Characterisation of fouling behaviour on membrane filtration of aggregated suspensions

Author:
Kovalsky, Peter

Publication Date:
2008

DOI:
https://doi.org/10.26190/unsworks/20661

THE UNIVERSITY OF NEW SOUTH WALES

School of Chemical Sciences and Engineering

Characterisation of Fouling Behaviour on Membrane Filtration of Aggregated Suspensions

A thesis submitted in fulfillment of the requirements

of the degree of

Doctor of Philosophy

By

Peter Kovalsky

April 2008

Acknowledgements

Thanks to Dr Graeme Bushell for providing solid support throughout the thesis and being the inspiration for the technical aspects of the project. The standard of rigor owes to your experience in flocculation. You certainly showed me what a challenging area this is.

Thanks to Professor David Waite for being a great co-supervisor. Your experience made sure we got through to the end. You are as sharp as a razor and I expect that your greatest work is still to come.

Thanks to the Australian Research Council for providing the Australian Postgraduate Award. Without such an exceptional scholarship it would not be possible to do full time research. Also, thanks to Anjou Recherche/Veolia Water for providing additional support and funding for the project. I hope we get another chance to work together in the future.

Thanks to the School of Chemical Sciences and Engineering and the Centre for Water and Waste Technology for its support with instrumentation and professional assistance. John Starling did an excellent job of ensuring that the labs were a good environment to work in.

Finally, thanks to my family for encouraging me to further my education. Thanks to my partner Samantha for supporting me while I devoted my life to research and this thesis. And to the Australian education system, thanks for continuing to support maths and the sciences.

List of Publications

Kovalsky P, Bushell G. In situ measurement of fractal dimension using focused beam reflectance measurement. *Chemical Engineering Journal.* Aug 2005;111(2-3):181-188.

Kovalsky P, Santiwong S, Bushell B, Waite TD. Impact of Coagulation on the Structure and Hydraulic Properties of Fouling Layers in Submerged Membrane Filtration. In: Hahn HH, Hoffmann E, Ødegaard H, eds. *Chemical Water and Wastewater Treatment* Vol IX. London: IWA Publishing; 2007:279-288.

Kovalsky P, Gedrat M, Bushell G, Waite TD. Compressible Cake Characterisation from Steady State Filtration Analysis. Paper presented at: IWA International Conference on Particle Separation, 2007; Université Paul Sabatier, Toulouse, France.

Kovalsky P, Gedrat M, Bushell G, Waite TD. Compressible cake characterization from steady-state filtration analysis. *AIChE Journal.* Jun 2007;53(6):1483-1495.

Kovalsky P, Bushell G, Waite TD. DEM/CFD analysis of cake consolidation: implications for filtration of flocculated matter. Paper presented at: IMSTEC, 2007; University of New South Wales, Sydney, Australia.

Wang, X.M.; Kovalsky, P, Waite, T.D. Multiphase flow models in quantifying constant pressure dead-end filtration and subsequent cake compression. 2. Concentrated slurry filtration and cake compression. Journal of Membrane Science (2008), 308(1+2), 44-53.

Wang, X.M. Chang, S, Kovalsky, P. Waite, T.D. Multiphase flow models in quantifying constant pressure dead-end filtration and subsequent cake compression. Journal of Membrane Science (2008), 308(1+2), 35-43.

Kovalsky P, Wang XM, Bushell G, Waite TD. Application of Local Material Properties to Prediction of Constant Flux Filtration Behaviour of Compressible Matter. *Journal of Membrane Science.* 2008;in press.

Kovalsky P, Bushell G, Waite TD. Permeability of simulated fractal structures under compressive loads, (paper in preparation).

Kovalsky P, Bushell G, Waite TD, Implications of Shear on filtration of flocculated matter (paper in preparation).

Abstract

It is widely accepted that flocculation improves filtration performance by increasing cake permeability. This principle is important in submerged membrane filtration for drinking water applications where the feed material can potentially contain fouling components which prohibit the extended operation of the filter.

Less well understood is the impact of floc properties on the hydraulic properties of the fouling layer formed on the membrane or the impact of hydrodynamic conditions during treatment on the floc-fouling layer relationship. In order to advance knowledge of this area, a set of tools were developed to characterise the cake formed during constant pressure filtration in terms of the compressive yield stress and permeability as a function of solid volume fraction. Using an iterative procedure, the optimal parameters for these models are calculated as are pressure and solid fraction distribution profiles. Input parameters to the numerical analysis are flux and final cake height data obtained from batch filtration experiments which are driven to steady state. The calculated material properties are compared against piston and centrifuge data with good agreement.

Application of the material properties to constant flux filtration involved development of a numerical model for simultaneous consolidation and cake formation. Flocculated yeast was used as the test system with the predicted transmembrane pressure rise as a function of time under constant flux conditions compared with experimental data. Good agreement is observed between model and experimental trends. The close correspondence between experimental and predicted results also suggests that it may be possible to predict trans-membrane pressure rise during constant flux filtration on the basis of material properties determined through simple constant pressure steady state experiments. A good account of the data was also achieved through extension of the general equation to include an empirical model for the consolidation time constant.

These new tools were applied to characterise the cakes formed under well controlled shear conditions. To avoid complications with modeling the sheared filtration system, the filtration was performed below the critical shear rate for particle rejection. This was verified by in-situ particle counts and size measurement. The material properties

were determined for flocculated yeast filtered in a coni-cylindrical Couette at several shear rates below the critical shear. Comparison of the compressive yield stress showed that cakes subjected to shear required less compressive stress to collapse. It is shown that the general equation for constant flux could be modified to encompass this effect through inclusion of an empirical shear parameter. The transmembrane pressure rise is able to be described well by this model.

DEM particle simulation was performed to investigate the effect of floc size and structure on cake permeability. Flocs of known size and structure were placed in a virtual suspension and the process of consolidation simulated by application of a compressive force. The permeability of the cake was calculated by computational fluid dynamics at various stages of the consolidation showing that the larger compact floc showed the highest permeability despite the highly compact structures formed. Comparison of pore size distribution also confirmed that several larger pores remained after consolidation of the larger compact flocs. Further work needs to be undertaken to pin point the microstructural mechanism governing this behaviour and whether the presence of fluid passing through these pores under normal filtration flows affects the retention of permeability of cakes under compression. Furthermore, the shear environment required to minimise the detrimental effects caused by shear enhanced cake collapse and also to form flocs of compact structure and large size needs to investigated.

Table of Contents

Table of Figures

List of Tables

Symbols

A'	Smiles constant
A^*	Experimentally determined constant
A_c	Cake area (m^2)
A_H	Hamaker constant
A_P	Plate area (m^2)
c_s	Solid volume concentration (kg/m^3)
B'	Smiles constant
C	Arbitrary constant
C_1,C_2	Permeability function parameters
C_3,C_4,C_5,C_6	Compressibility function parameters
d_{floc}	Diameter of the floc (m)
d_p	Primary particle diameter (m)
d_1	Chemical dimension (indication of chain straightness)
D	Diffusivity (m^2s^{-1})
D_c	Capillary diameter (m)
D_f	Mass fractal dimension
e	Charge on an electron
E_d	Potential energy/rupture threshold when two particles are separated at a critical distance (J)
f	The probability of a load bearing structure is denoted by
$\mathbf{f_A}$	Force of attraction (N)
$\mathbf{f_b}$	Buoyancy force (N)
$\mathbf{f_c}$	Contact forces (normal and tangential) (N)
$\mathbf{f_{DLVO}}$	Interparticle forces (N)
$\mathbf{f_f}$	Friction forces (rolling and sliding) (N)
$\mathbf{f_H}$	Hydrodynamic force (N)
f_L	Friction factor (Re dependant) and
$\mathbf{f_R}$	Force of repulsion (N)
F	Force (N)
$\mathbf{F}$	Summation of all forces acting on particle *i* in vector form (N)
g	Gravitational constant (ms^{-2})
g_d	Radial distribution function
G	Shear rate (s^{-1})
G^*	Characteristic shear (s^{-1})
h	Local cake thickness (m)
h_o	Initial local cake thickness (m)
H	Cake height (m)
H_{ij}	Particle separation distance (m)
H_∞	Equilibrium cake height (m)
H_c	Capillary length (m)
H_f	Final cake height (m)
H_o	Initial cake/sediment height (m)
J	Flux ($Lm^{-2}hr^{-1}$)
J_i	Flux entering cake ($Lm^{-2}hr^{-1}$)

J_o	Flux exiting cake ($Lm^{-2}hr^{-1}$)
k	Carman-Kozeny constant
k_b	Boltzmann number
k_{col}	Product of collision frequency
k_d	Constant related to the fractal dimension D_f
k'_{EB}	Spring constant for bending motion
k_o	Dimensionless curvature of the potential well,
k_p	Permeability prefactor
k_s	Consolidation equation constant
k_1 and k_2	Modified general equation constants
k_3 and k_4	Shear equation constants
K	Permeability (s)
K'	Mean effective permeability (s)
K_d	Darcian permeability (m^2)
L	Total cake height (m)
m	Cake mass per unit area (kg/m^2)
m_i	Particle mass (kg)
M	Mass of the aggregate (kg)
Mi	Cumulative cake mass per unit area (kg/m^2)
M_2	Compressibility exponent
n	Compressibility exponent
n_m	Aggregate size (number of particles)
n_1	Related to the end to end length of chains (m)
n_i	Number of ions per unit volume, ($ions/m^3$)
N	No. of particles
N_{ave}	Average number of particles
N_i and N_j	Number of particles in flocs *i* and *j* respectively
P_i and P_j	Two flocs of different size,
P_k	Floc formed by joining *Pi* and *Pj* and
P_L	Liquid pressure (Pa)
$P_{L,Net}$	Net liquid pressure (Pa)
P_N	Normal pressure (Pa)
P_o	Preform cake pressure (Pa)
P_S	Solids pressure (Pa)
$P_{S,\infty}$	Solids pressure exerted by cake on membrane (Pa)
P_y	Compressive yield stress (Pa)
ΔP	Applied pressure (Pa)
ΔP_L	Liquid pressure drop (Pa)
Q	Volumetric flow rate (m^3/s)
r	Radius (m)
r_a	Inner radius (m)
r_b	Outer radius (m)
r_c	radial distance from the centre of the reference particle (m)
r_i and r_j	radius of the colliding aggregates *i* and *j* (m)
r_L	Linear measure of size (m)
r_1 and r_2	Radii of two adjacent interacting spheres (m)
R	Hindered settling function ($Pasm^{-2}$)
R_c	Cake resistance (m^{-1})
R_m	Membrane resistance (m^{-1})
R_N	Mean radius of gyration of the cluster (m)

S	Fragmentation constant
S_c	Consolidation factor ($s^{-1/2}$)
t	Time (s)
T	Temperature (K),
$\mathbf{T}_{EB}$	Elastic bending moment
U	Direct angle of contact,
U_c	Dimensionless consolidation coefficient
U_e	Two particle bond energy (J)
v	Fluid velocity (ms^{-1})
v_L	Migration velocity (ms^{-1})
v_{norm}	Normalised particle velocity (ms^{-1})
v_{pl}	Plate velocity (ms^{-1})
v_s	Superficial fluid velocity (ms^{-1})
$\mathbf{v_t}$	Particle velocity at time t (ms^{-1})
V	Cumulative filtrate volume (m^3)
V_i	Volume of the aggregate (m^3)
V_p	Volume of a particle (m^3)
V_s	Cake preform cumulative filtrate volume (m^3)
V_{Solids}	Total solids (m^3)
V_{Total}	Total volume (m^3)
W	Experimentally determined constant
x_1	Fitting parameter
x_a y_a	DLVO constants
x_{crit}	Critical size at which particle is rejected (m)
X	Experimentally determined constant
y	Plate separation (m)
y_1	Fitting parameter
z	Cake position perpendicular to filter plane (m)
z_i	Counter ion charge number.

Greek Letters

α	Specific cake resistance (mkg^{-1})
α_1	Shear rate constant
α_{ij}	Collision efficiency
α_0	Specific cake resistance at zero pressure (mkg^{-1})
β	Fitting parameter
β_{ij}	Collision efficiency
β_g	Rate of intermittence between gas slugs given (slugs/sec)
β_1	Shear rate constant
δ	Consolidation lag (Pa)
δ_f	Filtration parameter
δ_g	Gap width between aggregates (m)
ε	Porosity
ε_d	Dielectric constant of water
ε_o	Permittivity of free space ($C^2N^{-1}m^{-2}$)
ε_{res}	Residual pressure (Pa)
ϕ	Solid volume fraction
ϕ_∞	Steady state solid volume fraction

ϕ_f	Final solid volume fraction
ϕ_g	Gelpoint solid volume fraction
ϕo	Suspension Solid Volume Fraction
$\mathbf{\Phi}_{EB,ji}$	Summation of angular displacements (rad)
γ	DLVO constant
γ_1	Constant in Happel model
Γ_{ij}	Floc breakage constant
Γ_d	Distance between the centres of mass G1 and G2 (m)
ϑ	Moisture Ratio
φ	Size of the fractal structure (m)
κ	Inverse of the double layer thickness (m^{-1})
κ_c	Dynamic Compressibility (Pa^{-1})
κ_2	Equation pre-factor
κ_R	Ratio of inner and outer Couette cylinders
λ	Correction function for monodisperse particles
λ_s	Stokes drag coefficient.
μ	Dynamic Viscosity (Pas)
θ	Angle between cone and plate (rad)
θ_1	Angle that two contacting particles make (rad)
θ_c	Critical angle (rad)
ρ_L	Fluid density (kg/m^3)
ρ_S	Solid density (kg/m^3)
ρ_o	Average number of particle per unit volume (particles/m^3)
τ	Time constant (s)
τ_{LMean}	Mean shear stress exerted by the air scour (Pa)
τ_w	Crossflow shear stress (Pa)
τ_S	Shear stress (Pa)
Ω	Speed of revolution (RPM)
ψ_0	Stern potential (mV)
ψ	Applied Pressure (m H20)
ζ	Random variable uniformly distributed between 0 and 1

Subscripts

i	Subscript denoting cake slice number or particle of interest.
j	Subscript denoting adjacent particle.
n	Subscript denoting slice adjacent to membrane

Chapter 1: Introduction

1.1 Problem Statement

Significant savings in the overall cost of water treatment can be made during filtration if measures are taken to enhance flux. These measures include the use of coagulants to flocculate the material to be separated, back pulsing and periodic cleaning. Of interest in this study is improving the general understanding of how floc properties affect membrane filtration separation efficiency.

In membrane filtration plants which use coagulants, the flocculated material tracks a path through the flocculation tank before being drawn towards the submerged filter cake. As flocs pass through a process there can be a wide variation in shear magnitude which can potentially affect the rate of floc growth, floc breakage and floc structure. The implication of flocculated material passing through varying degrees of mixing intensities and durations is poorly understood from the point of view of optimising filtration performance.

Flocculation research is largely driven by the pursuit of industry to improve solid liquid separation. As such, it has been established in the literature that a wide range of factors including shear history (McCurdy et al. 2004; Selomulya 2001; Spicer et al. 1998), chemistry (Gregory and Dupont 2001; Machenbach et al. 2003) and temperature (Hiemenz and Rajagopalan 1997) affect the properties of a floc.

Measuring floc properties is not a trivial exercise, with measurement of floc strength and structure being mostly limited to laboratory measurements using specialised instrumentation or image analysis. Given these limitations, fundamental research into the impact of floc characteristics on filtration performance is constrained by floc characterisation. The strategies to cope with known limitations are discussed in a review of works on the topic of combined filtration and flocculation.

1.1.1 Industrial Motivation for Work

Demands of huge membrane area during solid-liquid separation are a general problem met in a larger scale filtration. A common strategy for this is cascading the membrane modules either in parallel or in series (Mulder 1996). The separation of natural organic matter for purification of drinking water presents a unique demand on process design in that particle loadings are low (i.e. less than 100 parts per million) and volumetric throughput is of the order of 100's of millions of litres per day. Submerged membrane filtration is relatively new technology highly suited to drinking water treatment that can be operated at low pressures (i.e. 30-70 kPa) to minimise the cost of processing a nominal volume of fluid per unit area per unit time. Like other forms of dead-end filtration, a reduction in performance due to resistance from accumulating material is inevitable (Crittenden 2004) which increases the energy requirement to process a fixed throughput.

For operation of submerged membrane filtration, it is routine to have backwashing and air sparging to remove the filter cake at periodic intervals (Scott 2004). However, this is not completely effective, with some hard to remove material remaining. A second cleaning cycle is typically conducted less frequently to remove this layer which is described as a "foulant". The cake filtration cycle is illustrated in Figure 1-1.

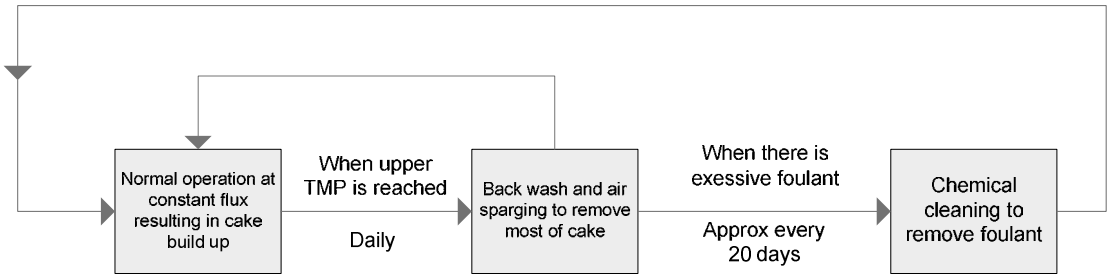

Figure 1-1 Operation of a submerged membrane filter in dead-end configuration requires backwashing when an upper transmembrane pressure (TMP) limit is reached.

The immediate scope of this work is to focus on the cake formed during normal daily operation. However, there are implications for improving the efficiency of the backwash and chemical clean if improved knowledge is gained from understanding

the material properties of the formed cake. The components of the cake which contribute to the resistance to flow are given in the following sections.

1.1.2 Cake Resistance in Submerged Membrane Filters

The concept of cake resistance can simply be described as the hindrance of flow through the membrane resulting from buildup of the solid suspension. The fundamental reasons for this flow resistance can be described by the Hagen-Poiseuille principle of flow through a tube such as described in standard fluid mechanics (Streeter and Wylie 1985) and transport phenomena textbooks (Bird et al. 2002). According to this principle the resistance to flow is inversely proportional to the void space between particles in the cake (i.e. as the void reduces in size the resistance to flow increases accordingly) represented as parallel cylindrical voids. In a macroscopic sense, it is convenient to quantify the space between particles by means of the porosity ε of the system (i.e. the volume of pores/total volume of the system).

For this research a physically measurable property of a particle system known as the solid fraction ϕ is utilised to describe the concentration of particles in a system which in a general sense can be related to the porosity as

$$\phi = 1 - \varepsilon \tag{1-1}$$

or experimentally as

$$\phi = \frac{V_{Solids}}{V_{Total}} \tag{1-2}$$

Several important variables commonly used in this thesis include:

i) *the suspension solid volume fraction* ϕ_o ; i.e. the solid volume fraction of the prepared suspension.

ii) *the gelpoint solid volume fraction* ϕ_g ; i.e. the concentration at which flocs encompass the whole suspension forming an interconnected network of particles.

iii) *the final solid volume fraction* ϕ_f ; i.e. the solid volume fraction of the layer adjacent to the membrane subjected to the greatest compressive stress from the weight of the material above.

The solid fraction profile of a cake formed during the standard gas driven filtration process is typically non-uniform with respect to position in the cake in the direction of cake formation for compressible materials (Cheremisinoff 1986).

At the end of any filtration cycle it is suggested that there are three contributing flow resistances acting in series. These are the consolidating cake layer, resistance from the fouling layer, and membrane resistance (Figure 1-2).

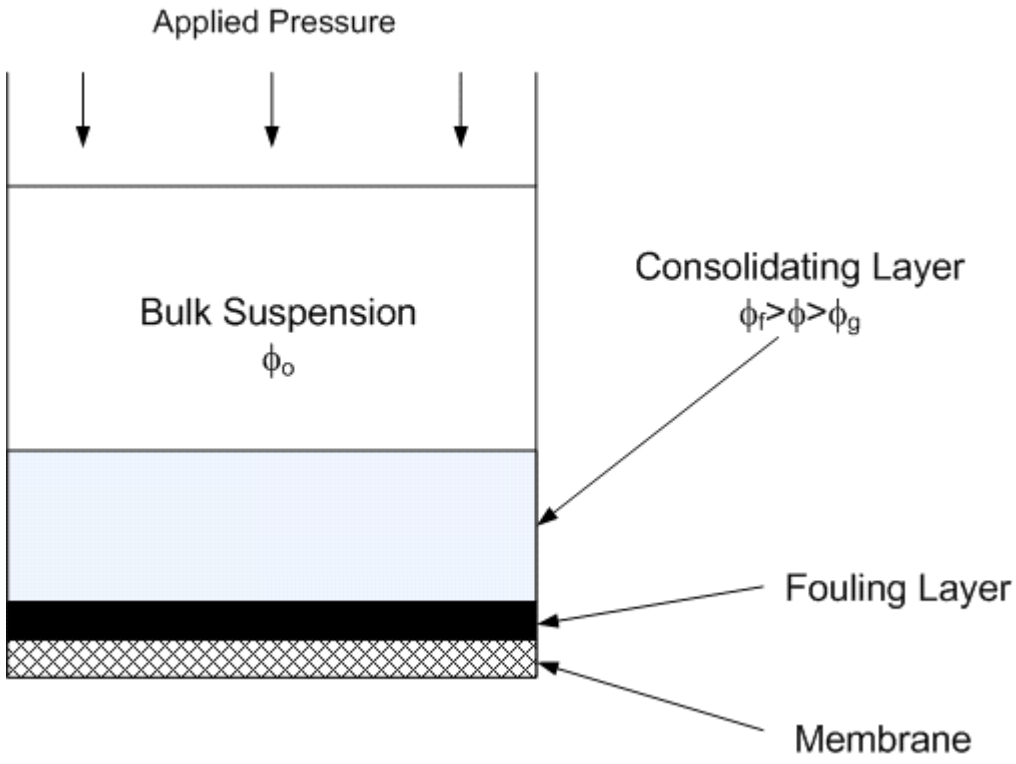

Figure 1-2 Resistance in dead-end filtration of feed water under constant flux operation.

Typically the solid fraction increases from the suspension/cake interface to the membrane such that $\phi_g < \phi < \phi_f$. The contributing resistances are believed to behave as resistances in series as described by Ruth et al. (1933) who described cake resistance based on an electric circuit analogy. A description of the resistance of the respective components is given in the following sections.

1.1.2.1 Resistance from Consolidated Cake

When the solids pressure imparted by cumulated hydrodynamic drag exceeds the compressive yield stress of the particle network, consolidation occurs. The change of solid volume fraction in the direction normal to the membrane surface is typically a monotonically decreasing function. This layer is where a large portion of the flow resistance occurs towards the end of an operation cycle.

By the application of crossflow shear, this layer can be removed to a certain extent (Altmann and Ripperger 1997). In general, if the force applied by crossflow shear is greater than the cohesive force in the consolidated particle network, the cake will be removed. Any solids remaining on the cake after application of crossflow shear is considered to be the permanent fouling layer.

1.1.2.2 Resistance from the Fouling Layer

At the beginning of a filtration cycle, the fouling resistance and membrane resistance are the only resistances to flow. These are not separately identifiable with experiments that do not start from a new membrane. However, there is evidence to suggest that, with time, resistance from the fouling layer increases. The mechanism responsible for the increase in resistance of a cleaned membrane is uncertain but it could be explained by the following contributions:

1) repeated compression/consolidation of the fouling layer increases after every cycle forcing the particles closer together thus increasing resistance;
2) continued growth of the fouling layer as application of shear and backwash fails to remove the consolidated cake layer;
3) pore blockage; and
4) chemical changes, cementation, crystallisation, precipitation, foulant adsorption (Li and Wang 2006) etc.

Figure 1-3 illustrates this increase in resistance due to the fouling layer as represented by an increase in the transmembrane pressure (TMP) required to sustain a constant throughput of permeate through the cake. It is quite clear that after each backwash that there is increase in resistance from the foulant layer. This is indicated by the post backwash pressure drop across the membrane getting progressively higher. Towards

the end of the chemical clean cycle, the post backwash pressure drop is significantly higher than the chemically cleaned membrane.

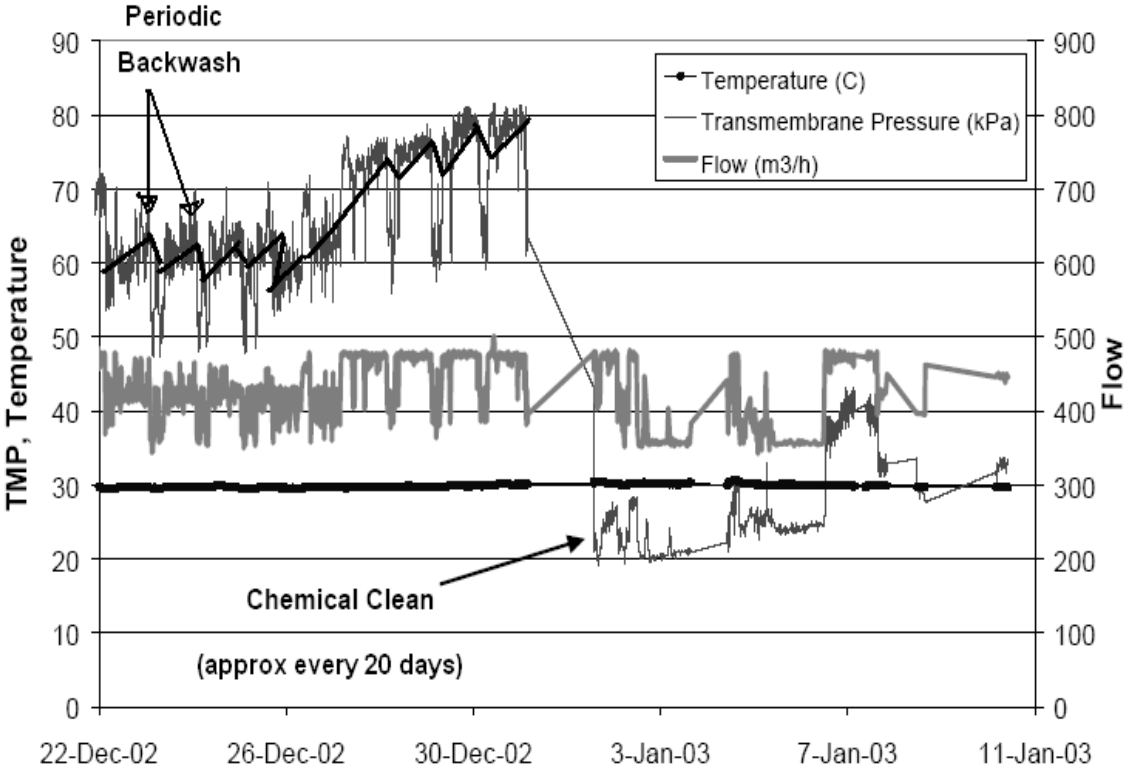

Figure 1-3 Real SMF data for a single cell operated approximately at constant flux (Scott 2004) The TMP is indicated to have periodicity initially then a clean mid way through the plot interval.

The resistance from the consolidating layer is given the most attention in this thesis, and to a lesser extent the fouling layer. In Chapter 3 a numerical technique for analysing cake filtration data to calculate the ϕ profile versus cake depth was developed. Insight into the removal of the fouling layer could be enhanced through a better understanding and characterisation of the solid volume fraction profile through the cake as Fuchs et al. (2006) demonstrates that pre-flocculation enhances the recovery of the membrane. Mo and Huang (2003) showed that alkaline cleaning can effectively restore most of the permeability.

1.2 Shear and Filtration

In practice, for any given combined membrane flocculation/filtration process, there are a limited number of critical processes (or factors) which can affect the performance of the filtration. The two critical processes identified in this research are the hydrodynamics of the process and the chemistry of flocculation. Given these critical processes, a limited number of control actions or variables can be identified which either directly or indirectly affect the filtration performance. Such control actions whether automatically or manually implemented may or may not be based on a mechanistic understanding of the process of filtration and flocculation.

A simplified flow diagram describing the indirect interaction between a design (controllable) parameter such as shear (left) and the resulting filtration performance (right) as a result of influence on the floc and cake properties (middle) is shown in Figure 1.4. The scope of this thesis is effectively captured in this diagram starting with a literature review along this scope together with development of new models and experimental data to support this. The four elements of this simple model can be described as follows:

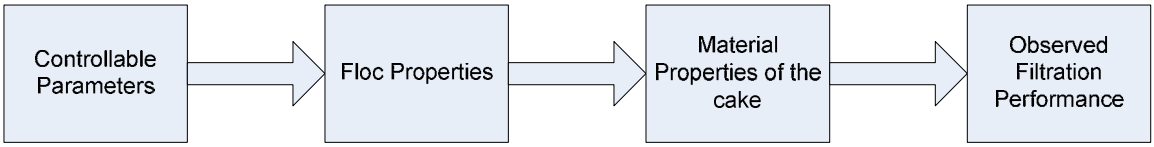

Figure 1-4 Flow diagram illustrating the indirect control of filtration performance through direct control of shear and chemistry. From left, controllable parameters could be floc dose, type, shear history which directly affect the floc properties. Once these flocs migrate onto the cake the flocs unite in a complete network where at this point can be characterised by the material properties. The material properties govern the filtration performance under the complete parameter space of pressure, flux, etc.

i) The first key area encompasses the *controllable parameters* which can be engineered to a high level of precision. Control of shear implies choice of impeller, position or spacing in tanks, impeller power input or speed, residence time or duration of mixing, and blending of chemicals. Similarly, reasonable control over chemistry of

the flocculation process through the addition of chemicals to control pH and coagulant dose is possible. Control of filtration throughput or pressure can also be regarded as a controllable parameter.

ii) The *floc properties* include those which may influence separation efficiency such as floc size, structure (e.g., as measured by fractal dimension D_f) and floc strength (in terms of particle bond energy). In practice, these parameters are not controlled directly and are a consequence of process design which is fixed at the time of construction. Flocculant dose are based typically on cost optimisation rather than chemical optimisation (i.e. maximum destabilisation). Flocculation detention times on the order of 10-20 minutes are typical in drinking water treatment processes prior to filtration (Crittenden 2004) which is a consequence of filtration design criteria rather than flocculation optimisation.

iii) The coverage in membrane filtration literature given to optimum filtration conditions based on floc properties lacks critical analysis of the mechanics governing this process. By proposing that the gel layer behaves mechanically like a consolidating bed (i.e. a thick filter cake subject to solid compressive stress) it is possible to approach the problem from a dewatering point of view. Essentially, *material properties* such as the permeability and compressive yield stress describe how a cake will respond to increasing solids stress as it is expected that the cakes response to stress also occurs in constant flux filtration (i.e. plant operation conditions).

iv) As will be presented in Chapters 3 and 4, the *filtration performance can be described* in terms of the material properties. These properties are used throughout the thesis to describe the mechanics of cake consolidation, with the process of cake formation being dealt with by conventional modelling.

In this research, the model presented in Figure 1.4 is the scope of the study. Through this concept a mathematical model was derived to describe “low shear” effects on filtration performance (i.e. the shear below which cake rejection or break-off occurs). By operating in the low shear regime ($<\sim 10 s^{-1}$), complications can be avoided with modelling cake formation rates.

1.3 Summary

As outlined in this section, part of the challenge of this work is to understand how the consolidating layer affects filtration performance or more specifically, the implications for the frequency of backwashing in submerged membrane filtration systems.

The focus of this study is on how shear affects filtration performance as a potential avenue for improving control over fouling of the membrane. The scope is limited to the case where the shear does not cause significant rejection of the material from the cake. Hence, the consolidation of the cake can be analysed without complications from unpredictable cake formation rates.

Furthermore, part of the focus of this study is to look at understanding how flocs behave mechanically under applied solids compressive stress. Chapter 5 looks at simulation studies into the consolidation of cakes formed from fractal aggregates as a way of investigating hydraulic behaviour of flocs under compression. This understanding relates to how the shearing during floc formation can result in improved cake permeability.

Chapter 2: Literature Review: Floc Properties and Filtration

In filtration, flocculation can be referred to as a size enlargement process in chemical engineering terms (Perry and Green 1997; Rhodes 1998). An increase in size of the material depositing on a cake induces an increase in the permeability of the cake both by providing a larger fluid pathway between depositing flocs and also within flocs themselves. Before reviewing filtration literature it is necessary to review the fundamentals of flocculation which is provided first in section 2.1. This section introduces the concept of flocculation and defines floc size and structure.

2.1 Flocculation Theory

The agglomeration of particles to form aggregates is a naturally occurring phenomenon characterised by a complex grouping of primary particles brought together by interparticle forces. The agglomeration of smaller primary particles in a liquid medium is commonly known as an aggregate or floc (Figure 2-1). Industrial separation processes that directly rely on the aggregation of particles include sedimentation, thickening, clarification, flotation and filtration. These types of applications are typically used in various stages of effluent treatment from mineral processing operations and municipal waste.

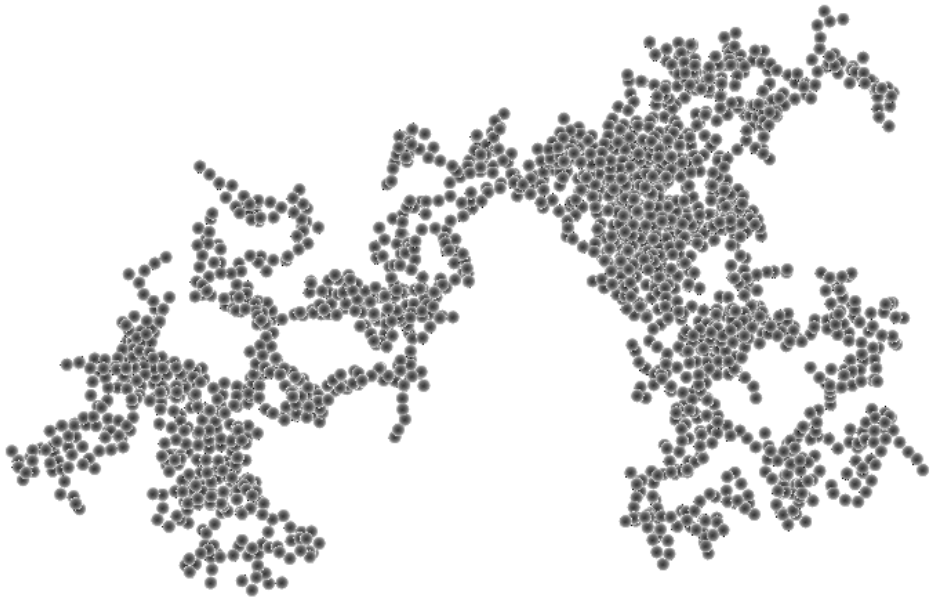

Figure 2-1 Computer simulated aggregate showing the spatial arrangement of particles. The entire structure is porous in nature which is believed to provide a hydraulic pathway for fluid to permeate when in contact with other flocs in a packed bed or cake.

The mechanism of aggregation can be described as the sticking of two particles upon collision. Several driving forces within a fluid environment bring about the collision of particles. These have been identified as:

- Brownian motion, which is driven by diffusion and is independent of shear effects;
- fluid motion, which is a shear-induced collision resulting from spatial variations in fluid velocity; and
- differential sedimentation, which is caused by the collision of two particles having different settling velocities.

Of these three mechanisms, shear-induced collisions are of the most importance as the Brownian force experienced by primary particles used in the experimental study is relatively small compared to shear force. Differential sedimentation effects are negligible due to particles experiencing sufficient agitation. Later the effect of shear on floc breakage will be discussed.

2.1.1 Characterisation of Flocs

Characterisation of flocs is fundamentally based on the spatial arrangement (i.e. loose or compact) and the number of particles within the structure (i.e. size). Physical properties of flocs such as porosity, permeability, density, floc size and floc structure are important parameters in the design of industrial equipment for a particular application.

In practical applications the process of flocculation is enhanced to yield favourable floc characteristics to maximise the efficiency of separation. Manipulation of floc properties is performed by variation of flocculent type, coagulants, flocculant dosage and shear environment during floc evolution. Coagulants effectively enhance the interparticle forces by reducing the repulsive double layer forces, acting to produce larger flocs. On the other hand, flocculants act more like glue providing an additional attractive force apart from van der Waals (Ravina 1993). For example, in practice, having larger flocs is hydrodynamically favourable if higher particle settling velocities are required to increase separation efficiency in a thickener.

2.1.2 Measurement of Floc Size

The ability to measure the size of flocs which are brought to the filter cake is an important requirement for this study. Such a task is difficult to achieve using some of the well refined techniques based around small angle light scattering as obscuration limits are exceeded at the high particle loadings in filtering suspensions.

It is possible to sample flocs to be brought offline for analysis. The process of transferring flocs whether by piping or pipetting results in some degree of floc breakage (Liao et al. 2006) and the eventual measured size no longer represents the sample bulk. Such limitations are the motivation for pursuing in-situ based techniques for sizing.

Image analysis involves the acquisition of many single floc images and subsequent measurement of size. A large set of data is created upon which the size distribution can be calculated. This technique often involves focusing a CCD camera into the process fluid using a macro lens. Such a technique is a viable option for in-situ measurement.

Alternatively, an instrument based around laser reflection which is suitable for the range of solids concentration looked at in this study was implemented. This is known as the Focused Beam Reflectance Measurement (FBRM) and a description is given in the following section.

2.1.2.1 FBRM

For this study the in-situ particle size measurement tool known as the focused beam reflectance measurement is used to measure floc size in the filtration vessel as the particles deposit on the cake.

The Lasentec Focused Beam Reflectance Measurement (FBRM) is marketed as an in-situ tool for sensing changes to size and shape of suspended solids in a general sense. The nominal range of solids concentration upon which most particle sizing instruments operate is typically quite narrow which is acceptable under laboratory conditions but not suitable for in-situ measurement. In comparison, FBRM is capable of operating over a wide range of solids concentrations from very dilute up to slurry type mixtures. This property alone gives it considerable appeal for being adapted for use as a floc characterisation tool, most particularly for industrial applications where solids concentration of process fluids can be quite broad.

The FBRM (model M400L-316K) consists of a laser scanning at a fixed high velocity (2m/s) housed in a rigid stainless steel probe which is inserted into a solid suspension (Worlitschek and Mazzotti 2003). Figure 2-2 illustrates the internal components of the probe. A spinning lens is used to generate the circular path tracked by the laser which is achieved through precise optical reflection and beam splitting. Ordinarily the light reflected back off the suspended particles is collected and passed back to the electronics where chord length is calculated based on duration of a high reflectance signal. The data is collected and reported as a chord length distribution.

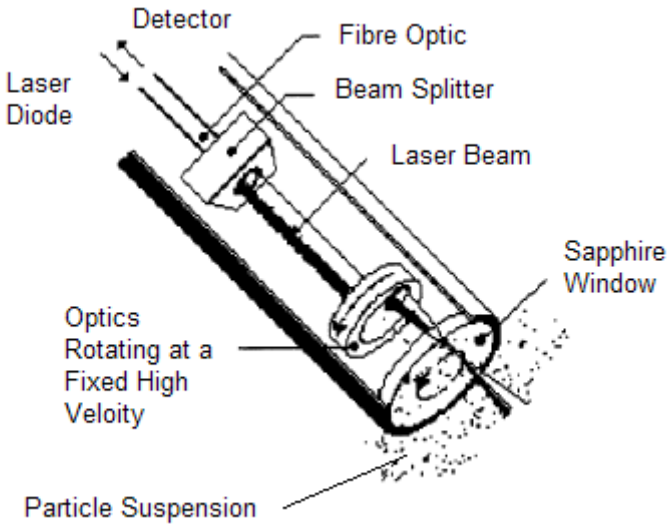

Figure 2-2 Schematic of the FBRM illustrating the principle of laser back reflection (taken from Ruf et al. (2000)).

The FBRM gives a reasonable estimate of floc size allowing the effects of shear on steady state floc size to be monitored.

2.1.3 Floc Structure and the Concept of Fractal Dimension

The concept of fractal geometry in nature was introduced by Mandelbrot (1967). Wide spread popularity of fractals can be attributed to this work. The morphology of aggregated particles was first showed to exhibit fractal structure by the experimental work of Forrest and Witten (1979). Their approach to characterising the fractal dimension made use of a transmission electron micrograph to obtain an image of the smoke particle aggregates.

Adaptation of the fractal concept to aggregation has led to the introduction of a macroscopic approach to qualitatively characterise the complex structure of flocs, referred to as the mass fractal dimension (D_f).

The mass fractal dimension is defined by

$$M \propto R_L^{D_f} \qquad (2\text{-}1)$$

where M is the mass of the aggregate, R_L is a linear measure of size and D_f is the mass fractal dimension. Figure 2-3 illustrates this relationship between mass fractal dimension and floc structure.

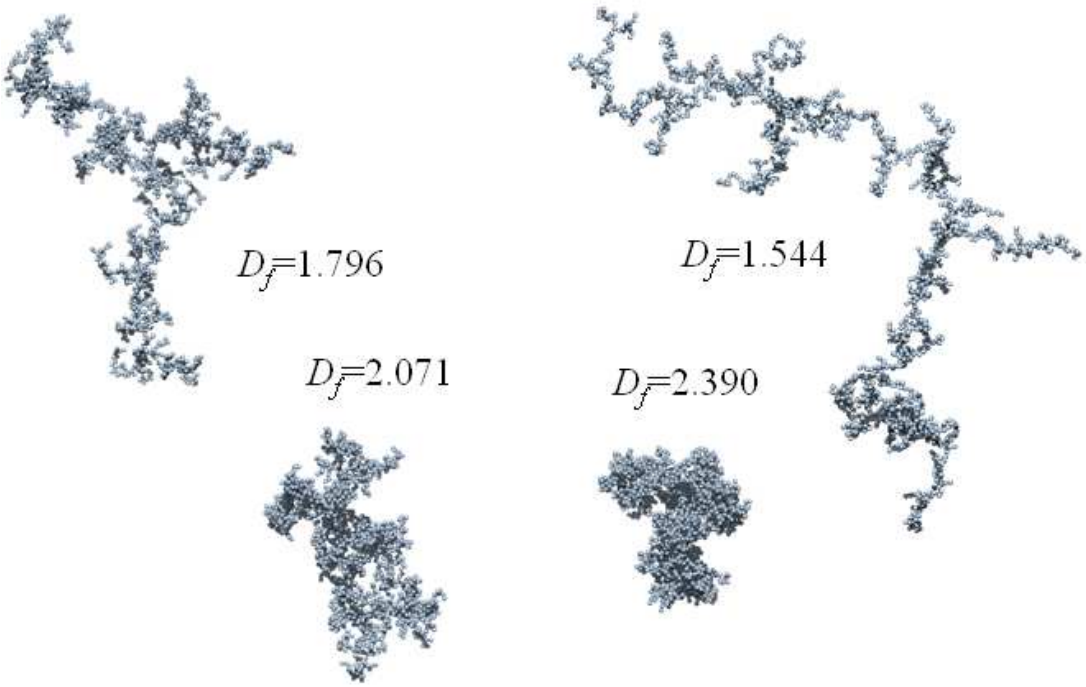

Figure 2-3 The mass fractal dimension is related to the structural arrangement of particles in the floc where a loose structure can be seen at low D_f and a compact structure at high D_f values.

There is evidence in literature which suggests that there is a correlation between fractal dimension and permeability of cake structure (Guan et al. 2001; Lee et al. 2003) presumably through some of the hydraulic characteristics of the original structure being retained after cake collapse (Antelmi et al. 2001; Waite et al. 1999).

Radiation (i.e. light, X-Ray) scattering has been used as a means for characterising the structure of aggregates (Sorensen 1997). This technique is based on the analysis of scattered radiation as a function of scattering angle. One method of analysis is based on the Rayleigh-Gans-Debye theory, which models the intensity of scattering from correlated particle pairs. The settling behaviour of particles also provides limited characterisation of the fractal structure of aggregates. The technique is limited in the sense that many of the hydrodynamically derived equations are based on non-porous

objects of a spherical nature (Bushell et al. 2002). Image analysis also provides a direct indication of particle morphology, which in itself is a significant advantage over the other two techniques. Box counting is primarily the method of analysis used in this instance.

Comparison in the literature between techniques has been uncommon until late (Bushell et al. 2002) making this topic a grey area in flocculation research. Inconsistencies between the various experimental approaches are reported in literature. Liao et al. (2006) reported that the observed fractal dimension was inconsistent between the three techniques (i.e. light scattering, settling and ex-situ image analysis) under controlled sampling conditions. Such inconsistency can potentially be attributed to the intrusive nature of measurements and in-situ methods are preferable. A study by Kovalsky and Bushell (2005) is an example of a promising technique for in-situ measurement of floc structure based on the unprocessed FBRM data.

A survey of literature has shown that floc size and fractal dimension can potentially influence filtration performance. The relevance of floc properties to filtration performance is the foundation of this thesis. The hydraulic influence of these fractal assemblages when they pack to form a cake forms the basis for the theory of “flocs and filtration”.

2.1.4 Effect of Shear on Floc Properties

The process of flocculation involves the collision and subsequent bonding of particles to form a floc. When short range forces between particles encourage particle sticking then conditions are conducive to flocculation. A number of processes including Brownian motion, differential settling and shear forces encourage particle-particle collision with the relative importance of these various processes being determined particularly by the size and density of the particles involved. When particles are above a certain size, the effects of Brownian motion are small. Alternatively, if the particle density is approximately equal to that of the liquid phase then flocculation driven by differential settling effects is minimal. Under certain conditions, shear effects can be the dominant mechanism for inducing particle collisions.

Shear effects are critical to both floc growth and floc breakage. In this section the focus is placed on the factors which govern the steady state achieved between floc breakage and floc growth for a given shear magnitude. These factors are explored through use of the well accepted population balance model of flocculation. This model is introduced below and referred to in subsequent sections as justification in meeting experimental design criteria.

2.1.4.1 Model for Floc Growth (Population Balance)

Flocculation occurs when short range repulsive forces are overcome and particle collision and bonding is favourable. When particle sticking is favourable, the smaller individual particles come together and result in formation of large assemblages. Both the collision frequency and collision efficiency govern the kinetics of floc growth. A rigorous accounting process is necessary to manage the possible combination of collisions between units of various sizes in order to model this process.

The foundations for such a model can be presented in terms analogous to a chemical reaction where

$$P_i + P_j \xrightarrow[\Gamma_{b,ij}]{\beta_i} P_i \equiv P_j \xrightarrow{\alpha_{f,ij}} P_k \qquad (2\text{-}2)$$

where P_i and P_j are two flocs in a system of different size, $P_i \equiv P_j$ represent a pair of particles that have approached each other closely enough that they affect each other's subsequent motion, P_k is the floc formed by joining P_i and P_j and β_{ij}, $\alpha_{\phi,ij}$ and $\Gamma_{b,ij}$ are rate constants for the respective reactions.

The rate constants are critical features of the model as they govern where the particular steady state concentration of the constituents will lie. The collision frequency function β_{ij} are influenced by long range forces such as shear. The functions $\Gamma_{f,ij}$ and $\Gamma_{b,ij}$ are what govern the formation and breakage of the P_k floc given they are in the region where short range forces such as van der Waals forces act to reduce the separation between the P_i and P_j units and encourage contact. Smoluchowski's Equation (von Smoluchowski 1917) describes the rate of irreversible flocculation; i.e.

$$\frac{dn_m}{dt} = \frac{1}{2}\sum_{i=1,\, j=m-i}^{i=m-1} k_{ij} n_i n_j - n_m \sum_{i=1}^{i=\infty} k_{im} n_i \qquad (2\text{-}3)$$

where the first term in the equation describes the rate of growth of numbers n of m sized aggregates and the second term describes the rate of disappearance of aggregates to become larger aggregates. Constant k_{ij} is the product of both collision frequency β_{ij} and collision efficiency α_{ij} such that

$$k_{ij} = \alpha_{ij} \beta_{ij} \qquad (2\text{-}4)$$

By introducing the collision efficiency into this equation it is possible to model the effects of shear on the rate of floc growth.

At a particle interaction level, fundamental physical models for two particle interactions can be introduced into the flocculation rate model. In a laminar flow field, particles that travel with the fluid flow but lying on different fluid streamlines can potentially be brought together because of flow field velocity gradient. For example, consider two particles traveling in adjacent streamlines with different velocities; the associated velocity difference causes a collision (see Figure 2-4). By definition the collision frequency at shear rate G (dv/dx) is given by (see section 6.1 for definition of G)

$$\beta_{ij} = \frac{4}{3} G (r_i + r_J)^3 \qquad (2\text{-}5)$$

where r_i and r_j are the radius of the colliding aggregates. An improved correlation which takes into account the effect of floc structure on floc radius is given by

$$\beta_{ij} = \frac{4 G r_o^3}{3} k_c^{\frac{-3}{D_f}} \left(N_i^{\frac{1}{D_F}} + N_j^{\frac{1}{D_f}} \right)^3 \qquad (2\text{-}6)$$

where N_i and N_j are the number of particles in the floc (Selomulya 2001). From equation 2-3 and 2-5, a simple quantitative model accounts for the effect of shear on floc growth. However, a more complex model is needed to account for floc breakage which is not accounted for in equation 2-3.

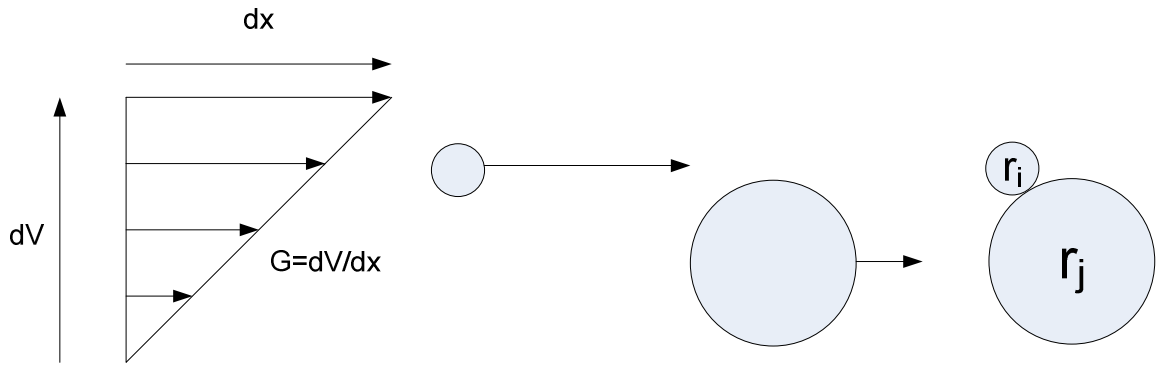

Figure 2-4 Flocculation induced by particle collision in adjacent fluid streamlines.

Kusters (1991) introduced the lumped discrete population balance model which takes into account floc breakage by adding additional terms to the population balance model. This is given as

$$\frac{dN_i}{dt} = \sum_{j=1}^{i-2} 2^{j-i+1} \alpha_{i-1,j} \beta_{i=1,j} N_{i-1} N_j + \frac{1}{2} \alpha_{i-1,i-1} \beta_{i-1,i-1} N_{i-1}^2$$
$$- N_i \sum_{j-1}^{i-1} 2^{j-i} \alpha_{i,j} \beta_{i,j} N_j - N_i \sum_{j=1}^{\max_1} \alpha_{i,j} \beta_{i,j} N_j - S_i N_i + \sum_{j=1}^{\max_2} \Gamma_{i,j} S_j N_j \qquad (2\text{-}7)$$

where the first four terms describe the loss and growth due to collision of different size flocs. The fifth term accounts for floc breakage due to fragmentation and the sixth term accounts for the rate of gain of flocs from breakage of larger flocs according to a fragmentation model.

A simple empirical model for the fragmentation constant S in the breakage terms (5th and 6th terms) is given by

$$S_i = A^* G^W V_i^X \qquad (2\text{-}8)$$

where A^*, W and X are experimentally determined constants and V_i is the volume of the aggregate.

There are several models which describe the floc breakage constant Γ (Selomulya 2001). These are based on binary breakage, multiple fragment breakage and normally distributed breakage but it is not necessary to go into great detail on these options here.

On examining the various rate constants and the equation which governs the population balance it can be seen that there are many factors which contribute to the rate of growth of flocs in a system. When the system is at steady state such that $dN/dt=0$, it is easy to see that the features which govern the kinetics of growth also govern the steady state size of flocs. This can essentially be summarised as a balance between breakage and formation of flocs when shearing forces are dominant.

2.2 Filtration theory

Flocculation theory and filtration theory appear to be two very distinct and separate disciplines. When one consults an encyclopaedia on the filtration topic (Cheremisinoff 1986) there is little mention of floc size or fractal dimension in any of the equations or models describing filtration. This perhaps owes to the relative ages of the two disciplines. For example, cake filtration theory was one of the most popular topics in chemical engineering at the beginning of the 20th Century in a statement made by Tien (2002). On the other hand, the discovery of Forrest and Witten (1979) arrived in the later part of that century. Some of the recent works on flocs and filtration will be discussed in this section.

Conventional filtration theory originated with the works of Ruth et al. (1933) and his pioneering work on compressible cake filtration. The extension of Darcy's Law to filtration and variations on this such as the parabolic rate law (Rushton 2000) are examples of the application of filtration theory. In this section cake filtration theory is discussed and the current knowledge on how floc properties are related to this body of theory is reviewed.

Fundamentally, filtration modelling involves the mass and momentum balance of the solid and liquid phases (Lee and Wang 2000). Filtration theory in the context of this research is approached as a tool to analyse filtration data (i.e. permeate mass versus time data) to gain further insight into mechanical properties of the cake such as local compressibility and local permeability.

The concept of the "standard filtration approach" will be developed in the following sections as a contrast to the material properties approach developed in this thesis.

Firstly, a review of theory related to flow through packed beds will be given as a precursor to filtration theory which builds on these fundamental concepts.

2.2.1 Flow Through Packed Beds (Carman-Kozeny equation)

Generally, it is understood that flocculation enhances filtration performance by increasing the interfloc porosity (space between flocs) and intrafloc porosity (space within flocs) to provide a permeable structure for fluid to pass through (Waite et al. 1999).

The fundamental theory governing fluid transport through a medium of packed uniform spheres can be described by the Hagen-Poiseuille principle (Bird et al. 2002). Consider a force balance of fluid passing through a narrow tube/capillary (Figure 2-5). The Hagen Poiseuille equation is given as

$$\frac{\Delta P_L}{H_c} = - \frac{32 \mu v}{D_c^{\,2}} \qquad (2\text{-}9)$$

Where H_c is the length of the capillary, D_c is the diameter, v is the fluid velocity, ΔP_L is the pressure drop and μ is the fluid viscosity. Figure 2-5 illustrates a capillary bound by packed spheres.

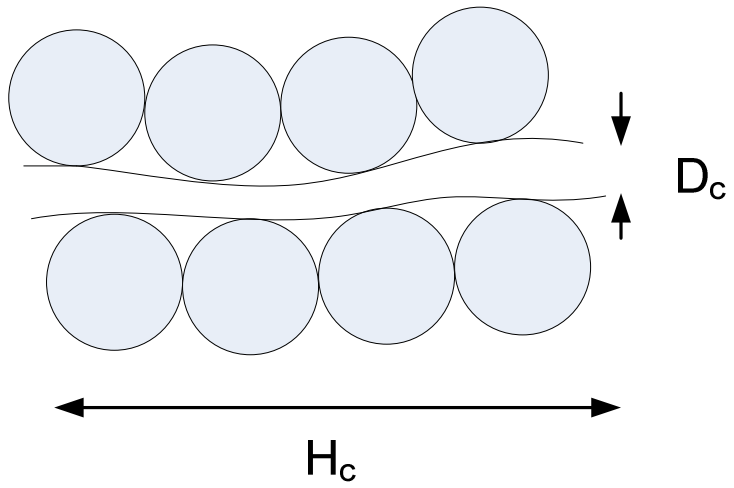

Figure 2-5 Hydraulic pathway enclosed by particles comprising the packed bed.

For highly permeable material, gravity or capillarity is a sufficient pressure to sustain flow through the packed bed. For filter cakes where capillary size is of the order of a few microns, additional mechanical driving force such as a pump is required.

The combined works of Carman and Kozeny provided a model for laminar flow through packed beds based on the Hagen-Poiseuille principle (Carman 1939). A derivation for the mean capillary diameter based on the porosity and sphere diameter can be substituted into equation (2-2) giving pressure drop through a bed of incremental thickness *dh* as

$$\frac{dP_L}{dh} = \frac{k\phi^2}{(1-\phi)^3 d_P{}^2 v_S} \tag{2-10}$$

where *k* is a constant, ϕ is the solid fraction, d_p is the particle diameter, P_L is the liquid pressure and v_s is the superficial fluid velocity. This equation, otherwise known as the Carman-Kozeny equation, relates the driving force per unit length required for a given porosity of the bed. For systems of single spheres, this correlation is reasonable, but for flocculated systems it is not an accurate approximation as the apparent porosity is a poor representation of the hydraulic characteristics of the cake. This is because the pore size distribution is polydisperse (i.e. high degree of non-uniformity).

Despite the shortcomings of the Carman-Kozeny relationship, the model describing the hydraulic characteristics of packed beds has provided a valuable foundation and is often a reasonable starting approximation. These concepts are expanded on further in this Chapter.

2.2.2 Standard Filtration Approach

The classical filtration equation derived from the original published works of Darcy (1856) relates flux *(J)* through a porous medium covered in a porous cake to both the pressure applied across the filtration medium *(ΔP)* and the resistance of the cake *(R_c)* and membrane *(R_m)*

$$J = \frac{1}{A_c}\frac{dV}{dt} = \frac{\Delta P}{\mu(R_c + R_m)} \tag{2-11}$$

where J is defined as the rate of change of cumulative filtrate volume V per cake area A_c and μ is fluid viscosity. The assumption is made that the resistance of the cake layer is directly proportional to the amount of mass deposited on the filter with mass accumulating in direct proportion to the volume of suspension filtered; i.e.

$$R_c = \alpha \frac{c_s V}{A_C} \tag{2-12}$$

where α is the specific cake resistance and c_s is the solid volume concentration. The specific cake resistance α is inversely proportional to the permeability of the formed cake.

The process of calculating α from filtration data requires integration of Darcy's Law giving the parabolic rate law

$$\frac{t}{V} = \frac{\mu c_s \alpha_{av}}{2A_c^{\,2}\Delta P} V + \frac{\mu R_m}{A_c \Delta P} \tag{2-13}$$

Experimentally α is obtained from constant pressure filtration data (i.e. the slope of t/V versus V plot).

Several workers adopt the standard filtration approach to describe the filterability of flocculated suspensions. A paper published by Chu et al. (2003) is directly related to the subject of floc size and filtration performance. In that work, Chu looks at the duration of mixing on non-steady state floc growth and the resulting effect on specific cake resistance. This work implemented a submerged membrane filter (SMF) in a dead-end configuration filtering flocs formed and subjected to various mixing times exhibiting different floc sizes. The results showed that larger flocs were more filterable. Model development provided a correlation between α and floc size.

The accuracy of such an approach is limited by the transferring of flocs manually from suspension to measurement which induces floc breakage. The effect of shear at the filter may suggest that larger flocs would presumably be transported away from the cake. By this reasoning it is likely that the measure of specific cake resistance is a convoluted result of several system variables in addition to floc size.

Another possible explanation for the observed correlation in α by Chu et al. (2003) is that the hydraulic properties of the cake are strongly affected by the flocculation progress, i.e. a significant portion of the flow resistance is due to non-aggregated primary particles being present in the system. To test this, one would simply need to carry out the flocculation after the system had reached maximum floc size and filter the flocs at various times past this point.

Works of the nature of Chu et al. (2003) provided valuable direction in apparatus design and interpretation of filtration data.

2.2.3 Modified Carman-Kozeny Approach

As described in section 2.2.1, the Carman-Kozeny model is derived from the fundamental model of flow through parallel capillaries. For cakes formed from uniform spherical particles, the Carman-Kozeny equation can be rearranged as (Waite et al. 1999)

$$\alpha = \frac{180(1-\varepsilon)}{\rho_s d_P^2\, \varepsilon^3} \tag{2-14}$$

where ρ_s is the density of the solid. The porosity of the packed bed can be calculated from the size and structure characteristics of the floc by the following equation (Jiang and Logan 1991)

$$\varepsilon = 1 - \left(\frac{d_{floc}}{d_p} \right)^{D_f - 3} \tag{2-15}$$

where d_{floc} is the diameter of the floc, and d_p is the primary particle diameter, and D_f is the fractal dimension. One could simply substitute equation 2-8 into equation 2-7 and directly relate the floc size and structure to the specific cake resistance. Guan et al. (2001) first attempted to assess the accuracy of this proposed model given by

$$\alpha \propto \frac{1}{(d_{floc}/d_p)^{3-D_f} \left(1 - \frac{1}{(d_{floc}/d_p)^{3-D_f}} \right)^3} \tag{2-16}$$

Guan used static light scattering to measure floc size and mass fractal dimension according to Rayleigh-Gans-Debye theory (Sorensen 1997). According to the modified Carman-Kozeny equation, the quantitative relationship between floc size/structure and filterability (i.e. specific cake resistance) can be represented on a 3D multivariable plot (Figure 2-6).

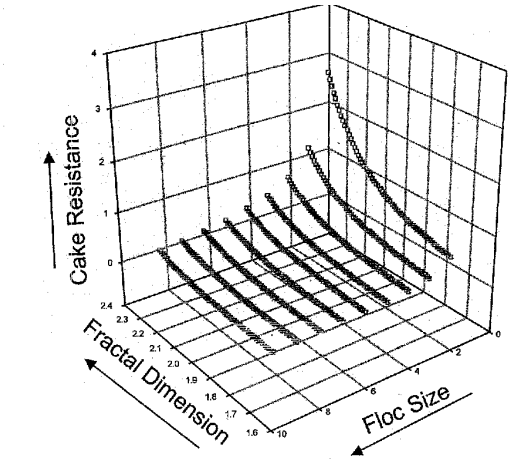

Figure 2-6 Relationship between specific cake resistance and floc properties taken from Lee et al. (2003)

With the measurement of floc size via light scattering being limited to ex-situ, it is almost impossible to make the particle characterisation representative of the material depositing on a filter cake using this technique. This implies there will be systematic error arising from floc breakage or growth as the flocs transport from the point of measurement to the filter cell.

Lee et al. (2003) went on to refine the process of using the modified Carman-Kozeny equation and further investigated the effect of floc size on specific cake resistance with varying shear rates. The framework for theoretical treatment of the floc size and structure in filtration presented by Lee is a good starting point for induction to the concepts described in this thesis.

Lee et al. (2003) conducted filtration at several shear conditions to vary size and structure and the subsequent iron hydroxide floc mass filtered in a dead-end configuration. Similar to Guan et al. (2001), Lee used light scattering analysis to measure floc size and fractal dimension. Cake filtrate data was analysed through the

traditional cake filtration model to extract the specific cake resistance by plotting t/V versus V according to parabolic rate law.

Overall, these authors were able to demonstrate that larger flocs produce filter cakes of lower specific resistance. However a large degree of uncertainty is present in the measurement of floc size/structure by ex-situ means. Furthermore, flocculated particles comprised of dense particles will settle out by gravity, upon which it is no longer appropriate to describe cake formation by equation 2-2 (for vertically orientated filtration systems). After reviewing the relevant literature which applies the standard cake filtration model, a steady state filtration approach, derived to be independent of floc settling effects, is necessary for this project. This is a large motivating factor for the development of the steady state filtration model described in Chapter 3 that is formulated around the basis of the "cake material property". Cake material properties, described in the next section, are analogous to key concepts in standard filtration terminology such as specific cake resistance.

2.3 Influence of Cake Material Properties on Filtration Performance

Compressional rheological theory has long been associated with the modelling of solid-liquid separation processes such as thickeners (Landman et al. 1988; Usher and Scales 2005). The dewaterability of a thickener bed describes the efficiency of the expression of water from within the porous bed structure. Parameterisation of the dewaterability of a thickener bed can be formulated into physically measurable properties of the materials. The compressibility (one-dimensional response of an elemental slice of the bed to compressive pressure) and permeability (the hydraulic property describing the conductivity of fluid though the slice) are two measurable material properties which govern the dewaterability of the bed.

Characterising the material properties of the cake essentially describes how the permeability and compressibility changes as a function of local solid fraction. The compressibility of a material is defined as the compressive yield stress $P_y(\phi)$ and local permeability function given by $K(\phi)$.

The ease of which a material is dewatered or collapses in response to the pressure can be quantified by the diffusivity of the material which is given by Landman et al. (1999)

$$D(\phi) = \frac{(1-\phi)^2 \frac{dP_Y(\phi)}{d(\phi)}}{R(\phi)} \qquad (2\text{-}17)$$

where $P_y(\phi)$ is the compressive yield stress, $R(\phi)$ is the hindered settling function which in essence is an indication of the flow resistance (or inverse permeability) and $D(\phi)$ is the diffusivity.

The hindered settling function is related to the Darcian permeability K_d according to the following relationship (Green 1997)

$$K_d(\phi) = \frac{\mu}{R(\phi)} \frac{(1-\phi)}{\phi} \qquad (2\text{-}18)$$

The concept of diffusivity is found in soil science in the study of consolidation (White et al. 2003). The works of Landman et al. (1995) lends itself to adaptation in other areas of pressure filtration. Many of the concepts of dewatering can be usefully applied to various filtration configurations as has been shown by Stickland et al. (2006) in modelling plate-frame filters and centrifugal drum filtration (Barr and White 2006).

The principles of dewatering are proposed to apply to membrane filtration in conceptualising the cake collapse associated with a reduction in filtration performance. A material with high dewaterability is disadvantageous in water treatment as it almost certainly implies that a rapid decrease in permeability follows a rapid expulsion of fluid and collapse of the cake structure.

2.3.1 The Relationship between Floc Properties and Material Properties in the Condensed Phase

Even if flocculent dose is optimal (whether flocculation proceeds by charge neutralisation or sweep flocculation), there is potential for improvement in filtration efficiency by optimising the influence of hydrodynamics on floc growth and structure.

It is widely accepted that large flocs give improved hydraulic characteristics of the cake. It is now apparent that even with addition of flocculants or coagulants, the problems associated with non-flocculated systems (i.e. a high resistance cake typical of closely packed primary particles) are still observed. This results from collapse of the cake structure under compressive load, thus reducing the size of the pores available for the passage of fluid. The role that shear plays in this problem has yet to be investigated and is of particular interest in this research.

While the presence of large flocs is generally considered to increase the hydraulic conductivity of a cake, there are a number of reasons why this may not be the case. These include:

1) the presence of extracellular polymeric substances (EPS) which migrate with the permeate flow through the cake and deposit in the inner layer of the cake causing a fouling layer. This concept is explored in detail by Hermowicz (2007). In an ideal situation this type of problem can be avoided by removing the EPS or colloidal matter in a centrifuge as is the case in our yeast system. Although this is useful on a bench scale, it will not be helpful in industrial practice;

2) unpublished data based on use of alum as a coagulant show that flocs formed by this mechanism result in cakes that do no provide adequate strength to resist collapse and thus a rapid decrease in permeability results as the weak structure yields under relatively low stress compared to a coagulant such as aluminium chlorohydrate (Santiwong 2008); and

3) membrane pore blocking caused by smaller particles detaching from flocs under compressive stress in the cake.

Points 1 and 3 are well studied causes of reduced membrane performance and represent the majority of focus in membrane literature. On the other hand, it is less well known how the transfer of momentum from the liquid to solid phase (as later described in section 3.2.2) and subsequent build up of solids stress is affected by the properties of the uncompressed solid itself. In order to shed light on this process a

review of literature concerning the microstructural effects of compressive yield stress is given below.

2.3.1.1 Effect of Floc Size, Structure and Strength on Compressive Yield Stress

Recall that compressive yield stress is a material property which describes the cakes one-dimensional response to compression. Several studies have attempted to examine the microstructural characteristics of flocs undergoing compressive stress. The implications of self-similar or fractal structures to the compressibility of beds was presented by Kranenburg (1994). The relationship between self-similar structure and the yield stress is reported to be power law in nature; i.e.

$$P_y \approx \varphi_P^{\frac{2}{3-D_f}} \tag{2-19}$$

where φ is the size of the fractal structure. This work was one of the first in describing the fundamental links between the compressive yield stress and floc properties.

Several works build on such an approach. Most notable are the works of Potanin et al. (1995) in which a model for weakly aggregated fractal networks under small static loads was introduced. The concept of fractal aggregates in consolidating beds is conceptualised by treating the network as a system of overlapping aggregates connected by load bearing chains which can be created or broken due to shear. Potanin and Russel (1996) further developed the model to investigate the effect of size of flocs on the compressive yield stress according to the following equation

$$P_y \approx k_o^{1/2} n_1 \frac{U_e}{r^2 \sigma_g} \phi^{\gamma_y} \tag{2-20}$$

$$\gamma_y \equiv \frac{3}{3-D_f} \tag{2-21}$$

where k_o is the dimensionless curvature of the potential well, n_1 is related to the end to end length of chains (related to floc size), U_e is the two particle bond energy, r is the primary particle radius and δ_g is the gap width between aggregates. For larger flocs,

the compressive stress required to cause the yielding of a load bearing chain is higher than is the case for smaller flocs and, as such, is likely to give higher filtrate throughput at a fixed pressure.

Channell et al. (2000) have examined the effect of microstructure on compressive yield stress through compression rheology experiments on flocculated zirconia and alumina at constant pH. The consolidating bed is thought to compress in a way that both rearrangement of aggregates in the bed and rearrangement within individual aggregates occur. A model fit is able to recover information about the consolidating unit size from experimental data which is assumed to be the floc size during careful pre-shearing of the suspension. This model provides useful qualitative verification of the microstructural influences on compressive yield stress. As this model is empirical in nature its application is limited and cannot be used in a predictive sense.

In more recent studies, Botet and Cabane (2004) simulated the process of consolidation and presented a theoretical model for the consolidation of colloidal sediments under uniaxial mechanical pressure. The model used by these authors is a variant of the Discrete Element Method (DEM) and some components are uniquely different to the model presented later in Chapter 5, such as treatment of bonds as a collection of connecting springs at multiple points on adjacent spheres.

Quite distinct behaviours are observed depending on disruptive energy E_d which is defined as potential energy and the rupture threshold when two particles are separated at a critical distance. For low E_d the behaviour of the network is plastic with a significant quantity of bond breakage and reformation events.

For higher E_d the behaviour of the bed is of an elastic nature and the mode of collapse is better described as a system where displacement of particles occurs but yielding of load bearing chains is unlikely. Thus, remnants of the original fractal structure will remain during the consolidation process. This is an important observation and can potentially have very significant implications for membrane filtration if the model is accurate. For example, filter cakes formed from flocs can retain the initial permeability despite having undergone extensive collapse. This will be investigated in Chapter 5.

2.4 Gas Driven Filtration versus Piston Driven Filtration

In submerged membrane filtration, partial vacuum is applied at the outlet drawing the influent water through the membrane. This is similar to the classical laboratory gas driven filtration system such as a hyperbaric filtration cell, where gas pressure forces the fluid (at the gas/liquid interface) through the membrane and, in the process, compacts the material deposited on the cake.

Consolidation studies traditionally involve the use of a piston driven device where pressure is directly exerted on the particle network forcing the fluid out of the network and through the membrane. The manner in which the load is applied makes it an ideal choice for modelling the consolidation as the pressure exerted on the cake is uniform (i.e. does not vary spatially through the cake at steady state) allowing calculation of the local solid fraction directly. It is for this reason that a piston filtration approach has been chosen to validate the numerical "cake integration" approach introduced later in Chapter 3.

A number of other investigators have used piston devices to measure compressibility and permeability characteristics of porous assemblages. Notable works include those by de Kretser et al. (2001) and Usher et al. (2001). Although piston filtration is ideal for characterising material properties, such experiments are constrained by the piston geometry where it would be difficult to modify the filtration cell to accommodate in-situ size measurement and/or shearing. This makes gas filtration desirable as there are less geometrical constraints and it is akin to the real world filtration process of interest. Hence, throughout this thesis, the dewatering properties of a material were determined based on gas filtration data.

2.5 Summary

A review of the standard filtration theory was presented with a view to demonstrate recent works on filtration of flocculated matter. Fundamentally, the flow though filter cakes is analogous to flow though packed beds of a porous nature, a concept that is described by the Carman-Kozeny relationship. The complication of flow through structured arrangements of particles such as in cakes formed from fractal aggregates

deviates away from the ideal packed bed structure. The modified Carman-Kozeny relationship was presented as a conceptual platform for modelling the hydraulic characteristics of these structures.

Reviewing the works of Guan et al. (2001), Chu et al. (2003) and Lee et al. (2003) reveals that a plateau has been reached in attempting to advance the adaptation of the standard filtration approach to better characterise the filtration of cakes formed from fractal aggregates. This current limitation prohibits thorough investigation of the impact of hydrodynamics on filtration performance involving related theory presented in these works.

Reviewing the basic principles of cake filtration has identified potentially valuable applications for developing a technique for measuring and parameterising the local material properties cake in membrane filtration in terms of a permeability function $K(\phi)$ and compressive yield stress function $P_y(\phi)$. A numerical technique for measuring these properties is developed in Chapter 3 and experimental validation of the technique given. Chapter 4 then details the implementation of the local material properties in determining the submerged membrane filtration (SMF) behaviour.

With the theoretical framework for characterising filter cakes in place, an investigation into the role of floc size in filtration is developed in Chapter 5. The permeability of compressible cakes was investigated by Discrete Element Method (DEM) simulations in conjunction with CFD analysis. The results have widespread implications on how the fouling from gel layer is understood which is described in this work as a system of soft compressible spheres at high packing density.

Chapter 6 articulates a model by which shear affects filterability of flocculated matter. An experimental investigation is carried out using the steady state filtration apparatus described in Chapters 3 and 4.

Chapter 3: Measurement of Cake Material Properties

In this Chapter a methodology for characterising dead-end filtration is presented. A numerical technique for assessing the filterability of a flocculated system based on laboratory scale dead-end filtration data is demonstrated using the terminology adopted by soil physicists and thickener specialists interested in water flux through consolidated porous solids. The approach described here is central to the thesis allowing contributions to be made to the body of scientific knowledge through subsequent application in Chapters 4 (justification of methodology to describe industrial systems), 5 (interpreting and analysing the data at a micromechanical level) and 6 (application to improve the general understanding of the effect of shear on filtration). This novel approach of characterising cakes is key to development of the stirred filtration cell in that the material properties can be calculated from standard filtration apparatus. This provides a way of understanding how shear affects the micromechanical properties of a cake.

3.1 Background

The rationale for the approach adopted here is based upon the fact that solids loadings in drinking water filtration are relatively low (<100ppm) and, over short time scales at least, it can assumed that the accumulation of new material onto a cake is negligible with the cake reaching a pseudo-steady state with respect to thickness and material properties. In this study the extent of consolidation of the cake at steady state and the flux through this consolidated cake is of interest.

This Chapter also addresses the complexities of modelling filtration in gas driven filtration systems under conditions typical of those encountered in low pressure submerged membrane filtration. It is proposed that the technique developed here could be utilised as an in-situ tool for measuring the dewatering (consolidation) properties of the suspended material based on real plant filtration data.

Availability of an in-situ method for characterising the material properties of suspended solids in raw water is important in ascertaining the characteristic of the materials which contribute to poor filterability. This is particularly important for constant flux filtration and optimisation of the frequency and intensity of filter cleaning.

The approach described here is a numerical technique for quantifying the dewatering properties of a material which, concomitantly, enables determination of the extent of consolidation during filtration. The key dewatering properties are the permeability (ease of fluid passage through the cake) and compressibility (a measure of the strength of the particle network). The technique is based on assuming reasonable mathematical forms for permeability $K(\phi)$ and compressive yield stress $P_y(\phi)$ functions. Evaluation of the accuracy of the functions and their unknown parameters is undertaken by substituting these functions into a momentum balance equation and integrating across the cake to compare the calculated pressure drop with the measured pressure drop. An iterative process is applied to select $K(\phi)$ and $P_y(\phi)$ function parameters such that the difference between the measured and predicted pressure drops is minimised.

Complications from simultaneous sedimentation, consolidation and cake filtration are avoided by taking a "steady state" approach to addressing transient effects in vertically orientated filtration systems. The works of Burger et al. (2001) and Font and Perez (2007) describe the level of attention needed to deal with simultaneous settling of flocs and filtration for what would appear as a relatively trivial modelling task.

3.1.1 Justification for New Filtration Approach to Measure Material Properties

In a review paper by Tien (2002), the opinion amongst many academic engineers is that the field of filtration is well studied and only few problems remain in this area. With the development of new solid liquid separation processes such as membrane filtration, resurgence in this area has come about in recent times. Tien states that major future efforts should be spent on developing new procedures of determining cake properties such as measuring compressive stress and permeability. Such a view is somewhat shared by Svarovsky (2000). The only true rigorous approach to filtration theory is by local characterisation of the cake. Such an approach is not widely

accepted by the filtration/engineering community perhaps due to the degree of uncertainty amongst the various methodologies.

Being able to quantify features such as the local permeability and compressibility of a material and to assess the impact of these properties on the macroscopic behaviour of the consolidated material is of industrial significance. For example, understanding the connection between flocculent choice and operating conditions and the impact on the material properties of the resulting accumulated solid or "cake" is critical in performance of processes such as sludge dewatering and membrane filtration.

3.1.2 Compressible Cake Modelling

The review of literature presented in section 2.2 mainly discussed non-compressible cake filtration (i.e. a material that is rigid in the packed bed phase and doesn't respond to compressive pressure to dewater the structure). Some materials behave in this fashion and the filtration behaviour of such materials is well understood (Svarovsky 2000). Materials found in water treatment processes such as natural organic matter (NOM) are found to be highly compressible and by this nature present a challenge for membrane filtration separation.

Added complexity arises for modelling materials that are compressible. To account for this it is necessary to address how the permeability of the cake changes with pressure. Tiller (1953) proposes the following model for the average specific cake resistance

$$\alpha_{av} = \alpha_o \Delta P^n \qquad (3\text{-}1)$$

where α_o is the specific resistance at unit pressure drop, and n is an indication of the cake compressibility. Typically, the value of α_{av} and n are measured experimentally.

For modelling the filtration behaviour of highly compressible material such as those developed from flocs, this approach has real limitations as there is likely to be significant variation from the average specific resistance within the cake (Tiller et al. 1999), particularly as a gradient in pressure through the cake is to be expected. It is thus necessary to analyse compressible cakes based on local cake properties rather than average cake properties, however such analysis is relatively complex if

undertaken whilst the cake mass is increasing and undergoing consolidation. The problem is simplified here by considering a steady-state filtration approach in which cake mass is constant and consolidation has ceased.

3.1.3 Recent Work on Cake Characterisation

Investigators concerned with the optimisation of the performance of filter presses have given particular attention to the characterisation of cakes formed from highly compressible material (Landman and White 1997).Variation in cake properties with time is commonly described by the momentum balance for the filtration process (Landman et al. 1995), i.e.

$$\frac{\partial \phi}{\partial t} = \frac{\partial}{\partial z}\left[D(\phi)\frac{\partial \phi}{\partial z} - \phi \frac{\partial H}{\partial t} \right] \qquad (3\text{-}2)$$

where ϕ is the solid volume fraction, z is the distance in the direction of cake formation, t is time, H is cake height and D is cake diffusivity (which is a function of solid volume fraction). By solution of equation 3-2, it is possible to deduce the local cake properties.

Several authors propose solutions to this momentum balance equation. Landman et al. (1999) propose a solution using a similarity substitution to obtain an equation for the cumulative outflow of the form

$$V = \beta t^{\frac{1}{2}} \qquad (3\text{-}3)$$

where V is the outflow due to consolidation of the cake and β is obtained from the slope of a t/V versus V curve. It is important to note that this equation will only be valid where the outflow is exclusively due to collapse in the cake and not due to the additional contribution from supernatant passing through the cake. This may well occur when the initial suspension consolidates/settles under its own weight leaving a layer of clear supernatant above which is subsequently pushed through the cake. In this situation, the experimentally derived value of β could potentially be overestimated with the extent of overestimation being dependant on the nature of the particle system.

In the approach presented here, particle network is allowed to consolidate under gas pressure until $d\phi/dt = 0$ and $dH/dt = 0$, thus eliminating the complexities of dynamic cake behaviour such as settling and consolidation. By taking this steady state approach it is possible to obtain the solid fraction profile by reducing equation 3-2 to

$$\frac{d\phi}{dz} = \frac{C}{D(\phi)} \tag{3-4}$$

where C is an arbitrary constant and the solid fraction profile is only a function of the diffusivity $D(\phi)$. The diffusivity function $D(\phi)$ can be expressed in terms of the compressive yield stress $P_y(\phi)$ and hindered settling function $R(\phi)$ as equation 2-17. Given the steady state filtration assumption, a numerical technique was developed to calculate the local solid fraction profile $\phi = f(z)$ based on compressive yield stress and permeability (analogous to the inverse of the hindered settling function). This local solid fraction profile was used as the basis for evaluating permeability and compressibility functions.

3.1.4 Compressive Yield Stress $P_Y(\phi)$ and Permeability $K(\phi)$

The permeability of a porous medium is a measure of how easily a fluid can pass through the medium. For single spheres arranged uniformly, this can be modelled by the Carman-Kozeny relationship (Carman 1939) given by equation 2-10. For flocculated material this is a poor estimation of the pressure drop as there is a wide distribution in cake pore size, leading to an overestimation of the pressure drop. In this work, the functional form was not restricted to any particular model; rather, an unrestricted functional form which suitably describes the permeability of a wide range of materials was chosen.

The studies reported here characterise the compressibility of filter cakes in terms of the compressive yield stress $P_y(\phi)$ which is defined as the pressure required to compress a cake to a given solid volume fraction. This is valid anywhere above the point at which flocculated particles form a continuous network (gelpoint). Some notable works looking at the measurement of the compressive yield stress and permeability include those by de Kretser et al. (2001) and Usher et al. (2001). The measurement involves a piston driven filtration device operated in a stepped pressure

manner with expelled fluid mass versus time logged and analysed in order to calculate the material properties.

For filtration, it is important to characterise the compressibility of cake, as a small change in solid fraction can lead to a change in permeability of several orders of magnitude (Waite et al. 1999).

There are numerous functional forms for compressive yield stress models. Amongst the most straightforward is the power law used by Green and Boger (1997)

$$P_Y = \kappa_2 \phi^{M_2} \tag{3-5}$$

This has been observed to describe the compressibility of salt destabilised systems of zirconia. Physically, this model suggests that for every incremental increase in solid fraction, there is an increase in the number concentration of interparticle bonds for a given volume of cake. The force required to induce a yielding in the bond network appears to increase as a power law with solid fraction, where the magnitude of the exponent M_2 quantifies the strength of the particle network.

Smiles (1970) also observed that for soils, the solid volume fraction varies with applied pressure in a logarithmic fashion though he parameterised this in terms of the moisture ratio (ϑ) and the overlying water head (ψ); i.e.

$$\vartheta = A' - B' \ln(\psi) \tag{3-6}$$

where

$$\vartheta = \frac{1-\phi}{\phi} \tag{3-7}$$

Similar behaviour has been described for a variety of soil and clay type particles by White et al. (2003). However, the suitability of this model for systems is questionable since negative moisture ratios are predicted at high solid pressures. Furthermore, the moisture ratio predicted as $P_S \rightarrow 0$ does not equate to the gelpoint moisture ratio due to the discontinuous behaviour of the function at this limit. As a result of these inconsistencies, this model was considered unsuitable for this work.

Channell et al. (2000) have shown that flocculated alumina nano-particles exhibit non power law compressive yield stress. The results clearly show that cakes formed from highly flocculated material exhibit greater strength initially but then converge to a power law form at higher solid fractions. Similar behaviour was observed by Gladman et al. (2005) in studies of the dewatering of slurries treated with polymeric flocculants.

In the studies reported here, an unrestricted functional form is used that encompasses all these types of behaviour. As described later in this paper, a model of logistic form is shown to be both suitable and convenient for the purpose of demonstrating the approach.

3.1.5 Review of Other Numerical Approaches

A variety of alternate techniques to those used here have been developed in order to address the need for characterisation of local filter cake properties that develop in pressure (or vacuum)-driven filtration systems.

Philip (1955) suggested a numerical method involving material coordinate transformation of equation 3-2. It is possible to predict the local cake properties using this technique if one assumes a moisture ratio versus pressure function of the form shown in equation 3-6.

Wakeman (1978) suggested an integration technique for solution of the differential equations describing cake formation. This technique requires an intrusive method for determining liquid pressure through the cake (i.e. Pitot probe or similar) or alternatively using a resistivity technique. However, varying the initial solids concentration is likely to bias cake permeability for flocculated systems due to inconsistent floc size between measurements. Additionally, intrusive probes cannot be used for thin cakes as they will probably bias cake measurement.

Recently, Johansson and Theliander (2007) incorporated constitutive relationships between cake resistance and solid fraction into the Wakeman approach to model compressible cake filtration. Difficulties were encountered in modelling both low and high pressure regions of the cake.

Lu et al. (1998b) used a numerical technique for analysis of flux data. This approach gives local cake properties but is highly model-dependant and, as such, is not well suited to application across a wide range of materials and conditions. The Lu approach uses the Carman-Kozeny relationship to describe the expected pressure drop across a section of cake. This approximation is suitable for non-flocculated suspensions but, given the heterogeneity of pores in cakes formed from flocculated suspensions, it may well over-estimate the pressure drop.

A unified numerical model for filtration and expression was developed by Sorensen et al. (1996). Biological sludge cakes were simulated using this technique showing that a thin layer of cake was responsible for the bulk of pressure drop. In this study constitutive pressure relationships were also used. Kocurek and Palica (2005) further developed this approach and provided experimental validation showing good agreement.

It is clear from this brief review that a more robust way of determining cake properties at a local level would be useful. Attempts thus far at numerically modelling compressible cake filtration processes appear to simplify what are traditionally very complex processes to mathematically model. A numerical model for steady state filtration will be presented in the next section which was motivated by the numerical modelling works to date.

3.2 Theoretical Basis

A technique for quantifying the compressive yield stress and cake permeability from steady state filtration data is described here. The key to this approach is the procurement of reliable and consistent filtration data and final cake heights or average moisture ratios. Using these values as input data, a numerical integration is performed over the cake depth to calculate the compressibility and permeability functions that most accurately reproduce the observed filtration behaviour. The estimation of these dewatering properties is free of model assumptions and, as such, has the potential for quite general application.

3.2.1 Material Properties

The equations used to describe the material properties are chosen to be logistic for the compressive yield stress and power law for the permeability. The equation describing the permeability of the cake is given by

$$K(\phi) = C_1(1-\phi)^{C_2} \tag{3-8}$$

where C_1 and C_2 are parameters. The local specific cake resistance is related to the permeability defined here as

$$\alpha(\phi) = \frac{1}{\mu K(\phi)} \tag{3-9}$$

The logistic form of the inverse compressive yield stress function is given by

$$\phi = \left[\phi_{cp} - \frac{1 + C_3 e^{\frac{-\log P_S}{C_5}}}{1 + C_4 e^{\frac{-\log P_S}{C_6}}} (\phi_{cp} - \phi_g) \right] \tag{3-10}$$

where, C_3, C_4, C_5 and C_6 are parameters and ϕ_g is the gelpoint of the material which is the solid volume fraction of the unconsolidated cake taken to be ϕ_g=0.05 from equilibrium settling height tests and log P_S is the logarithmic form (i.e. $\log_{10}(P_S)$). This is a reasonable estimate as small deviation in the gelpoint does not affect the material properties calculation as the permeability of the unconsolidated cake matter has a low pressure drop compared to the layers adjacent to the membrane. The parameters C_1 to C_6 are calculated based on the numerical technique of Kovalsky et al. (2007). The procedure determines the parameters via a non-linear unconstrained optimisation configured to minimise the error between simulated and experimentally measured steady state filtration data.

In physical terms the C_2 parameter is analogous to a permeability exponent and essentially describes how the permeability of the cake decreases locally as the material consolidates. For certain materials the C_2 parameter is larger in magnitude for gelling materials and Extracellular Polymeric Substances (EPS) that are conventionally associated high specific cake resistance (Cho and Fane 2002).

Parameters C_3 to C_6 define the shape of a log-logistic function and, for the purposes of this study, are obtained here by empirically fitting experimental filtration data. While the compressive yield stress of a filter cake is indirectly affected by a variety of factors including the size (Channell et al. 2000), fractal dimension (Kranenburg 1994) and strength (Botet and Cabane 2004) of particles and/or aggregates that make up the cake, assignment of physical meaning to C_3 to C_6 is non-trivial and beyond the scope of this investigation.

Although the choice of the mathematical form of P_y is arbitrary for material property determination, the logistic form was chosen for use here as it appropriately describes the non-power law behaviour observed by Gladman et al. (2005) encompassing the observed resistance to compression at low pressures and the physical limit of a system at high pressures. Figure 3-1 illustrates two arbitrarily chosen logistic curves for "strong" and "weak" cakes. In both instances the curves share the same asymptotic behaviour but, at any given equilibrium solid fraction, the "strong" cake will require greater compressive stress (work) compared to the weak system to induce a yielding of the network of particle-particle bonds in the system.

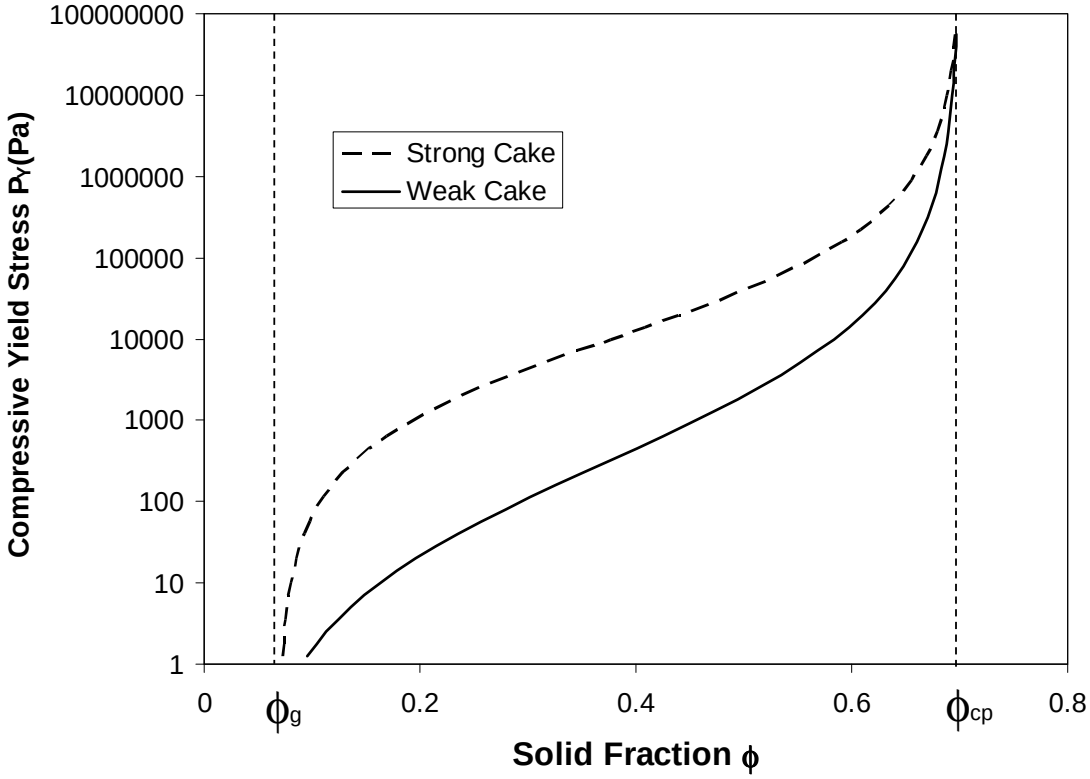

Figure 3-1 Material property parameters C_3 to C_6 define the shape of the log-logistic curves. The shape of the curve is qualitatively related to floc size, strength and structure in a general sense.

3.2.2 Numerical Integration Overview

The numerical technique used here involves conceptualising the total cake mass as an accumulation of discrete slices. A momentum balance is performed for each slice in a sequential manner. This is performed from the top of the cake to the bottom of the cake as the force external to a slice is exerted from above. Based on the assumption that the solid particles are not deformable, the momentum balance is given by

$$\frac{\partial P_L}{\partial z} = -\frac{\partial P_S}{\partial z} \tag{3-11}$$

where P_L is the local liquid pressure and P_S is the local solid pressure. P_S will always be close to P_y if the drainage of fluid is the rate determining step in the dynamics of collapse (Green 1997) and thus

$$P_s(z,t) = P_y[\phi(z,t)] \tag{3-12}$$

The numerical cake integration procedure performs this force balance in a discrete manner on the basis of a slice of fixed mass. For each cake slice the pressure drop is defined as follows

$$dP_L = \frac{J}{K(\phi)} dm \tag{3-13}$$

where dP_L is the trans-slice liquid pressure drop, J is the steady state filtrate flux which is a constant through all slices, dm is the incremental cake mass with units of kg/m^2 and $K(\phi)$ is the mass-based permeability which is defined for this study. The mass-based permeability compares to the Darcian permeability K_d according to the following equation

$$K_d = \frac{K\mu}{\rho_s \phi} \tag{3-14}$$

where ρ_s is the particle density.

To quantify the local solid pressure P_S or liquid pressure drop ΔP_L relative to the applied pressure, equation 3-13 is integrated; i.e.

$$\Delta P_L = P_S = J \int_0^{M_i} \frac{dm}{K(\phi)} \tag{3-15}$$

where P_S is the cumulative solid pressure due to the force imparted by the cake (of mass M_i), dm is the nominal slice mass and J is the flux obtained from filtration experiments. Equation 3-15 was evaluated numerically as detailed later in section 3.2.3. By definition, the solid pressure corresponding to the equilibrium local solid fraction is equivalent to the compressive yield stress.

If the experimentally determined J values are substituted into equation 3-15, selecting an appropriate form for function K, the following criterion is expected to be satisfied

$$P_{S,n} = \Delta P_J \tag{3-16}$$

where ΔP_j is the pressure applied during the steady state filtration which resulted in measured steady state flux J_j where subscript j denotes the particular filtration runs at a series of applied pressures. To calculate the solid pressure exerted on the membrane, defined as $P_{S,n}$, equation 3-15 is integrated across the whole cake. Thus, a form for $K(\phi)$ must be assumed first then iteratively refine its parameters such that the convergence criterion is met. In addition, a functional form of the solid fraction dependence on P_S (i.e. the inverse compressive yield stress function $\phi(P_S)$) is required for the numerical integration. The inverse function is chosen as a logistic function (i.e. equation 3-10) can be put forward as a concise functional form for the compressibility behaviour. The logistic function cannot in principle be used to describe $P_y(\phi)$.

For the correct $K(\phi)$ and $\phi(P_S)$, the criteria set by equation 3-16 must be met independent of applied pressure. To ensure that this is the case, filtrations are performed for at least five different nominal pressures ΔP_J and the best permeability and compressibility fits obtained to the complete data set.

For the reciprocal arrangement where the material properties are known, it is possible to calculate the filtrate flux by the procedure described here. An iterative procedure is required to calculate J such that the following relationship is obeyed

$$J\int_0^M \frac{dm}{K(\phi)} - \Delta P_J = 0 \qquad (3\text{-}17)$$

where J is the calculated filtrate flux and ΔP_J is the applied filtration pressure.

3.2.3 Numerical Integration Procedure

The numerical integration of equation 3-15 is performed in discrete slices denoted by subscript i from i=0 (top of cake) to i=n (slice adjacent to membrane). Before evaluating the model parameter guess, the synthetic properties are generated for each slice, namely the solid fraction ϕ_i. To achieve this, the process of consolidation under pressure was simulated to achieve a cake which is at steady state. The compressive yield stress function $P_y(\phi)$ is introduced in combination with the numerical integration to calculate the solid fraction for successive slices. The process of consolidation is done via the following iterated procedure:

1. Assume initially that the entire cake is at the gelpoint solid fraction ϕ_g by assigning this solid fraction to each slice.

2. The calculations described in steps 2 to 4 are performed for each slice starting at i=0 (top). First, the experimentally measured steady state flux J_j was imposed and then the pressure drop corresponding to the current slice $dP_{L,i}$ calculated (equation 3-13).

3. Equation 3-15 was evaluated numerically to calculate the pressure on the next slice $i+1$.

$$P_{S,i+1} = \int_0^{M_i} \frac{J}{K(\phi)} dm = \Delta P_i + \Delta P_{i-1} + ... + \Delta P_o \qquad (3\text{-}18)$$

where M_i is the sum of cake mass above and including the current slice.

4. Based on the compressive yield stress function and the imposed solid pressure calculated by equation 3-18, the solid fraction of the next slice $i+1$ was calculated.

It is again stressed that the choice of functional form is flexible. This assumed form is suitable for the range of materials characterised in work.

If the process of steps 2 to 4 is repeated sequentially for each slice from $i=0$ to $i=n$ the solid fraction profile of the entire cake can be calculated.

5. Calculate the residual pressure $\Delta P_{res,j}$ as follows

$$\Delta P_{\mathrm{Re}s,j} = \Delta P_j - P_{S,n} \qquad (3\text{-}19)$$

where $P_{S,n}$ is the solid pressure imposed by the entire cake at the final slice $i=n$ and ΔP_j is the experimental trans-cake pressure drop. Based on the calculated solid fraction profile, each solid fraction was calculated again by repeating steps 2-4 until the change in residual pressure $\Delta P_{res,j}$ does not differ by more than 0.1% with successive iterations. At this point the cake is at steady-state. Figure 3-2 illustrates a typical iteration.

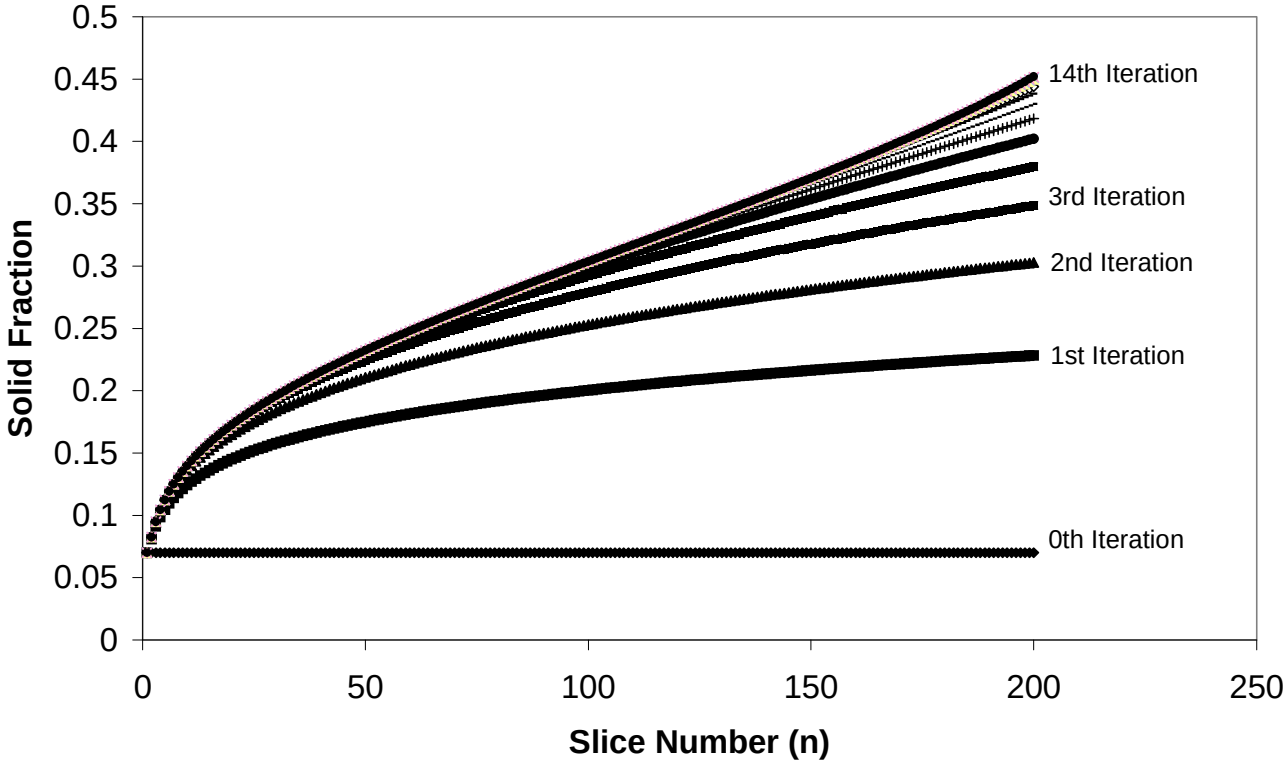

Figure 3-2 Typical Iteration showing convergence of solid fraction profile for a given guess of C_3 to C_6.

To test the consistency of the model, equal $K(\phi)$ and $P_y(\phi)$ functions for several pressures were substituted. The loop is run for each of the nominal pressures used in the gas filtration experiment 12.5, 25, 50, 100 and 200kPa and flux obtained. If the residual pressure is approximately equal to actual filtration pressure for each run such that $\Delta P_{res,j}=0$ for all j , then it can be concluded that the model parameters are correct.

To assess the accuracy of the chosen parameters for the permeability and compressibility model, a sum of squares error calculation is performed such that

$$\varepsilon_{\text{Res}} = P^2_{\text{Res},12.5} + P^2_{\text{Res},25} + \ldots + P^2_{\text{Res},200} \qquad (3\text{-}20)$$

The key to the numerical integration technique is to converge the parameters $C_1 \ldots C_6$ such that the error ε_{Res} is minimised.

The parameter convergence process is managed using a non-linear unconstrained optimisation based on the Nelder-Mead simplex method. By setting up the cake

integration as a parameter optimisation problem, quick convergence to the most likely fit will result.

Additional weight were also given to converge the parameters according to matching the measured cake height with the calculated cake height H_∞, given by

$$H_\infty = \sum_{i=0}^{n} \frac{dm}{\rho_s \phi_i} \qquad (3\text{-}21)$$

where ρ_s is the solid density and *dm* is the mass of cake in slice *i*. This is crucial to obtaining a unique solution, as it reduces the degrees of freedom in the calculation. Thus, particular care must be taken with the cake height measurement post-filtration, especially with materials which form cakes which have a tendency to break off and for thin cakes.

A schematic of the algorithm is given in Figure 3-3. Typically convergence takes around 5 minutes (Pentium 4 with 1GB of RAM) depending on the accuracy of the initial guess.

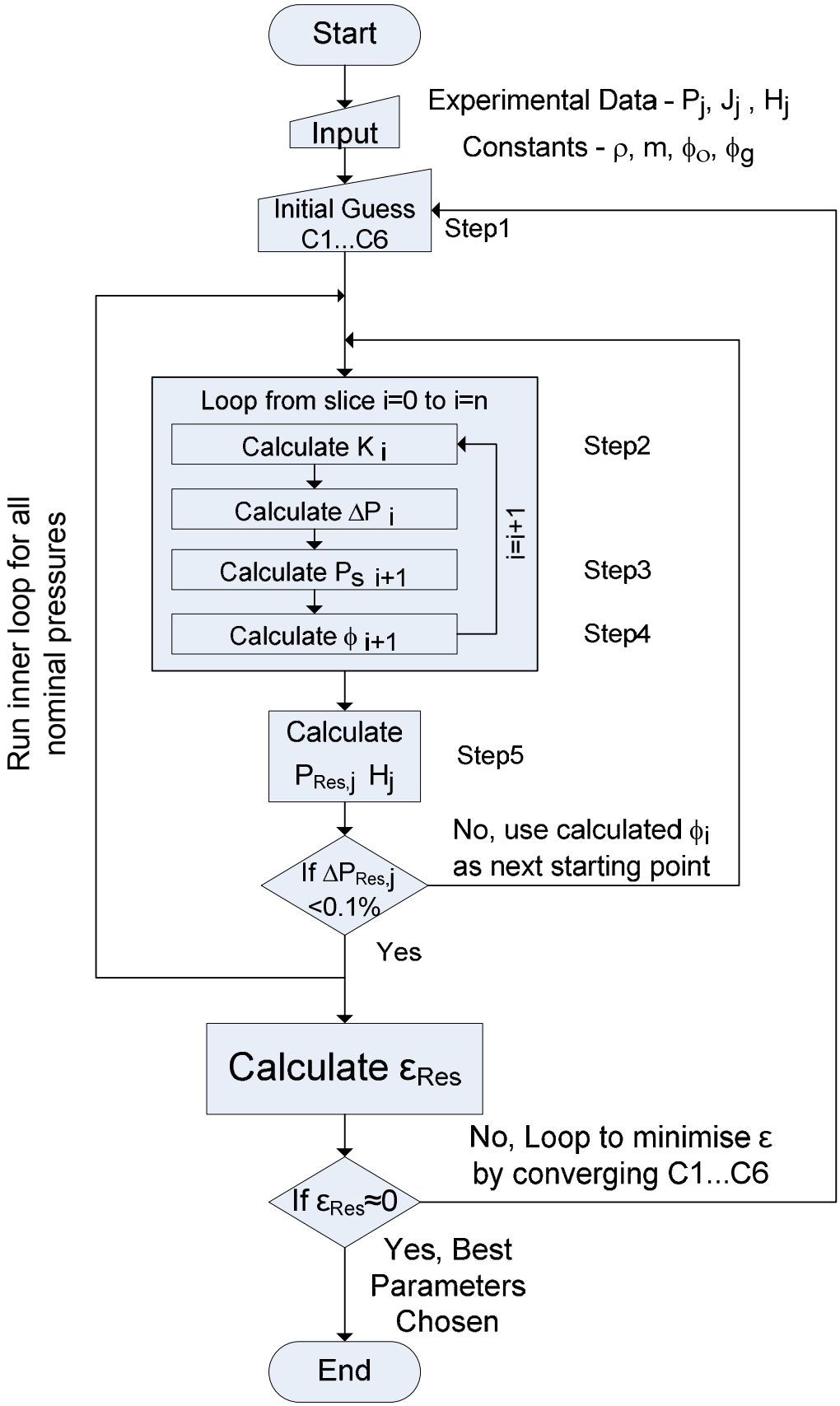

Figure 3-3 Flow diagram of procedure for selecting the optimum model parameters.

A separate iteration as given by equation 3-18 was performed to back calculate the "ideal" flux values given the 6 parameter fit, which is then assigned as predicted response values. These ideal values are calculated based on zero residual pressure and hence is a theoretical perfect fit. Based on this a sum of squares error can be calculated along with an R-square correlation coefficient as a measure of the accuracy of the model fit. This is illustrated in Figure 3-4.

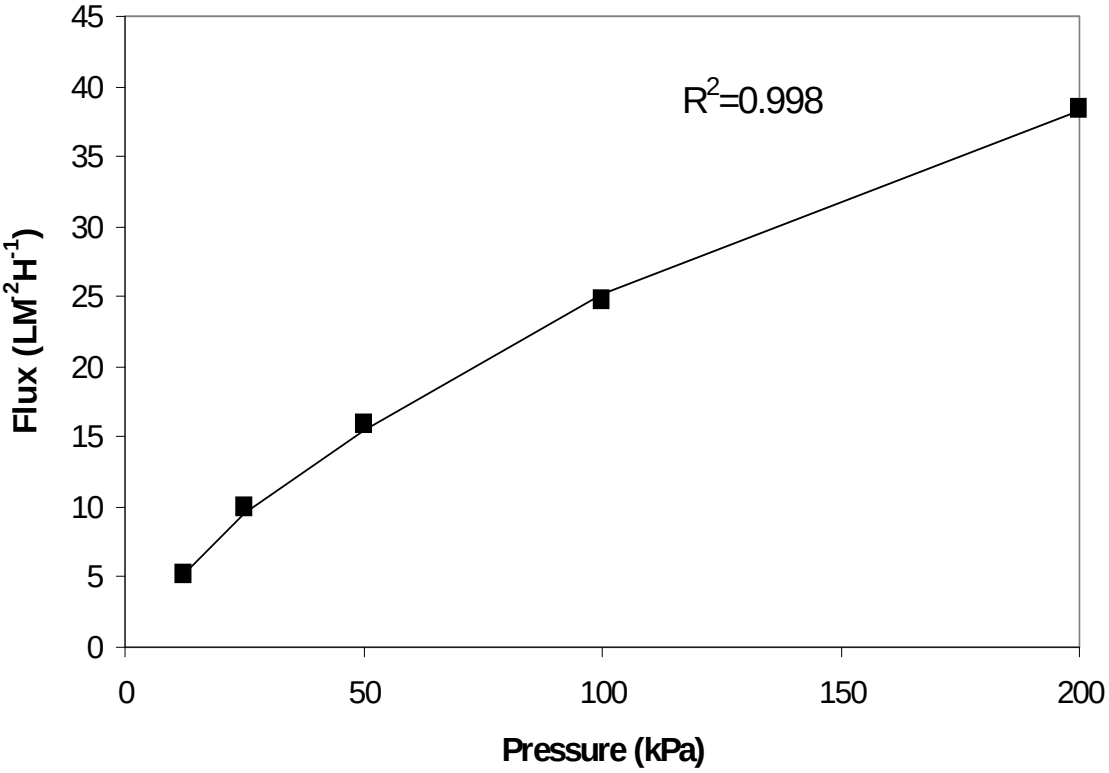

Figure 3-4 Fit of experimental data (■) to ideal flux trend (solid line) calculated based on zero residual pressure for 10 μm zirconia.

3.3 Materials

The experimental component of this work involves the acquisition of filtration data for input to the "cake integration" procedure. For the experimental work three types of particles with distinctly different characteristics were chosen in order to validate the technique. For each particle system, pressure filtration studies were undertaken for at least five nominal pressures and a stepped pressure piston filtration study was performed in order to validate the deduced compressibility model. Additional

comparisons between the model deduced from filterability studies and results obtained using a centrifuge technique were undertaken in order to validate the deduced model in the moderate to low pressure range. The permeability model was also validated using a compression-permeability (CP) device known as a Rowe Cell. The Rowe Cell differs from other odeometers in that there is provision for directly measuring the permeability of a sample in addition to determination of its compressibility.

3.3.1 Particle Preparation

Two types of zirconia (ZrO_2) were used as model particles in this study, both of which have well behaved and reproducible characteristics. Zirconia has been used in numerous other compressibility studies including de Kretser et al. (2001), Usher et al. (2001), Green and Boger (1997) and Channell et al. (2000). The zirconia particles (Aldrich Chemical Company, Milwaukee, Wisconsin, USA) possessed a specific density of 5.850 and exhibited mean particle sizes of 5μm and 10μm. The zirconia suspensions were prepared in 0.1M KNO_3 with 10mM sodium tetraborate tetrahydrate used to buffer the suspension at a stable non-flocculating pH of 8.8. Acetic acid (0.1M) was added to the stirred zirconia suspensions in order to reduce the pH to the isoelectric point of pH 7.3 where flocculation occurred. For the zirconia system the steady state floc sizes were approximately 90μm for the 5μm zirconia and 70μm for the 10μm zirconia as measured in-situ by focused beam reflectance measurement (FBRM) using a Lasentec (model M400L-316K).

Yeast was also chosen for the validation work as an example of a soft biological particle typical of those found in wastewater treatment. Two types of yeast were chosen. Bakers yeast supplied by Tandaco was used, having a mean particle diameter of 5μm and specific density of 1.40. Optimum flocculation for these yeast particles has been observed by Jin and Speers (1998) to occur at pH between 4 and 5. The floc size was approximately 120μm as measured with the FBRM. Dried yeast supplied by Fluka was also used. While this material has similar mean particle size and specific density to the Tandaco yeast, particle size measurement indicated that smaller flocs occurred at pH 4.5 with mean floc size attained of <20μm.

The preparation of yeast suspensions is somewhat more complex than that of zirconia. According to Hughes and Field (2006), it is necessary to wash the yeast as the transmembrane pressure rise for washed yeast cells has been found to be lower than that for unwashed yeast, implying that there may be extracellular polymer (EPS) present in the unwashed yeast. For this reason, the yeast was dispersed in milli-Q water and sonicated with a high power sonicator (Model Misonix) for five minutes at an intensity of 24W in a volume of 0.5L. Following sonication, the sample was centrifuged at 3000 RPM and 10 ^{o}C for 15 minutes using an Allegra 25R centrifuge. The supernatant was decanted and the yeast washed in a manner identical to the first washing procedure, except that sonication was undertaken with a Consonic Model SM 2200 sonicator as only a lower power sonication was necessary to redisperse the yeast. The washed yeast was resuspended in milli-Q water and flocculation induced by lowering the pH to approximately 4.5 with 0.1M acetic acid dosed into a high shear environment created by a four blade axial impeller operating at 500 RPM. To encourage flocculation, the suspension was subsequently stirred with the impeller for five minutes at a reduced speed of 250 RPM.

A clay type soil material was also used. The soil is heterogeneous in nature (Tweed River, Queensland, Australia). This particle system was chosen to further illustrate the flexibility of the approach described above. The soil particle size was measured using static light scattering and found to have a mean particle size of 15μm. The soil was stored in its sampled state with care taken to maintain the moisture content close to that of the original sample. The soil exhibited a specific bulk density of 2.6. The floc size varied between 50 and 60 μm as measured with the Lasentec FBRM.

The soil was prepared by dilution will milli-Q water to a solid fraction of 0.05 and a total volume of 200 mL. The soil was stirred at 1000 RPM in order to disperse the particles. The stirring speed was lowered to 250 RPM and 0.1M acetic acid added to bring the pH down to 3.5 in order to induce flocculation. Stirring was continued for five minutes.

3.4 Methods

3.4.1 Filtration Cell

Steady state filtration data was obtained using the dead-end batch filtration cell shown in Figure 3-5. A pressure controller (Bronkhorst 602C) was used to maintain a precise and constant transmembrane pressure in the 12.5 – 200 kPa (± 0.1%) range, and filtrate flow data was logged using an electronic balance and standard PC. For all experiments, Sartorius 0.2μm cellulose acetate membranes were used.

A schematic showing the dimensions of the filtration cell and key features is shown in Figure 3-6.

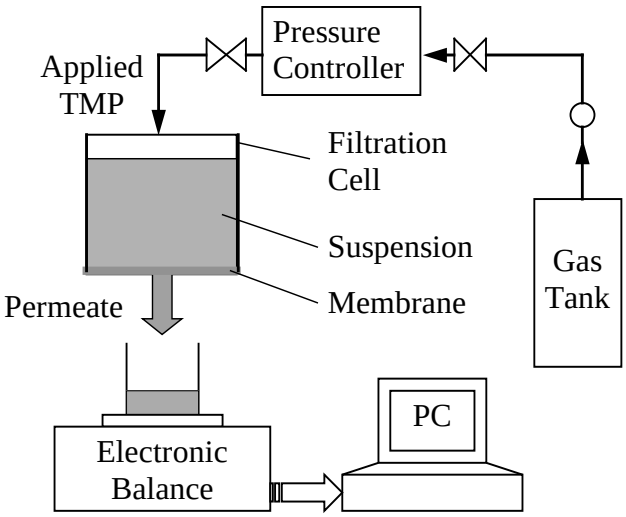

Figure 3-5 Schematic diagram of the experimental set-up used for filtration studies showing data acquisition system and pressure supply and control.

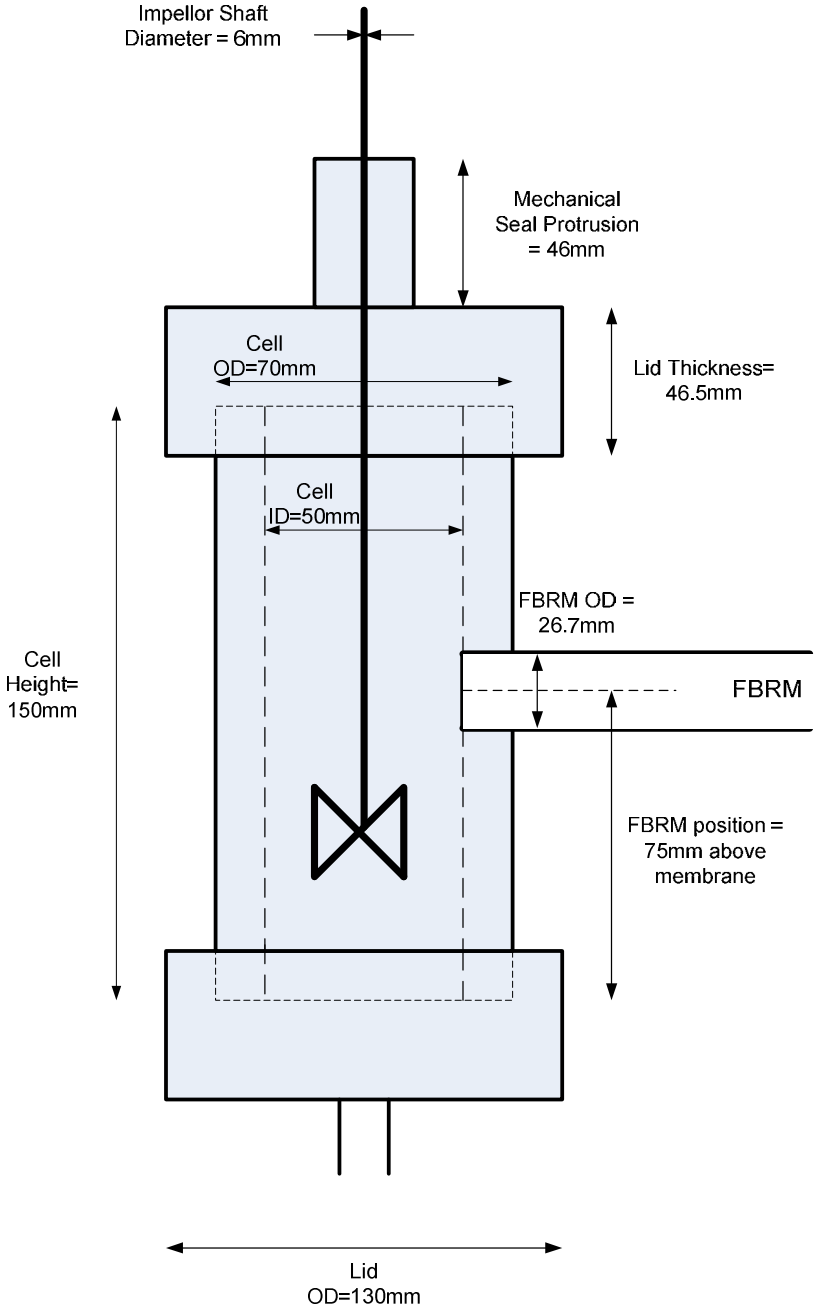

Figure 3-6 Schematic of stirred filtration cell showing dimensions and placement of key features.

3.4.2 Experimental Procedure

The flocculated suspension was poured into the filtration cell and allowed to settle. Depending on the system, the filter cake was allowed to consolidate for up to 30 minutes to within 5% of the expected steady state height (Figure 3-7), where ϕ_g and ϕ_∞ represent the gelpoint solid fraction and solid fraction at $z=0$ respectively. After

settling, the system was pressurised, the valve opened and permeate mass sampled at fixed intervals. The filtration was continued until the flux reached steady state at which point it was stopped.

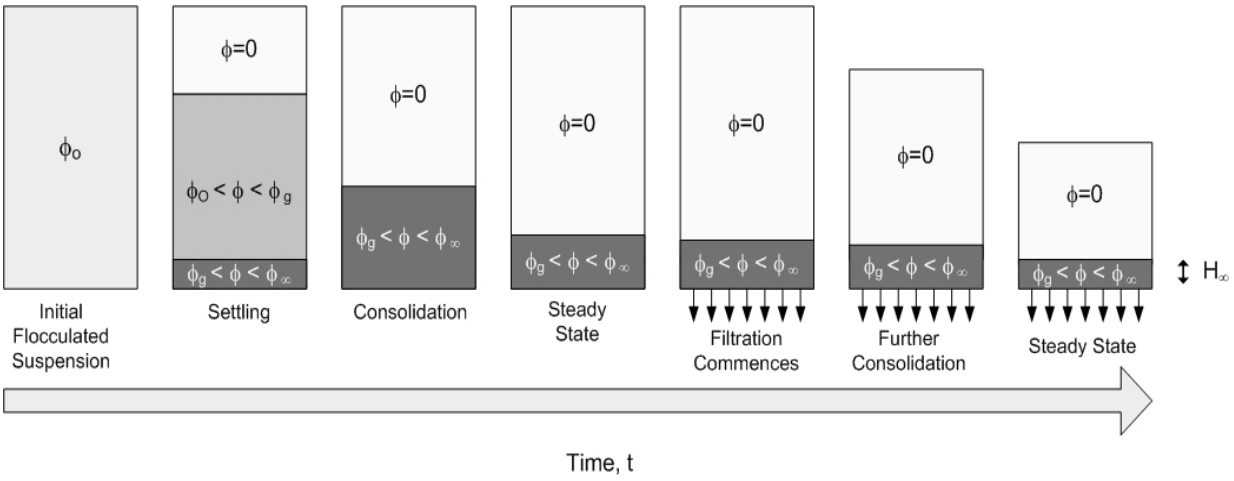

Figure 3-7 Timeline showing consolidation to steady state prior to filtration. Filtration is commenced and run to steady state (i.e. *dJ/dt=0*).

3.4.2.1 Measurement of Cake Height

The cake height was required as an input to the numerical technique and particular care was taken to ensure this parameter was measured to within 5% error. Two techniques were employed here:

1) *Volume displacement technique* - Any remaining supernatant was removed with special care to ensure that the solid was not disturbed. The cake height was then measured using a volume displacement technique. This involved transferring the wet cake to a volumetric flask of suitable size with care taken to preserve the water within the cake structure. Water was then added to the volumetric mark and the volume of cake determined from the flask volume minus the volume of water added. With the volume of the cake known, the final cake height was calculated as follows

$$H_\infty = \frac{V_C}{A_C} \qquad (3\text{-}22)$$

where V_c is the cake volume and H_∞ is the steady state cake height. By using high particle loadings, cake volumes of around 20 cm^3 were typically formed. In general,

the volume displacement technique relies on a sufficiently large cake to minimise measurement error. For thin cakes, a more precise technique would be necessary. It should be noted that it is important to stop the filtration before all the water is expelled from the filtration cell, as error will be introduced if cake desaturation occurs. From direct observation of cake height in separate experiments, it was found that the error associated with this technique is within 3% at 20mm and 5% with cakes of 10mm thickness. This error arises from losses of material during separation of supernatant.

2) *Optical micrometer technique* – For thin cakes a micrometer with a fibre optic cable tip mounted to the tip was fitted to the filtration cell (Figure 3-8). The procedure involved determining a reference point height at the membrane surface before filtration. After filtration the micrometer was lowered until the point at which the tip touched the cake surface. At this point a change in the light intensity was observed at the receiving end of the fibre optic connected to an optical/electrical converter. This acknowledges the precise point of contact where the reading was made. The device is rotated through 90 degrees and the measurement repeated. The average of four measurements was taken.

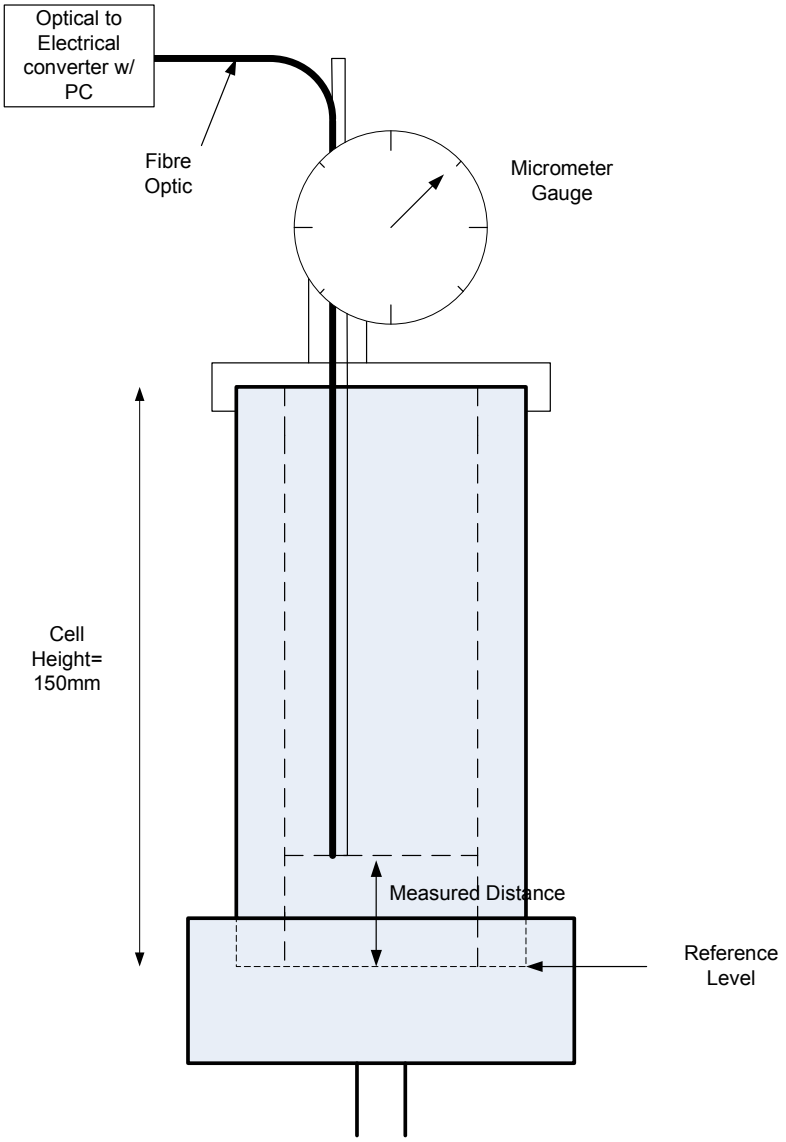

Figure 3-8 Optical micrometer fitted to the filtration cell normally post filtration to measure cake height directly.

3.4.3 Compressive Yield Stress

Comparison measurements of the compressive yield stress were undertaken by piston filtration (odeometer) and centrifuge settling techniques.

3.4.4 Odeometer (Rowe) Cell

To validate the method described above, the Rowe Cell was used to directly determine the compressive yield stress for the materials of interest. For a piston driven system, the force applied by the piston is equal to the force of the interparticle bonds acting to oppose the compaction of the cake. As a result, the network stress is uniform throughout the cake leading to uniform cake porosity when the cake is at equilibrium. Given this condition, we can calculate the solid fraction of the cake under piston load

$$\phi_f = \frac{\phi_o H_o}{H_f} \qquad (3\text{-}23)$$

where ϕ_o is the initial solid fraction, H_o is the initial suspension height and H_f is the final cake height. Alternatively, ϕ_f can be measured by oven drying the wet cake. For piston filtration, the compressive yield stress is equal to the applied piston pressure corresponding to the equilibrium solid fraction ϕ_f.

3.4.4.1 Experimental Equipment

The piston filtration device used in these studies was a Rowe Cell (Head 1980) of diameter 76.2 mm and recommended for sample heights of 30 mm. The cell itself consists of three parts: the body, the cover and the base. All three components are made of copper. The cell body is clamped between the base and cover by long tie-bolts as shown in Figure 3-9.

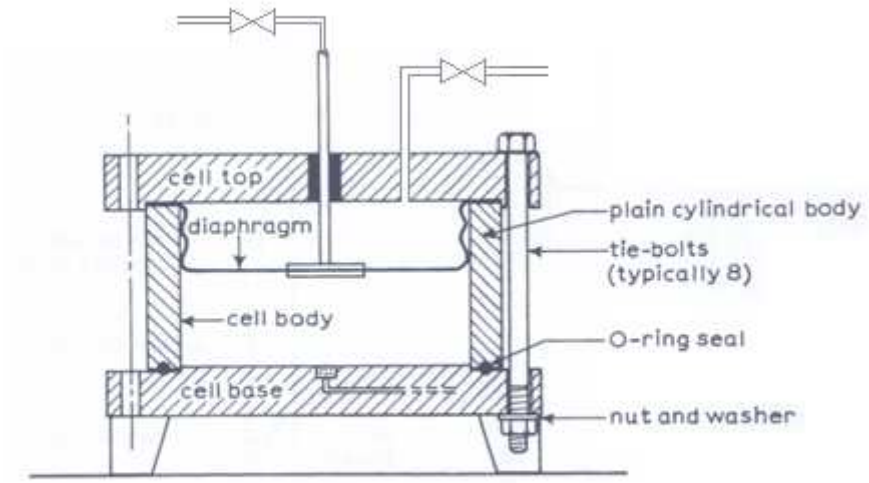

Figure 3-9 Rowe Cell cross section schematic showing the assembled unit used to measure compressibility and permeability. The pressure source connected to the centre channel of the piston is connected to fluid reservoir used for permeability measurement. The second pressure source (offset) is supplied to the diaphragm used for compressibility measurement (Diagram adapted from Head (1980)).

For the studies described here a 0.45μm Millipore membrane on a thin polyester filter support was used. The piston pressure was regulated using a pressure controller (Bronkhorst 602C). The permeate exited the Rowe Cell at its base and was weighed on a computer-logged electronic balance.

3.4.4.2 Experimental Procedure

The flocculated particles were poured into the Rowe Cell and the particles allowed to settle and consolidate under gravity. After consolidation the clear supernatant was removed using a syringe. To ensure constant pressure distribution over the filter cake, a thin aluminium plate was placed between the piston and the cake. Following closure of the cell top, pressure was applied at a starting value of 12.5 kPa and filtrate collected until no further liquid was expelled. The pressure was then stepped up to 25 kPa (then 50, 100 and 200 kPa) and the process repeated. The moisture ratio of the

zirconia filter cake was obtained by oven drying at 120 ^{o}C for 24 hours. The moisture ratio of the yeast cake was best determined from cake volume as oven drying tends to remove cell water in addition to the free water. The cake height (and subsequently volume) was easily determined using a digital calliper. Knowing the final moisture ratio, the moisture ratios at the lower pressures could be back calculated by mass balance based on the volume of permeate expelled from the Rowe Cell at each pressure step.

The Rowe Cell filtration of zirconia was performed from a starting solid fraction of 0.06. The collected filtrate volume versus time data are shown in Figure 3-10 where the distinct stepped pressure phases during the filtration are evident. Initial consolidation times are typically 1-2 hours depending on the material. Once the cake had consolidated to the equilibrium height at the initial pressure, subsequent pressure steps required about 15-30 minutes to reach equilibrium.

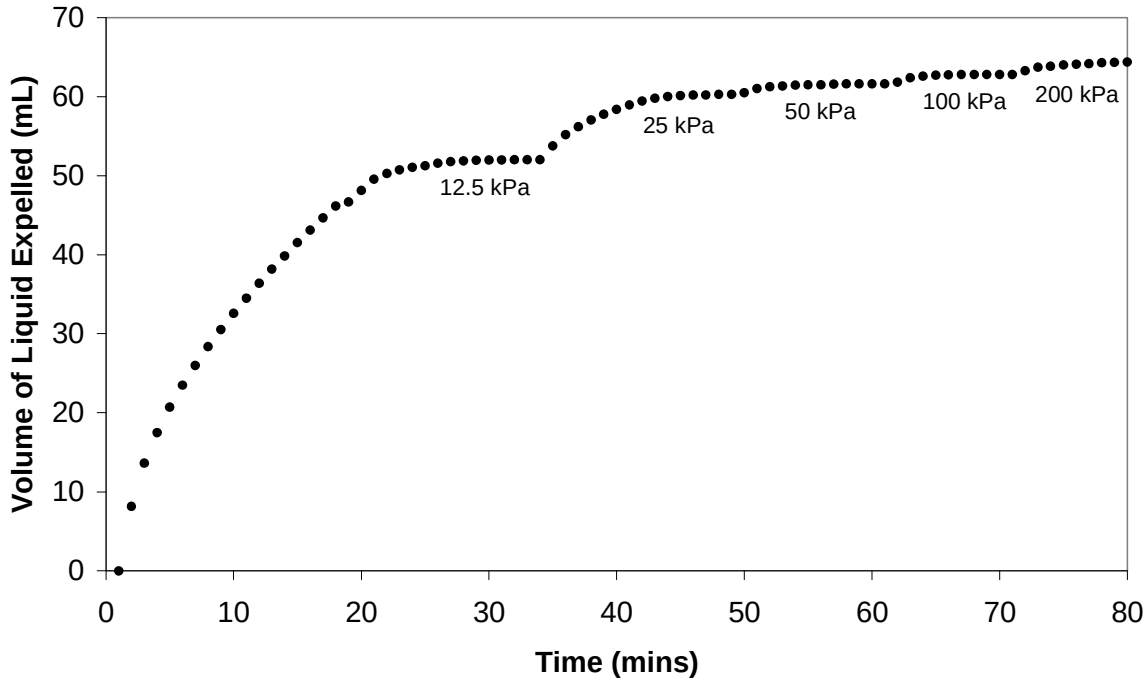

Figure 3-10 Rowe Cell filtrate collected as a function of time for the 5μm zirconia at pH 7.3. Similar trends are observed for the other flocculated materials upon compression.

3.4.5 Equilibrium Height Settling Tests (Gravity and Centrifuge)

The centrifuge used was a Spintron GT – 175 with capacity for 16 tubes, top speed of 4000 RPM, maximum volume of 4 x 250 mL and radius *r* of 160 mm. To ensure a constant radial stress distribution throughout the sample, it was necessary that flat bottomed tubes were used. Transparent, 50 ml conical bottomed centrifuge tubes were used with the flat bottom created by injecting a small quantity of silicone sealant into each tube using a syringe. The silicone was allowed to set in an upright position for 24 hours.

3.4.5.1 Experimental Procedure

In the multiple speed equilibrium sediment height technique, the equilibrium sediment height H_{eq} and gravitational constant g are obtained. By using this raw data, $P_y(\phi)$ and the solid fraction can be calculated using the mean value theorem of Buscall et al. (1987). The mean value 'approximate' solution for $P_y(\phi(0))$ is a very good solution to the compression equation (Green 1997); i.e.

$$P(0) \approx \Delta\rho_s \phi_o H_o g \left(1 - \frac{H_{eq}}{2r}\right) \tag{3-24}$$

$$\phi(0) \approx \frac{\phi_o H_o \left[1 - \frac{1}{2r}\left(H_{eq} + g\frac{dH_{eq}}{dg}\right)\right]}{\left[\left(H_{eq} + g\frac{dH_{eq}}{dg}\right)\left(1 - \frac{H_{eq}}{r}\right) + \frac{H_{eq}^2}{2r}\right]} \tag{3-25}$$

Particular experimental procedures were used for soil and yeast, as described below.

3.4.5.2 Soil

A defined volume of suspension was placed in a tube, typically to 90-95% of the tube capacity. The sample was then centrifuged for 30 minutes at a constant speed. The supernatant was poured into a beaker and the tube with compacted soil weighed. To measure H_{eq}, water was added to the filter cake until there was a volume of 40mL in

the tube. The equilibrium sediment height could then be calculated by volume difference. The tube was weighed and the supernatant returned to the tube. The speed of centrifugation was then increased and the procedure repeated. Five to seven equilibrium heights for different speeds were required.

3.4.5.3 Yeast

The experimental procedure for yeast was almost identical to that used for soil except that the height was obtained by measuring the interface between the sediment and the supernatant and an average of the highest and lowest parts of the interface determined.

3.4.6 Permeability

Permeability of consolidated cakes was obtained using the Rowe Cell but operated in a different manner to that used for determination of compressibility. The principle behind the permeability measurement is to compress a known amount of material to steady state with a known piston pressure. A second pressurised fluid source is connected to the Rowe Cell inducing fluid under pressure (the so-called “pore pressure”) to pass through a channel on the centre axis of the piston towards the cake. By simultaneously applying a piston pressure and a pore pressure, it was possible to compress the material to a known solid fraction and to then force fluid through the cake. By simply rearranging equation 3-13, the permeability of the cake could be determined from the measured flux.

Prior to examining the permeability of the various particulate assemblages, a pure water flux test was run on the Rowe Cell with sintered plate, reservoir and filter paper in sequence. The calculated permeability was measured at several pressures and was consistent at 1.5×10^{8} Pa/flux units. This represents a pressure drop of less than 3% of the lowest applied pressure and was considered acceptable for the purposes of the investigation reported here.

3.4.6.1 Procedure

Particles were prepared as described previously and transferred to the Rowe Cell. The aluminium plate was replaced with a permeable sintered plate to allow passage of

fluid. The sintered plate was underlaid with a layer of filter paper in order to prevent particles from permeating back past the plate, and to provide a seal between the plate and the outer ring. The plate was then placed onto the consolidated material. Piston pressure was applied to the plate thereby consolidating the underlying material. Filtrate was expelled from the Rowe Cell until no further consolidation occurred (i.e. the steady state flux was zero).

At steady state, a solution of known composition held in a 2L reservoir was passed through the cake by applying a defined pore pressure. In these studies, a solution of the same composition to that used in flocculation was employed in order to reduce the likelihood of cake rearrangement due to change in ionic strength or pH. The filtrate volume was logged at fixed intervals to enable calculation of the flux. According to equation 3-13, a constant flux is expected as the filtration is being performed at steady state. $K(\phi)$ can thus be calculated based on the measured constant flux and applied pore pressure ΔP_L with ϕ obtained from the Rowe Cell compressibility experiment.

This procedure was repeated for each of the nominal pressures. For each pressure, equal pore and piston pressures were applied to minimise further consolidation.

3.5 Results and Discussion

3.5.1 Filtration

For each material, filtrations were performed separately over a range of nominal pressures. The filtrations were allowed to continue to steady state (i.e. until there was no further change in flux). This is illustrated for zirconia in Figure 3-11, where it can be seen that filtration to steady state typically takes approximately an hour. Filtration runs longer than one hour was typically not necessary given the amount of material used.

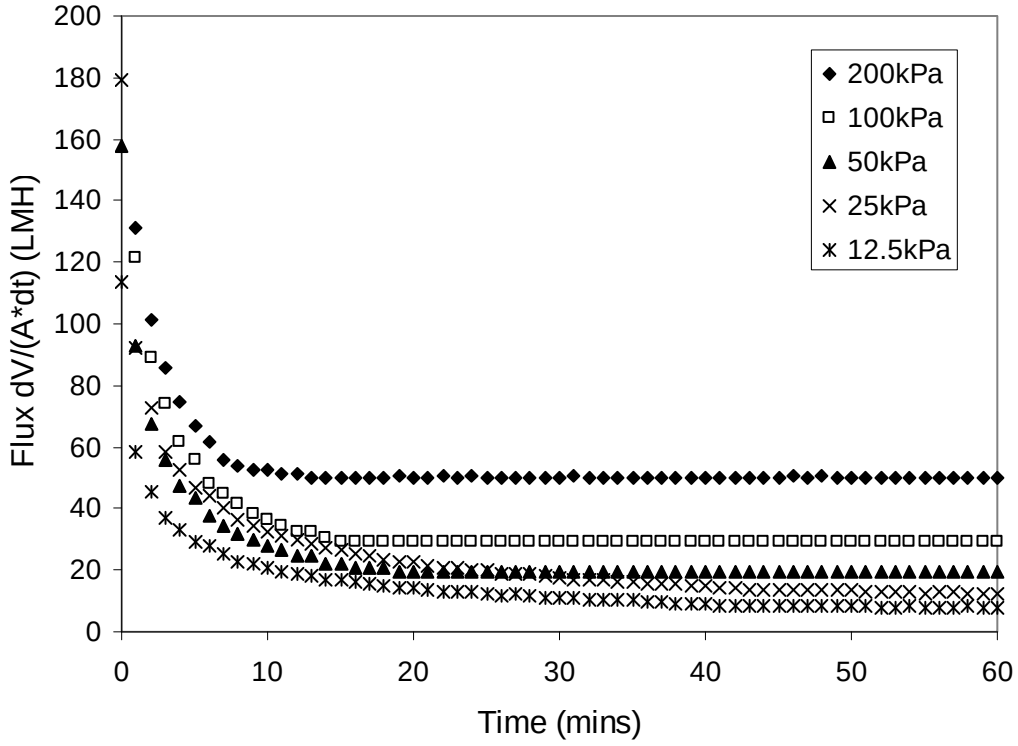

Figure 3-11 Filtration of zirconia illustrating the time it takes for steady state flux to be reached. Steady state is typically reached within an hour.

A plot of the steady state flux versus nominal applied gas pressure is given in Figure 3-12. For each system a trend expected for a compressible cake is seen with a nonlinear relationship between flux and pressure. For both yeast systems a maximum flux is observed followed by a decrease at higher pressures. This maximum flux is referred to as the cut off flux above which compaction effects lead to reduced permeability and outweigh the effect of increased pressure. It is noteworthy that similar behaviour is often encountered in water and wastewater treatment systems.

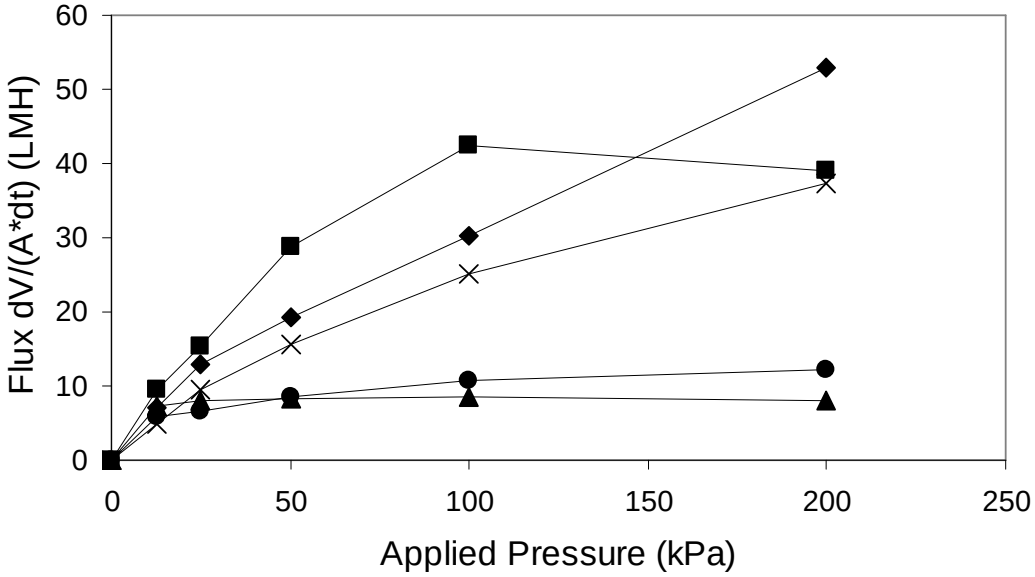

Figure 3-12 Steady state flux versus applied nominal pressures (■) flocculated yeast pH 4.5 (▲) smaller yeast flocs pH 4.5 (♦) 5μm zirconia pH 7.3 (x) 10μm zirconia pH 7.3 (●) soil pH 3.5.

A summary of the calculated parameters are given in Table 3-1 with R^2 values indicating the quality of fit to the data. These parameters are obtained directly from the output of the calculation for the analysis of each set of flux/pressure data for the five systems. For all systems there is an acceptable level of correlation with R^2 values close to 1. The sensitivity of the correlation coefficient to change in parameter value is shown in Figure 3-13 for the 5μm zirconia system. These results show that particular parameters are less sensitive to variation in input data. If this is observed over a wide variation of input data for a certain system then it is possible to set the parameter as a constant. This can be useful as fewer data points are required to meet the required degrees of freedom for the analysis.

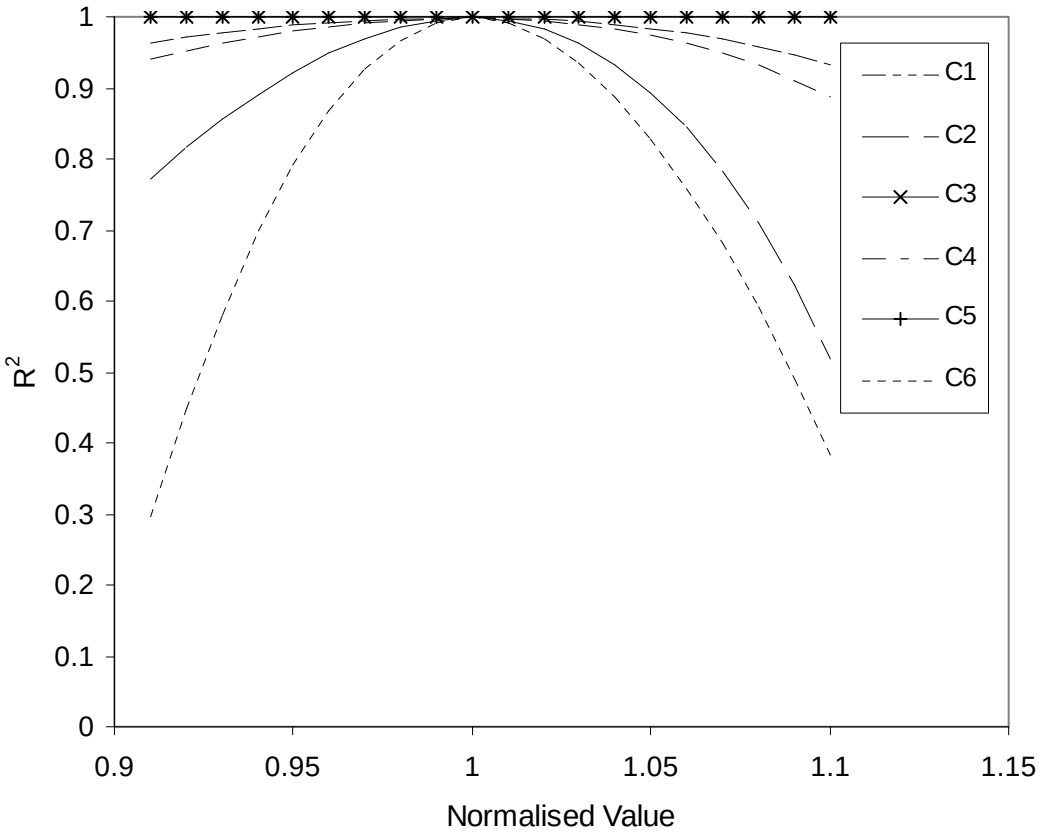

Figure 3-13 Sensitivity of correlation coefficient to change in optimum constant values for 5μm zirconia.

Table 3-1 Summary of parameters calculated by numerical analysis of steady state filtration data.

	C_1	C_2	C_3	C_4	C_5	C_6	R^2
Zirconia 1	3.82E-08	4.53	0.0137	0.0888	1.43	-1.69	1.000
Zirconia 2	3.31E-08	3.62	0.0579	0.0557	3.45	-1.31	0.999
Yeast 1	3.45E-09	1.84	-0.0238	0.00700	3.06	-0.710	0.988
Yeast 2 [1]	1.26E-6	7.09	0.0986	0.0797	0.55	-1.35	0.978
Soil	7.75E-09	11.7	0.215	0.0349	10.4	-1.41	0.987

1. Permeability functional form as $K=C_1*(\phi-0.3)^{C2}$

3.5.2 Compressive Yield Stress

The final solid fraction of the Rowe Cell compacted cake was measured by oven drying. As described earlier, the subsequent solid fractions for the lower pressures could be back calculated based on the volume of filtrate eluted at each pressure step. Thus, it was possible to generate compressive yield stress versus solid volume fraction plots for each particle system of interest. The Rowe Cell compressibility data is compared with the values predicted from the numerical cake integration fits to the filtration data (indicated by the solid line) for the various particle systems of interest shown in Figure 3-14.

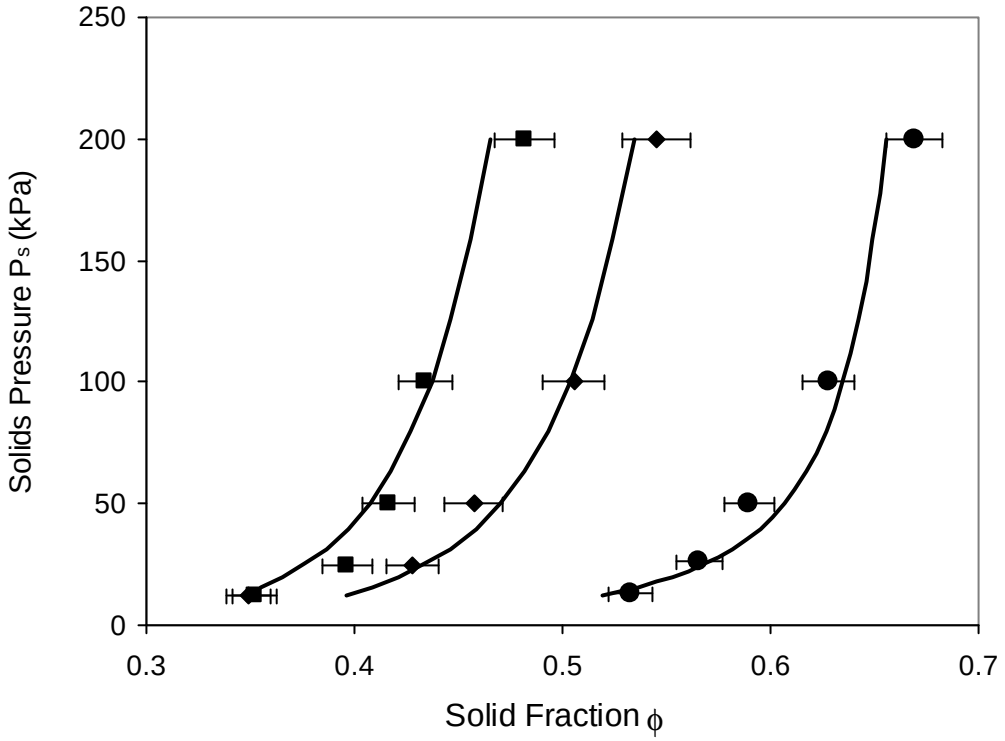

Figure 3-14 Comparison of the filtration experiment-calculated compressive yield stress (solid lines) versus direct measurement via Rowe cell - (■) 5μm zirconia , (♦)10μm zirconia, (●) flocculated yeast. Note that the solid lines are not a fit to the data shown in this figure.

For the 5 μm zirconia (Figure 3-14), the predicted P_y versus ϕ plot obtained from the converged model derived from the gas filtration data appears to agree well with the data obtained from the piston filtration studies in the moderate to high pressure range. There does not appear to be any systematic deviation of the model from the piston filtration data. The error bars indicate the uncertainty associated with the measurement of the solid fraction using direct cake height measurement. For the 10μm zirconia (Figure 3-14), the converged model fit also appears to agree well with the piston filtration data. Similarly, results from the yeast filtration show a good fit against the Rowe Cell data in the moderate to high pressure range as shown in Figure 3-14. Error in the measurement of cake height propagates to the final result, but the model results typically fall within the expected range.

For the moderate to low pressure range, centrifuge experiments were performed to compare to the converged model fit. The results for the yeast exhibiting small floc size are shown in Figure 3-15 and demonstrate that the model derived from gas filtration data provides a good description of the compressibility of the material in this range.

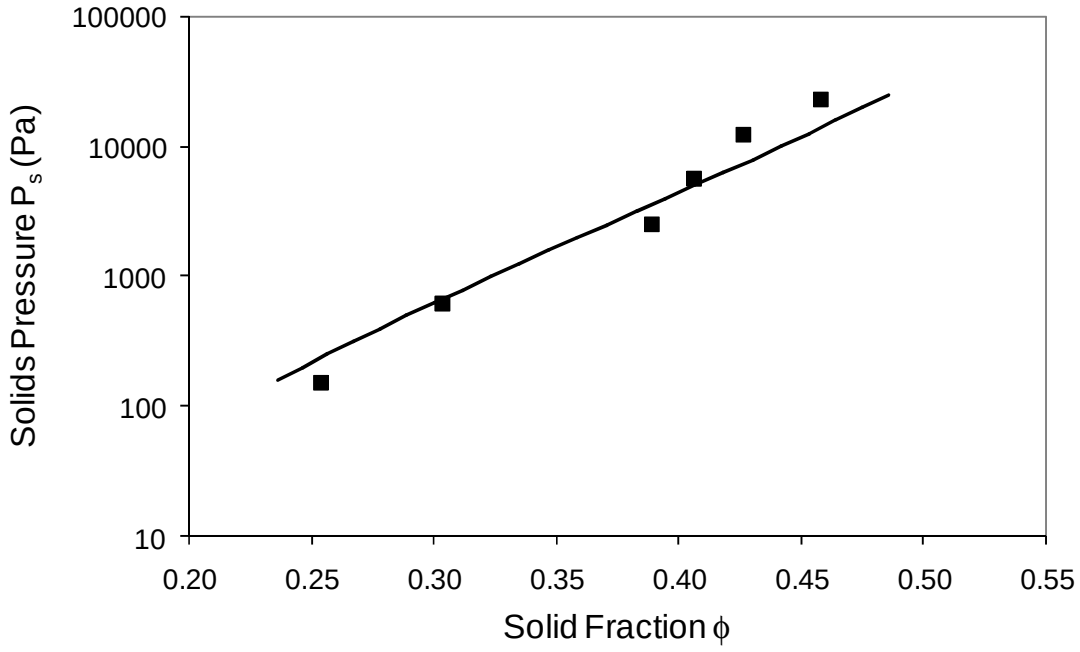

Figure 3-15 Comparison of the calculated compressive yield stress versus centrifuge measurement for the smaller yeast flocs pH 4.5. Error bars for centrifuge points were omitted as the range is sufficiently small.

All three techniques for measuring the compressive yield stress of the soil are overlaid in Figure 3-16 and demonstrate very similar P_y versus ϕ behaviour. This is particularly satisfying as each of the methods is quite independent of one another. A slight difference is apparent between the centrifuge and odeometer results, with the centrifuge technique indicating slightly higher solid volume fractions for a given applied pressure than is suggested by the odeometer analysis. The difference between these two methods of validation is most likely due to elastic deformation leading to an underestimate of the compressive yield stress to an extent that is difficult to quantify.

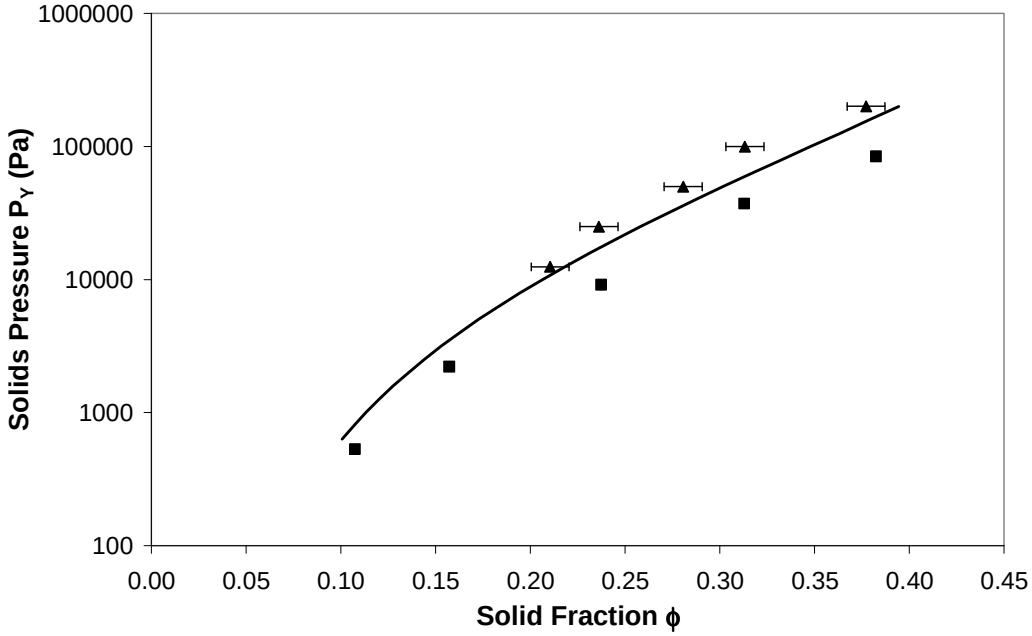

Figure 3-16 Comparison of the filtration-derived soil compressive yield stress (solid line) versus Rowe Cell (▲) and centrifuge measurements (■). Error bars for centrifuge points were omitted as the range is sufficiently small.

The choice of a logistic functional form for P_y appears to be satisfactory for the range of particle systems examined in filtration experiments with convergence of model parameters in all cases. Use of conventional power law forms such as equation 3-5 would not converge to an acceptable residual pressure in any of the systems. This illustrates that it is necessary to consider non-power law behaviour, particularly at low solid fractions when modelling filtration processes of flocculated systems. The functional form used here takes this low solid fraction behaviour into account. At the same time it is shown to be convenient for the numerical analysis with only four parameters required to encompass the variety of behaviour observed with minimal computational burden. It should be noted however that, although the logistic function used here is convenient, any functional form, including piecewise polynomial, could also be used.

3.5.3 Permeability

The permeability data obtained for zirconia, soil and yeast samples compressed to achieve a range of solid volume fractions is presented in Figure 3-17, along with the model predicted permeabilities for the various materials (derived from the gas-driven filtration runs). The predicted behaviour is observed to be comparable to the Rowe Cell measurements for the flocculated yeast and zirconia. However, it is significantly higher than the Rowe Cell measurements for the soil system and lower than the Rowe cell measurement for the smaller floc size yeast. A possible explanation could be that both techniques calculate permeabilities that are accurate representations of the respective systems and the difference is due to inherent manner in which piston and gas filtrations are performed. For example, it is possible that there is a difference in the structure of the pores of the different cake materials, which arises from different flow histories which are unique to the nature of each technique. The most significant difference is the high initial flux that is common to gas filtration which, in this case, is approximately an order of magnitude higher than the steady state flux for all materials. This was not observed in Rowe Cell filtration with steady state flux being reached almost instantaneously as the consolidation process has been induced beforehand in a separate process (via the piston).

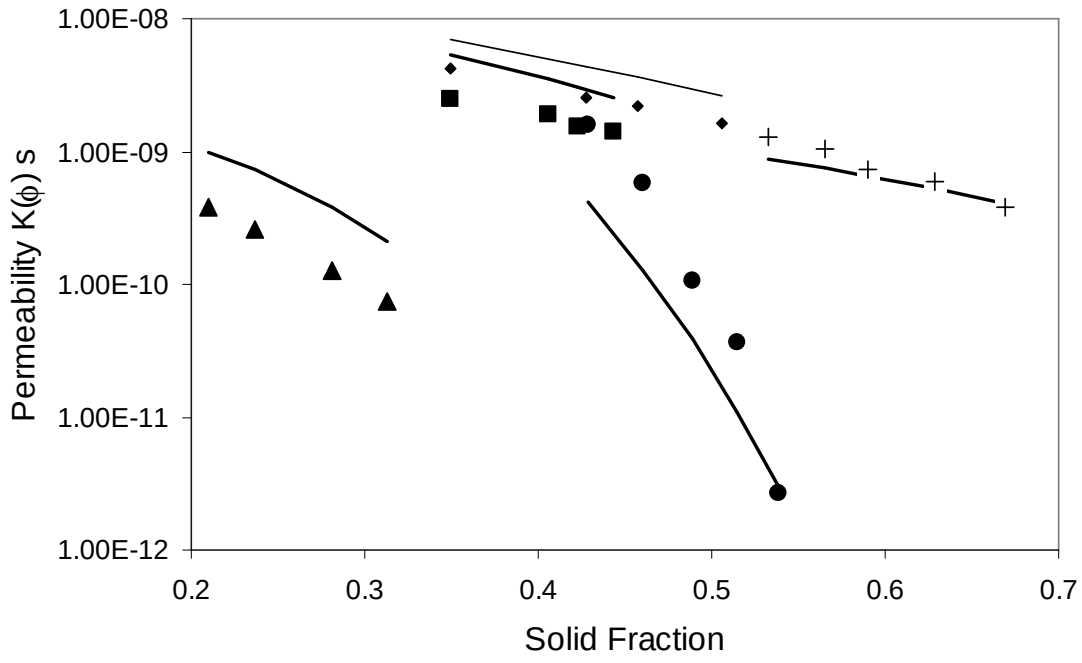

Figure 3-17 Permeability of cake material, measured directly versus the model fit for soil (▲), smaller yeast flocs (●), flocculated yeast (+), 5 μm zirconia (■) and 10 μm zirconia (♦).

It is important to recognise that the technique described here is suitable for systems that exhibit a low cut off flux (as observed particularly for the small yeast flocs). Although the yeast exhibits quite normal compressive behaviour, the permeability of the material, particularly at higher solid fractions, is several orders of magnitude lower than the other materials examined. This suggests that the pore size distribution of the small yeast flocs is much smaller than for the other material and is possibly more reflective of a non-flocculated system.

As shown by comparison with the Rowe Cell permeability measurements, the functional form selected to describe permeability is suitable for the range of solid fractions encountered in this study.

3.5.4 Cake Height

The measured cake heights and corresponding calculated heights are compared in Figure 3-18. This figure shows good agreement between the experimental and

calculated heights within the range of experimental error. For the larger cakes, less error was observed by the volume displacement technique as larger volumes to losses in the transfer stage are proportionally smaller. Some points fall outside the range of error but it is stressed that the calculated fit here reflects the trend based on the best fit of the material parameters C_1 to C_6 to the gas filtration results.

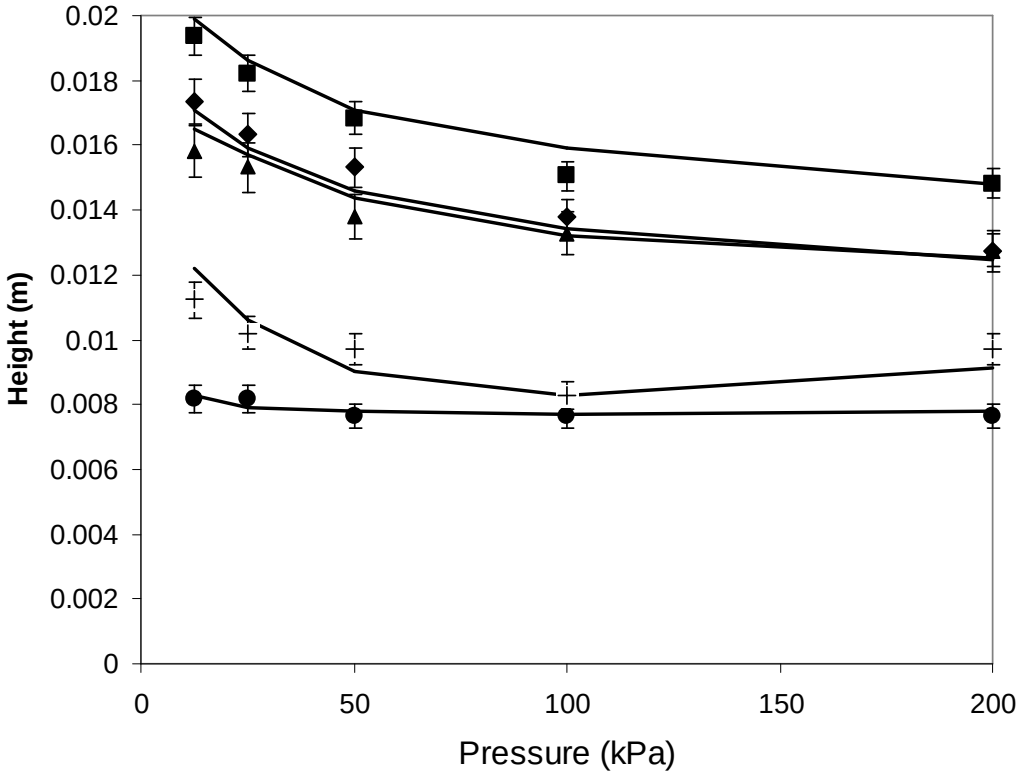

Figure 3-18 Comparison of measured cake height versus calculated ideal cake for soil (▲), smaller yeast flocs (●), flocculated yeast (+), 5 μm zirconia (■) and 10 μm zirconia (♦).

3.5.5 Source of Errors

Although the model fit calculated from the numerical cake integration provides comparable results to those determined by independent means, systematic and random errors are present. The most significant random error is due to the limitation in the accuracy of the cake height measurement. Random error in this measurement is typically less than 5%, depending on the final cake height. The error is magnified significantly for much smaller cakes and is thus the reason why solids loadings are

selected that generates cake which is greater than 5mm in thickness. Other random errors arise as a result of differences in shear magnitude and pH between each filtration, however, care was taken to minimise this.

Systematic errors arise from trapped air between the piston and the cake in the Rowe Cell technique. This certainly leads to higher than calculated solid fractions, as the dead volume of filtrate in the exit tube is expelled by air being pushed through the cake. In addition, the permeability dependence on flux history is postulated as the reason for the difference between the gas filtration-derived model and Rowe Cell results. To verify this one could manually limit the flux during the early stages of consolidation until steady state appears to be reached before removing the imposed flow restriction. The relationship between permeability and flow history is discussed further in Chapter 5.

3.6 Conclusion

A steady state filtration technique has been described that appears to be suitable for characterising cakes formed from flocculated materials. By driving gas filtration to steady state, stable flux data was obtained as input values for a numerical cake integration procedure. Model parameters for all particle systems examined had converged based on residual pressure minimisation criteria and compared favourably to direct measurements of permeability and compressibility.

Estimation of the compressive yield stress function based on the cake integration approach described here appears to be consistent with data obtained by odeometer (Rowe Cell) and centrifuge methods for all five particle systems examined. In addition, the calculated permeability for all systems is comparable to that predicted by the gas filtration-derived model. This suggests that the model forms used here for both the permeability (power law) and compressibility (logistic function) are suitable for this type of application. It is stressed that the model selection is not restricted to these functions and can essentially be of any mathematical form provided that the ideal calculated flux gives a reasonable fit to the experimental data.

Chapter 4: Constant Flux Filtration from Material Properties

In this Chapter the methodology described in Chapter 3 was applied to modelling constant flux filtration. In a review of literature, difficulties with existing approaches to the modelling of filtration of compressible materials under constant flux conditions are addressed and a new approach to modelling simultaneous consolidation and cake build-up based on dewatering theory is presented. Flocculated yeast is used as the test system with the predicted transmembrane pressure rise as a function of time under constant flux conditions compared with experimental data.

The work described here is essentially a practical application of measured cake material properties seeking to develop better predictive tools for membrane filtration. In this Chapter, shortcomings of the conventional filtration approach are discussed. This includes the assumption that the material properties are constant as the cake evolves and instantaneous in reaching some nominal average specific cake resistance.

4.1 Introduction

The separation of particulates such as clays, oxides and micro-organisms from waters and wastewaters via dead-end filtration is widely used in the water industry. Although these membrane systems are typically pressure controlled to deliver constant flux (Ho and Zydney 2002), a reduction in performance due to resistance from accumulating material is inevitable.

The pressure in dead-end systems controlled to constant flux will continue to rise until it becomes necessary to remove the accumulated material by introduction of back-flushing, bubbling or some other means of agitation to cause cake displacement. Given that initiation of cake removal is normally triggered by pressure rise to a certain threshold value, prediction of the rate at which pressure increases is important in predicting the likely frequency of cake removal that will be required.

Typically, the type of dead-end systems traditionally associated with a high potential for fouling and subsequent increase in cake resistance are submerged membrane filters (SMF) and membrane bioreactors (MBR). In MBR systems, approaches to avoiding TMP rise include:

i) ensuring that the permeate flow rate is well below the critical flux of the dominant foulant; and

ii) reducing the set point flux in order to delay the onset of rapid TMP increase (Cho and Fane 2002).

Other operational strategies can be employed to further delay the onset of rapid TMP rise but are limited by an inevitable consolidation of the cake and associated reduction in cake porosity.

Traditionally it is believed that this rapid onset in TMP rise is related to the critical flux below which permeability of the filtration system is effectively constant and above which permeability decreases (Pollice et al. 2005). Studies have shown this not to be the case with small changes in permeability observed very early in the cake evolution (Le-Clech et al. 2003) suggesting that the phenomenon is not directly related to the critical flux.

Clearly lacking is an analytical approach which provides insight into how the composition of the suspended matter affects filtration. In order to develop such an analytical approach, it is critical to understand and apply the underlying principles governing the change in cake porosity and permeability when the cake is subjected to compressive stresses. The accumulation of new material onto the cake contributes to consolidation as this increases the compressive stress exerted on the lower layers of the cake.

In this study, the process of simultaneous cake consolidation and cake growth was examined for dead-end filtration systems in order to model the transmembrane pressure rise for a given set of material properties. From a practical point of view, focus is placed on the compaction of the material under applied solids pressure and the ability of the particle network to withstand compressive stress. To do this it is

necessary to describe the filtration process in terms of the compressive yield stress, P_y, and the permeability, K, of the accumulating cake.

A theoretical approach to modelling consolidating cakes will be described in this Chapter. The model allows simulation of the trans-membrane pressure rise as a function of processed volume at constant flux given the material properties P_y and K, where these parameters are determined using the method of Chapter 3. A rigorous, one-dimensional force balance is solved numerically in order to calculate the incremental rate of consolidation with superimposed flow representing the filtrate passage through the cake. It was demonstrated that the conventional analytical solution to the problem leads to large errors as a result of assumptions that are not justified for highly compressible systems. Approaching the problem numerically allows the formulation of a solution free of these assumptions and to account for non-linearity in the filtration process.

4.2 Background

In this section the conventional approach is described for predicting the pressure rise for compressible cakes under constant flow conditions. Particular attention is given to the process of consolidation as cake formation is a relatively trivial matter. The conventional approach based on specific cake resistance (α) is described first.

For incompressible materials, the specific cake resistance is constant with time and pressure. Thus, if the flux is maintained constant, an expression for constant flux filtration in terms of the pressure increase with time is given by rearranging equation 2-11

$$\Delta P_L = \alpha \mu c_s \frac{Q^2}{A_c^{\,2}} t + \mu R \frac{Q}{A_c} \qquad (4\text{-}1)$$

where Q is the volumetric flow rate. Thus a plot of pressure P against t will be a straight line if the material is incompressible. In compressible cake filtration, layers of the cake consolidate under the pressure of material above and as a result of fluid drag with the eventual extent of consolidation depending on the pressure exerted. The resulting change in specific cake resistance through the filtration process is one of the

major reasons why non-linear P vs. t relationships is typically encountered in compressible cake filtration at long filtration times. Thus, to accurately describe the time dependent increase in pressure, it is necessary to account for the change in specific resistance with applied pressure and time. This dependency is commonly described by the power law constitutive relationship as presented in equation 3-1.

It should be noted that no account is taken in equation 3-1 of the time it takes for the material to consolidate with an apparent assumption that the specific cake resistance reaches its steady state instantaneously at a particular pressure. This is only a reasonable assumption if the cake consolidation is not the rate limiting step, such as may occur if the feed concentration is very dilute, or if the hydrodynamic resistance to water expression from the consolidating cake does not dominate permeate flux.

In addition to the issue of time dependent changes in specific cake resistance, it is important to note that, for highly compressible systems, the average specific cake resistance does not adequately describe the hydraulic conductivity of the cake as there is significant variation of the cake properties within the cake (Tiller et al. 1999). Hence, throughout this Chapter, the focus will be on local (i.e. depth dependent) cake properties rather than average cake properties.

Lu et al. (1998a) developed a numerical technique involving local cake properties to simulate constant flux filtration. The cake is described as a series of discrete slices for numerical convenience. The dynamic component of this method is based around cake formation rates and consolidation considered to be instantaneous according to the relationship between specific cake resistance, porosity and solid compressive pressure.

During constant flux filtration the rate of pressure rise is attributable to both cake growth and consolidation. To model each component a constant flux filtration experiment is considered in which addition of fresh material to the cake ceases but filtration continues. According to equation 4-1 it would be expected that no further increase in cake resistance would occur if solid feed was no longer introduced to the system. An illustration of the possible effects of this abrupt cessation of solid loading on rate of pressure build up for slow and fast consolidating materials is shown in Figure 4-1.

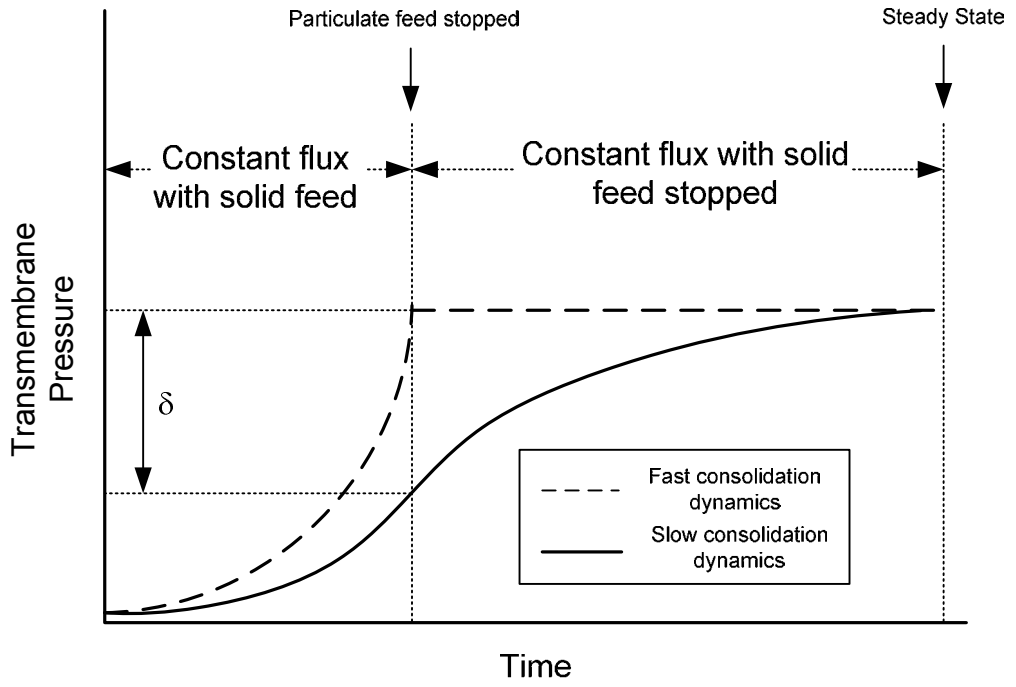

Figure 4-1 TMP rise during constant flux cake filtration followed by passage of clean suspension at constant flux for arbitrary systems of fast and slow consolidation dynamics.

In practice, real systems exhibit varying degrees of consolidation behaviour and it is important to account for this effect. Where the magnitude of δ (see Figure 4-1) is appreciable, it is clearly no longer appropriate to assume instantaneous (fast) consolidation. Consolidation dynamics may be described by the filtration momentum balance equation expressed in terms of local cake properties (equation 3-2). By solution of equation 3-2, it is possible to deduce the local cake properties.

Several authors propose solutions to this momentum balance equation. Landman et al. (1999) propose a solution leading to an expression for the consolidation ratio given as

$$U_c = S_c\sqrt{t - t_f} \tag{4-2}$$

where t-t_f is the effective duration of consolidation (t_f being the time of filtration prior to the consolidation stage). The dimensionless consolidation ratio is defined by

$$U_c = \frac{H_o - H}{H_o - H_\infty} \tag{4-3}$$

where H is the cake height, H_o the height at the beginning of consolidation and H_∞ the equilibrium consolidation height. The factor S_c is in equation 4-2 is given by

$$S_c = \frac{\delta_f}{H_o - H_\infty}\left[\frac{k_s(1-\phi_o)^2}{\phi_o r(\phi_o) h_o^2}\left(\frac{V_P}{\lambda_s}\right)\right]^{\frac{1}{2}} \qquad (4\text{-}4)$$

where δ_f is analogous to the conventional β (i.e. equation 3-3), k_s is a constant, V_p is the volume of particle or floc and λ_s is the Stokes drag coefficient for the particle.

While the function δ_f is obtained by solution of the filtration equation (equation 3-2), determining the floc volume and Stokes drag coefficient is difficult. Additionally, Landman pointed out that the above approach is only reasonable at short filtration times. As such, this approach is not particularly useful in many filtration applications as significant decreases in permeability are encountered at long filtration times where the solid fraction approaches its equilibrium state.

Creep consolidation is a separate phenomenon to the dewatering model described by Landman. Creep consolidation effects in the dewatering of cellular materials was identified by Lanoiselle et al. (1996) and is of relevance to yeast filtration and possibly natural organic matter (NOM) in water treatment systems. It is believed that this process is the slow expression of extracellular water migrating from within the cell structure and becoming free to join the bulk flow of permeate.

Creep consolidation in filtration was modelled by Shirato et al. (1986) who proposed an approach to time-dependant consolidation over a wide range of filtration pressures. In this approach, three kinds of retardation time (i.e. consolidation retardation) are considered. The first is a retardation time associated with liquid flow resistance of a Terzaghi (elastic) element, the second is a retardation time associated with a Voigt (viscous) element, and the third is a retardation time associated with creep deformation of the particulate bed. More recently, Christensen and Keiding (2007) showed that modelling the creep behaviour in pressure filtration of activated biological sludge gave a better account of the observed filtration trend. While creep deformation is expected to be important at long consolidation times, it is recognised that this timescale is considerably longer than those associated with liquid flow

resistance and, for the purposes of simplicity, will be ignored in development of the numerical model.

Buscall and White (1987) have modelled the consolidation problem and present a constitutive equation of the form

$$\frac{D\phi}{Dt} = \kappa_c(\phi, P_S)[P_S - P_y(\phi)] \tag{4-5}$$

which is valid for $P_S > P_y(\phi)$, where κ_c represents the dynamic compressibility of the cake. For application to filtration it was assumed that $P > P_y$ everywhere due to hydrodynamic drag. By considering the work done on the cake due to consolidation under applied solids pressure, an expression for the rate of work done can be developed. Assuming that this is equal to that of viscous dissipation from flow that results from displacement leads to the following expression for the dynamic compressibility

$$\kappa_c(\phi) = \frac{9\phi\left[1-(6\phi/\pi)^{1/3}\right]^2}{\mu(1-\phi)} \tag{4-6}$$

This expression will not be particularly useful in filtration as significant fluid energy is introduced to the specified system boundary that has otherwise not been accounted for. This energy is introduced as the superimposed flow (at a rate proportional to the inlet flux J_i) in addition to the liquid expelled due to consolidation. Hence, the expression given here is likely to underestimate the consolidation time for filtration.

Kapur et al. (2002) provide useful insight into the assumptions necessary to model the process of cake consolidation. The assumption is made that the rate controlling step of consolidation is determined by drainage of fluid from the porous structure. The governing equation developed by Kapur et al. is

$$\frac{dH}{dt} = -k'\frac{(1-\phi)^3}{\phi^2}\frac{\Delta P_L}{H} \tag{4-7}$$

where *k'* is the Carman-Kozeny constant. Basically, the assumption needs to be made that the rate of consolidation (*dH/dt*) is exclusively a result of the balance of the fluid driving force ΔP_L and resistance in terms of the Carman-Kozeny relationship. Hence,

the rate of expulsion per unit area of membrane is equal to the rate of consolidation. Applying this form to filtration is problematic. For example, encountering fluid influx from outside the system boundary is a certainty in the form of supernatant influx at a flux of J_i. An additional term would be required in equation 4-7 to account for the superposition of this influx with the expelled volumetric flow rate due to consolidation. Furthermore, this model is limited to systems describable by the Carman-Kozeny relationship.

In this Chapter, a flexible form of the governing equation for consolidation is formulated and a numerical solution to this equation developed. This is important as the fouling layers formed on membranes during water and wastewater treatment possess hydraulic characteristics which depart significantly from cakes formed from uniform packed hard spheres which prohibits use of restrictive models describing cake permeability.

4.3 Theory

A numerical technique is developed here which enables prediction of the rate of cake consolidation. The trans-cake pressure drop is equal to the solids pressure at the membrane, $P_{S,\infty}$. The technique seeks to calculate this pressure differential as a function of time or, given the flux, as a function of processed volume. The TMP is calculated as the sum of $P_{S,\infty}$ and the pressure drop across the membrane.

A model is proposed where the rate of consolidation at any point in the cake explicitly accounts for local flux, solids pressure and flow resistance due to the cake. Darcy's Law is used to quantify the flow resistance where, in the context of this work, the driving force $\Delta P_{L,Net}$ is the difference in fluid pressure between some point in the cake and the cake exit, which drives the fluid through the cake below that point at a rate of J_{Net}.

This approach is illustrated in Figure 4-2 for a thin cake slice. The slice can be thought of as a sponge subject to a solids pressure P_S which expels water and contributes to the bulk flow of permeate which exhibits a local flux J. As a result of this additional flux, an additional fluid pressure drop is generated at the lower plane of

the slice. It is stressed that $P_{L,Net}$ is a "virtual pressure" used as a calculation aid in determining J_{Net}.

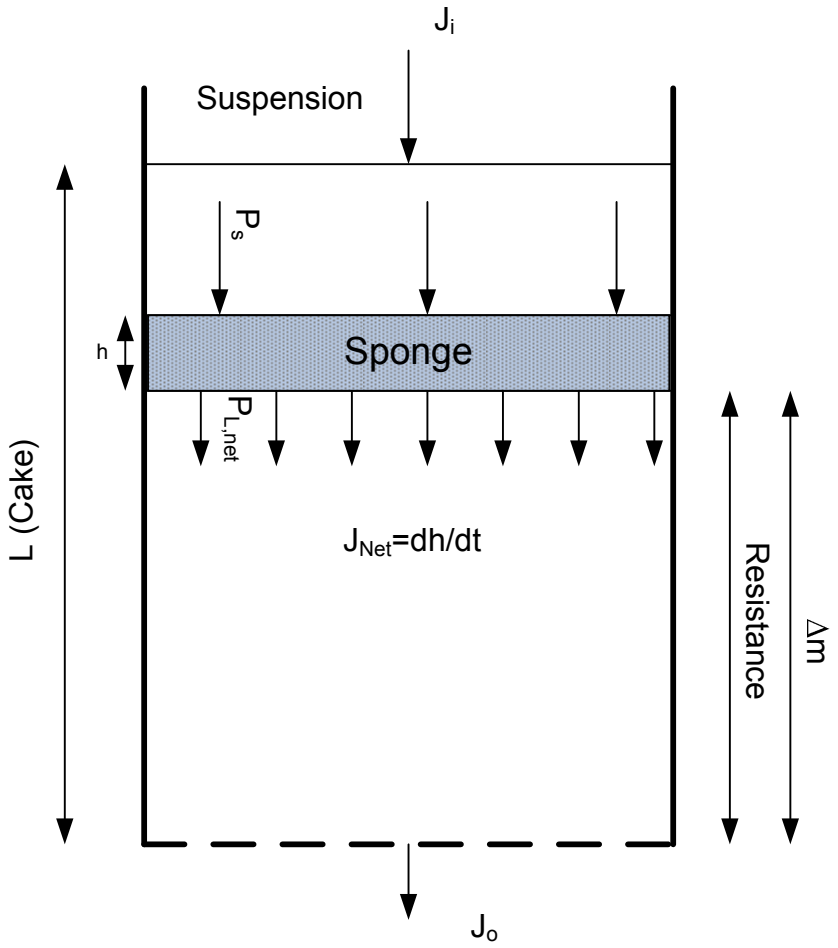

Figure 4-2 Darcy's Law applied in conjunction with the sponge analogy

The rate of consolidation (*dh/dt*) of the imagined sponge and resulting addition to the flux will be governed by Darcy's Law such that it is proportional to the driving force divided by the resistance. A pressure balance is performed on the slice (Figure 4-3) and the net fluid pressure $P_{L,net}$ which results from this process is given by

$$P_{L,net} = P_N - P_y \tag{4-8}$$

where P_N is the normal pressure which is exerted by the cake below and P_y is the compressive yield stress which represents the mechanical resistance of the cake to compression. The net fluid pressure is ultimately the key factor that determines the change in cake thickness (*dh/dt)* which arises due to displacement of water from a

cake slice of fixed solid mass (i.e. water being squeezed out of the “sponge” shown in Figure 4-2). An analogy to help explain Figure 4-3 is to visualise free falling with a set of scales with a 1kg weight on it. The reading on the scale is zero until a force acts from the bottom of the scales. Once the scale is stationary on the ground, the balance reads 1kg.

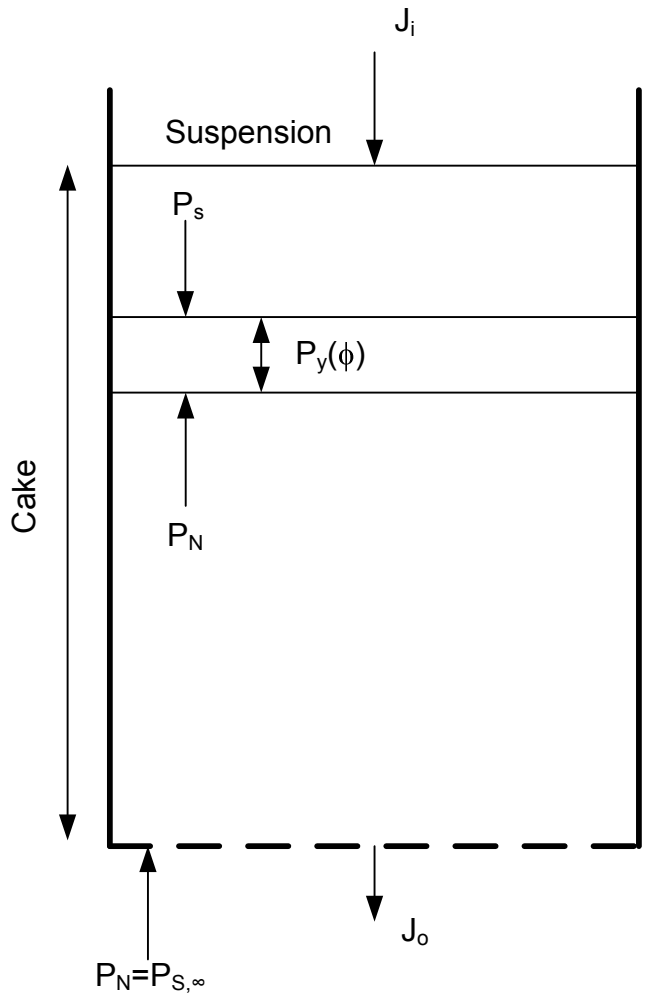

Figure 4-3 Pressure Force Balance on the slice illustrating the pressure forces involved governing the expulsion of liquid from slice. The squeeze force experienced by the cake slice is governed by the normal pressure force P_N where the maximum squeeze occurs when the cake layers below are stationary and thus $P_N=P_S$.

The normal pressure P_N is indicative of the consolidation motion of the lower layers. If the cake slice is in free fall due to consolidation of the layers below the particular

slice of interest, P_N will be zero. Alternatively, if little consolidation of the cake below the slice occurs then $P_N=P_S$ and maximum consolidation of the slice will take effect. In physical terms equation 4-8 states that the residual solids pressure imposed on a solid element that does not contribute to mechanical deformation of the solid network is realised as hydrodynamic force expressing the fluid from the slice.

The resistance encountered by the liquid in the cake is non-uniform with respect to position in the cake and can be deduced if the local solid fraction profile and permeability is known. Darcy's Law was used to quantify the relationship between driving force, resistance to flow and the magnitude of flow. As the permeability (inverse resistance) is non-uniform through the cake, Darcy's Law (section 2.2.2) was reformulated to account for this such that

$$J = \frac{\Delta P_L K(\phi)}{\Delta m} \tag{4-9}$$

where Δm is the mass of a thin layer of cake and ΔP_L is the liquid pressure relative to the outlet. The derivative of equation 4-9

$$\frac{dJ}{dP_L} = \frac{K(\phi)}{\Delta m} \tag{4-10}$$

describes the rate of change in flux with fluid pressure. At any point in the cake, the total flow exiting a slice is the sum of the inlet flow J_i and expelled flow J_{Net} due to consolidation; i.e.

$$J = J_i + \int_0^{P_{L,Net}} \frac{K(P_S)}{\Delta m} dP_L \tag{4-11}$$

where the second term is the integral of equation 4-9, Δm is the mass of the cake between the local slice and the membrane (Figure 4-2) and ΔP_{Lnet} is the net fluid pressure (which can be calculated using equation 4-8). Here the permeability is expressed as a function of solids pressure rather than liquid pressure though these material properties are directly related. The cumulative drag force and the local solids pressure P_S may be calculated using the momentum balance valid for point to point contact between particles (Tiller and Huang 1961)

$$\frac{\partial P_L}{\partial z} = -\frac{\partial P_S}{\partial z} \qquad (4\text{-}12)$$

where P_L is the absolute fluid pressure present because of the applied filtration pressure. The liquid pressure is assumed to be distributed across the cake cross section and solid pressure P_S defined as a "pseudo-solid compressive pressure" according to Tiller and Huang (1961). This assumption is reasonable for deformable particles, such as yeast, if the compressibility function is consistent with the definition that solid pressure is cross section averaged rather than a contact area pressure between deformable spheres. Lin et al. (2003) describe an alternate approach to dealing with the filtration of deformable spheres according to the latter definition. These concepts were extended by Lin to look at the implications of measured particle deformation on cake permeability according to the Carman-Kozeny relationship.

For the methodology described in this Chapter, such treatment of particle deformation is not critical as the concept of permeability is addressed as a top down approach and as such, influences of changing local hydraulic dimensions are lumped into the calculated permeability model parameters. Such an approach is reasonable for non-uniform systems of particles that are not easily described by the Carman-Kozeny relationship.

The momentum balance (equation 4-12) relates the local liquid and solid pressures and thus the integral in equation 4-11 can be evaluated. The permeability of the cake layers below any given layer is non uniform making use of equation 4-9 difficult. To simplify this the mean effective permeability *K'* of the lower cake was calculated with known local pressure P_L and flow J_i using

$$K' = \frac{P_L}{J_i \Delta m} \qquad (4\text{-}13)$$

where P_L is the absolute fluid pressure and J_i the local fluid flux.

In order to simplify the integral in equation 4-9 and thus calculate an expression for the rate of consolidation a linear approximation was made based around the mean effective permeability such that

$$J_{Net} = \frac{dh}{dt} = \frac{P_{L,Net}}{K'\Delta m} \tag{4-14}$$

As mass is conserved, make use of the following expression

$$h_o\phi_o = h\phi \tag{4-15}$$

where h_o and ϕ_o are the slice height and solid fraction at the previous time step respectively. Thus

$$\frac{d\phi}{dh} = -\frac{h_o\phi_o}{h^2} \tag{4-16}$$

Now

$$\frac{d\phi}{dt} = \frac{d\phi}{dh} \times \frac{dh}{dt} \tag{4-17}$$

Using equations 4-14 and 4-16. the following expression is obtained for the rate of consolidation

$$\frac{d\phi}{dt} = -\frac{h_o\phi_o}{h^2}\frac{P_{L,Net}}{K'\Delta m} \tag{4-18}$$

As described in the next section, equation 4-18. can be applied to all cake slices sequentially from the top of the cake to the bottom.

In the work described above, the simplifying assumption was made that $J_i >> J_{Net}$ and hence the local flux is considered to be J_i through the cake and thus $J_o \approx J_i$. This is checked at the end of every calculation. If this assumption was not correct, overestimation of the TMP would result. The concept of expelled liquid resulting in flux increase in the direction of the membrane is illustrated in Figure 4-4.

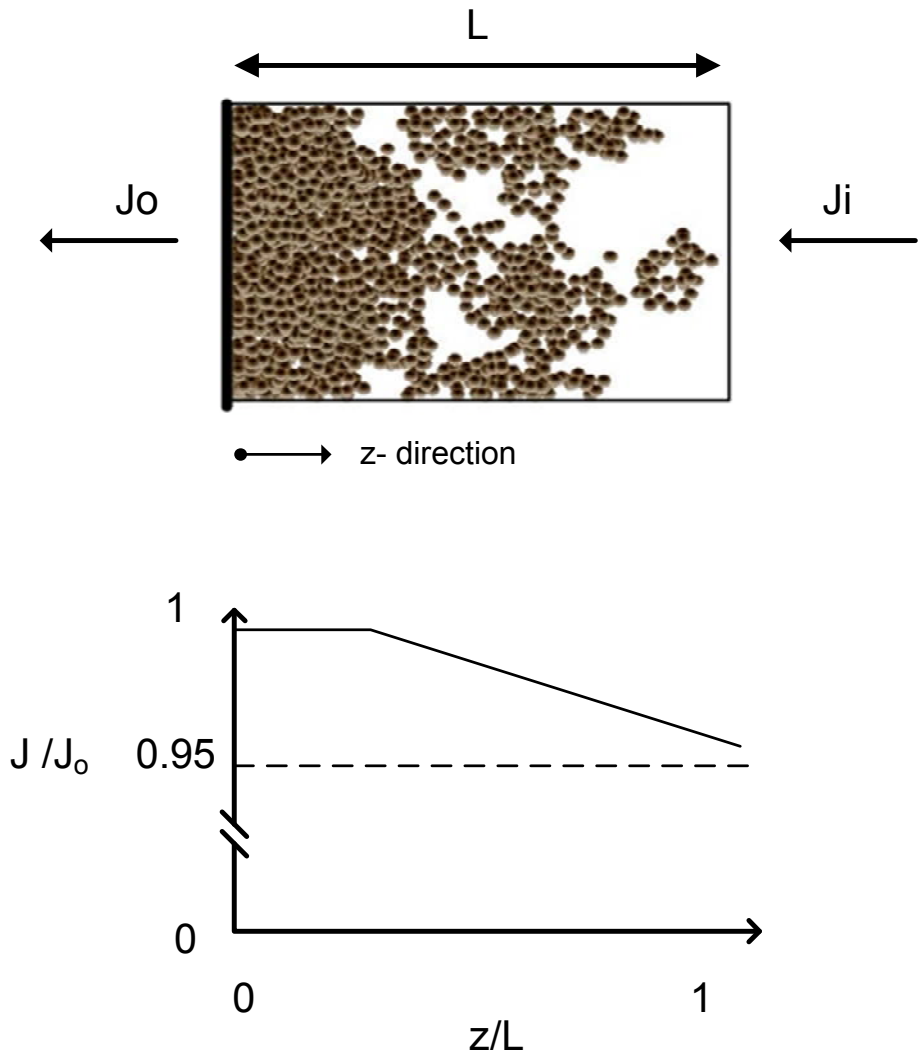

Figure 4-4 The variation in local flux to outlet flux ratio J/J_O through the cake due to accumulation of expelled liquid as shown in this conceptual diagram.

When J_i/J_O is calculated to be less that 0.95, a first order correction was made to account for the contribution to bulk flow by the expelled liquid. This simple approximation is sufficient as the bulk of pressure drop through the cake is in the region where J/J_O is approximately unity.

It is noted that J_i/J_O is a function of both solids loading and magnitude of the flux. For the solids loading used it this work (ϕ_0 = 0.011) and flux range 15 to 50LMH it is rare to encounter J_i/J_O less than 0.95 even though it has been reported in literature that this can be as low as 0.85 in membrane filtration (Tien and Bai 2003). As the

concentrations used in this study are higher than that encountered in most membrane filtration applications the assumption that $J_i \approx J_O$ would appear reasonable.

4.3.1 Application to Predicting Constant Flux Filtration

The steady state filtration approach was used to develop the initial solid fraction and solids pressure profiles in the cake based on the material properties $P_y(\phi)$ and $K(\phi)$. Subsequently, a numerical technique was used which enables simulation of simultaneous consolidation and cake formation and calculation of the resultant TMP rise for a given processed volume.

In the initial state (t=0) there are a fixed number of solid layers (slices) which make up the preformed cake deposit. A number of constants are introduced initially and the properties of each layer including solid fraction, local solids pressure and local liquid pressure are subsequently tracked as are global parameters such as time and processed volume.

During solution, equation 4-9 is used to calculate the flux exiting each slice. It was assumed that the fluid flow during constant flux filtration is equal everywhere and also assumed that accumulation of flow is negligible. As discussed previously in section 4.3, this assumption is reasonable for moderately dilute systems. The solids pressure on any slice is given by

$$P_{S,i+1} = \int \frac{J}{K(\phi)} dm = \Delta P_i + \Delta P_{i-1} + ... + \Delta P_o \qquad (4\text{-}19)$$

where the integration is performed numerically through the addition of pressure drop across each slice (denoted as i) above the current slice all the way to the top of the cake (i.e. i=0). Knowing the solids pressure, the pressure balance can be calculated (equation 4-8) before proceeding to calculate the rate of local consolidation given by equation 4-18. By selecting a time step that is sufficiently small, the consolidation process can be simulated and the change in solid fraction given by

$$\phi_{t+\Delta t} = \phi_t + \Delta t \frac{d\phi}{dt} \qquad (4\text{-}20)$$

where a time step of 0.01s is chosen as an optimum balance between computational expense and accuracy. In principle, consideration must be given to factors such as particle concentration and local consolidation rate in selecting a suitable time step (i.e. smaller time step for concentrated systems and/or fast consolidating systems and vice versa).

Additional slices were introduced at fixed intervals in order to mimic the addition of mass during filtration and the procedure of calculating the local profiles repeated for each time step. The material was added at the gelpoint solid fraction ϕ_g. Initially, the addition of new material disrupts the state of the slices below and consolidation occurs because of the additional compressive stress imposed by the developing cake.

The procedure described above is repeated until an exit condition is reached. The exit condition was specified to be when the total TMP reached 150 kPa. It is unlikely to encounter pressures greater than this in submerged membrane filtration practice. A flow diagram of the approach used is given in Figure 4-5.

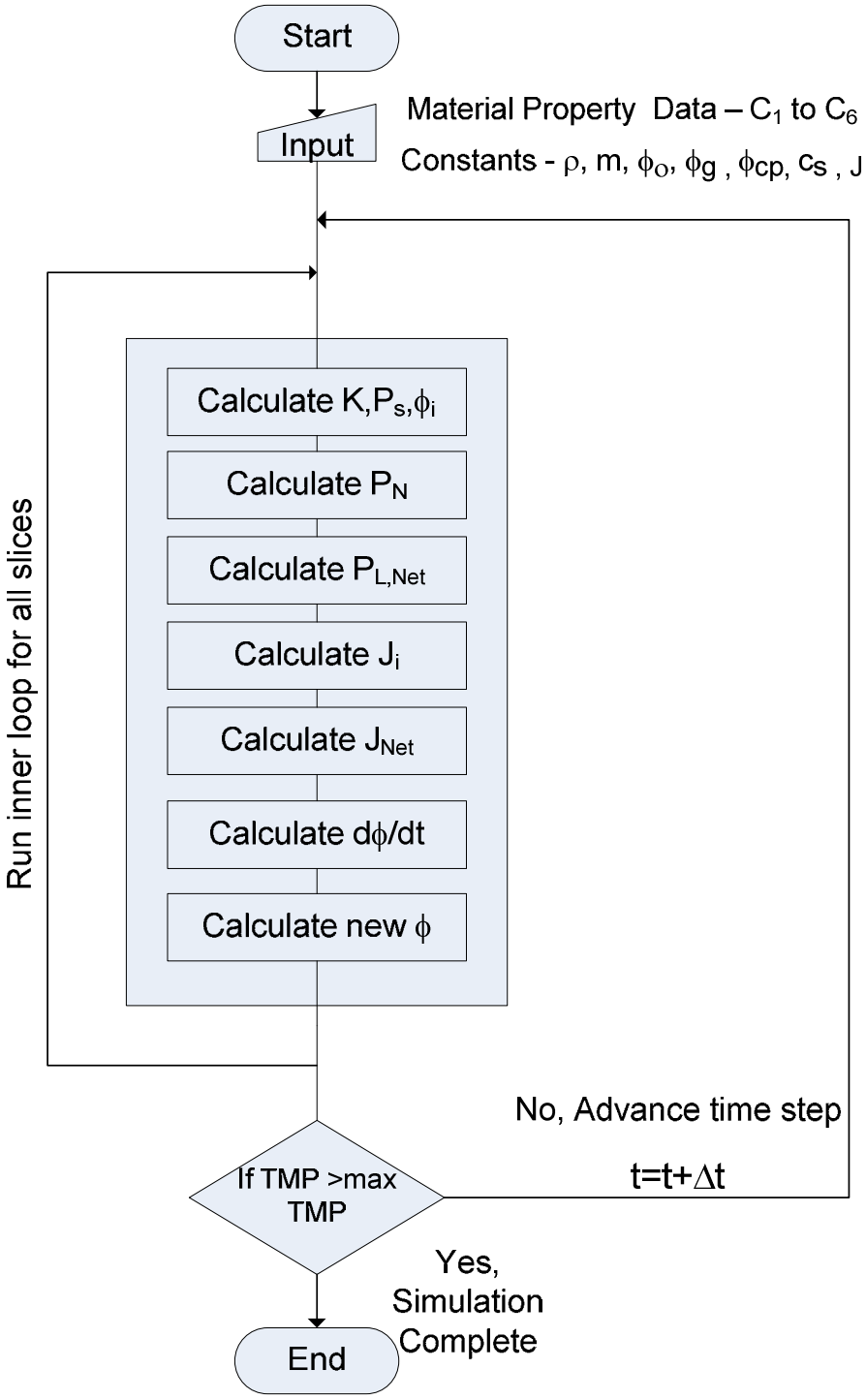

Figure 4-5 Flow diagram for calculation of TMP rise based on material properties

4.3.2 General Equation for Constant Flux

A modified form of the general equation for constant flux given by equation 4-1 is proposed incorporating an additional term to account for the transient elements in the consolidation process. Two transients governing the dewatering of the cake in this

work have been identified. These are the dewatering dominated by cake resistance and creep consolidation. The transient effects can be simplified to one time constant (Christensen and Keiding 2007) and modelled as a single transient according to the following equation

$$\alpha(\Delta P_L, t) = \alpha_0 \left(1 - e^{-\frac{t}{\tau}}\right) \Delta P_L^n \tag{4-21}$$

where τ is the consolidation time constant. Substituting equation 4-21 into the general equation for constant flux (equation 4-1) gives

$$\Delta P_L = \alpha_0 \left(1 - e^{\frac{-t}{\tau}}\right) \Delta P_L^n \mu c_s \frac{Q^2}{A^2} t + \mu R \frac{Q}{A} + \Delta P_0 \tag{4-22}$$

where P_0 is the pressure drop of the pre-formed cake. From this model it is possible to deduce the consolidation time constant by a sum of square error (*SSE*) minimisation routine. This is given by

$$SSE = \sum_{i=1}^{n} (\Delta P_{L,\mathrm{model}} - \Delta P_{L,\exp})^2 \tag{4-23}$$

where $\Delta P_{L,model}$ is the values calculated from equation 4-22 by iteration corresponding to some time t and $\Delta P_{L,exp}$ is the experimentally measured pressure drop at the equivalent time. The time constant τ and compressibility parameter n is varied to reduce the SSE resulting in a value that best fits the experimental data. For a series of experiments run at several different constant fluxes, n is independent of flux. Hence, the routine is configured to calculate τ as a function of flux J and an n value common to all flux values.

4.4 Experimental

The steady state filtration method detailed in Chapter 3 was used to determine the material properties of flocculated yeast prepared both at and away from the pH_{pzc}. Using these material properties, simulations of the TMP rise over time for various constant fluxes were undertaken using the method described above. For direct

validation of the simulated results, filtration at constant flux was performed measuring the TMP rise with accumulation of cake mass.

The experimental rig used to both extract P_y and K and to undertake the constant flux studies is a variation of the setup described in section 3.4.1. For the purposes of the studies reported here, a 1.5L reservoir was added in series with a 250mL batch filtration cell in order to simulate the gradual, continuous introduction of material to the membrane during the constant flux studies. Through use of a stirred reservoir containing the flocculated material, it was assumed that the batch filtration cell behaves as a plug flow vessel (Figure 4-6). By material balance, the rate at which mass of solids leaving the pressurised reservoir must equal the rate at which mass deposits on the cake provided that accumulation of material in the reservoir and cell is avoided. One possible source of non uniform flow of yeast out of the reservoir was associated with settling in the tube. To counteract this it is necessary to operate above 15 LMH and to select a tubing diameter appropriate to the density of the material being examined. For yeast, 1/16" tubing was found to be satisfactory. For systems close to the density of water, 1/8" tubing was found to be acceptable.

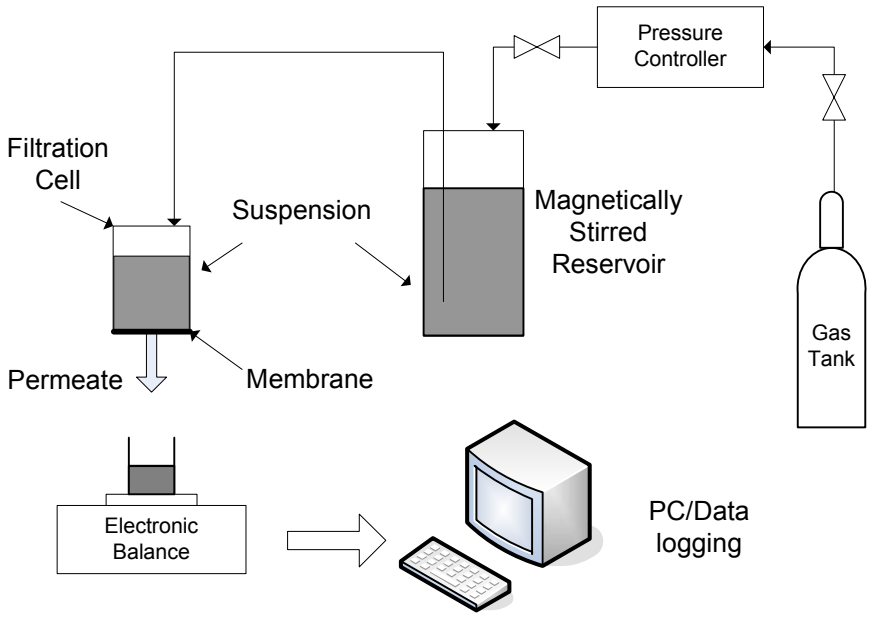

Figure 4-6 Experimental setup for filtration

The filtration cell shown in Figure 4-6 is circular with cross-sectional area of 19.6 cm^2 and height of 15 cm. The cell features a mechanical seal around the shaft of the impeller which allows for in-situ stirring in order to distribute the material evenly

across the membrane and cake (Figure 4-7). A 4-blade axial impeller positioned 12 cm above the membrane was used at a stirring speed of 5 RPM which was sufficient to achieve even distribution yet not induce uplift of material from the cake. The impeller was mounted to the lid via a mechanical seal to retain air tightness. The impeller was driven by a Faulhaber 2224 series micro motor and 1000:1 reduction gearbox powered by a variable voltage (0-12V) power supply. The motor/gearbox was mounted on the lid of the filtration cell via a custom bracket.

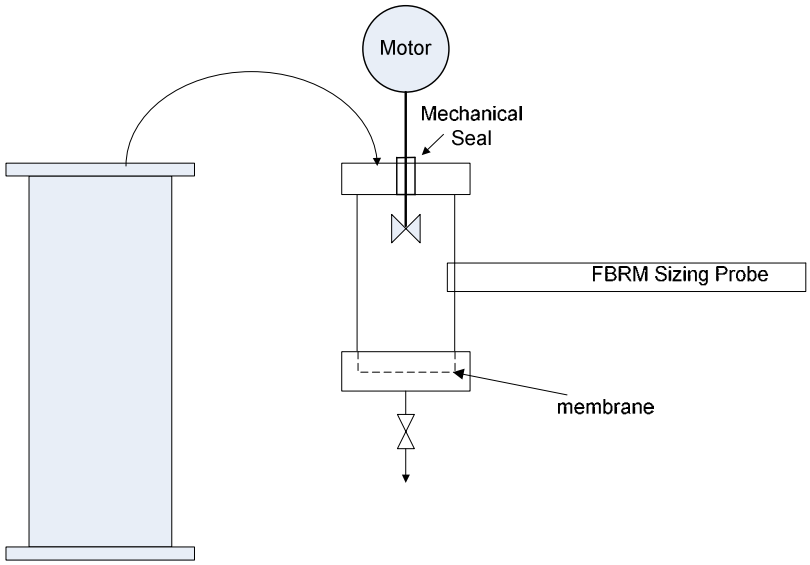

Figure 4-7 Filtration Cell Schematic (connected to the 1.5L magnetically stirred reservoir).

Particle number and size were determined using the in-situ focused beam reflectance measurement (FBRM) instrument. The FBRM probe was positioned flush with the inner wall of the vessel and provided a measure of the chord size distribution and particle counts. A hole with diameter matching the FBRM was bored through the filtration cell with an O-ring fitted to the perimeter of the hole. This allowed the FBRM to interface the cell fluid and at the same time retain a seal to maintain pressure in the cell. The installed probe enabled assessment of the consistency of size and particle loading. Monitoring of particle counts also provided an indication of whether plug flow conditions were met.

4.4.1 Constant Pressure Filtration

In order to determine the material properties of the yeast particles, 14g of yeast was washed in a centrifuge at 3,000 RPM and 10^{o}C for 15 min using an Allegra 25R centrifuge then added to Milli-Q water to make up 1.4L of suspension. The filtration cell and reservoir were filled with this suspension. The reservoir was placed on a magnetic stirrer to suspend the particles and flocculation initiated by reducing the pH to either 2.7 or 4 by the addition of 0.1M acetic acid. A constant pressure was applied to the reservoir, driving the suspension into the filtration cell. The yeast was retained on the membrane and the permeate collected in a vessel on a balance, the weight of which was logged continuously to determine permeate flux. Steady state was reached when no further change in flux was observed during filtration. This occurred after all the suspension was displaced from the reservoir and material settled in the filtration cell. The cake was preserved in its wet state and height immediately measured using a micrometer. This entire process was repeated at five different pressures in order to obtain sufficient data to perform the material properties computation.

4.4.2 Constant Flux Filtration

The procedure for constant flux filtration was similar to that used in constant pressure filtration thereby ensuring that consistent material properties were maintained for both types of filtration. Initially 14g of washed yeast was prepared the same way as described in constant pressure filtration. The filtration cell and reservoir were filled with this suspension and fixed pressure applied to the cell to “pre-form” the cake. This was done because the minimum pressure achievable with the experimental setup was 12.5kPa and operating at constant flux below these pressures was not possible. Thus, it was necessary to operate at constant 12.5kPa filtration until steady state was reached with the pre-formed cake. This typically took 15 minutes. The reservoir containing the remaining 1.2L was then connected to the filtration cell (as in Figure 4-6) and gas pressure applied. The flux was computed by the PC and feedback control applied to maintain the set point flux. The TMP rise was logged by the PC. The applied pressure induced transfer of the yeast suspension from the reservoir to the filtration cell at the base of which the yeast particles accumulated. The pressure continued to rise (in order to sustain the flux) until 150 kPa was reached at which point the filtration was terminated.

This entire procedure was repeated for several fluxes between 15 and 50 LMH. The TMP versus processed volume was recorded in each case and used for validation by direct comparison with the simulated cake consolidation and growth results based on the material properties measured using the constant applied pressure method.

4.4.3 Stopped Feed Experiments

To further examine the time dependence of consolidation, an experiment was undertaken in which flow was continued but solid feed was stopped. From this experiment an approximate indication of the lag associated with the consolidation was gained by measuring the time taken to reach steady state after the suspended solid flow is stopped. This result can be compared to the model predicted response based on the steady state material properties and simulation procedure described in this Chapter.

Experimentally the solid feed was abruptly stopped at 50 kPa by disconnecting the supply reservoir, decanting the feed and replacing it with clear filtrate. The pressure supply was reconnected and constant flux filtration resumed after a delay of less than 1 minute.

4.5 Results

Both the steady state material properties deduced from the constant pressure steady state investigations and the comparison of calculated and observed TMP versus processed volume data represent key outcomes of this work. The results of constant flux filtration studies of pH 2.7 flocculated yeast and the predicted relationship based on the numerical analysis presented in this work (i.e. the simulation output) are shown in Figure 4-8. The predicted TMP rise based on the conventional approach (i.e. equation 4-1) is also shown in this figure (and discussed in more detail later). The numerical analysis was also configured to model “instant consolidation” such that the solid fraction profile at any point in time was determined directly from the equilibrium relationship between solid pressure distribution and compressibility function. It should be noted that the analysis of the results of Figure 4-8 are ongoing through this section.

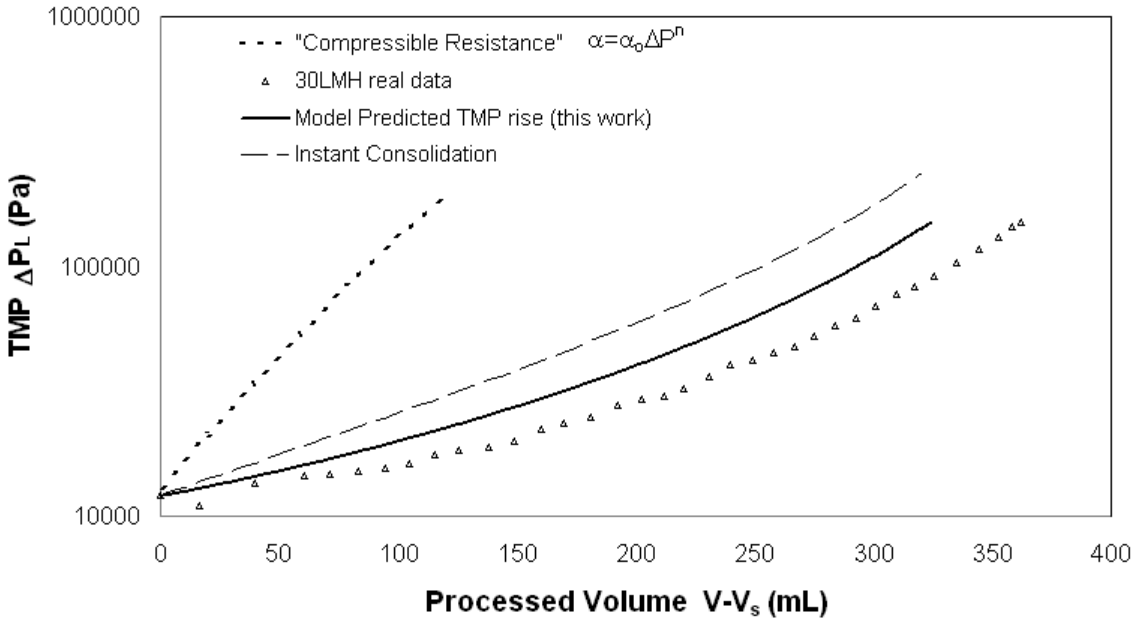

Figure 4-8 Comparison of constant flux filtration behaviour as calculated by standard filtration approach, by model prediction based on assumption of finite consolidation (this work), by model prediction based on instantaneous consolidation and measured experimentally for yeast pH 2.7 at 30LMH.

The constant pressure filtration results for the five nominal pressures used are shown in Figure 4-9 for yeast at both pH 2.7 and pH 4.0. Monotonically increasing flux with increase in pressure is observed in both cases with a higher flux for any given pressure observed for the yeast flocculated near the pH_{pzc} of the yeast (pH 4.0) compared to that at the lower pH. These results were used in calculating the material properties of both yeast cakes using the method of Chapter 3. The values of the coefficients C_1 to C_6 that are included in the material properties expressions and obtained by comparison of model and experimental data are shown in Table 4-1. The resulting compressive yield stress and permeability were calculated and are compared (for the pH 2.7 aggregated yeast) with results directly obtained by odeometric measurement in Figure 4-10.

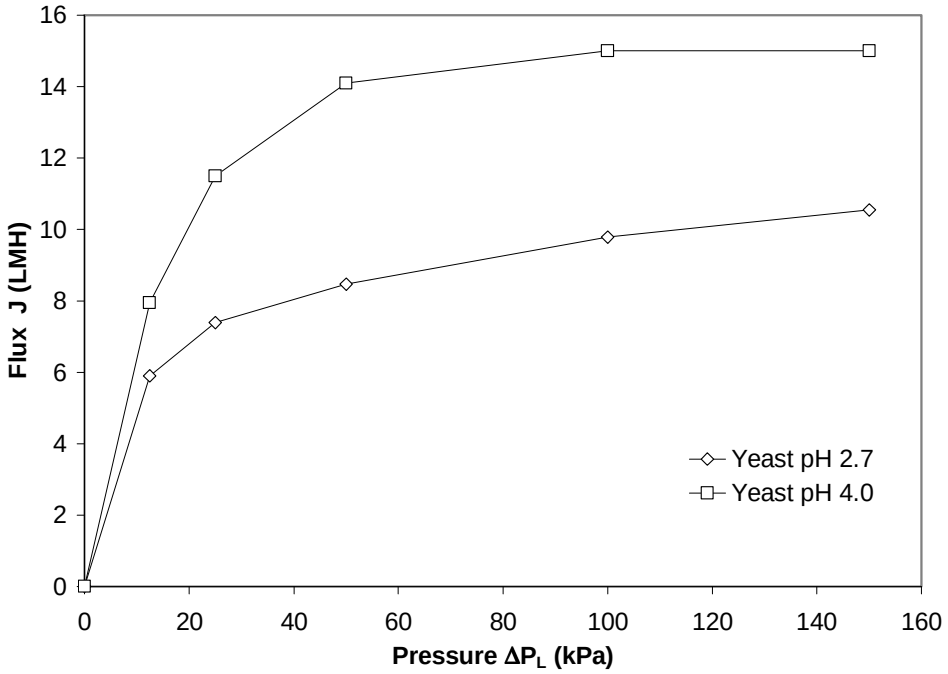

Figure 4-9 Steady state flux versus constant applied pressure for flocculated yeast pH 2.7 and pH 4.0.

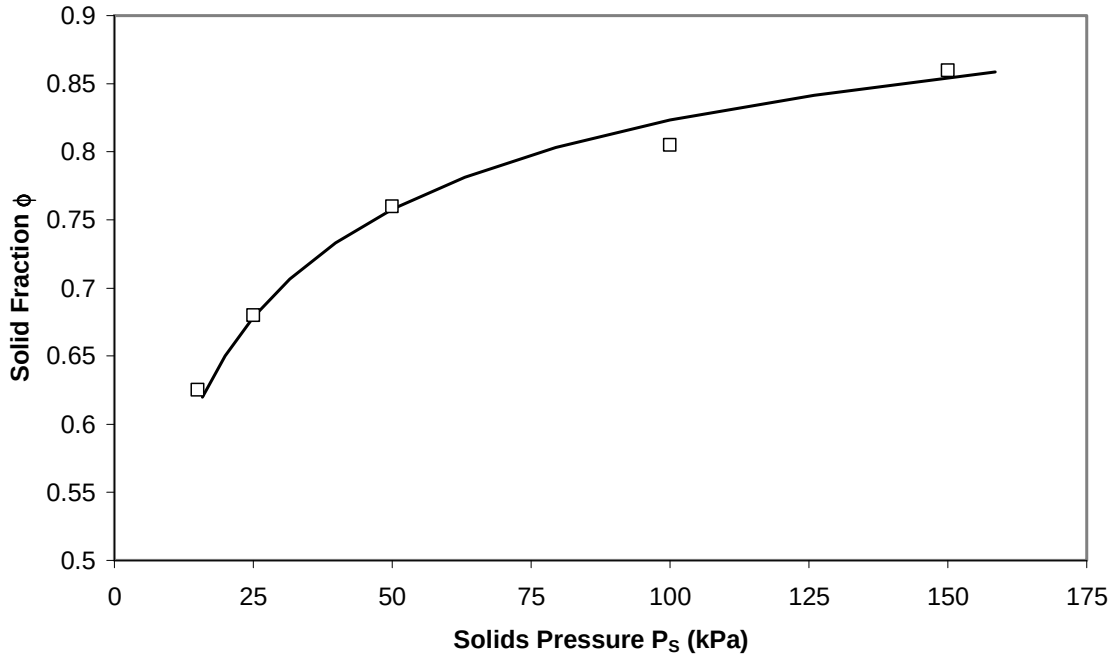

Figure 4-10 Comparison of Compressive Yield Stress by direct measurement (Rowe Cell - squares) and calculated by steady state filtration analysis for flocculated yeast pH 2.7 (solid line).

Table 4-1. Summary of parameters calculated by steady state filtration

	C_1	C_2	C_3	C_4	C_5	C_6	R^2
Yeast pH 2.7	4.69×10^{-9}	2.88	0.156	0.0043	0.0004	-0.741	0.98
Yeast pH 4.0	2.08×10^{-9}	4.02	-0.123	0.021	0.0003	-0.995	0.97

This result demonstrates the validity of the steady state filtration approach to material property determination of the yeast cakes examined here. The value for the close packed solid fraction ϕ_{cp} was determined to be 1 for this work which implies that the material is highly compressible in nature allowing packed spheroids (yeast cells) to deform and compact beyond the theoretical close packed solid fraction for uniform spheres of approximately 0.64 (Meireles et al. 2004).

The material properties results obtained via the steady state analysis were used to calculate the TMP rise using the method described earlier. A comparison of the computed and experimentally determined TMP increase with processed volume V-V_s for constant flux filtration of the pH 2.7 yeast sample for a range of fluxes is shown in Figure 4-11. Here, V_s is the equivalent processed volume required to preform a cake prior to the constant flux period and is typically around 200mL. The results shown in Figure 4-11 show good agreement between experimental and simulated TMP rise for all set point flows. Slight differences may be attributable to systematic errors related to a lag in the system created at the starting point of filtration. As the filtration commences with clear solution, a lag is involved as the system equilibrates to plug flow conditions. It appears that this lag is approximately 50mL based on the results shown in Figure 4-11. It is worth noting that creep consolidation could also contribute to this lag with the two transients difficult to deconvolve.

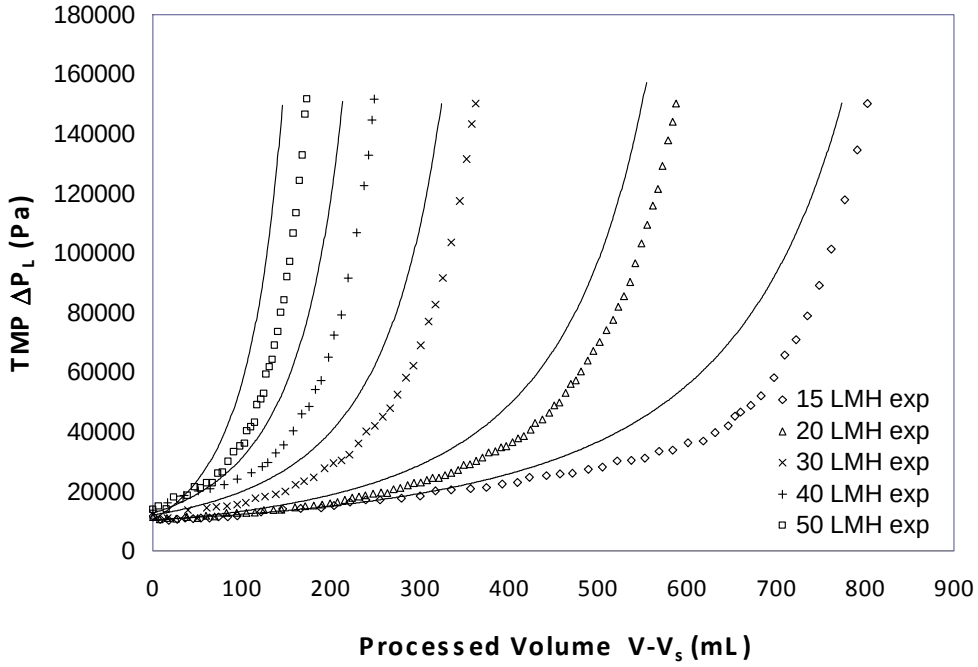

Figure 4-11 Comparison of TMP rise for 50, 40, 30, 20 and 15 LMH from left to right for experimental (exp) constant flux filtration(dotted lines) and simulated based on measurement of P_y and K (solid lines) at pH=2.7.

Figure 4-12 presents a comparison of the second yeast system flocculated at the optimum pH of 4. The agreement between simulated and experimental TMP rise is quite good for the 40 and 50 LMH cases and is better overall compared to pH2.7. This could be due to the faster overall filtration time which negates the consolidation effects. In Figure 4-13 a plot of the particle counts with time is shown for this system as determined using the Lasentec FBRM. These plots confirm that a lag occurs before the system reaches a consistent solids loading. The lag appears to be of the order of 20-30 minutes (equivalent to about 50mL) for the system to reach 90% of the final state and would be sufficient to account for the small difference between experimental and simulated TMP rise that is observed. There is certainly scope for improvement here as a consistent system could be achieved through a redesign of the apparatus to eliminate the transient effect.

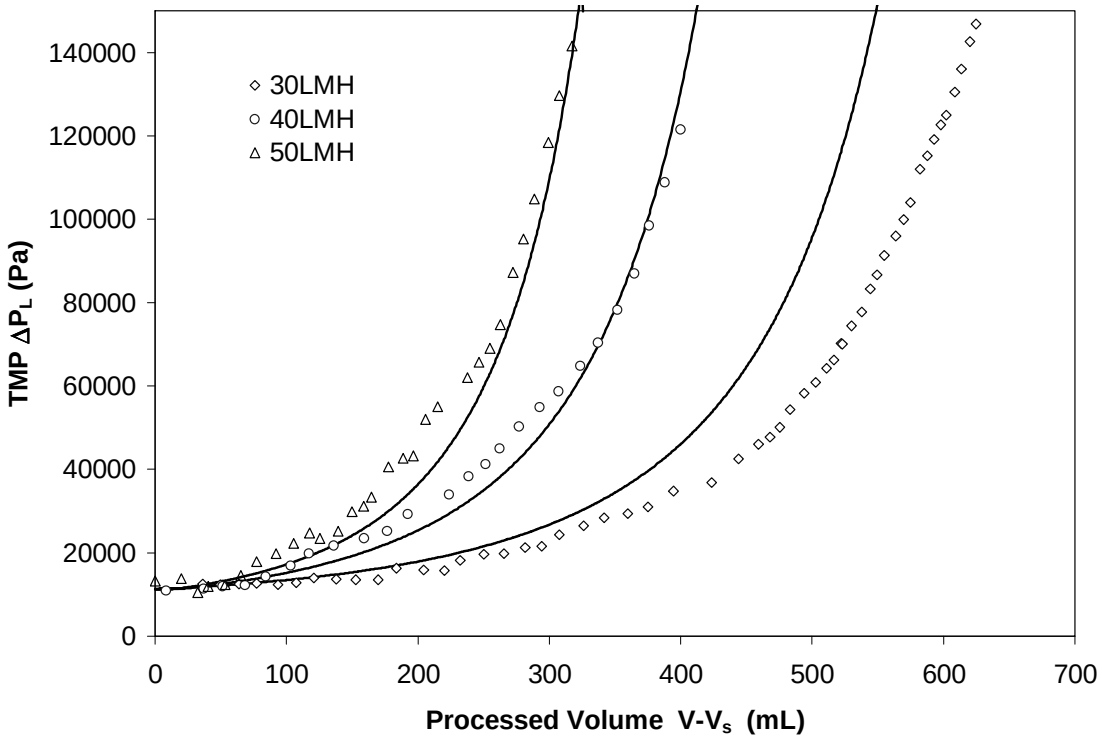

Figure 4-12 Comparison of TMP rise for 50, 40, 30, LMH from left to right for experimental constant flux filtration (dotted lines) and simulated (solid lines) for yeast pH=4.0.

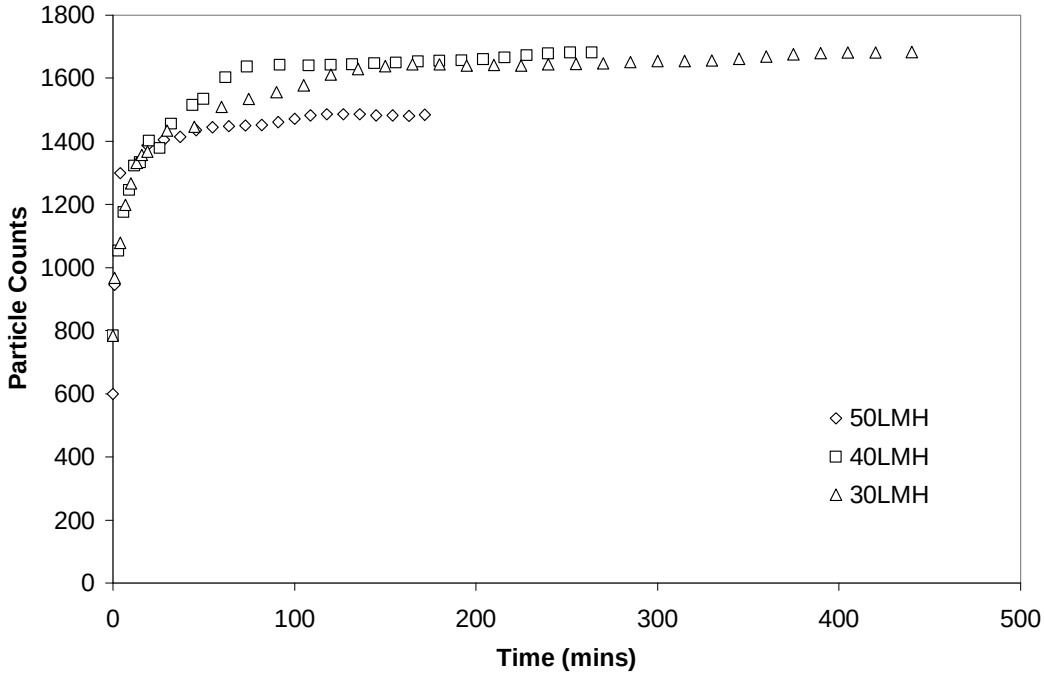

Figure 4-13 Measurements of particle counts taken with the Lasentec FBRM showing evolution to steady particle loading in the filtration cell (Yeast at pH4.0).

4.5.1 Comparison to Standard Filtration Approach

The standard filtration approach can also be readily applied to the constant pressure filtration data in order to obtain the specific cake resistance α. The constant flux pressure rise was calculated using equation 4-1 enabling comparison with the experimentally measured trends. Comparison of the results shown in Figure 4-8 obtained by the conventional approach with those obtained using the approach developed in this paper serve to illustrate the limitations of standard models that neglect local cake properties. To calculate the specific resistance, the standard t/V versus V plot was generated and the slope of the linear region determined (Figure 4-14).

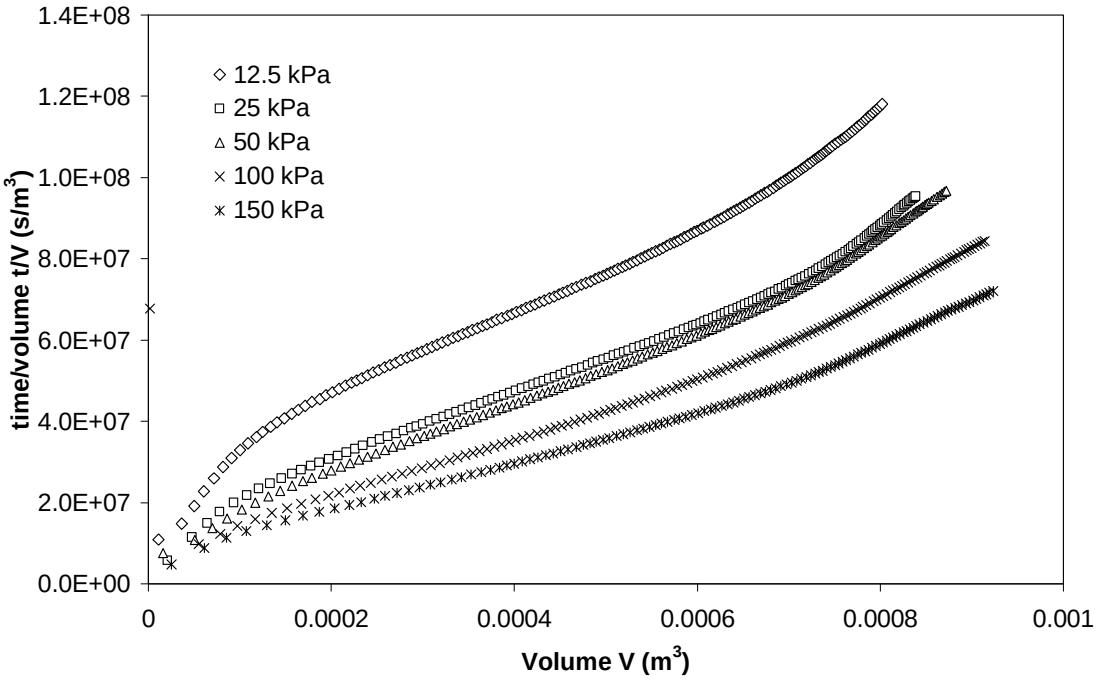

Figure 4-14 *t/V* versus *V* for flocculated yeast.

The calculated resistance values show definite dependence on pressure confirming the compressible nature of the yeast cakes. The degree of compressibility is represented by the power law exponent in equation 3-1. A log-log plot of resistance versus pressure is shown in Figure 4-15 and a compressibility of n=0.86 calculated.

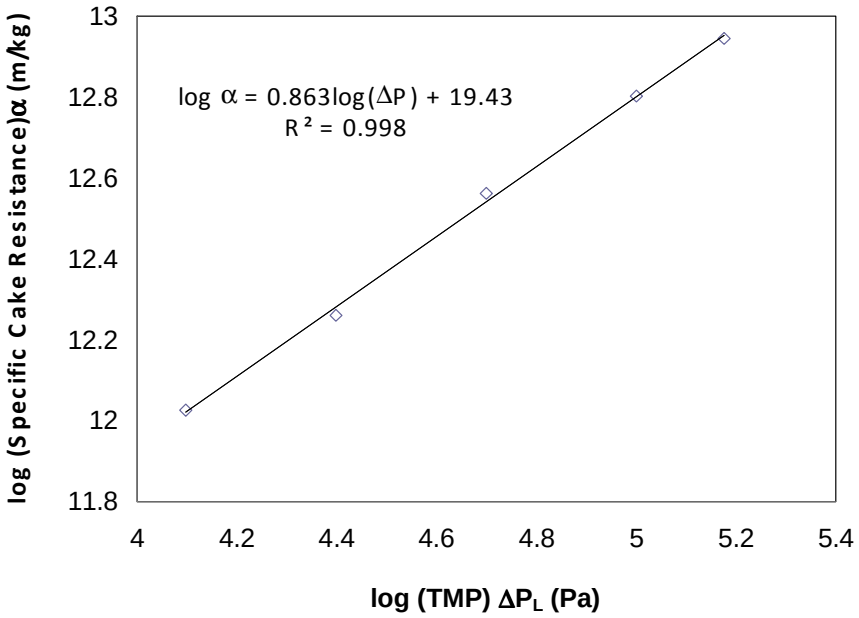

Figure 4-15 Compressibility of flocculated yeast cake.

It is stressed that the compressibility exponent measured via these means is not a local property and represents the dependence of **average** specific resistance on pressure. The value here was then used in the subsequent calculation of the constant flux behaviour of the flocculated yeast material. An average specific resistance (α_{av}=4.8e12), based on an average between 12.5 and 150 kPa, was used with the conventional constant flux equation 4-1 to represent a simple approximation of the constant flux behaviour. In addition, a better approximation was obtained by accounting for the pressure dependence of α and hence an iterative scheme is used to incorporate equations 3-1 and 4-1. The resulting constant flux trends for both of these approaches are compared in Figure 4-8 to the results obtained using the computational method developed in this paper and the experimentally determined constant flux results.

Of particular interest in Figure 4-8 is the extent to which the predicted rate of pressure increase is greater than the experimentally determined rate of increase. This steeper rise in pressure is consistent with an assumed average specific resistance with respect to cake depth. However the extent to which the additional assumption that the specific

resistance is reached instantaneously (for any given P_S) contributes to a faster TMP rise is unclear. To explore this issue the constant flux model was configured such that the simulated cake formation and consolidation processes occur instantaneously. By assuming that the steady state solid fraction ϕ_∞ is a function of the known solids pressure

$$\phi_\infty = \phi(P_s) \tag{4-24}$$

the resulting local permeability profile was calculated and the resulting pressure rise determined. As can be seen in Figure 4-8, the pressure rise for the assumed instantaneous consolidation results in a faster TMP rise with the difference between the standard filtration approach and experimental result most likely associated with the fact that an average specific resistance has been assumed. For a given mass of cake, too much weighting is placed on the low porosity region of the cake and hence is an over estimate of the specific cake resistance. This issue is unavoidable as the non-uniform porosity profile is inevitable in compressible cakes such as those formed from flocculated yeast.

4.5.2 Stopped Feed Experiments

The result of an abrupt cessation of the yeast feed at a constant rate of 50 LMH is shown in Figure 4-16. The observation that pressure continues to rise indicates that the consolidation process is far from instantaneous. This trend was observed on all occasions when stopped feed experiments were conducted and is not isolated to the single result shown here. However, to convey the concept, only a single experimental result is shown.

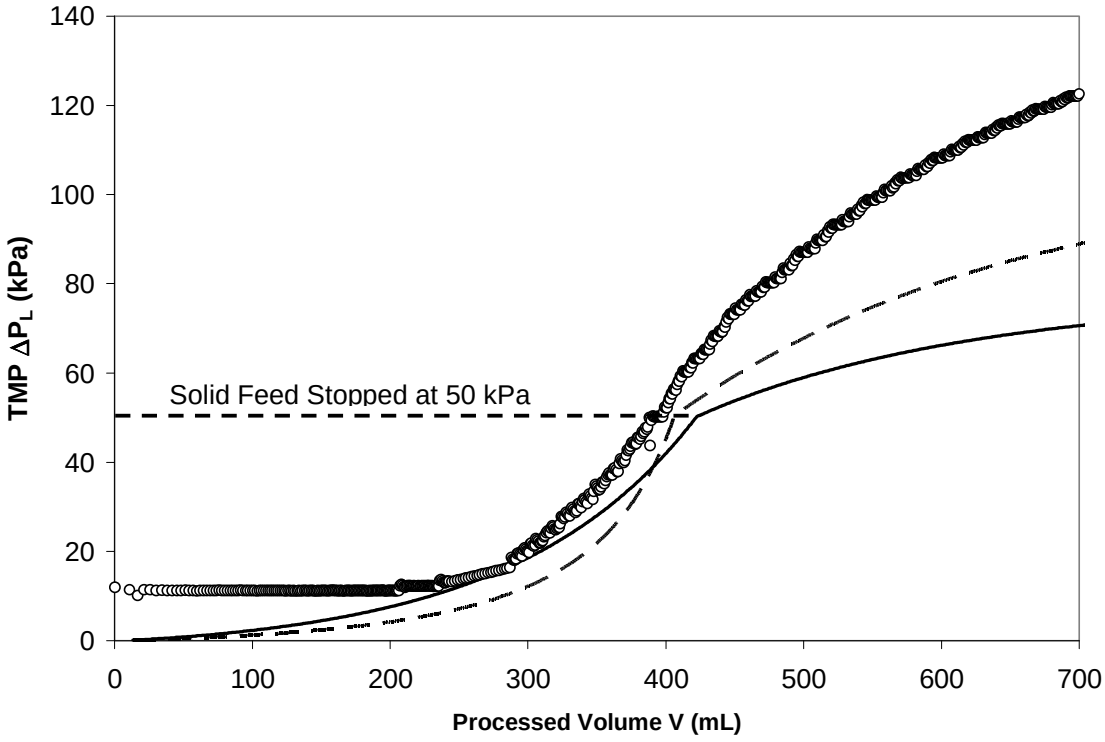

Figure 4-16 TMP response to change in feed conditions for constant flux filtration of yeast 50 LMH (o), model predicted (solid line) and sensitivity to 50% increase in permeability exponent (dashed line).

Also presented is the model predicted response to a step change in the feed. The model predicted TMP rise is not as large as that observed experimentally. The significant difference between observed and predicted TMP increase is of concern and suggests that there may be other consolidation mechanisms at play that lead to further consolidation of the cake. Figure 4-16 also shows the expected change in TMP rise as a result of a 50% increase in the C_2 parameter to a value of 3.9. An artificial increase in this parameter has the effect of decreasing the overall permeability of the simulated cake to yield a theoretical response curve that matches the experimental one. It is not unreasonable to suggest a perfect fit between model data can be obtained through adjusting this permeability exponent. However, no fundamental insights would be gained from such an approach. In order to reproduce the experimental response curve it may be necessary to model other time dependant effects in addition to simple cake resistance retardation effects. Phenomena such as creep consolidation may account for the remaining pressure difference between the model and experimental data with additional attention to this issue discussed in the following results section.

4.5.3 Parameter Fitting the General Equation with Time Constant

As was shown in section 4.5.1, the general equation (equation 4-1) for constant flux filtration was a poor fit to the experimental data. This was due mainly to the inaccuracy of the power law constitutive relationship (derived from standard *t/V* versus *V* data) in describing the compressibility of the yeast material. This is related to the degree of non-uniformity through the cake. Furthermore, the issue of transient effects in the consolidation of the cake confounded this issue. For example, in the absence of transient compensation, trying to describe the experimental data with a single compressibility exponent (*n*) across all flux (*J)* is not possible. This results in large error between model and experimental data.

A modified general equation with time constant for consolidation was derived in section 4.3.2 and fitted to the experimental data here. A sum of square error minimisation routine was implemented to derive the compressibility parameter and time constants. Figure 4-17 and Figure 4-18 show the model fit and corresponding time constants for the constant flux filtration runs. In all runs, with the exception of 15 LMH, good fits of the experimental data result. The exception at 15 LMH is possibly due to settling effects beginning to dominate over the longer experimental run.

Thus, a sensible approach to modelling constant flux filtration is to numerically deduce the compressibility exponent from constant flux filtration data rather than from *t/V* versus *V* data. As stated in the previous section, the *t/V* on *V* approach is a poor approach to characterising the cake as a there is significant issues with averaged cake properties and hence, values derived from this approach are not generally applicable to all filtration.

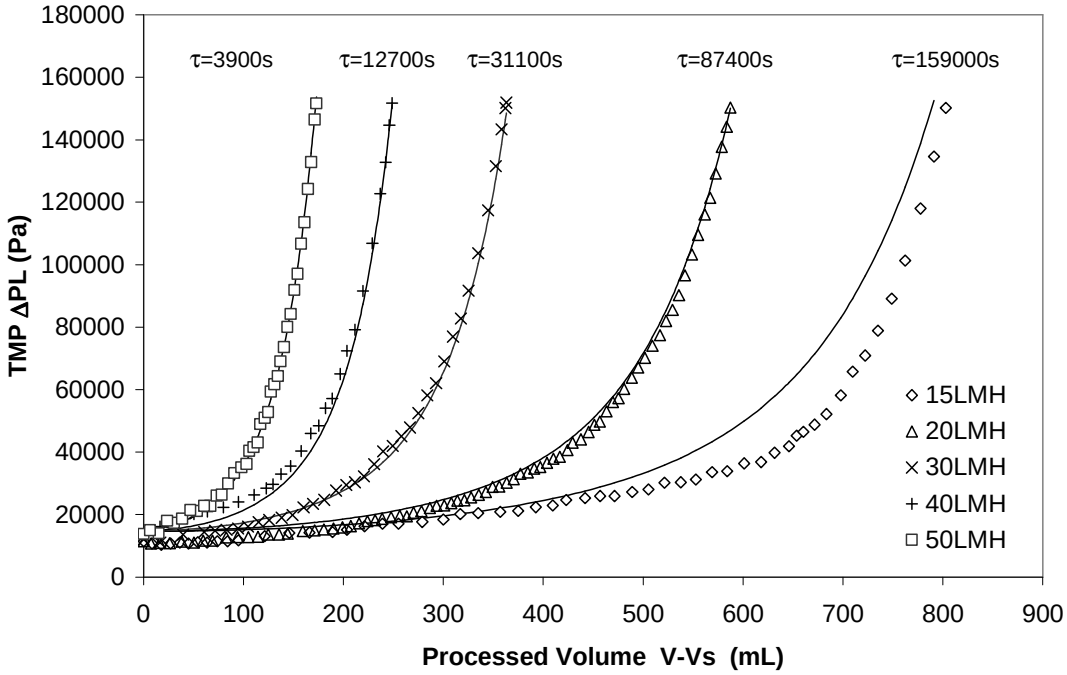

Figure 4-17 Time constants for consolidation calculated from SSE minimisation routine for yeast at pH 4.0. The modified general equation appears to be an excellent fit to the data. The calculated common value for the compressibility *n* was 0.835.

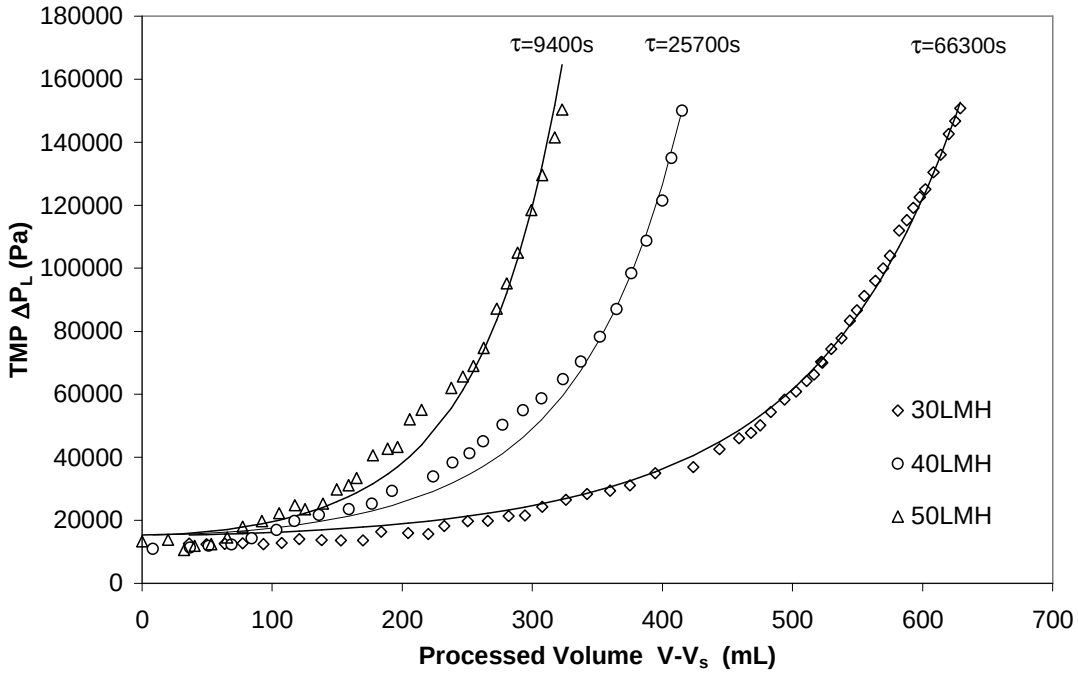

Figure 4-18 Time constants for consolidation calculated from SSE minimisation routine for yeast at pH 2.7. The calculated common value for the compressibility *n* was 0.799.

For both yeast filtrations at pH 4.0 and pH 2.7, the time constant is plotted as a function of steady state flux in Figure 4-19. A power law function empirically describes this relationship very well in both yeast cases. Such a result implies that as one increases the rate of filtration one gets a faster response from the consolidating cake, presumably because there is a greater amount of compressive force acting to bring the cake to equilibrium faster.

In reality, the dynamic behaviour of the cake is a complex function of the applied pressure, compressive yield stress, permeability and creep behaviour. It was possible to calculate the time constant from the cake simulation described in section 4.3.1, but the values calculated were of the order of 10-30% of the actual experimental values. This could imply that there is a considerable creep component for the yeast material that can't be accounted for by conventional mechanical models. Thus a better approach for industrial applications may be to resolve the time constant empirically rather than attempt to model the complex mechanical behaviour from the material properties.

From an optimisation point of view, if a cake were to exhibit a gentle slope (power law exponent in the τ versus J relationship), then effectively the operation of the filter can be extended over a wider range of flux values before the inevitable sharp rise in pressure occurs. In addition, for materials which exhibit a steeper slope, it may be economical to operate at the lower flux.

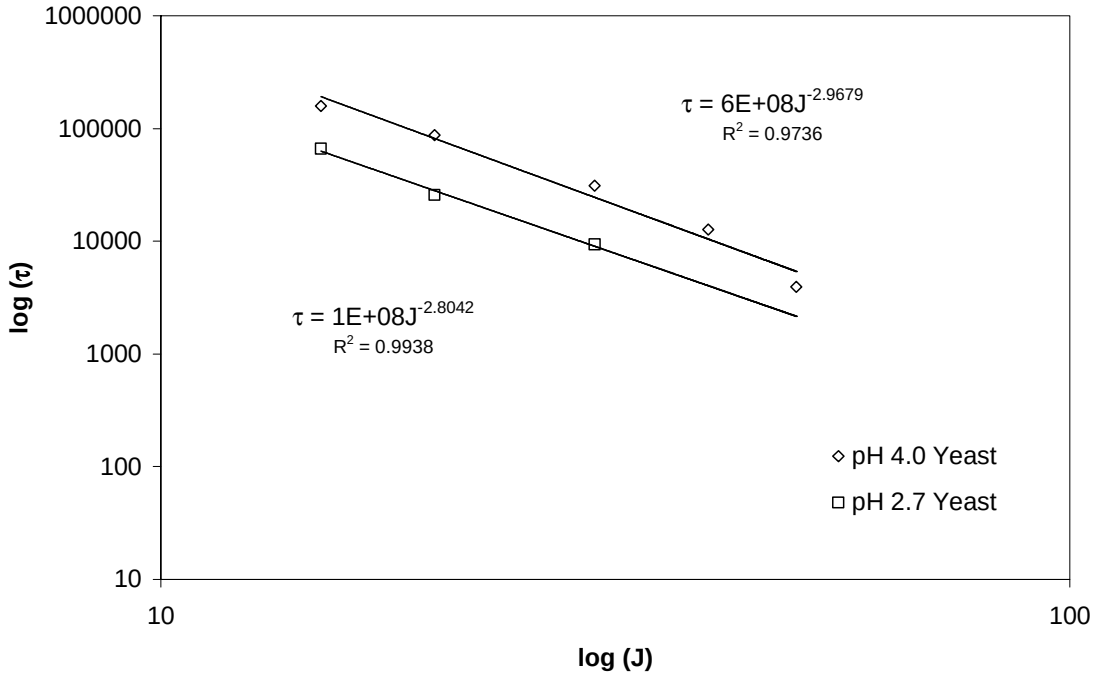

Figure 4-19 Log-log plot of consolidation time constant versus flux showing that a function of power law form describes this relationship well.

4.6 Conclusion

In this study, it was demonstrated that it is important to consider the variation in cake properties as a function of cake depth for theoretical treatment of constant flux filtration, at least for a compressible assemblage such as aggregated yeast. A new technique for predicting the constant flux behaviour for a yeast particle system for a given set of material properties (compressive yield stress and permeability) has been demonstrated. Good agreement was observed between experimental and simulated TMP rise, based on independently measured material properties. The remaining difference is likely attributed to additional consolidation effects not accounted for in this study. Comparison with the standard filtration approach suggests that significant

improvements in predicting the TMP rise are gained from accounting for local cake properties, though attention to phenomena contributing to slow consolidation of compressible cakes is also required. This is a possible reason for the discrepancy between experimental and simulation results as the systematic difference in pressure drop (i.e. simulation pressure drop is higher than experimental for all results) appears consistent with this.

A modified general equation based on the standard filtration approach was derived to take this slow consolidation effect in account. Where a system exhibits slow creep behaviour, it was shown that it is possible to empirically model a time constant. An empirical approach in cases where creep behaviour is not well described by mechanical modelling can be satisfactorily approached through empirical modelling from a set of constant flux filtration results.

Chapter 5: Simulation Studies into Floc Properties and Filtration

The fundamental reason why pre-coagulation is advantageous in membrane filtration is related to the enhanced permeability of the cake layer that results from increased cake porosity. Fluid can either be transmitted through pores enclosed within the floc structure or between the pores created by adjacent packed flocs. Commonly, a reduction in filtration performance with time occurs and can be attributed to the extensive collapse of the cake network which occurs under applied solids stress. Particulate simulation of cakes formed from consolidated fractal aggregates can potentially reveal how the pores change during collapse. In this Chapter, a methodology for simulating the particle physics governing the dewatering of a cake formed from flocs of precisely controlled size and fractal dimension is described.

5.1 Aims

The fundamental principles governing the transmission of fluid through the porous cake structure were detailed in section 2.2.1. The hydraulic pathway favours the largest pores according to equation 2-9 (i.e. ΔP is inversely proportional to the pore size squared). A particular focus of the study reported in this Chapter relates to examination of the characteristics of the pores in the cake as the overall cake volume decreases through use of particle physics simulation. Figure 5-1 illustrates the change in pore size of the largest flow pathways as the cake collapses under pressure. In this chapter this phenomenon is explored with a view to quantitatively characterising the pores in the cake for different starting suspension characteristics (i.e. size, structure and bond strength).

Section 2.2.1 also describes how flocs provide both interfloc and intrafloc porosity when brought together as a network of interconnected particles. The hypothesis is proposed that as the network consolidates and the void space is displaced by solid mass, a proportion of the pores retain their size more effectively. The implication of the statement being true is significant in that it would potentially explain why

flocculation is advantageous in cakes that have undergone extensive collapse (i.e. there are still some larger pores that could support flow despite extensive collapse).

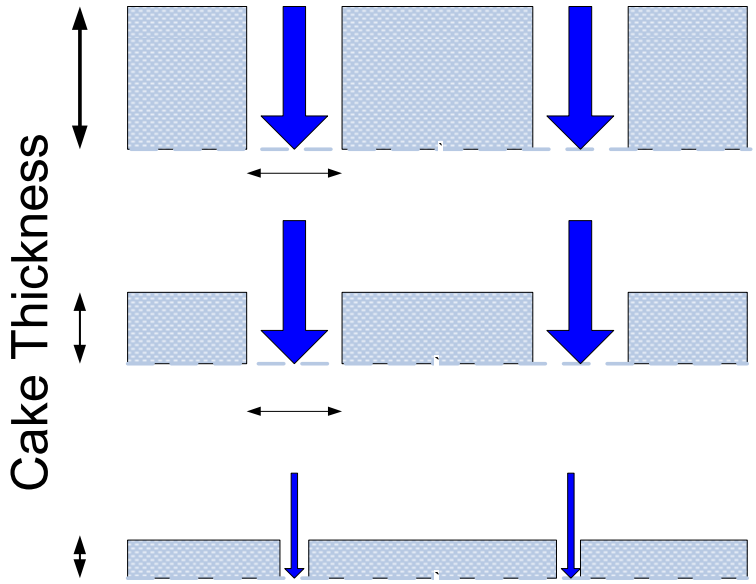

Figure 5-1 **Conceptual diagram illustrating the** change in pore size with collapse in overall cake volume.

5.2 Background

The study of flow through flocs has been aided by the novel use of microscopy tools such as CLSM (confocal laser scanning microscopy) to produce 3D-structures of flocs. Recent studies by Chu on activated sludge flocs have provided intimate detail on the nature of advective flow through pores supported by CLSM coupled with CFD analysis (Chu and Lee 2004a, Chu and Lee 2004b). The interior structure of flocs was shown to be heterogeneous with pore tortuosity paying an important role in flow retardation. Major findings from these studies were that larger pores support the bulk of flow transmitted through a bed structure comprised of flocs. The fractal dimension was determined to not significantly affect flow pattern (Chu et al. 2005). It was also observed with activated sludge floc that there was a two level structure (Chu et al. 2004) in the sense that the geometry of larger pores differed from that of smaller pores. These findings represent some of the most significant experimental insight into the nature of fluid transport through flocs. However, it must be pointed out that the work of Chu focuses mainly on relatively unconsolidated floc assemblages and is not directly applicable to membrane filtration.

Attention to some of the issues associated with cake collapse in membrane filtration was raised by Cabane et al. (2002) in a study in which the structure of membrane cakes was examined. A non-intrusive method of small angle scattering verified that extensive collapse of the fractal structure occurred but flagged that strengthening the bonds between particles, possibly by chemical conditioning, could result in a structure which could resist collapse.

The nature of the collapse in these thin cakes formed from fouling gels has remained largely unknown. Meireles et al. (2004) conducted an experimental investigation into the fouling of membranes using yeast as a model contaminant. In that study, a surface layer effect involving a highly compressed skin of yeast cells is one possible scenario for cakes exhibiting high resistance. This presumably arises because of a significant pressure gradient across a monolayer of yeast spheroids. However, the pressure distribution associated with this scenario would imply a large proportion of the cake being in a loose, unconsolidated state. This was not observed in Chapters 3 and 4.

The alternate hypothesis is that the pressure gradient is less steep and arises because of cell deformation through the entire cake. This is more consistent with experimental observations in Chapters 3 and 4 as yeast cakes appear uniformly firm at moderate pressures.

The compressive deformation of yeast cells in some ways can be similar to the syneresis effect experienced by gels in the sense that there is significant reduction in porosity when the phenomena occurs (Vandijk and Walstra 1986). The yeast cell is a soft hydrated entity composed of a high proportion of bound, extracellular water and, as such, is a good model to mimic the compressibility and permeability of gels. Thus yeast was chosen for this particular study as it also meets the criteria of having high sphericity and monodispersity, a useful feature as the simulation of cake collapse is naturally of uniform spheres.

5.2.1 Permeability of Cakes Undergone Collapse

The permeability of packed beds has been studied extensively and the principles can be applied to some extent to membrane filtration. The use of the Carman-Kozeny

relationship is common in membrane literature owing to its general applicability to a wide range of systems however it has been identified to be a good approximation only for solid volume fractions greater than 0.5 (Veerapaneni and Wiesner 1996). Happel and Brenner (1965) derived an approximation for the constant *k* in the Carman-Kozeny equation based on solution of the Navier Stokes equation. This expression has been used in several numerical filtration models including Lu et al. (1998b) as a mechanistic *P* vs. ϕ relationship.

The Happel model provides a better description of the Darcian permeability as the solid volume fraction approaches the dilute limit (Happel 1958)

$$K_d = \frac{2a_P^2}{9\gamma_1^3}\frac{\left(3-\frac{9\gamma_1}{2}+\frac{9\gamma_1^5}{2}-3\gamma_1^6\right)}{(3+2\gamma_1^5)} \qquad (5\text{-}1)$$

where $\gamma_1 = \phi^{1/3}$. Both the Carman-Kozeny and Happel models will be compared to results of this study.

The Brinkman (1947) model is an extension of Darcy's Law describing the flow through a porous spherical shell. Kim and Yuan (2005b) applied this model to assessment of the impact of fractal aggregates on specific cake resistance. This work was based on a simple hydrodynamic model with a solid core and porous shell being replaced by a fractal aggregate.

For an ideal aggregate with quadratically increasing permeability with size, the permeability is given by (Kim and Yuan 2005a)

$$K_d(r) = k_P r^2 \qquad (5\text{-}2)$$

where k_P is the permeability prefactor. This ideal aggregate was the subject of a subsequent study by Kim and Yuan (2006) into the specific cake resistance of a swarm of aggregates formed in the diffusion-limited-cluster-aggregation (DLCA) regime. The approach used by Kim and Yuan (2006) is particularly useful in the approach to the dilute limit. However, this approach is limited in it can not address cake collapse or, in the context of the current study, inter-aggregate overlap.

The models presented here to some extent describe the hydrodynamic behaviour of flocs and the resulting cakes over a range of conditions. However, these models were not explicitly derived to account for the history of the floc particularly after they form an interconnected network and extensive collapse results in a loss of the original fractal identity. A suitable approach to address this issue is by way of characterising the permeability as a measurable hindered settling function $R(\phi)$ as described by Landman and White (1992). Recent works by Usher et al. (2001) and de Kretser et al. (2001) demonstrate rapid techniques for determination of this parameter. By explicit determination of this parameter the dependence on floc history can be incorporated into the parameterisation of the material properties as constitutive relationships. Such an approach was employed in Chapter 3 by way of the unrestrictive permeability function approach.

The work presented in this chapter shows that the permeability of a cake formed from fractal aggregates of different size and structure can potentially exhibit history dependence after extensive collapse. The implications for membrane filtration are significant as the approach to modelling permeability of collapsed cakes would require this additional consideration.

5.3 Methodology

The rigorous simulation of a consolidating cake based around computational particle physics has been developed in these investigations. A workflow is developed here which integrates several independent functions to provide a tool for simulating floc consolidation. Associated metrics were also developed to enable direct comparison of predicted results with real experimental data. The procedure involves generation of virtual flocs which essentially are a set of coordinates and radii for each particle which makes up the floc. When spheres are overlaid at the centre of these coordinates and structure visualised, the image of a floc becomes apparent (Figure 5-2). When this routine is called upon sequentially, a virtual suspension of randomly generated flocs can be created. A suspension of flocs is represented as a list of spheres which comprise the entire suspension. When this is plotted, the suspension bound by the simulation boundaries take shape (Figure 5-3). This suspension forms the starting point for the rigorous particle simulation outlined in the workflow (Figure 5-4).

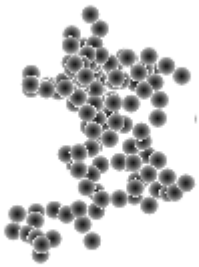

Figure 5-2 2D Image of a floc created by placing black circles at sphere coordinates in order of furthest to nearest.

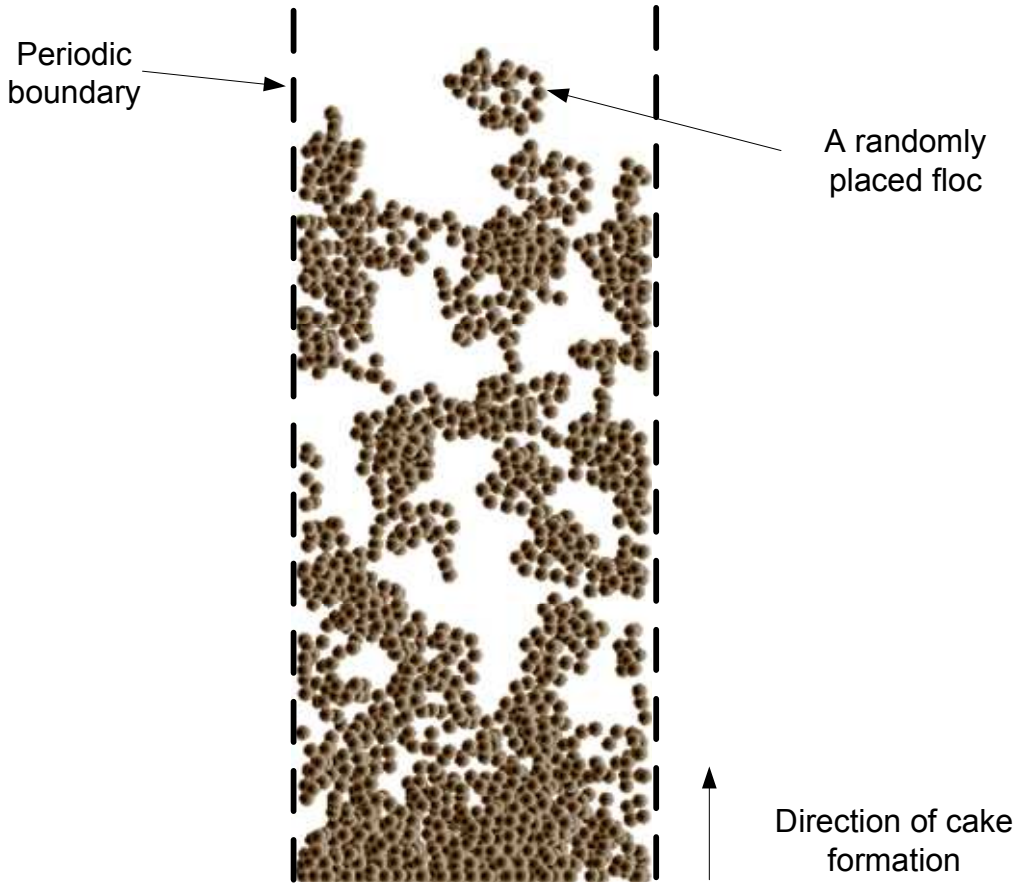

Figure 5-3 DEM suspension comprised of randomly placed flocs.

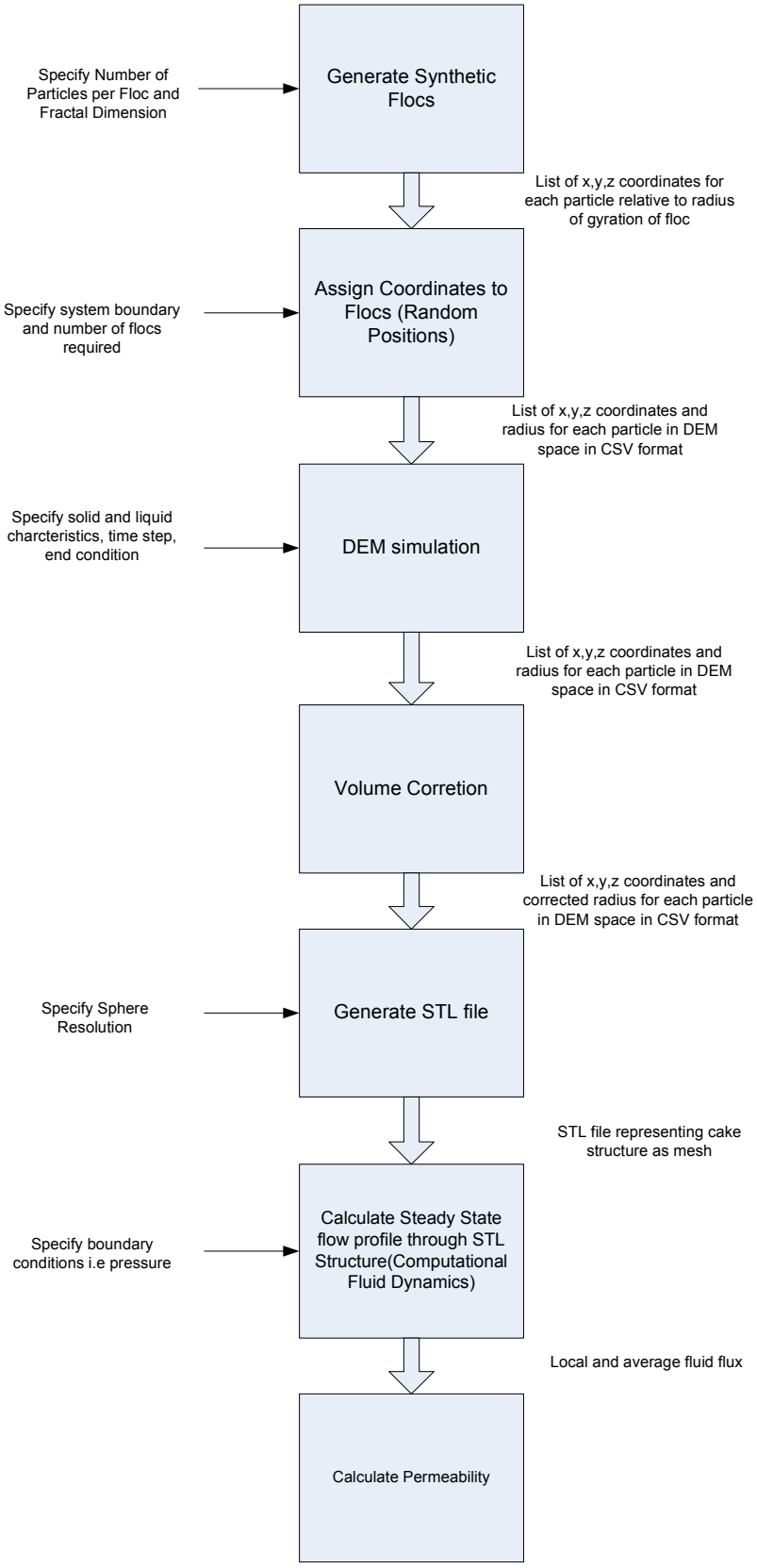

Figure 5-4 Workflow describing method to simulate cake consolidation.

For this work, the process of consolidation was induced by exerting a compressive stress on the DEM particle bed equivalent to the local solids pressure experienced in filtration runs in Chapters 3 and 4. The extent of dewatering was adjusted to approximately equal that measured during filtration runs by tuning the physical interaction between particles. The resulting virtual cake structure is a series of highly packed sphere coordinates similar to a real yeast system (Figure 5-5). Such a format can easily be converted to a CFD compatible mesh in order to measure the hydraulic characteristics of the structure. Details of the DEM implementation are given in the following section.

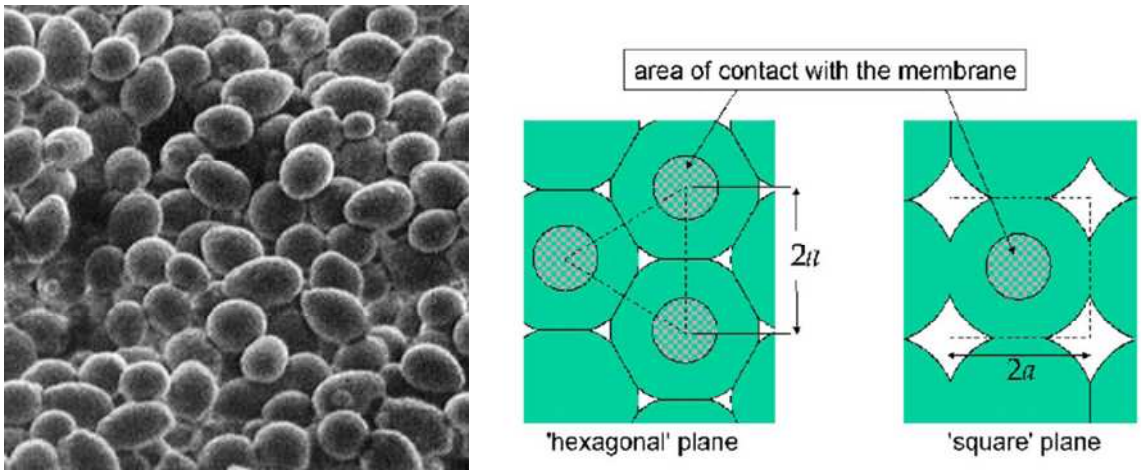

Figure 5-5 SEM image of packed yeast cells showing spherical shape of discrete particles(left) and packing of deformable spheres taken from Meireles et al. (2004) (right).

5.3.1 Discrete Element Method

The DEM approach developed by Cundall and Strack (1979) models and mimics the physics and interactions of discrete individual particles in a virtual system and is implemented as a rigorous particle simulation. The physical specifications such as mass, radius and position are first made for each discrete particle in the model environment. Properties of the filtrate liquid phase are specified in terms of density, viscosity and temperature. In addition to this, the properties describing the system chemistry are accounted for in terms of electrolyte strength for DLVO systems (i.e. theory describing electrostatic interactions based on the work by Derjaguin, Landau, Verwey and Overbeek) and empirical particle interaction models for non-DLVO

interactions. Newton's second law is implemented in a discretised manner, integrating over discrete time steps to predict the succeeding velocities and positions of all particles in the system.

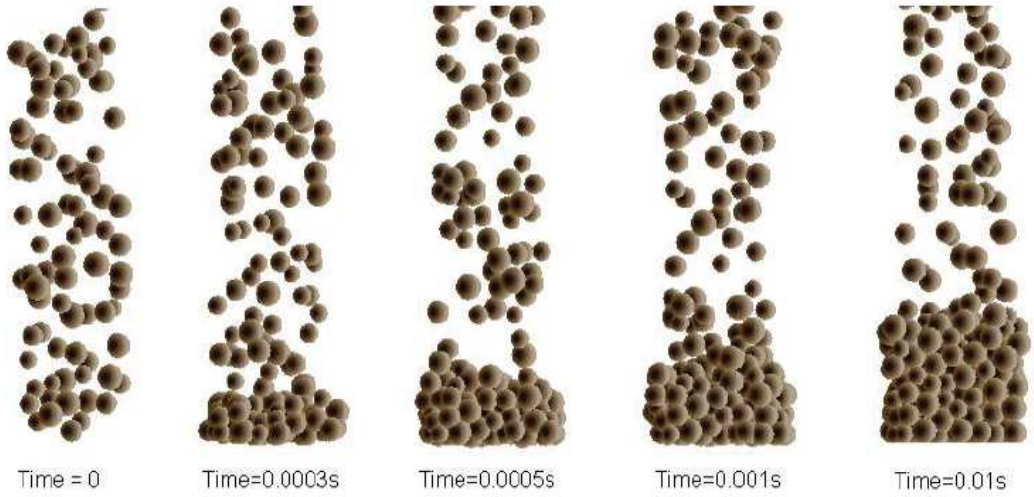

Figure 5-6 Evolution of a system of several hundred particles in response to a simple downwards acting hydrodynamic force with a particle-impermeable membrane at the bottom of the Figure.

The results obtained through simulation are precise geometrical information about the particle positions in the cake at various stages of consolidation. Extraction of pore size information is also possible in addition to a geometrical structure that can be analysed by conventional CFD methods (Selomulya et al. 2006).

5.3.1.1 Similar DEM Work by Others

Others have attempted to examine the dynamics of packing of spheres (Zhang et al. 2001) using DEM. Zhang aimed to uncover the most dominant mechanism of resistance to collapse in the sphere packing structure. This work is conceptually a similar problem to that investigated in the DEM simulation in that concepts relating to forces that act to resist collapse in cake structure will be encountered. Physically, the key differences are that for the yeast system there are additional hydrodynamic forces due to permeate flow and liquid medium instead of gaseous medium. Zhang concluded that interparticle friction forces are the main mechanism resisting compaction of the stable structure. This is a reasonable conclusion as their DEM

results clearly demonstrated a strong dependence of packing density on friction coefficient in the presence of gravitational force only. For filtration systems it is suspected that friction contributes to the network strength, over which there is virtually no control.

The mechanisms of cake collapse were studied by Botet and Cabane (2004) using synthetic fractal aggregates. These investigators verified that structural effects remained after consolidation due to the original fractal structure in the so called elastic regime. The proposed behaviour of cake collapse for structures of low compressive yields stress was closer to traditional plastic behaviour (i.e. fluid behaviour consistent with random bond breakage and reformation). For systems comprised of strong fractal backbones, an elastic behaviour was observed. In all regimes, the convergence at high solids compressive pressure was found to resemble closed packed spheres. As these spheres were quoted as being hard, the study is limited and does not necessarily reflect compressible spheres like yeast.

Ni (2001) also examined the process of cake formation based on the principles of particle packing using DEM. This study incorporated a fluid dynamic algorithm to account for particle-fluid interactions during the cake formation process. The scope of this study was mainly centered on comparison with conventional filtration models and hence the simulation was configured to directly simulate the cake formation process (i.e. building up of a cake). As the suspensions were not structured, the average cake solid fraction remained relatively constant during the cake formation process and thus insight into the effects of cake compaction were limited. In this Chapter, an elemental approach (fixed mass slice) was taken mimicking the methodology described in Chapter 3 rather than mimicking the entire cake filtration process as described in the study by Ni (2001).

5.3.1.2 Mechanics of DEM

The DEM simulation accounts for all forces that are imparted on each particle. The calculations are performed in rectangular coordinates (i.e. x, y and z directions). The translational movement $\Delta\mathbf{s}$ during time step Δt is given by

$$\Delta \mathbf{s} = \mathbf{v}\Delta t + \frac{\mathbf{F}\Delta t^2}{2m_i} \tag{5-3}$$

where **v** is the particle velocity, m_i is the particle mass and **F** is the summation of all forces acting on particle *i* which is given by

$$\mathbf{F} = \sum_{j=1}^{k} (\mathbf{f}_{c,ij} + \mathbf{f}_{f,ij} + \mathbf{f}_{DLVO,ij}) + m_i\mathbf{g} + \mathbf{f}_H + \mathbf{f}_B \tag{5-4}$$

In the above equation $\mathbf{f}_c$ represents contact forces (normal and tangential), $\mathbf{f}_f$ represents friction forces (rolling and sliding), $\mathbf{f}_{DLVO}$ is the interparticle forces, $m_i\mathbf{g}$ is the gravity force, $\mathbf{f}_H$ is the hydrodynamic force and $\mathbf{f}_b$ is the buoyancy force. Implementation of Newton's second law is performed in a discretised manner to predict velocities of particles at the next time step. This is given by

$$\mathbf{v}_{t+\Delta t} = \frac{\mathbf{F}_i\Delta t}{2m_i} \tag{5-5}$$

where $\mathbf{v}_{(t+\Delta t)}$ is the velocity at the next time step. The DEM loop sequence can be condensed into three main calculations as shown in Figure 5-7.

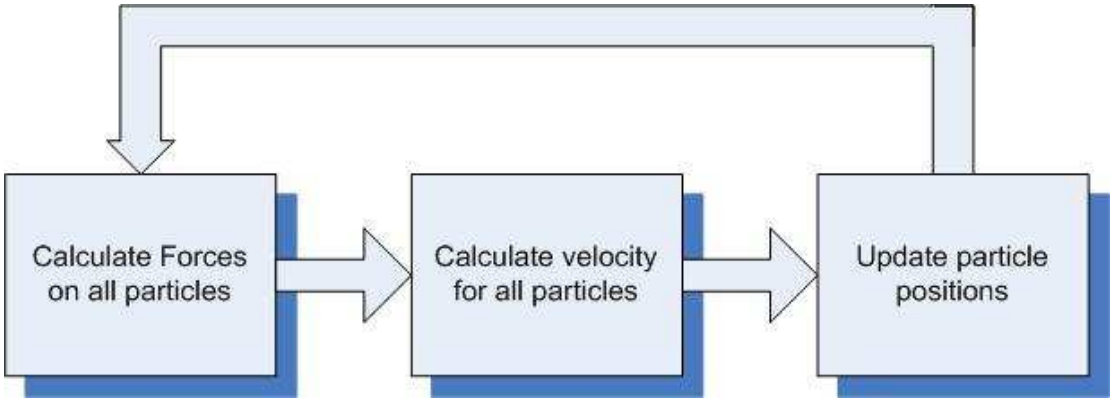

Figure 5-7 DEM loop sequence for calculation of particle movement. Time is incremented by Δt at the end of every loop.

This loop presented in Figure 5-7 is continued until a stop criterion is met. The results of this analysis are particle positions, velocities, etc, upon which a wide range of theoretical analysis could be performed.

5.3.1.3 DEM Setup and Execution

Ideally the most realistic simulation would involve millions, perhaps billions of individual spheres in a filtration column. Instead the computational expense of this exercise restricts particle numbers to a couple of thousand. A discrete approach is required to simulate a microscopic element of a reasonable number of particles. At any point in the cake, a fixed volume element of fixed mass is subject to a solid compressive pressure which results from cumulative drag force exerted by the fluid on the cake above. For the DEM the solid compressive pressure was emulated as a downward piston force exerted on the uncompressed cake. The forces are resolved at discrete time intervals and the motion of consolidation typically proceeds to a steady state (i.e. where the force contained in the bonds in the particulate network equals the downward piston force).

5.3.1.4 Colloidal Interactions in DEM

One of the most important elements for accurate simulation is the model to describe particle-particle interactions. Long range colloidal interactions are modelled based on DLVO theory (Shaw 1992). This model accounts for the electrostatic interaction profiles between charged particles which arise when particles are brought into contact with a polar medium such as water. This leads to the formation of an electric double layer which arises when ions of opposite charge to the surface are attracted and distributed around the particle. The interaction is based around a summation of van der Waals forces arising from induced dipoles between two particles and electrostatic repulsion resulting from like charges in adjacent electric double layers.

Electrostatic interactions arising from the mutual electric double layer repulsion can be represented by a model based around the solution to the Poisson-Boltzmann distribution. For the DEM, a model by Reerink and Overbeek (Shaw 1992) was chosen to describe the repulsive interaction between two spheres separated by distance H_{ij} and of radii r_1 and r_2 which is given by

$$\mathbf{f}_R = \frac{64\pi\varepsilon_d r_1 r_2 k_B{}^2 T^2 \gamma_1 \gamma_2}{(r_1 + r_2) e^2 z_i{}^2} \exp(-\kappa H_{ij}) \qquad (5\text{-}6)$$

where ε_d is the dielectric constant of water, k_B is the Boltzmann number, T is the temperature (K), e is the charge on an electron and z_i is the counter ion charge number. For equal spheres this reduces to

$$\mathbf{f}_R = \frac{32\pi\varepsilon_d r k_B{}^2 T^2 \gamma}{e^2 z_i{}^2} \exp(-\kappa H_{ij}) \tag{5-7}$$

where γ is given by

$$\gamma = \frac{\exp(z_i e\psi_o / 2k_B T) - 1}{\exp(z_i e\psi_o / 2k_B T) + 1} \tag{5-8}$$

and ψ_0 is the stern potential (mV) which is reasonably approximated by the zeta potential (Shaw 1992). κ denotes the inverse of the double layer thickness and this is expressed as

$$\kappa = \sqrt{\frac{e^2 \sum_i n_i z_i{}^2}{\varepsilon_o \varepsilon_d k_B T}} \tag{5-9}$$

where n_i is the number of ions per unit volume and ε_o is the permittivity of free space.

The attractive potential between two spheres of radii r_1 and r_2 separated by distance H_{ij} is given by an expression derived by Hamaker (Shaw 1992) to account for van der Waals interactions

$$\mathbf{f}_A = \frac{-A_H}{12}\left[\frac{y_a}{x_a{}^2 + x_a y_a + x_a} + \frac{y_a}{x_a{}^2 + x_a y_a + x_a + y_a} + 2\ln\left(\frac{x_a{}^2 + x_a y_a + x_a}{x_a{}^2 + x_a y_a + x_a + y_a}\right)\right] \tag{5-10}$$

where $x_a$and y_a are given by the following equations

$$x_a = \frac{H_{ij}}{r_1 + r_2} \tag{5-11}$$

$$y_a = r_1 / r_2 \tag{5-12}$$

A_H is known as the Hamaker constant which is characteristic to the material being studied. A value of $2.5\text{x}10^{-21}$ was used for this study (Hsu et al. 2001).

The combined electrostatic interaction is then given by

$$\mathbf{f}_{DLVO,ji} = \mathbf{f}_R + \mathbf{f}_A \qquad (5\text{-}13)$$

which is routinely implemented at equation 5-4 for the summation of forces on individual particles. This force is fairly significant in the process of flocculation and potentially significant in the behaviour of the cake. However, in a packed bed state, the dynamic rolling friction force, surface friction and elastic bending moment have an equally significant effect on how the cake behaves. These will be discussed in the following sections.

5.3.1.5 Friction Forces

Lu and Hwang (1993) studied the mechanism of cake formation and examined the influence of the critical friction angle on particle packing (Figure 5-8). The angle that two contacting particles make is θ_I in this figure. For particles depositing with high critical friction angle (i.e. the angle that can be sustained before the particle slips passed) the formed cake structure was found to be more porous in nature. At low critical angles θ_c=0, the cake resembles a close packed arrangement of particles.

Upon compaction by a compressive load such as in pressure filtration, the friction forces would contribute to providing strength to the network. However, for spheres packed in an electrolyte medium, the effects of electrostatic interaction may be dominant over friction forces at a particle-particle interaction level. Thus, the model presented by Lu and Hwang (1993) is only a limited representation of the process of cake filtration.

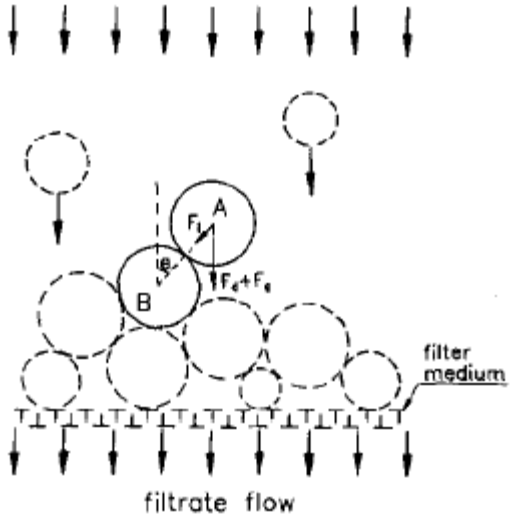

Figure 5-8 Frictional forces on a particle in a packed bed taken from Lu and Hwang (1993).

More detailed development of the friction forces between particles involves consideration of the dynamic rolling friction and elastic bending moment. A summary of each is given as follows:

i) *dynamic rolling friction;* The dynamic rolling friction is the force between two particles as they roll on each other. As this force is not critical to this study it will be considered analogous to surface friction shown in Figure 5-8. For this complicated topic the reader is referred to the work of Khan (2007) on the implementation of dynamic rolling friction in DEM.

ii) *elastic bending moment*; The elastic bending moment can be thought of as the rotational component of a spring interconnecting two particles that can both rupture upon separation by a critical distance or rupture if the angular displacement relative to the original contact position exceeds a critical angle. Figure 5-9 illustrates the elastic bending moment $\mathbf{T}_{EB}$ acting for the case where the bond is stretched by angular displacement from the original orientation. For this work it is calculated by

$$\mathbf{T}_{EB} = k_{EB}^{'} \left(\mathbf{\Phi}_{EB,ji} \right)_{total} \tag{5-14}$$

where $(\Phi_{EB,ji})_{total}$ is the summation of angular displacements at successive time steps since bond formation and k'_{EB} is the spring constant for bending motion. According to this equation the torque is proportional to the angular displacement from the original point of contact. When the angular displacement exceeds a critical limit, the bond breaks and the angular displacement is reset to zero.

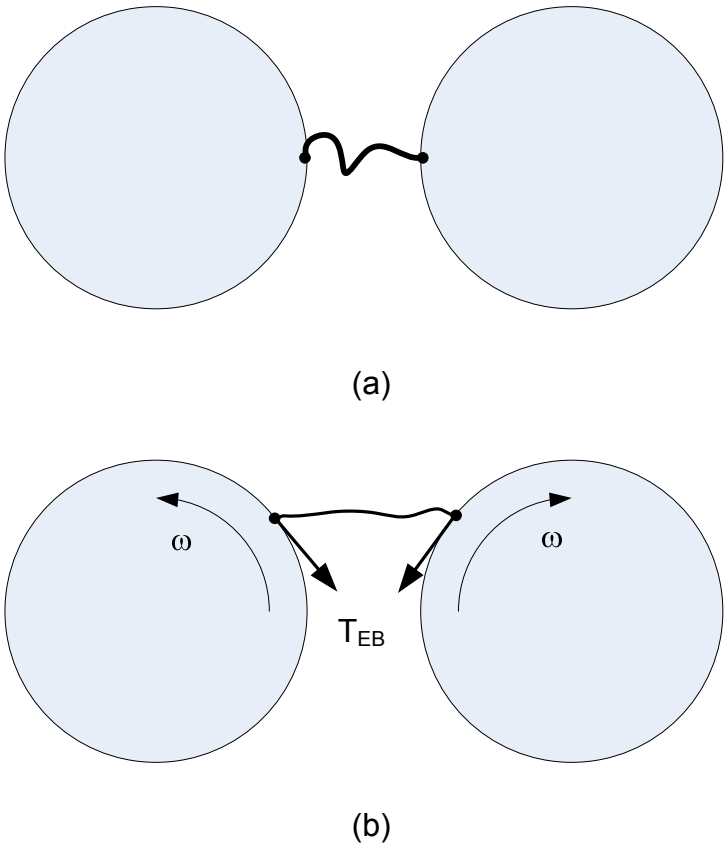

Figure 5-9 (a) bond between two particles and (b) after some angular displacement results in an elastic bending moment T_{EB} on each particle to retract the bond to its original angular position.

Both the critical limit and spring constant k'_{EB} are important parameters governing the compressive behaviour of the cake. For example, Figure 5-10 (a) illustrates a floc resting on a surface and (b) after some time the forces contained within the particle network, comprised of DLVO forces and friction forces with elastic bending moment, oppose the gravitational force and the floc retains its structural identity. However, in (c) where the forces contained in the structure comprised of only DLVO forces and friction forces (no elastic bending moment), the structure does not withstand collapse

(Khan 2007). For real yeast systems, the bed structure is retained under gravity for at least several times its own weight as was frequently observed in the experimental work. This stresses the importance of the elastic bending moment in recreating cake behaviour.

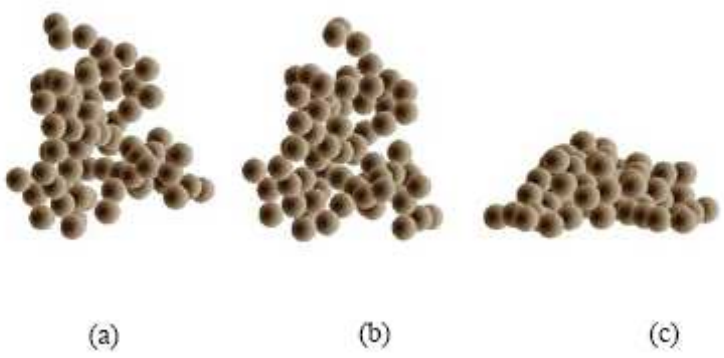

Figure 5-10 Simulation of a DEM floc sitting on a surface subjected to gravitational force (a) for different parameters, (b) after some time with elastic bending moment, (c) after some time without elastic bending moment (From Khan 2007).

In the simulation study the elastic bending moment parameters were adjusted such that the simulated compressive yield stress of the cake approximately mimicked the experimentally measured values. Exact reproduction of the behaviour was not sought as the hydraulic properties of the cake rather than the compression or shear rheology are the focus of this study.

5.3.1.6 Hydrodynamic Force Modelling in DEM

For this study, creeping flow around a sphere is assumed, and as such, Stokes law can be used to describe the viscous flow around the DEM spheres. For flow through a network of concentrated particles, the free draining approximation is made where the force exerted on each particle is proportional to the bulk fluid flow. This approach has been implemented previously in particle simulation studies by Doi and Chen (1989) which required relatively little computational time and is highly suitable for DEM. The resulting force exerted on a sphere of radius r by creeping flow is given by Stokes law as

$$\mathbf{f_H} = 6\pi r \mu \mathbf{v_t} \qquad (5\text{-}15)$$

where r is the particle radius and $\mathbf{v_t}$ is the particle velocity at time t.

It should be noted that the 1-D hydrodynamic force described here is not to be confused with the Lattice Boltzmann CFD technique applied at the end of the simulation to rigorously calculate the flow through the cake. Due to the computational expense required to calculate force of the permeating fluid on the particle at every time step during the simulation, the calculation was not implemented in the DEM. Hence, the consolidation and associated microstructural effects will be explained in the absence of fluid. The implications of such a compromise are uncertain as the local structural changes, particularly in the pores with fast moving fluid, could result in failing to reproduce pore erosion effects. Such an effect is suspected to be a potential mechanism to explain how pores retain their size during consolidation. But due to the lack of a realistic representation of the fluid this cannot be simulated.

5.3.2 DCLA Simulation (Synthetic Floc Generation)

The initial component of the workflow in the simulation procedure involves the preparation of virtual suspensions of flocs of known size and structure. Settling of the flocs and application of solids compressive pressure via a virtual piston compresses the flocs into a cake.

The generation of virtual flocs involves calculation of particle coordinates which make up the floc structure. The calculation is based on diffusion limited cluster aggregation (DLCA) and uses an algorithm to generate the coordinates of primary particles which make up a floc structure in three dimensional space. A tunable parameter can be presented to the algorithm which directly varies the floc fractal dimension from 1 to an upper limit of 2.55.

The Cluster-Cluster Aggregation (CCA) simulation was based around the Off-Lattice Variable-D Model as described by Thouy and Jullien (1996). To start with, the size of the floc which is intended to be created through simulation is controlled through choosing a number of identical spherical particles of unit diameter to be considered in the run. The process of simulated cluster-cluster aggregation is created through statistically modelled collision and sticking of primary particles at first, and as they

pair up, these pairs meet up with other pairs and the doubling growth continues in this fashion forming progressively larger clusters of 2^i particles at the i^{th} iteration step.

To control the structure of the aggregate being formed, a number of rules are imposed to the sticking of cluster to cluster during aggregate growth. These rules are geometrically modelled to incorporate into an iterative scheme which looks at two potentially matching clusters and determines where and how they should join to create the desired structure (D_f). The rule for sticking two aggregates (1) and (2) of N particles is chosen to satisfy

$$\Gamma_d^{\,2} = k_d^{\,2} R_N^2 + 1 \qquad (5\text{-}16)$$

where $\Gamma_d = G_1G_2$ is the distance between the centres of mass G_1 and G_2 of the clusters when they are in the sticking position, $R^2_N = (R^2_N(1)+R^2_N(2))/2$ is the square of the mean radius of gyration of the clusters and k_d is related to the input fractal dimension D_f by

$$k_d = 2\sqrt{4^{1/D_f} - 1} \qquad (5\text{-}17)$$

Knowing the parameter Γ_d given by equation 5-16 and centres of mass of clusters G_1 and G_2 the simulation randomly chooses a particle belonging to cluster (1) and a particle from cluster (2) and all possible geometrical arrangements are evaluated when they are joined in this way to ensure no overlap. Sticking of clusters (1) and (2) must also obey the following condition

$$\theta = \pi\zeta^{\sqrt{\frac{2}{D-1}}} \qquad (5\text{-}18)$$

where θ is the direct angle of contact, ζ is a random variable uniformly distributed between 0 and 1. For D_f=3, this ensures that θ is uniformly distributed between 0 and π and at the opposite extreme this reduces to θ=0 promoting the formation of a linear chain of particles when D_f=1. Figure 5-11 illustrates two clusters with centres of mass G_1 and G_2 potentially joining at J_1 at an angle θ.

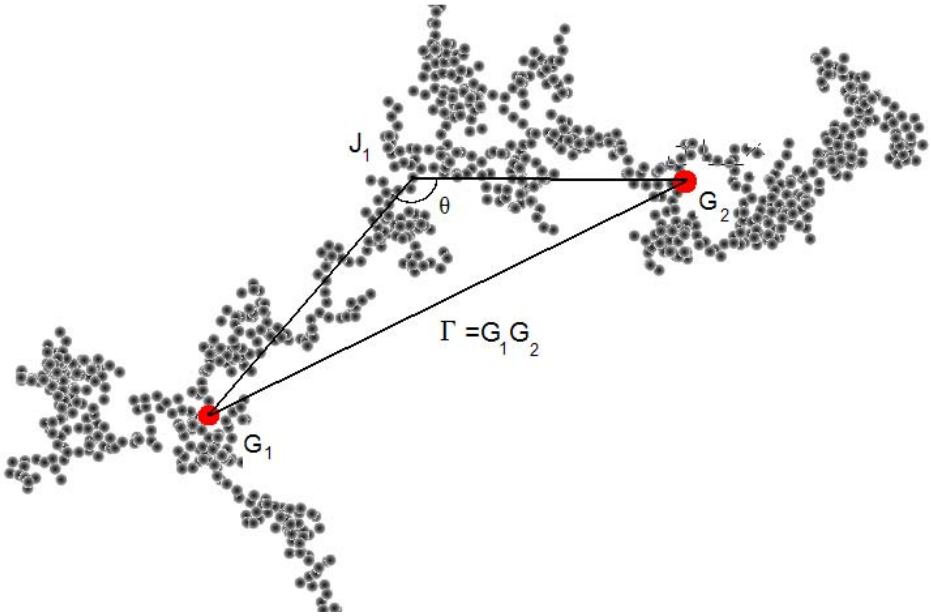

Figure 5-11 Illustration of two equally sized clusters forming a bond at J_1.

In evaluating the joining of cluster (1) and (2) at J_1 such that the criteria is met, the position of G_2 is moved in a circular arc with the arc centre aligning with the axis made by extending the line G_1J_1. The centre of mass of the floc at G_2 is rotated in such away that the angle of contact θ is maintained. If the rule criterion is not met for all possible positions on the arc a new random pair of particles are evaluated in the same way and the procedure is repeated until the sticking rule is met.

In this simulation a modification was made to the procedure described by Thouy and Jullien (1996) which incorporates a tuning parameter to select the fractal dimension of the simulated floc which replaces equation 5-17. This tuning parameter controls the over lap of the two clusters as a factor between 0 and 1 with 0 attempting to create a straight line of particles (D_f=1) and 1 creating a compact structure of D_f=3. The iterative joining of clusters is performed until one cluster remains which is the final aggregate concluding the simulation.

For the purposes of this experiment, the simulation is based on flocs made up of 1, 7 and 36 primary particle coordinates with tuning constants chosen to generate data that would yield a variety of flocs with a wide spread of fractal dimensions (Table 5-1). Several hundred flocs of each structure in Table 5-1 were simulated and stored in a database.

Table 5-1 Summary of data generated through CCA Simulation.

Tuning constant	Mass Fractal Dimension (D_f)
0.2	1.25
0.4	1.5444
0.45	1.6633
0.475	1.7257
0.5	1.7956
0.525	1.879
0.55	1.9726
0.575	2.0707
0.6	2.1803
0.62	2.2897
0.64	2.3902

5.3.3 Computational Fluid Dynamic Modelling

Lattice Boltzmann based simulation is used to compute the flow through the packed bed comprised of particular geometries determined from discrete element simulations. Using this technique it was possible to calculate the flow through a bed based on specified pressure drop and hence, the local permeability of the solid cake element of known solid fraction can be determined. This allows direct comparison with experimentally deduced local permeabilities of packed yeast spheroids.

5.3.3.1 Correction for Soft Particle Overlap

For a bed of soft monodisperse spheres it is perfectly reasonable to have a scenario where compression under moderate to high stress gives solid fractions which exceed the close packed solid fraction.

For a bed of virtual spheres whose spatial arrangement potentially exceeds the close packed solid fraction it is possible to have particle-particle overlap. In DEM, spheres are usually fixed in radius for the duration of the simulation. As the soft DEM particles overlap, solid volume is lost. Without compensation the calculated permeability from CFD analysis would likely be overestimated.

A simple correction for this involves a 1st order approximation for conserving system mass. Consider an arrangement of three spheres in Figure 5-12. When two soft spheres overlap for an extended duration of time the overlap is likely due to close packing rather than a collision. Under these conditions the normal force between two overlapping particles is a balance of repulsion describable by the bulk modulus of the material and the force bringing the two particles together related to the transmission of compressive stress through the system. In DEM, such a scenario results in the closing of pores (Figure 5-12).

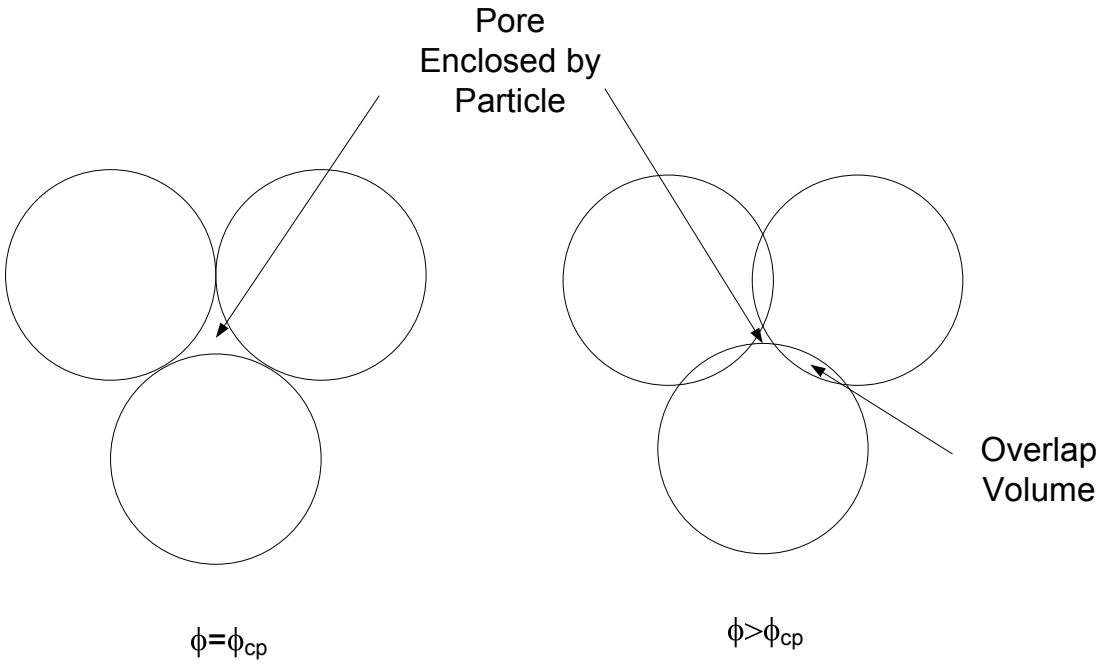

Figure 5-12 Pore formed by union of three adjacent particles reduces in size due to overlap correction in order to conserve total volume.

In a real system of soft particles, the same scenario results in a redistribution of volume to ensure solid volume conservation. For example, Figure 5-13 shows for the simple three sphere system how a flat contact between adjacent spheres results in a change in radius of curvature of the uncontacted region.

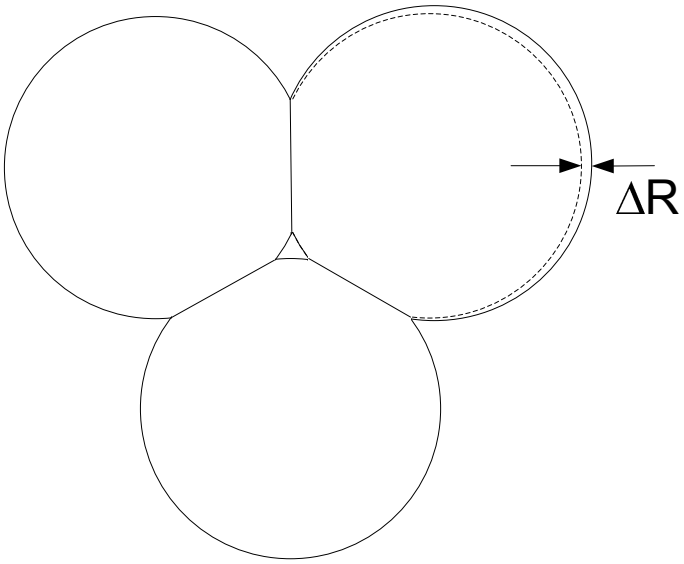

Figure 5-13 Representation of the union of three particles which creates a flow bottleneck.

Figure 5-14 illustrates the scenario where a small overlap between 1 and 2 will propagate to particle 3 in response to a correctional increase in volume 2. Naturally these changes will propagate across all particles in the network.

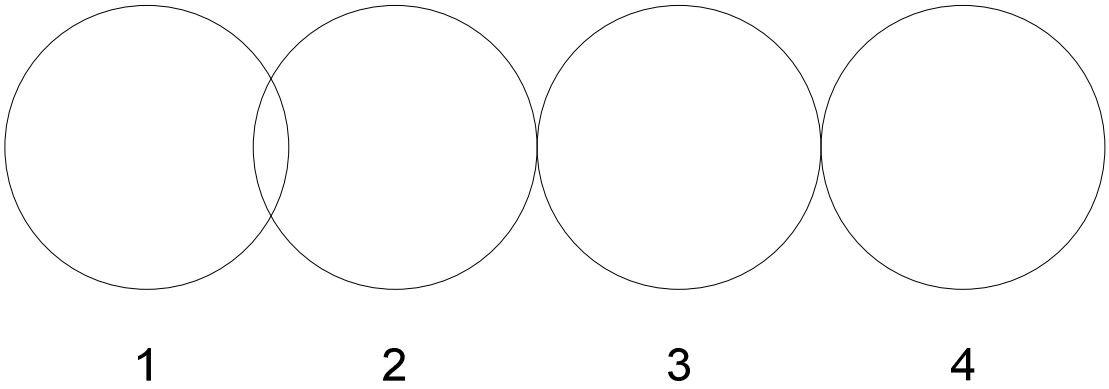

Figure 5-14 Propagation of volume overlap.

For the purposes of this work a simplifying assumption is made that each particle can only be affected by a maximum of two degrees of separation, the implications of this will be discussed in the results section. A rigorous treatment of the deformation of compressible spheres described by Lin et al. (2008) could also be considered in future iterations of this work.

5.3.4 STL Geometrical Mesh

STL, short for stereo lithography, is a file format common to 3D computer-aided-design (CAD) modelling applications. At the heart of the data structure is the triangular facet. These facets are what make up the 3D structure. Each facet consists of the three vertices (coordinates) and a vector normal to the plane of the triangle indicating the direction of the surface.

In this work the process of generating an STL file involves looping through each particle coordinate and building a list of triangular facets which make up the representation of the spherical particle. Each sphere can be a minimum of 4 facets (crude sphere or triangular pyramid) to infinite triangles (perfect sphere). However, the computational expense would limit having too high a resolution in the sense that the number of triangles are directly proportional to the amount of memory required to carry out the computation. Thus a modest number of 20 triangles were chosen to be accurate enough to model the hydrodynamic behaviour of creeping flow, but at the same time not too computationally expensive. The STL file can then be imported into the CFD software, Powerflow.

5.3.5 Fluid Simulation

A commercial Lattice Boltzmann simulation package, Powerflow by Exa Corporation (version 3.5), was used to simulate flow through the DEM cakes. The Lattice Boltzmann theory is derived from the kinetic theory of gases. The simulation environment is composed of a lattice grid where fluid particles are allowed to move between volume elements (Voxels) in a manner that conserves momentum, mass and energy. The solid phase is represented by surface elements (Surfels) which can interact with fluid particles. The simulation procedure involves tracking the velocity of fluid particles at discrete time steps through the volume defined by boundaries.

The Powerflow package allows for direct integration of STL geometries into the simulation. The STL geometry consists of triangular facets which combine to form a mesh which approximates a structure at specified resolution.

The permeability of the cake structure was calculated according to equation

$$K = \frac{1}{J}\frac{\Delta P_L}{\Delta m} \quad (5\text{-}19)$$

using parameters averaged across the cake cross section as reported by the simulation output.

5.4 Simulation and Experimental Procedure

In this section a description of the procedure implemented to execute the workflow described in Figure 5-4 is given. Specific detail of parameters used and routines are provided here. Comparison with experimental data is made in the results section. Detail will be provided of how the experimental data was obtained and analysed in order to make direct comparison between simulation and experimental results.

5.4.1 Simulation

The structure of this section is orientated in line with Figure 5-4. The purpose of this section is to provide detail of the parameters used in this study for the respective components.

5.4.1.1 Generation of Flocs

The aim of the DEM was to examine the effect of floc size and structure in suspension on the microstructural properties of the consolidating cake. For this work, particle numbers corresponding to floc sizes of 1, 7 and 36 particles were simulated. The corresponding fractal dimensions of 1.8, and 2.3 were simulated in every combination of floc sizes to create “loose” and “compact” floc structures representing two extremes. The limitation on floc size is due to the computational expense of such an exercise. The total number of particles in the virtual suspension is 2016.

5.4.1.2 Placement of Flocs and Equations

As described in the previous section, a database of flocs comprised of sets of primary particle coordinates was generated. For any given system, parameters such as particle mass concentration and x, y and z limits were specified. Flocs were placed in suspension by placing the centre of gyration of the randomly selected floc within the

simulation boundaries such there is no overlap with an adjacent floc. Flocs were placed sequentially with these conditions checked until the desired number of flocs was reached.

5.4.1.3 DEM Execution

The methodology of the DEM simulation is based around Figure 5-7. The executable code was developed in collaboration with Khan (Khan 2007) and compiled in C. Each executable was run on a Dell Quad Core Server SC1430 running 4 instances of the code simultaneously over a period of 4-8 weeks.

For simulation of dead-end filtration the DEM was set up as an incremental rectangular volume adjacent to the membrane of dimensions 100 μm by 100 μm with periodic boundary conditions in the x and y directions. The downward z direction is bound by a wall to simulate a permeable membrane which retains the solid in the cell (with a height of 1000 μm). Initially, a finite number of flocs of known size and structure were created and randomly dispersed in the virtual cell. For this system, all remaining voids are treated as being occupied by a fluid, in this case, dilute salt solution.

The DEM was executed using interaction parameters set to simulate yeast suspended in solution. Ordinarily, the DEM was run for a specified length of time or until a certain stop criterion was met. For simulation of dead-end filtration, the stop criterion was when the fastest moving particle in the system reached a low termination velocity suggesting that the cake had reached a kinetically stable state.

5.4.1.4 Radial Distribution Function

The radial distribution function is a measure of the spatial uniformity of particles around a nominal particle. Such information pertains to the permeability of the cakes in the sense that non-uniform pore distribution will favour a lowering in the resistance to flow due to the presence of macropores.

The radial distribution function $g_d(r)$ is given by Yang et al. (2000)

$$g_d(r) = \frac{dN_{ave}(r)}{4\pi r^2 dr \rho_o} \qquad (5\text{-}20)$$

where $N_{ave}(r)$ is the average number of particles found in a shell of thickness dr at a radius r from the centre of the reference particle and ρ_o is the average number of particle per unit volume.

5.4.2 Pore Size Calculation

In addition to characterisation of the DEM cakes by CFD, measurement of pore size was performed using the technique of Khan (2007). The procedure involves picking a point in the cake at random and placing a sphere of increasing radius until overlap with the nearest particle in the bed was reached (Figure 5-15). With sufficient random points selected, a reasonable statistical representation of the bed can be made. However, this method tends to underestimate the permeability in that the presence of a pore is regarded as an isolated entity and is not considered in conjunction with neighboring pores.

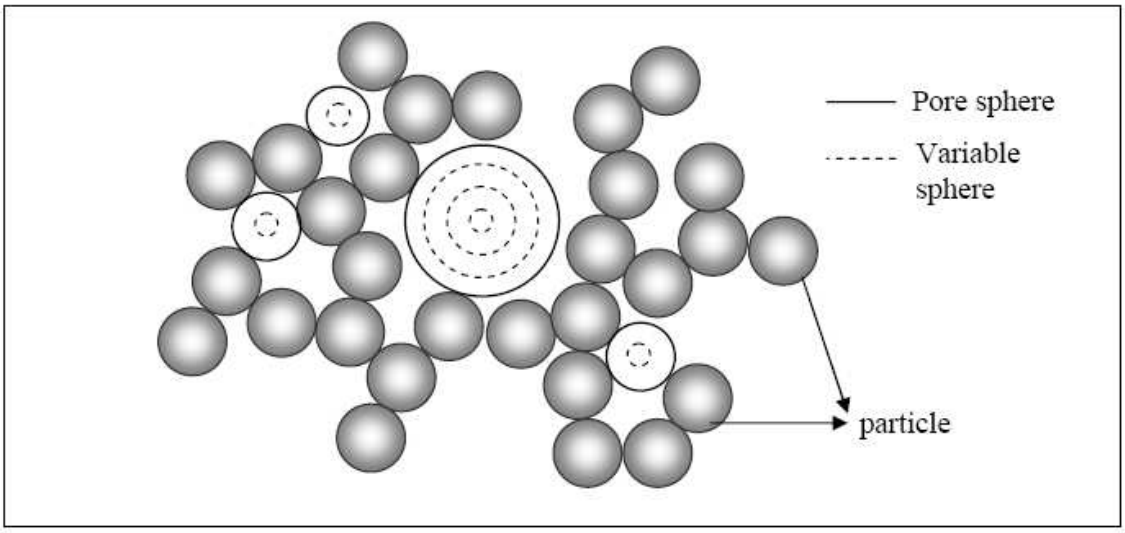

Figure 5-15 Calculation of pore size was performed by Monte Carlo type simulation of picking random points in the cake structure and determining equivalent sphere that would fill the pore gap. (Taken from Khan (2007)).

5.4.3 DEM Parameters

The results section provides details of the execution parameters and raw results for the DEM including selected graphical representations of the data structures. Choice of parameters was primarily directed toward approximating the compressibility of the real suspension rather than performing a rigorous exercise. Thus, certain assumptions were made in choosing the parameters. Table 5-2 shows a summary of the parameters used.

Table 5-2 Table of parameters used in DEM study.

Properties		Value	Justification
System Properties	Hamaker Constant Ha	$2.5x10^{-21}$	Particle force interaction profile taken from Hsu et al. (2001)
	Relative dielectric constant	81	
	Double layer thickness	1.19nm	
	Zeta potential	-4mV	
Particle Properties	Number of particles Np	2016	
	Particle Mean Radius	2.5μm	Malvern Mastersizer D(4,3)
	Poisson's ratio of particle	0.24	
	Density of particle	1400 kg/m3	Measured Experimentally
	Young's modulus, E	100000 Pa	
	Kinetic friction coefficient	2	Values were iteratively chosen to match the DEM observed compressive yield stress to experimentally measured
	Dynamic rolling friction coefficient	2.8	
	Elastic bending moment coefficient	$2x10^{-13}$	
	Limit of elastic bending	$1x10^{-24}$	
Fluid Properties	Fluid Viscosity	0.001002 Pa.s	For Water at 20^{o} C
	Fluid Density	1000 kg/m3	
Wall and compression particle properties	Youngs modulus	$1x10^{8}$	Harder than particle
	Poisson's ratio	0.24	Same as particle

5.5 Results

Presented here are detailed results relating to the permeability of virtual cakes formed by DEM simulated consolidation physics. Emphasis is placed on the size and number of large pores found in these cake structures as these pores can potentially support the bulk of the flow through even the most compact structures. Discussion is made of the likelihood that the number of larger pores are favoured by initially larger flocs which,

when brought together to form a loose but porous cake structure, will contain large pores that resist size reduction more efficiently during cake collapse.

Quantification of the hydraulic properties of the cake is presented directly in terms of CFD measured permeability as well as indirect characteristics such as radial distribution function and pore size distribution. Some of these characterisation tools are validated against synthetic packing structures as detailed in the next section on CFD validation.

5.5.1 CFD Validation

The validity of the CFD tool as a means to calculate the permeability of a porous cake was tested on a simple cake structure composed of a uniform packing of spheres. The specific cake resistance would be expected to conform closely to the Carman-Kozeny equation which is based on the assumption of perfectly uniform porous structures such as that described here and hence this test represents an ideal validation.

A face centered cubic arrangement of spherical particles was formed to calculate the coordinates of particles up to any desired cake dimension. A 15 by 15 by 5 arrangement of particles forming a uniform cake is pictured in Figure 5-16.

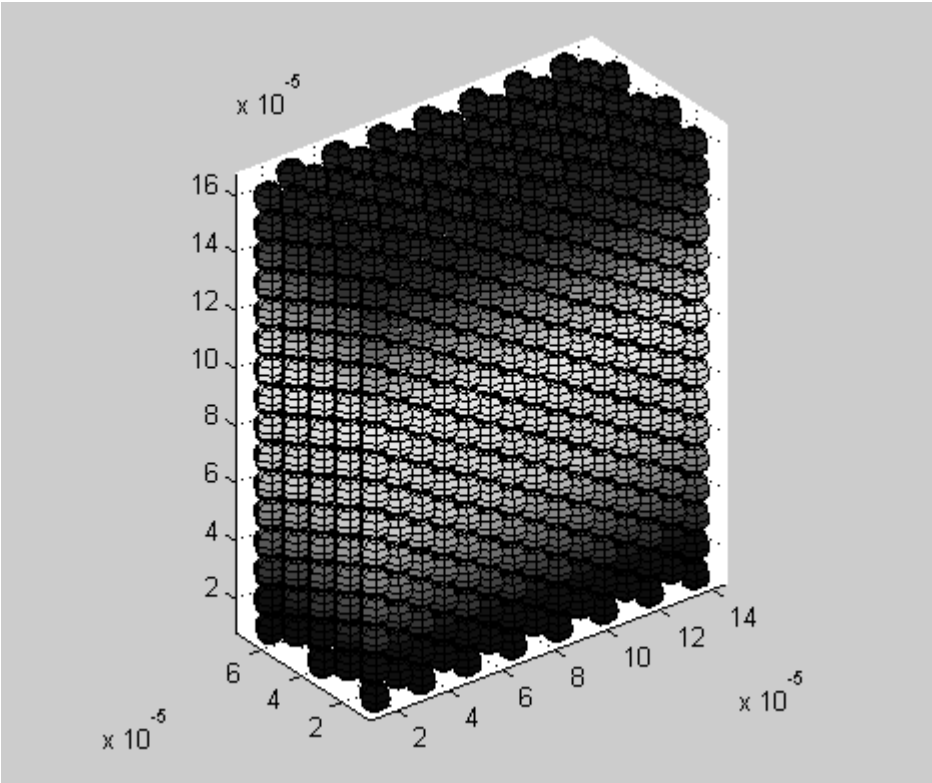

Figure 5-16 Face centered cubic arrangement of spheres created as a cake slice for validation purposes.

The permeability of the uniform cake was calculated by the CFD method. The distribution of flow is presented in Figure 5-17. In this instance the flow distribution is perfectly even across the face of the cake.

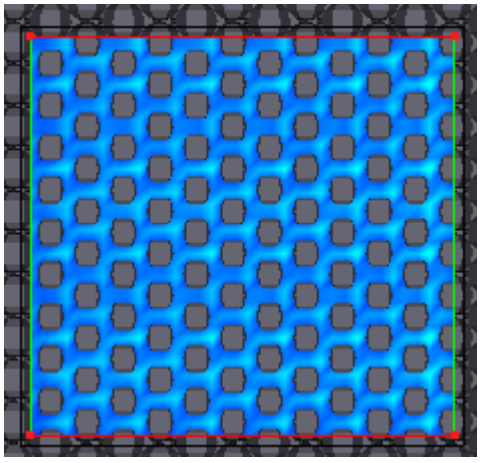

Figure 5-17 Flow visualisation showing velocity magnitude (light shade indicates higher velocity) for flow through a uniform cake slice of face centered

cubic packing of spheres. The specific cake resistance calculated by the CFD technique was $2.56x10^{-14}$ (mkg^{-1}).

Comparison of the permeability of the face centered cubic arrangement of spheres to the Carman-Kozeny calculated specific cake resistance returns a value within 10% of theoretical. This indicates that the CFD methodology used here is reasonable for calculating the specific cake resistance at high packing densities.

5.5.2 Raw DEM Results

Virtual suspensions comprised of flocs of precise size and structure was created as described in section 5.4.1.2. DEM simulates the consolidation of these suspensions firstly under gravity as shown in Figure 5-18 (left) and then by simulated piston solids compressive pressure (middle). The information of interest is the size distribution of pores in the cake as the consolidation proceeds to highly compact structures. Figure 5-18 (right) is the corresponding bottom view of the cake represented by the middle figure showing clearly the pores through which fluid could pass through directly.

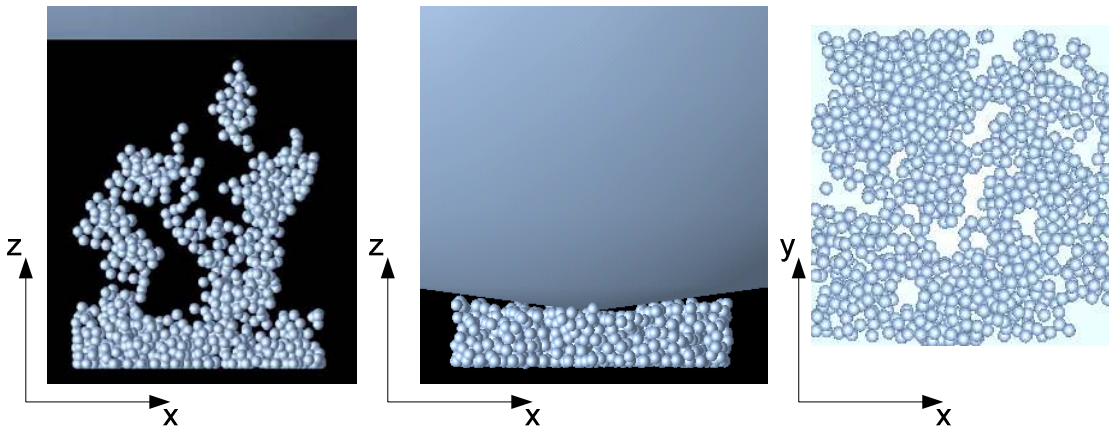

Figure 5-18 Flocs settling under gravity to form a cake viewed along the x-axis (left). Application of compressive pressure by way of an improvised piston (middle). Bottom view (along z-axis) of cake showing pores right through cake structure despite the entire structure collapsing (right).

5.5.3 CFD Visualisation of Flow

When the pores (as shown in Figure 5-18 (right)) have profiles which extend the height of the cake, such pores provide a path of least resistance for the fluid. Figure 5-19 shows the distribution of flow across a cake containing pores of this nature. In this instance, the volumetric flow through a large pore which extends the height of the cake is greater than the sum of all the smaller pores. This demonstrates the effect of larger pores on the overall hydraulic characteristic of a cake slice. The results section is focused on how these pores behave in response to cake collapse.

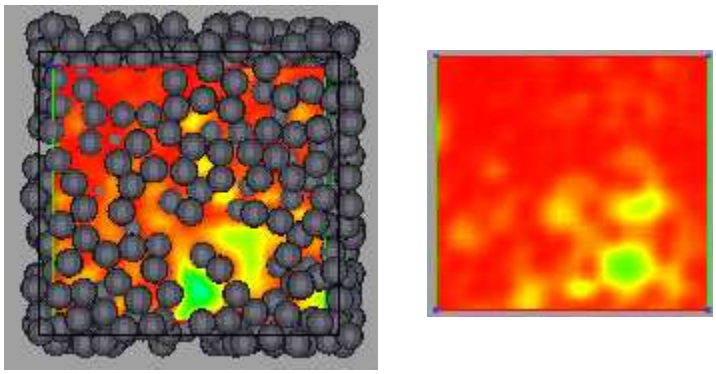

Figure 5-19 Distribution flow across face of the cake showing preferred flow through region of larger pore (light shade indicates higher flow velocity). Pictured on the right is the same flow pattern as on the left with particles omitted from the figure.

Figure 5-20 shows pressure isosurface corresponding to the cake structure in Figure 5-19. This visualisation closely corresponds to the percolation of fluid though the cake slices showing the fluid passing more quickly through the path of least resistance.

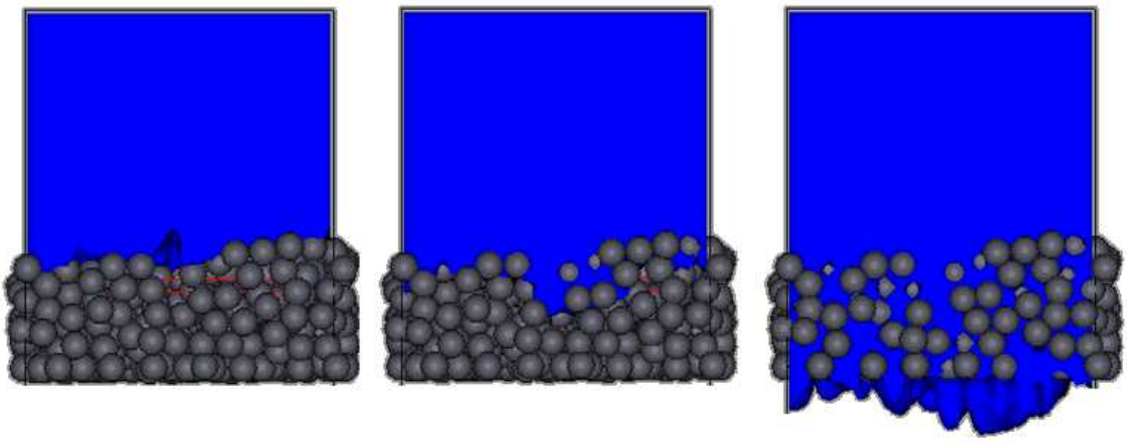

Figure 5-20 Pressure isosurface (i.e. boundary of the advancing fluid front) showing path of least fluid resistance towards the region with larger pores.

5.5.4 Effect of Floc Size on Local Pore Size

A suspension of randomly selected flocs was simulated with DEM. Primary particles and flocs comprising 7 and 36 particles with fractal dimension D_f=1.8 and D_f=2.3 make up the 5 simulated systems. The mean pore size was calculated by averaging the pore size distribution obtained by the method described by Khan (2007). The mean pore size was calculated at ϕ=0.15, 0.3, 0.45, 0.6 and 0.8 and plotted in Figure 5-21. As the cake consolidates under the applied solids compressive pressure a reduction in average pore size was observed uniformly as a result of physical displacement by the solid phase.

Comparing across the 5 simulations at ϕ=0.15 the pore sizes at the larger floc size at both fractal dimensions are largest (Figure 5-21). As the cake consolidates, there is a pattern showing that the flocs of 7 and 36 particles at D_f=2.3 have the largest pore size towards the latter stages of the consolidation. However, the difference is marginal with the comparison of average sizes not providing adequate information pertaining to the hydraulic characteristic of the cakes.

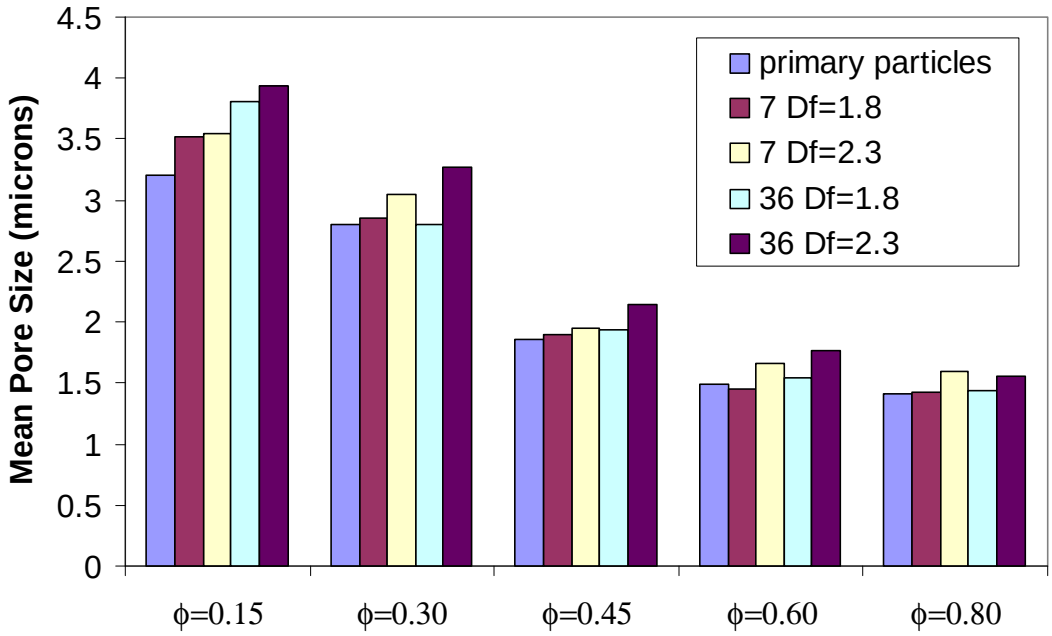

Figure 5-21 Local mean pore size calculated by method of Khan 2007 showing a tendency for flocs of compact structure to retain overall larger pores.

As the resistance to flow is proportional to the square of the hydraulic radius, the pore size distribution provides sufficient information to make inference about the permeability of the cake. Figure 5-22 to Figure 5-27 shows the pore size distribution for ϕ=0.15 to ϕ=0.8 respectively. At ϕ =0.15 it can be seen that larger pores are more frequent in the larger flocs. Looking at ϕ=0.8 the overall pore size distribution has reduced as expected and large pores are of the order of 10 to 12 μm. These size pores were not found in the primary particles case and the 7 particle/D_f=1.8 simulation. Such a result almost certainly implies that the highly compact cakes formed from larger, and particularly more compact flocs, will yield the most permeable cakes. This cannot be quantified based on the information in the pore size distribution alone. CFD calculated permeability combined with the results presented here should be more conclusive in showing that larger flocs of compact structure are more permeable.

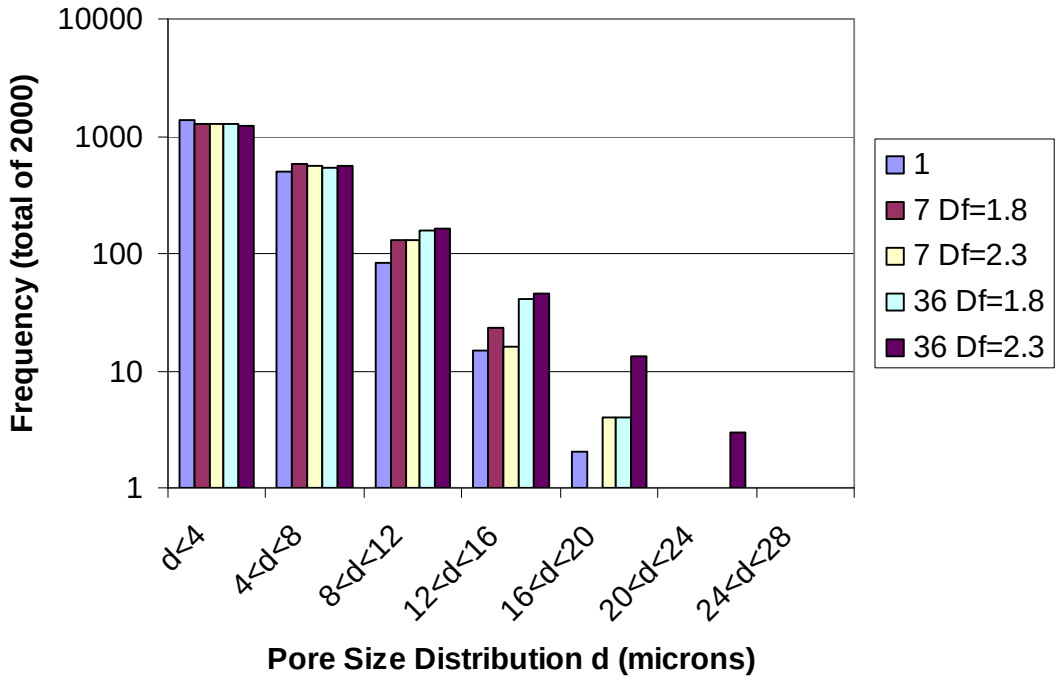

Figure 5-22 Pore size distribution for the 5 DEM simulations at ϕ=0.15.

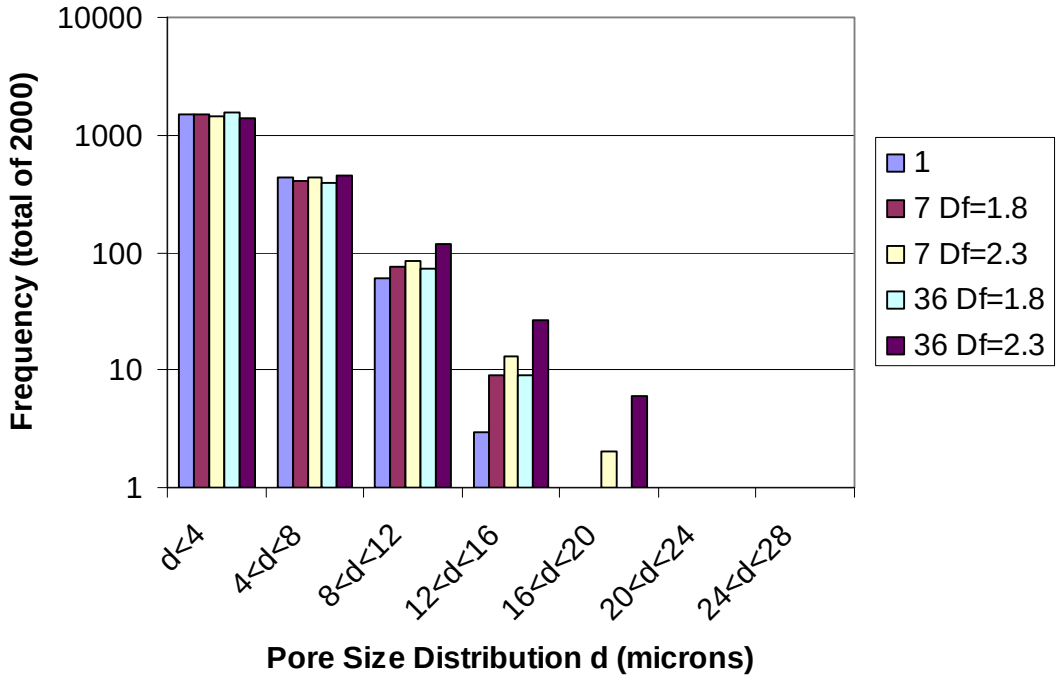

Figure 5-23 Pore size distribution for the 5 DEM simulations at ϕ=0.30.

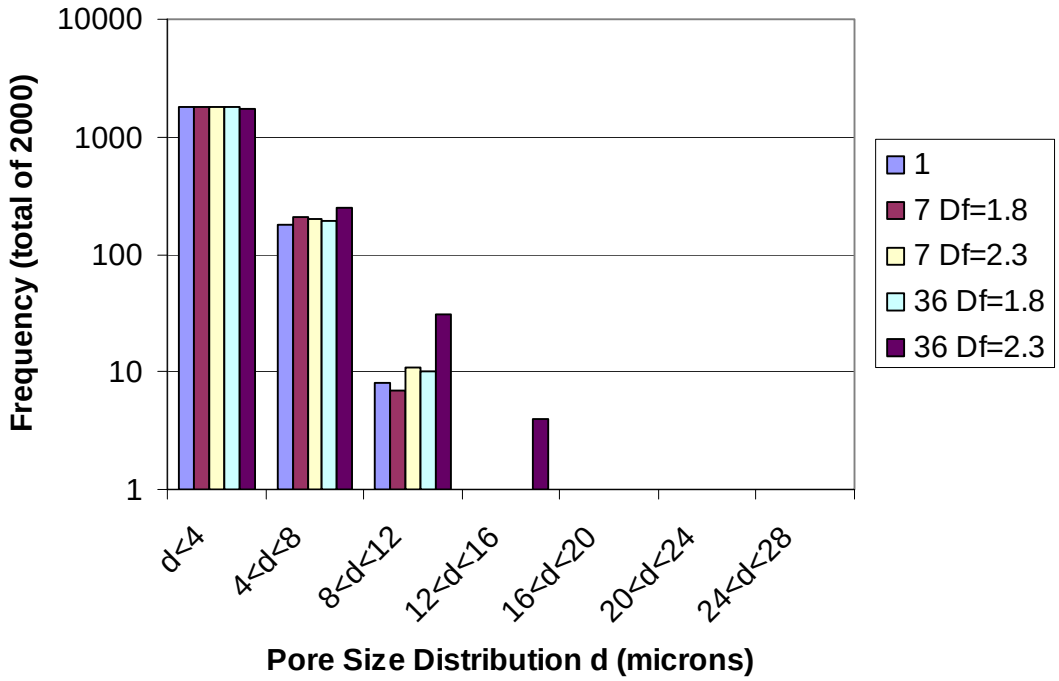

Figure 5-24 Pore size distribution for the 5 DEM simulations at ϕ=0.45.

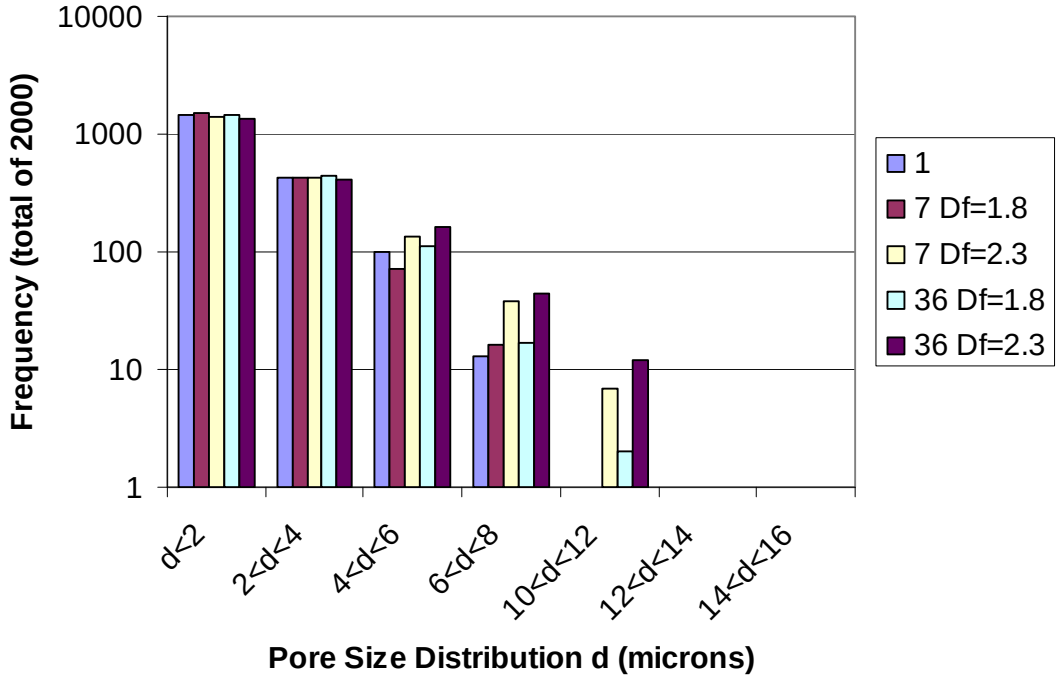

Figure 5-25 Pore size distribution for the 5 DEM simulations at ϕ=0.60.

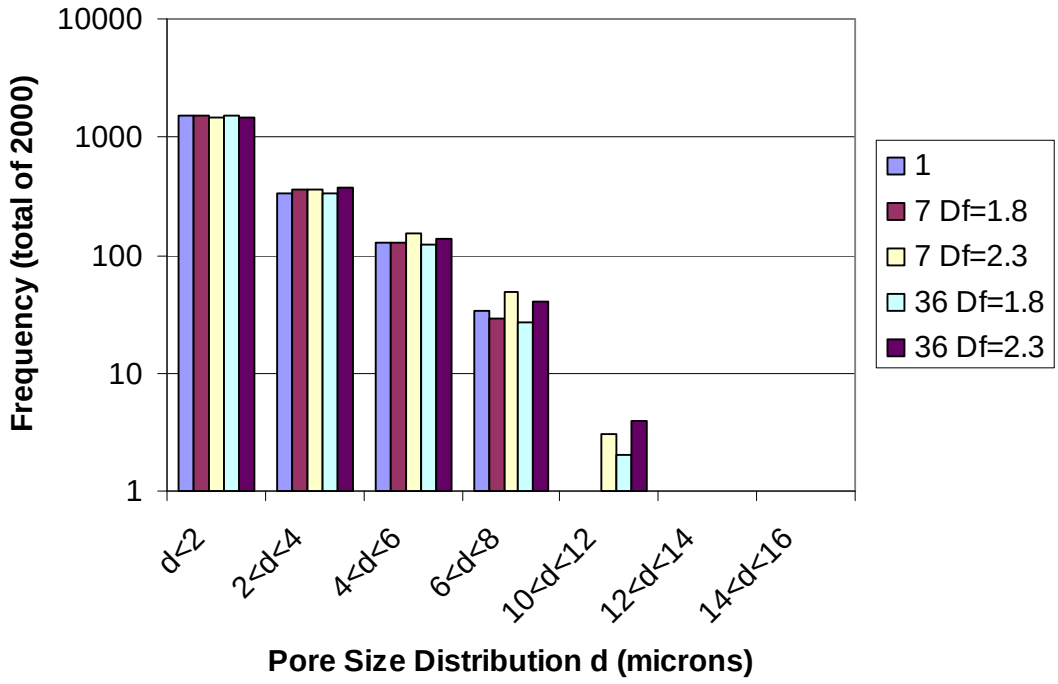

Figure 5-26 Pore size distribution for the 5 DEM simulations at ϕ=0.80.

5.5.5 Radial Distribution Function

Radial distribution functions for the 5 simulation results are presented here to identify any structural differences on an overall scale rather than localised "large pore" differences. The radial distribution functions for all 5 simulations at ϕ=0.80 are compared in Figure 5-27 where the x-axis is the normalised distance *r/R* (i.e. the distance from the origin divided by the sphere radius). All 5 plots overlay and appear identical The result described in section 5.5.4 showing larger pores at all stages of consolidation is not a common feature of the overall structure with the bulk of the cake appearing relatively uniform in packing with peaks at *r/R*=1.75 and further away at *r/R* =3.5. These peaks are consequence of having monodisperse spheres.

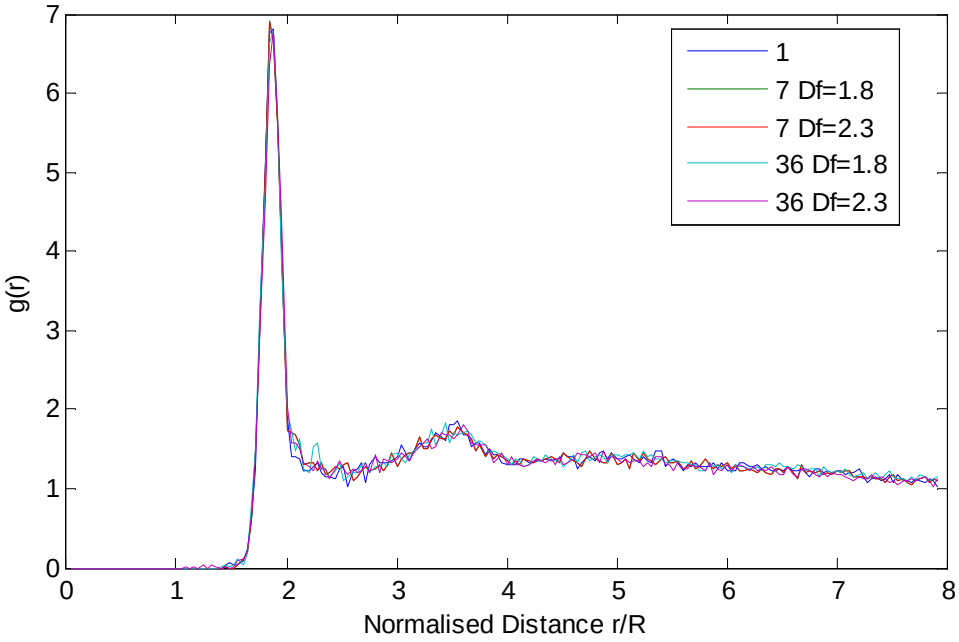

Figure 5-27 Radial distribution compared for each of the 5 simulations at ϕ=0.80 showing identical functions.

5.5.6 Permeability of DEM cakes (CFD)

The permeability of the DEM cakes were calculated using CFD analysis and the results of these calculations are shown in Figure 5-28. Variation in permeability appears greatest at the looser packing and becomes narrower at higher packing densities. It appears in all instances that the highest permeability was observed for the 36 particle compact floc (D_f=2.3). Such a result would be expected considering the pore size distributions would favour this result. This result suggests that the cake structures formed from the larger compact flocs appear to retain their structure with the greatest efficiency or act as a buffer against cake collapse. This appears to be true even at low ϕ.

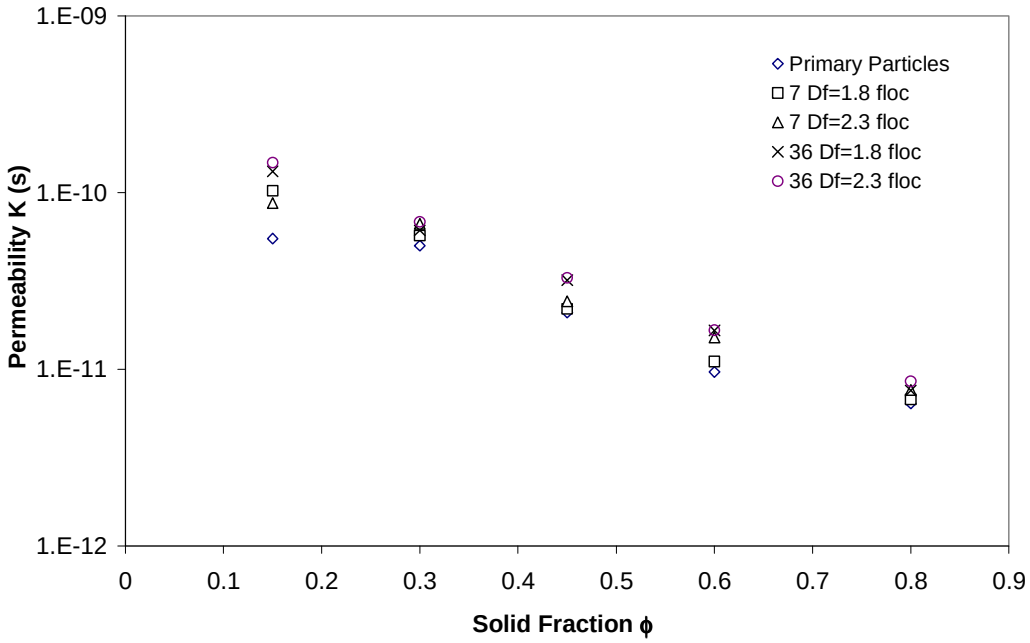

Figure 5-28 Permeability of DEM/CFD cakes for each of the 5 simulations.

Comparison to the Carman-Kozeny relationship and Happel model is given in Figure 5-29. Overall, the opposite trend to what one would expect for a polydisperse pore sized structure is observed (i.e. the Carman-Kozeny and Happel measured resistance is lower). A possible explanation for the difference at the loose packing end is that the calculated solid fraction was not representative of the whole cake due to settling stratification. In the DEM a considerable portion of the cake has settled, particularly at the bottom, and essentially a skin of higher density influences the hydraulic properties at low solid fraction. At higher density the two trends cross over.

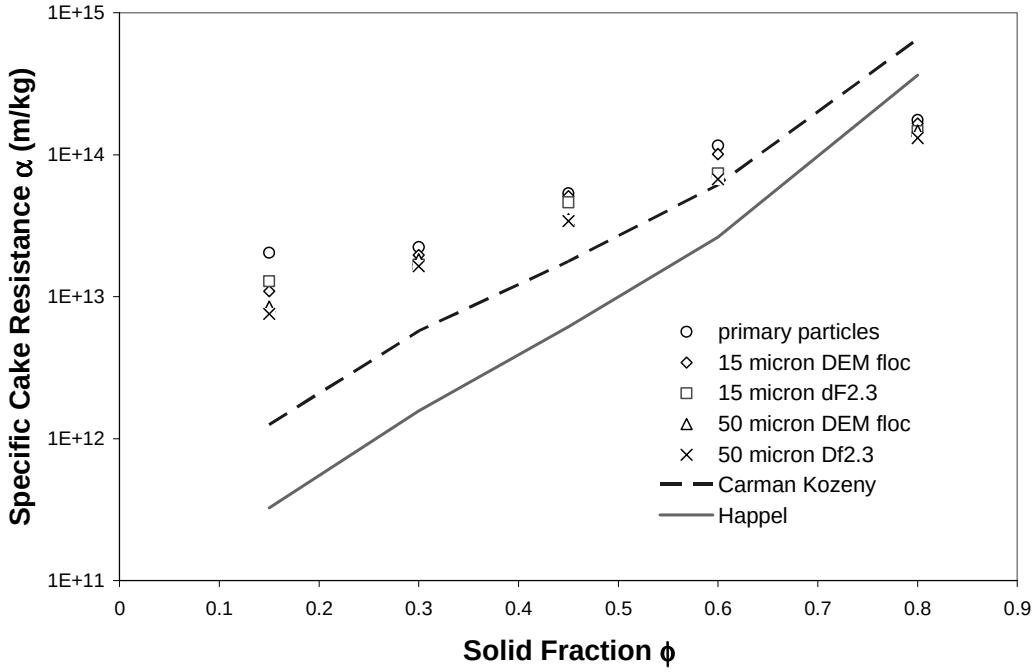

Figure 5-29 Comparison of DEM/CFD calculated cake resistance to Carman-Kozeny and Happel models.

Despite the result indicating the implication of floc size and structure for cake permeability, such a result does not have direct implications on filtration performance as the compressibility relationship is also of equal significance and the two must be considered together. However, for two cakes having reasonably equal compressibility, as may be the case for two flocs formed in the same chemical conditions, floc evolution may play a role in filtration performance (i.e. flocs depositing on the cake at different stages of growth could affect permeability). Consequently, the effect of shear also becomes important here as floc restructuring, breakage and growth all can potentially affect the permeability along the lines described in this chapter. In Chapter 6, the effect of floc size on compressibility will also be discussed.

It is also worthwhile noting that these findings contradict the modified Carman-Kozeny relationship presented in section 2.2.3 as it appear flocs of higher fractal dimension exhibit lower cake resistance after consolidation. This becomes apparent early on in the consolidation and is evident up to the highest packing densities. The hypothesis is proposed that higher D_f structures don't interpenetrate well and leave

larger intrafloc pores which provide a buffering porosity which acts to retain this spatial voidage during collapse.

A possible microstructural explanation is that although the structure is open in the unconsolidated state, as the stress carrying sections are weaker, parts of the cake break off and have a higher probability of filling the larger pores. As a tight floc does not fragment in the same manner due to its shape, it is likely that a yielding of a stress carrying element will result in an inwards (i.e. interfloc) displacement of porous space.

5.5.6.1 Comparison to Filtration Data and Analysis

The specific cake resistance calculated by CFD was compared to that measured by the steady state filtration technique (Figure 5-30). The specific cake resistance calculated for the DEM/CFD appears closest in agreement to the yeast pH 2.7 flocs for ϕ =0.15 to 0.60. The DEM/CFD trend does not follow the upward curvature of the experimental result at ϕ=0.8 in Figure 5-30. It is suggested that this is due to the particle overlap volume correction underestimating the required correction for a given overlap.

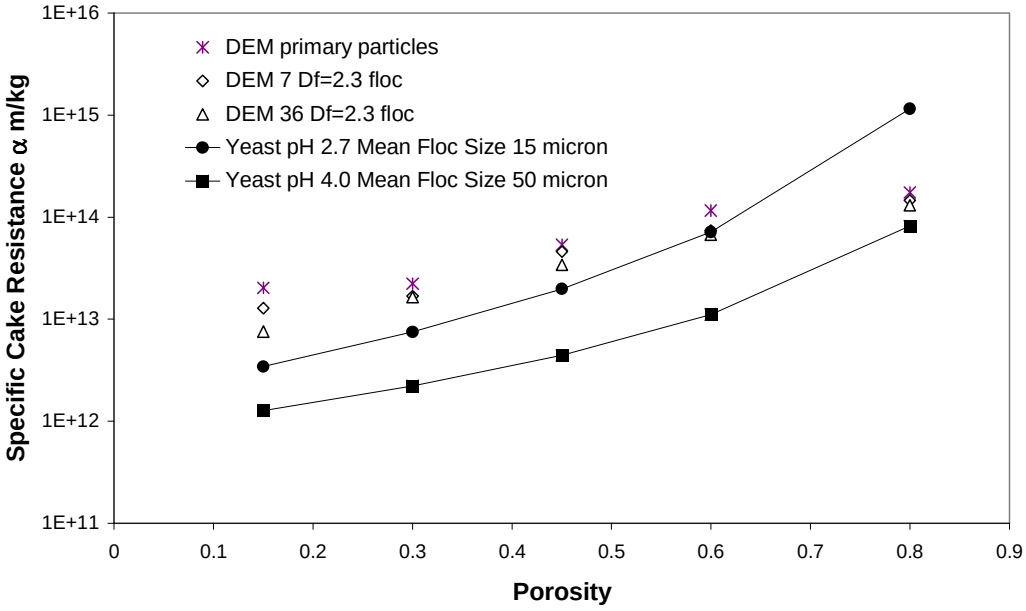

Figure 5-30 Comparison of specific cake resistance measured using the steady state filtration technique to DEM for yeast flocs.

A 7 particle DEM floc is close in diameter to 15 μm and the 36 particle floc close to 30 μm in diameter. The sensitivity of resistance to floc size in the DEM does not appear as large as in the experimentally measured result. This could be for the following reasons:

i) The mean measured chord size of 50 μm does not account for the polydispersity of the system or represent the floc size particularly well. Large flocs up to 500 μm are measured and could dominate the hydraulic characteristics of the cake. Thus it may not be appropriate to compare a mean measured floc size in a real polydisperse system with a monodisperse simulated floc suspension.

ii) There are other factors at play in the consolidation physics that result in pores retaining their size and volume with greater efficiency as the cake collapses. This could possibly be due to the interaction of the permeating fluid with the translational movement of particles as the cake collapses. Such details were not represented in the simulation.

Additional simulation studies would need to be conducted with larger DEM flocs when the computing resources become available.

5.6 Conclusions

The permeability of cakes formed from fractal aggregates was studied. The focus of this chapter was on simulated cakes of defined structure consolidating according to controlled physical conditions. Virtual suspensions comprised of monodisperse floc populations with precisely known particle number and fractal dimension (structure) were created. The permeability of these cakes was determined using CFD. Additional characteristics pertaining to the hydraulic properties of the cake such as radial distribution number and pore size distribution were also calculated.

Results show that the cakes formed from larger flocs had larger pores in a relatively unconsolidated state as shown in the pore size distribution. Larger pores were also favoured in the more compact floc. Larger overall pore size was also more frequent after cake collapse in the larger compact floc. Calculation of permeability by CFD showed that the largest compact floc had the highest permeability. It is reasonable to conclude that a higher frequency of large pores favours higher hydraulic conductivity of the cake.

Specific cake resistance for the DEM was compared to experimentally measured values. Although the two trends appeared similar, the DEM does not represent the experiment well for a number of reasons. The most important reasons include the fact that yeast flocs measured by the FBRM appear highly polydisperse with some flocs measured up to 500 μm. These types of flocs could dominate the overall hydraulic characteristics of the cake and cannot be simulated due to high computational expense. Another important difference is the absence of a rigorous implementation of a hydrodynamic force in the DEM physics. It is possible that the presence of fluid could affect the cake structure through effects such as tunneling or pore erosion. Future DEM work could look at pore erosion as a favourable characteristic of the cake. This would require a two-way DEM/CFD coupling.

Overall, considerable uncertainty still exists concerning the mechanisms governing the collapse in pore volume with overall collapse in cake volume. The findings

presented here however certainly have implications to how shear could affect the filtration characteristics of a cake through change in floc size and structure.

Chapter 6: Shear and Filtration

It is important in the filtration stage of any drinking water treatment process to obtain an efficient separation of the solid and liquid phases. Flocculation is often introduced prior to filtration because it improves the effectiveness of this separation process by influencing the hydraulic properties of the cake layer. Mixing is a key component of the flocculation process as it is critical to the blending of chemicals and encourages flocculation by increasing the frequency of contact between particles. This idea is well understood. On the other hand, the behaviour of a flocculated suspension that is subsequently subjected to compression in a sheared environment is poorly understood. A fundamental understanding of the mechanical behaviour of flocs in such an environment opens up new insights into the behaviour of the gel layer in membrane filtration.

In this Chapter an extra level of complexity is added to the filtration system by examining the effects of shear on dead-end filtration. A conceptual model for the effect of shear on the gel layer is presented and the impact of shear on fouling examined. Specifically, the effect of shear on suspended flocs, the effect of shear on cake dewaterability and the effect of shear as a means of detaching the cake from the membrane are examined experimentally.

The hypothesis is presented that *shearing the cake has a detrimental effect on filtration performance by compromising the strength of load bearing elements in the cake.* The implication for operation of membranes is significant in that the presence of shear is intrinsic to the operation of the filter. Shear can either be present in uniform (laminar) conditions or more likely present in turbulent conditions.

There are two confounding issues which make this study particularly difficult. The first relates to the proven benefit of shearing as a mechanism for removing a portion of the cake by lift. The second relates to the portion of cake unremoved by shearing that undergoes additional collapse because of shear stress. In this study, low shear experiments were undertaken to ensure consistent cake growth by avoiding shear

induced cake erosion. At the same time the shear must be high enough to distribute the material evenly within the cake.

Flocculated yeast is chosen as the model particle system in the studies reported in this Chapter. As shown in previous Chapters, yeast is a readily flocculating material. Under compressive stress the primary particles deform leading to solid fractions that can exceed that achievable by a close packing arrangement of uniform spheres. Despite this, the cakes formed from flocculated yeast at or near the pH_{pzc} tend to retain permeability in these highly compacted states, though are sensitive to further shear-induced collapse.

6.1 General Introduction to Shear

The concept of shear stress is best described in terms of molecular momentum transport. Newton's Law of viscosity is best demonstrated for the case of laminar flow between parallel plates. Consider the arrangement of two plates where one is fixed and the second plate is set in motion at fixed velocity v_{pl} (Figure 6-1). To sustain this motion a force F is required which is equal to

$$\frac{F}{A_p} = \mu \frac{v_{pl}}{y} \qquad (6\text{-}1)$$

where μ is the viscosity, F is the force applied per plate area A_p, v_{pl} the plate velocity and y the distance of separation between plates. The flow profile that is developed between the fixed and moving plates is illustrated in Figure 6-1. As suggested by the schematic, the steady state laminar flow profile is reasonably represented as a linear velocity profile.

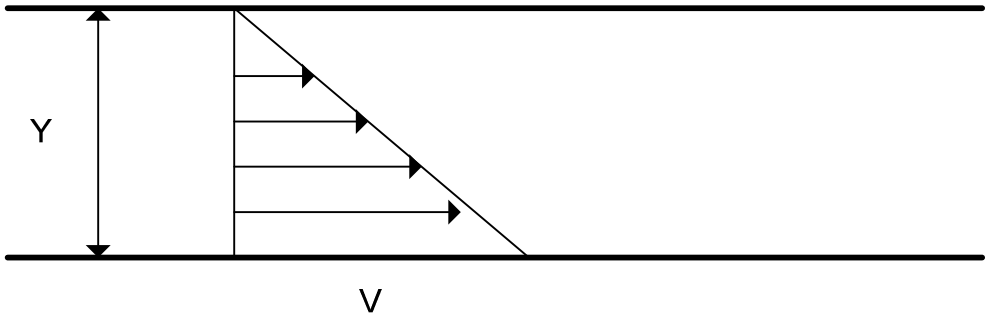

Figure 6-1 Laminar flow profile between stationary plate and moving lower plate of velocity *v* separated by distance *y*.

The constant of proportionality is defined for Newtonian fluids as μ, which is the viscosity of the fluid. The quantity of shear stress is defined as the force per unit area imposed on the plate and is given by

$$\tau_S = -\mu \frac{dv}{dy} \tag{6-2}$$

In flocculation studies it is conventional to define the shearing rate *G* as the velocity gradient which is given by

$$G = \frac{dv}{dy} \tag{6-3}$$

where the shear rate is reported in units of s^{-1}. This terminology is used throughout this Chapter.

6.1.1 Theoretical Considerations for Shearing Apparatus

Several basic objectives need to be met in choosing a suitable setup for studies in which the effect of shear on filtration is investigated. These are listed as follows:

1) Some shear is required to disperse particles such that a reasonably uniform distribution of material across the membrane is obtained upon settling. This effectively limits the lowest amount of shear possible to some non-zero value.

2) The shear rate in the bulk filtration cell needs to be the same as the shear rate at the membrane surface. Several well characterised geometries allow for this,

such as a cone and plate (Figure 6-2) and a coni-cylindrical Couette (Figure 6-3). However, the latter allows for in-situ floc size measurement. Thus, the assumption can be made that the floc size does not significantly vary between the point of measurement and the point at which they deposit on the membrane.

3) A possible design of a filtration apparatus to investigate the in-situ shearing effects on filtration performance is given by Vasan et al. (2002). This device is essentially a cone and plate arrangement with a permeable membrane incorporated on the lower plate side of the device. A schematic representation of the device is given in Figure 6-2.

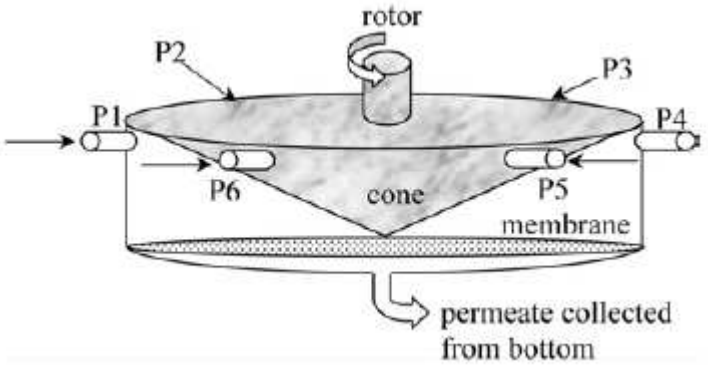

Figure 6-2: Cone and plate membrane design taken from Vasan et al. (2002). The device can be designed to deliver uniform shear in the region bound by the cone and membrane.

A design equation of such a device can be derived from the differential equations which govern the equations of motion and are given by

$$\tau_S = 2\mu\Omega\sec(\theta) \qquad (6\text{-}4)$$

where θ is the angle that the cone makes with the plate and Ω is the speed of revolution. If the angle of the design is suitably narrow, complications with Taylor vortices can be avoided. For present purposes, in-situ measurement of floc size can be achieved using an FBRM probe. Design of a cone and plate arrangement to incorporate an FBRM probe inserted at the vessel wall would require an unreasonably large vessel diameter if target shear rates were met and complications with Taylor

vortices avoided, due to the diameter of the probe. Furthermore, at low shears in a large vessel it would be difficult to distribute mass evenly across the cake due to floc settling.

For this study a coni-cylindrical configuration to investigate the effect of shear on filtration was chosen. This device was originally developed by Mooney and Ewart (1934) with the purpose in mind of eliminating end effects common to conventional Couette viscometers (Figure 6-3).

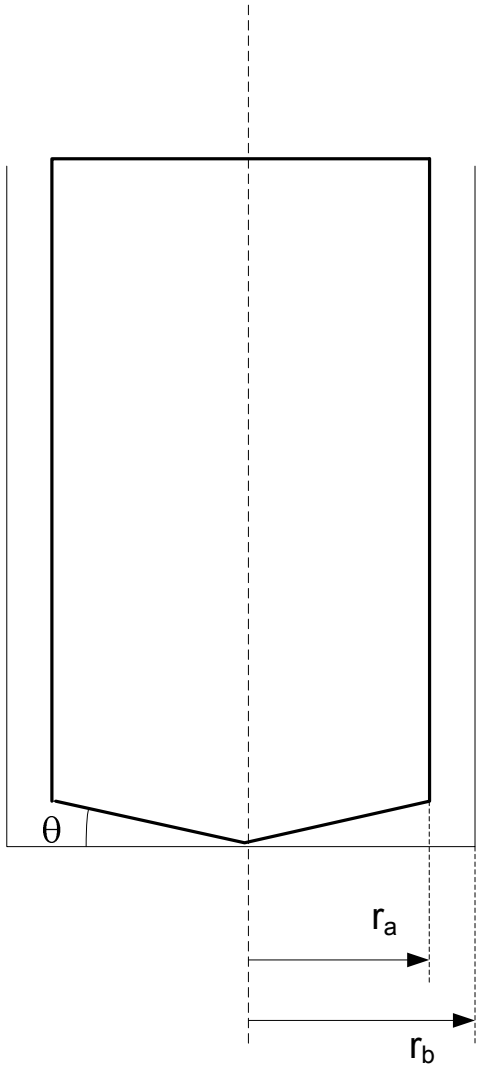

Figure 6-3: Schematic of coni-cylindrical Couette showing key dimensions governing the shear environment.

Essentially, the shear stress at the bottom of the device is the same as that experienced in the region between the inner and outer cylinders. The shear rate in the cylindrical component is given by

$$G = \frac{\kappa_R \Omega}{1 - \kappa_R} \tag{6-5}$$

where $\kappa_R = r_a/r_b$, r_a is the inner radius and r_b is the outer radius. The shear environment adjacent to the membrane bottom is essentially a cone and plate arrangement. A simple relationship which gives the shear rate in such an environment is given by Mooney and Ewart (1934)

$$G = \frac{\Omega}{\theta} \tag{6-6}$$

The vessel was designed with a modest κ_R of 0.9. At operational shear rates below $12s^{-1}$ Taylor Vortices are not expected to be significant and a range of low shear environments that are reasonably uniform can be generated.

6.2 Literature Review/Theory

The current state of knowledge on the relationship between shear and filtration performance across all four key areas, as presented in Figure 1-4, are empirical at best as was discussed in section 2.2.3. From a practical point of view, there appears to be little consideration in the literature of how a change in the controllable parameters (i.e. shear history) propagates through to a change in filtration performance (i.e. the constant flux behaviour of a given material). The intention of this review is to consolidate key concepts from established areas of literature to bridge this gap.

A more complex conceptual map, unmasking the physical mechanisms of each component in Figure 1-4 is presented in Figure 6-4.

Several of the mechanisms (each represented by numbered arrows) are well understood with a substantial body of underlying research. Reference to selected research of relevance to the various mechanisms is given in Table 6-1. The literature review is structured around the relevance of the various theories to the research

objectives of this Chapter. Part of the theory has already been covered in previous Chapters and is summarised in Table 6-1.

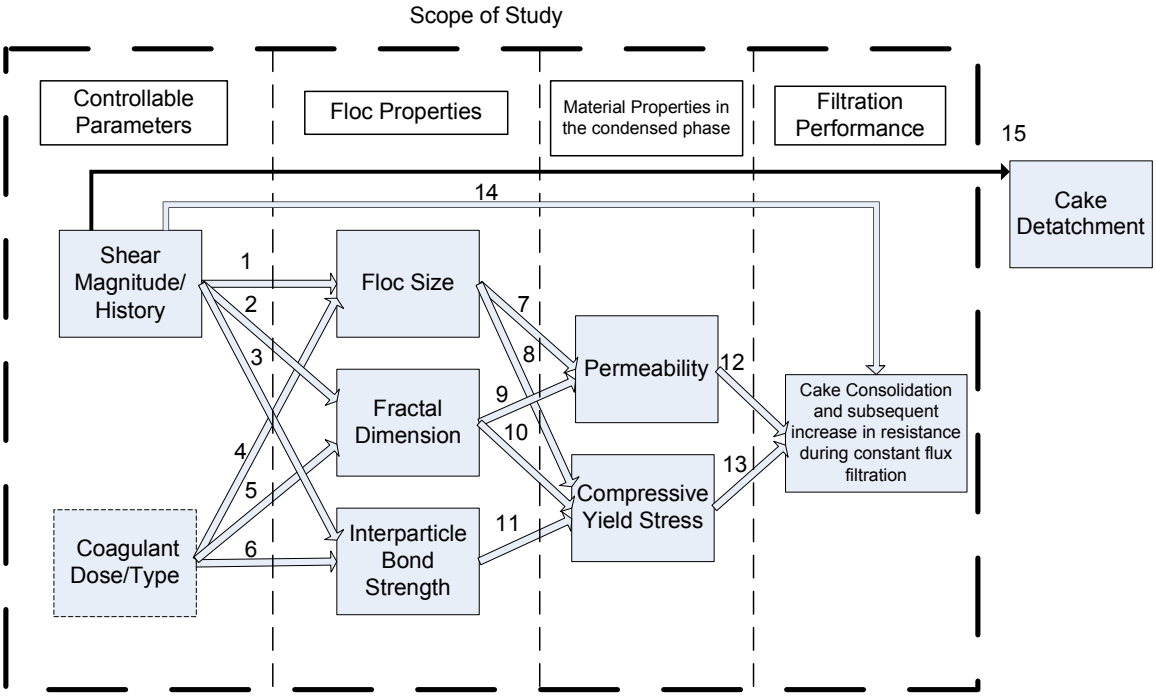

Figure 6-4 Conceptual map for the effect of shear on dead-end filtration presented as an unmasked representation of Figure 1-4.

Table 6-1 Summary of the mechanisms which comprise the complex relationship between shear and filtration described in Figure 6-4.

Mechanism	Description of Mechanism	Reference
1	Shear history affects the steady state floc size through breakage and growth.	Section 2.1.4.1
2	Shear history affects floc structure due to restructuring at long times.	Selomulya PhD 2001
3	Shear history affects bond strength due to repeated bond breakage and reformation.	Mc Curdy et al. 2004
4	Coagulant dose affects flocs size by affecting particle collision efficiencies and frequencies.	Section 2.1.4.1
5	Fractal dimension is characteristic of flocculent type, i.e. flocs formed by ACH have different structure to Alum.	Bottero et al. 1990
6	Coagulant dose affects total energy required to rupture a bond due to influence over the electric double layer.	Heimenz and Rajagoplan 1997
7	Floc size affects permeability as the space between flocs is retained upon overall collapse of the cake.	Chapter 5
8	Floc size affects compressive yield stress as the network structure has a 1 dimensional resistance to collapse because of the network of stress carrying bonds.	Section 2.3.1.1
9	Fractal dimension affects permeability in the unconsolidated state by providing interfloc porosity.	Section 2.3.1.1
10	Fractal dimension affects compressive yield stress as structure relates to the bond density which in turn relates to the energy required to rupture these bonds.	Section 2.3.1.1
11	The total energy required to yield a network of bonds relates to the strength of individual bonds.	Section 2.3.1.1
12	The permeability affects filtration performance by the volume of fluid that can pass though a given structure for a given input in liquid driving force.	Section 3.2.1
13	The compressibility affects filtration in the sense that a cake that resists collapse will remain more permeable over a wider range of pressures.	Section 3.2.1
14	The cake itself is affected by shear stress as it weakens the 1 dimensional response of the structure.	Section 6.2.1
15	High shear will cause a cake to detach from the membrane because of lift force.	Section 6.2.2

6.2.1 The Effect of Shear Rate on Cake Dewatering

The point of focus in this experimental study is the investigation of the effect of shear on a cake subject to compressive stress. The effect of shear is intrinsically present in the form of bulk fluid agitation at its lowest extreme. In the study of shear rate on filtration, these low shear effects are superimposed on other complex aspects of the sheared filtration system. Thus, understanding low shear effects on the cake receives priority before addressing more complex shear interactions with the filtration system.

A recent study by Gladman et al. (2005) observed a critical shear rate to be at the point where beneficial and detrimental effects in dewatering occur. The effect of post floc formation shear was investigated for a system of calcite particles and polyacrylamide polymer. Flocculation was conducted in a linear pipe reactor at $875s^{-1}$ and introduced to a low shear Couette environment where shear was maintained below $10s^{-1}$. The results of the study conducted by Gladman et al. (2005) showed that enhanced dewatering was observed as shear increased to $6s^{-1}$. Apparent maximum compressibility was observed at this shear due to densification of flocs in the condensed phase. Further increases in shear resulted in less dewatering but was difficult to account for.

A key difference between the work of Gladman et al. (2005) and what is proposed here is the method of shear. Gladman applied shear through the suspension mimicking the operation of a thickener rake. In membrane filtration, the shear is transmitted from the agitated liquid phase to the relatively stationary (highly viscous) cake phase. The shear rate in the cake phase is considerably less due to the vastly different viscosities. Furthermore, the shear rate in the cake is also difficult to measure. Thus, in the work presented here, the shear rate in the liquid phase will be quoted in modelling work.

The effects of combined shear and compression on aggregates in a Couette environment has been previously studied (Channell 1999). From this investigation it was concluded that shear affects the rate of filtration through a decrease in permeability associated with the shear enhanced consolidation of the network.

The assumed form for the shear dependant compressive yield stress $P_y(\phi,G)$ is derived from the principle of the kinetics of cluster rearrangement in a sheared field. By treating the problem as a formation and breakage of load bearing structures, the

qualitative dependence on shear can be modelled semi empirically through elementary reaction rate theory. The model is given by Channell (1999)

$$\frac{P_y(\phi,G)}{P(\phi,0)} = \left[1-\left(\frac{G}{G^*}\right)^{1/y_1}\right]^{x_1} \tag{6-7}$$

where the characteristic shear rate G^* is critical point describing the point at which load bearing chains are broken faster than that they can reform. The probability of a load bearing structure forming is denoted by f and behaves according to

$$\frac{df}{dt} = \alpha_1 G - \beta_1 f^{y_1} \tag{6-8}$$

where the rate constant α_1 relates to the breakage term due to shear and β_1 relates to the reform rate term. G^* is given as (β_1/α_1) and can be determined experimentally from rheological studies, or in this work by fitting the experimental data. Suggested values of x_1=1 imply a linear increase in $P_y(\phi,G)/Py(\phi,0)$ with increase in the probability of potential load bearing sites becoming available. In addition, for the system mentioned, y_1=2 appears to be also a reasonable value from experiments (Channell 1999).

It is important to note that the first term in equation 6-8 representing the breakage term is dependant on the velocity gradient (shear rate) through the cake as the localised movement of particles is a rate determined process rather than shear stress determined. In thickener dewatering this is insignificant as the shear rate and shear stress are equal through the sheared bed. However, in membrane filtration, although the shear stress in the agitated liquid phase is transferred to the cake phase, the velocity gradient in effect through the cake structure is considerably less than the fluid shear rate due to the differences in viscosity of the two phases (Figure 6-5). For example, a compressible cake subject to solids compressive stress will have a gradient in solid fraction ranging from the gelpoint to the maximum packing adjacent to the membrane. Consequently, the viscous properties of the cake will also vary accordingly with a gradient of increasing viscosity from the top of the cake to the bottom. Thus, equation 6-8 may not be an accurate model for describing the effect of

shear on membrane filtration. For this work the shear rate in the cake is approximated to be that of the fluid phase with the limitations clearly stated here.

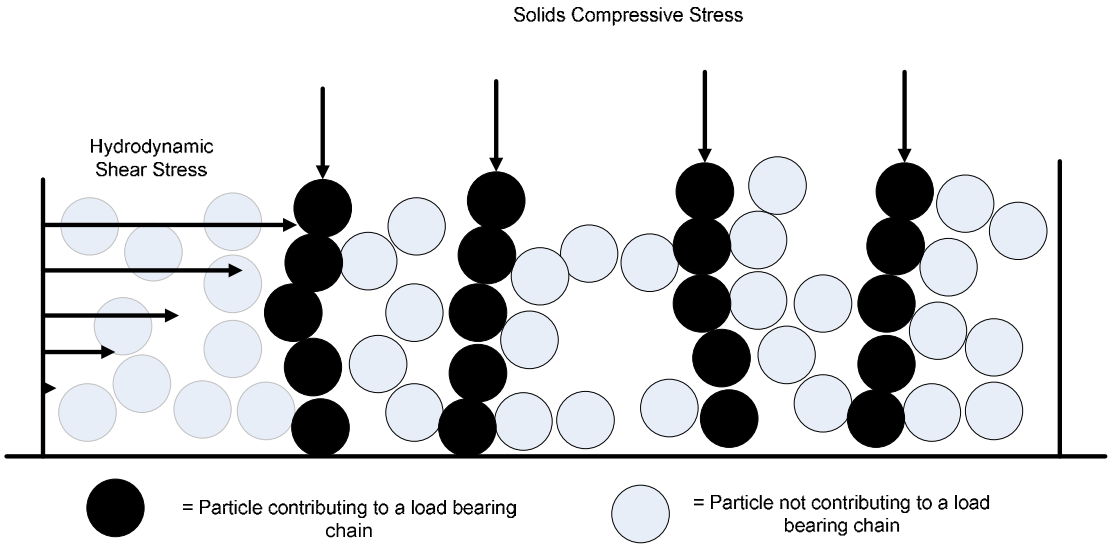

Figure 6-5 The shear rate acting through the cake results from the transfer of shear stress from the fluid phase to the cake through the cake/suspension interface.

Koenders et al. (2001) studied the external torsional (hydrodynamic) shear effects on dead-end cake filtration. Interesting findings from this study include the deduction that shearing the cake externally causes the orientation to change in the direction of the shear (with respect to apparatus axis) and thus weakening the one-dimensional response of the cake material. The implementation of parallel disc viscometry of the selected system by Koenders results in complex shear patterns that require additional theoretical consideration of the spatial shear distribution which made analysis difficult in this instance.

A significant finding from the work of Koenders et al. (2001) relating to orientation of the cake material in the principal direction of the shear stress could suggest that the load bearing members described by Channell (1999) could also be aligned in this fashion during the formation stage where the angle is somewhat related to the shear magnitude. This is a reasonable scenario if the compressive stress is low as what is experienced in the top layers of a cake. When these load bearing members are subject to higher compressive stress later in the filtration, the stress direction will be offset resulting in an effect which is described as reduced stiffness or more precisely, the

strength of the original unbroken load bearing members are effectively lower and prone to breakage. This provides a conceptual mechanism for shear to affect the cake behaviour at the suspension interface rather than by the transfer of shear stress to the cake as described by Channell (1999). The mechanism proposed by Koenders et al. (2001), which acts at the cake/suspension interface, is felt at later stages in the filtration long after the freshly deposited cake slice has left the loose condensed phase as fresh layers of cake form above it causing cake collapse.

The concepts discussed in this section present the strongest reason as to why it is unlikely that the effect of shear is solely on flocs themselves and the benefit associated with optimum floc shear could result in detrimental effects on cake permeability by reducing the stiffness of the fresh layers of cake. The implications here are that the same forces would be in play for biological systems such as MBR and SMF's where ambient shear is present.

6.2.2 Shear Assisted Rejection of Particles

The shear assisted rejection of particles is represented as mechanism 15 in Figure 6.4. The principles governing crossflow shear filtration (as opposed to dead-end) essentially rely on rejection of the retentate from the membrane by hydrodynamic back transport. Such provisions allow for continuous operation. Certain aspects of crossflow filtration literature are presented here as they are relevant to the intrinsic effects of shear on the cake in dead-end filtration.

In crossflow filtration, shear acts to prevent cake from forming below a critical flux by inducing back transport of particles away from the membrane (Mulder 1996). In this case a force balance taking into consideration the lift force induced by the drag against the force induced by permeate flow on the particle (Altmann and Ripperger 1997) can reasonably describe the physics of cake formation. Useful insights have been gained from studies of this nature to investigate novel methods to encourage particle rejection.

In recent times there have been many studies conducted into various mechanisms to create higher shear at the membrane surface to enhance shear assisted rejection of particulates, for example Al Akoum et al. (2002). Submerged membrane modules can

be made to vibrate at a known frequency and amplitude giving a new way to induce shear much higher than possible by forced crossflow velocities in the turbulent regime. Air bubbling is often thought of as a low-cost alternative to induce moderate shear as a means of providing an uplift force in hollow fibre modules. This is presented in the following section.

6.2.2.1 Cake Break Off By Air Sparging Shear

An example of the hydrodynamic characteristics of a common submersed membrane filtration module is presented here.

For simultaneous backwashing and air scouring, Laborie et al. (1998) proposed a model for shear stress at a cake based around turbulent flow conditions. Figure 6-6 illustrates the Memcor CMF-S submersible module. The geometry is designed so that there can be efficient use of air for scouring of the retenate side of the membrane.

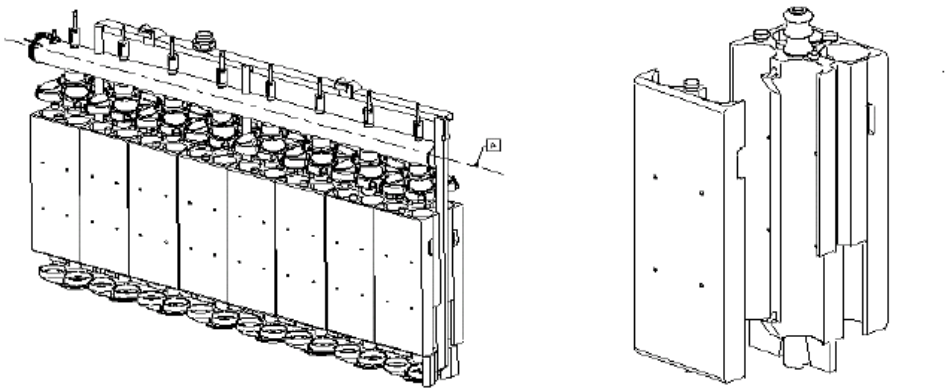

Figure 6-6 Submodule (Submersed Membrane Filter from Memcor CMF-S) in use at Sandhurst Drinking Water Treatment Plant (Scott 2004)

During air scouring there effectively is crossflow shear induced by both air induced film and liquid which is shown in the following figure. Best use of air scouring is made in the regime where gas is in a slug formation as shown in Figure 6-7 (Cabassud et al. 2001).

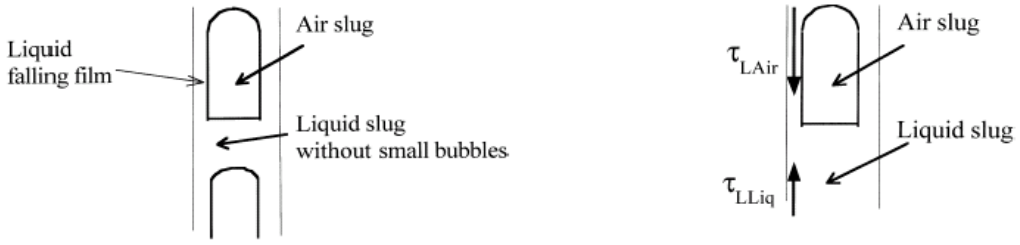

Figure 6-7 Shear at the air slug/cake interface representative of the shear on a cake in submerged membrane filtration. The high shear stress caused by a gas slug passing over the cake can potentially detach the cake and at the same time act as an additional dewatering stress.

The shear rate is given as follows (Laborie et al. 1998)

$$\tau_{L,Mean} = \beta_g \tau_{L,Air} + (1-\beta_g)\tau_{L,Liq} \qquad (6\text{-}9)$$

where τ_{LMean} is the mean shear stress exerted by the air scour, and β_g is defined as the rate of intermittence between gas slugs given by

$$\beta_g = \frac{L_{Air}}{L_{Air} + L_{Liquid}} \qquad (6\text{-}10)$$

The shear stress near the liquid and gas slug is given by

$$\tau = \frac{1}{2}\rho_L f_L v^2 \qquad (6\text{-}11)$$

where ρ_L is the liquid density, f_L is the friction factor (Reynolds number dependant) and v is the liquid velocity near the wall.

This area is worthy of investigation as significant fouling is still observed in air sparged systems above the critical flux. Perhaps the degree of fouling is not always reduced by shearing as some of the detrimental effects described in section 6.2.1 are present. Although air sparging is a quick way to induce shear in hollow fibre type systems, the actual shear rate experienced by the cake is highly variable. This issue is flagged as benefits of cake removal by shearing are useful but additional weaker tangential stresses can potentially act to dewater (collapse) the cake.

6.2.2.2 Floc Size and Shear Assisted Particle Rejection in Uniform Shear Environment

For this section the primary interest is predicting the range of shear which results in complete deposition to within a desired level of certainty. In this section a summary of literature concerned with the transport of particles in the vicinity of the membrane and the forces which govern particle migration will be given.

To predict whether or not a particle or floc attaches to the cake in a sheared environment requires calculation of the migration velocity. In the context of this work such knowledge is important as the experimental objective is to obtain complete deposition of particle matter. The migration velocity is the velocity at which a particle moves away from the membrane relative to fixed coordinates. If the migration velocity is less than velocity of the permeate, then it can be assumed that deposition of the particle or floc will occur. It is assumed that the deposit is irreversible as there is additional force acting in the direction of flow due to contact with a neighbouring particle once it makes contact with the cake.

The study of Altmann and Ripperger (1997) incorporates a crucial relationship between the size of a particle and the uplift force experienced by the particle as it approaches the condensed phase in crossflow filtration. The relationship given by Altmann and Ripperger (1997) is

$$F_L = 0.761 \frac{\tau_w^{1.5} d_P^{\ 3} \rho_L^{\ 0.5}}{\mu} \qquad (6\text{-}12)$$

where τ_w is the crossflow shear stress, d_P is the monodisperse particle size, ρ_L the fluid density and μ is the viscosity. Thus, a method for predicting cake formation can be developed based on a two dimensional force balance to confirm that the net force on a particle results in stable deposition, hence meeting the experimental objective.

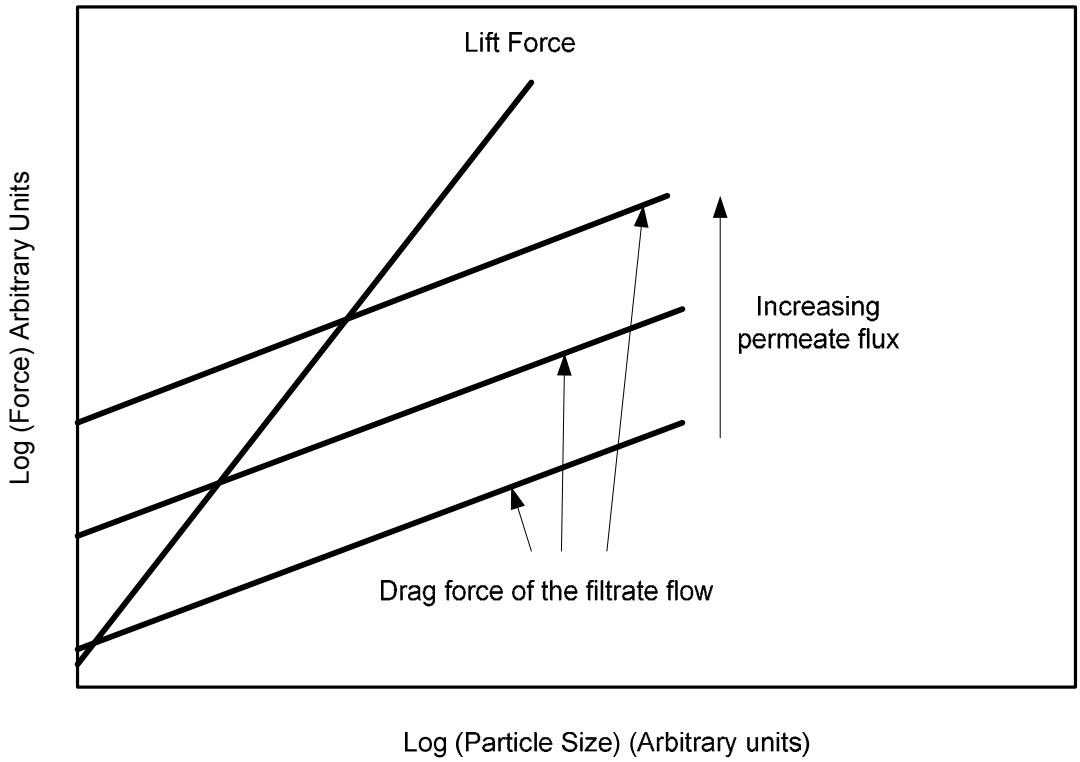

Figure 6-8 Particle migration away from the cake due to hydrodynamic shear is a balance of drag and lift force. At the point that the lift force exceeds the drag force the particle will migrate away from the cake. Such a process is particle size dependant (Altmann and Ripperger 1997).

As models like these are derived from the drag force experienced by spherical particles, the following problems arise:

1) Hindered movement effects caused by the presence of other particles need to be corrected for and in a highly concentrated state, the drag force experienced by the particle by permeate flow is likely to be larger.

2) The assumption of spherical particles is qualitative at best and likely to be an overestimate of the back transport experienced by a floc as hydrodynamic complications arise because of intrafloc flow. However, this can be compensated by substituting an equivalent hydrodynamic radius. It is uncertain whether back and forward transport are affected the same way by such an approximation but for the purposes here will suffice.

3) The effect of shear on the growth and/or breakage of flocs in the vicinity of the cake are neglected in the work of Altmann and Ripperger (1997). This is assumed negligible as the authors were working with monodisperse spheres. Without in-situ measurement it is difficult to account for this growth/breakage. (Note: an in-situ measurement in the vicinity of the condensed layer is provided in this work.)

Complications arise as flocs are rejected from the cake by shear which results in increasing particle concentration. Cake formation rates become difficult to predict with the accuracy required to model constant flux filtration. For this study, complications with particle rejection are avoided by operating at shear rates which ensure that the cake formation is uncompromised. This is achieved by operating at low enough shear rates ensuring that the drag force of permeate flow on the flocs is greater than the shear induced uplift force. Online measurement of particle counts validates this idea as flocs being rejected from the cake would result in an overall increase in counts over time. Provisions for this measurement are made in the experimental design.

6.2.2.3 Force Balance for Cake Removal

In order to ensure that the cake formation is not compromised by shear, rejection of particulates must be avoided. If the shear stress at the surface of the cake exceeds the binding force and permeate induced drag force on the cake, the result will be particle uplift.

To estimate the force required to rupture the compressed cake structure by crossflow shear is difficult. This requires knowledge of bond energy and number of bonds per unit area in addition to other parameters. Figure 6-9 illustrates a cake breaking off subject to crossflow shear. Because of stratification of the cake during filtration (non uniform ϕ in the z-direction), the compact layers will remain unless sufficient shear stress can overcome the tight network of bonds or short range forces between particles and the membrane surface.

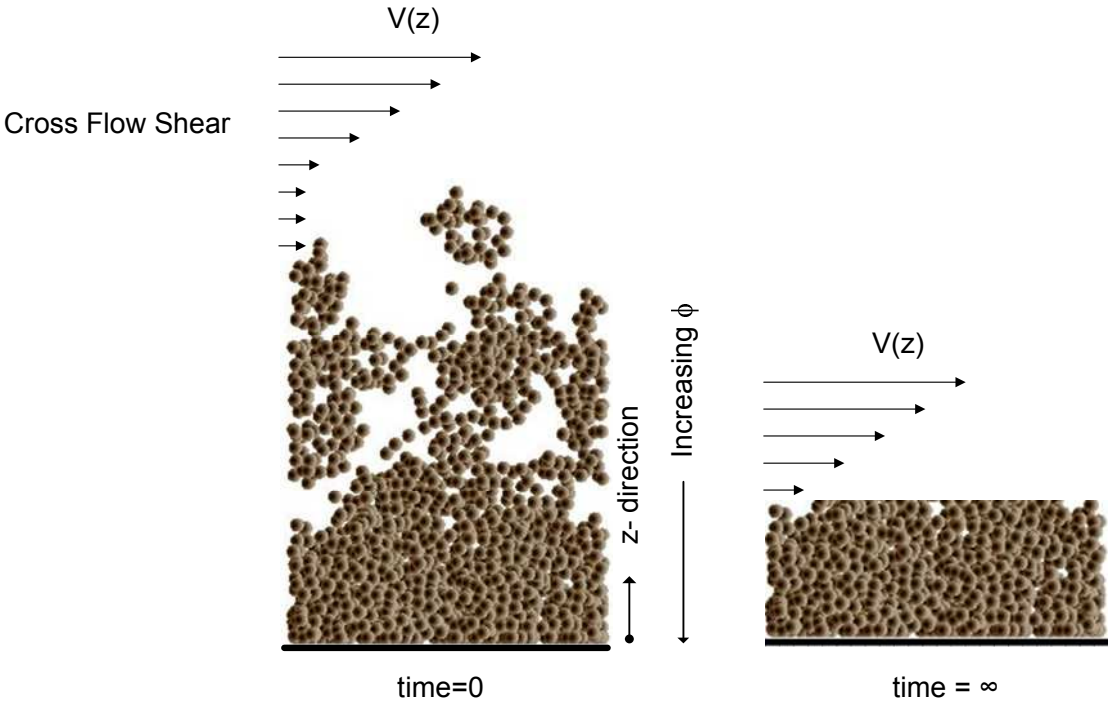

Figure 6-9 Cake detachment of loosely bound layers by shear stress.

To operate such that near complete retention of material on the cake occurs, the migration velocity must be less than the permeate velocity. The migration velocity is given by Altmann and Ripperger (1997)

$$v_L(x) = 0.0807 \frac{\tau_w^{1.5} \rho_L^{0.5}}{\mu^2} \frac{x_{crit}^2}{\lambda(x_{crit}, \phi_o)} \tag{6-13}$$

where the correction function λ for monodisperse particles of size x_{crit} is given by

$$\lambda(\phi) = \frac{4 + 3\phi + 3\sqrt{8\phi - 3\phi^2}}{(2 - 3\phi)^2} \tag{6-14}$$

The assumption of monodisperse spheres for this application is reasonable as the intended purpose of the calculation is to gain an appreciation for the sensitivity of particle back transport to shear.

If the migration velocity is greater than the superficial flow velocity then a particle will migrate from the surface. The normalised particle velocity is defined as

$$v_{norm} = \frac{v_L}{v} \qquad (6\text{-}15)$$

For v_{norm}>1, particle/floc detachment would occur. Figure 6-10 shows the effect of shear rate on normalised velocity for various monodisperse particle sizes. A "low" shear range was defined where a cake formed from yeast flocs would be sensitive to lift or detachment. The mean floc size as shown later is between 40 and 50 μm. Hence, according to this model, considerable effects on the cake would be felt at or above $10s^{-1}$.

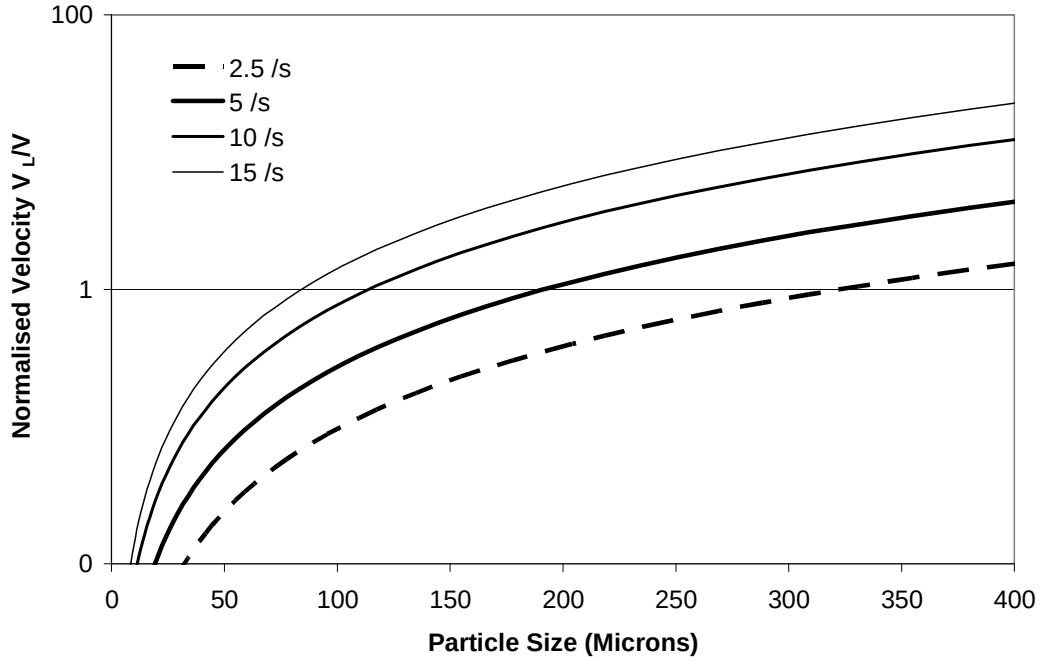

Figure 6-10 Effect of shear on cake lift as calculated by the two dimensional force balance showing the size at which a spherical particle is rejected (i.e. v_L/v=1) for different shear rates.

A model for the dependence of cake formation rate on shear stress would have been an ideal tool to describe the effect of shear on filtration, particularly in the regime where flocs are rejected from the cake. Due to complications with hydrodynamic forces on flocs in the vicinity of the cake it is difficult to extend the model of Altmann and Ripperger (1997) from the spherical case. Instead, the model is used to probe the effect of shear on cake formation at or below the critical shear at which significant particle rejection occurs.

The critical aspect of ensuring that the cake formation is uncompromised by shear induced rejection is through online particle counts measurement rather that through the force balance model presented here. The FBRM can be configured to detect an increase in suspension concentration (in-situ) which would ordinarily result from rejection of flocs from the cake. The model calculation will be presented later in the results section compared to the experimental results from particle counts.

6.2.3 General Model for Shear

A general equation is derived to account for shear effects in addition to the lumped transient model described in section 4.3.2. The effect of shear on compressive yield stress was presented in equation 6-7. This relationship is based on local cake properties and mathematically difficult to implement into a general equation. Instead an empirical shear relationship is proposed. As a cake becomes affected by shear, less pressure is required to compress the material to a given solids fraction. Hence, an increase in the overall compressibility (*n*) would be expected inline with what would be observed locally. Over a narrow shear range this can be approximated by

$$n = k_3 + k_4 G \tag{6-16}$$

Thus, for this work, a linear approximation is made across a relatively narrow range of shear. Substituting this relationship for compressibility into equation 3-1, the effect of shear on specific cake resistance for the low shear range is given by

$$\alpha = \alpha_o \left(1 - e^{-\frac{t}{\tau}}\right) \Delta P_L^{(k_3 + k_4 G)} \tag{6-17}$$

where k_3 and k_4 can be determined empirically from experimental data of TMP rise at different shear rates. The modified general equation for constant flux to include a shear term is given by

$$\Delta P_L = \alpha_0 (1 - e^{-\frac{t}{\tau}}) \Delta P_L^{(k_3 + k_4 G)} \mu c_s \frac{Q^2}{A_c^{\,2}} t + P_0 \tag{6-18}$$

The assumption must be made that cake formation rates are not affected below some critical shear rate and the time constant is independent of shear below this critical

shear rate. The critical shear rate in this instance is the shear at which the cake formation rate becomes affected by back transport rather than the definition of Channell (1999) that shear cause the material to collapse to the close packed solid fraction, or n=1. The shear at which lift begins to occur is assumed to be less than the shear which would cause collapse of the network.

The effect of shear on cake formation rate was shown to be non-trivial to model in section 6.2.2.1. Ideally, a term would be included in equation 6-18 to account for this. However, for simplicity, this regime is not modelled and is reserved for future work.

The empirical model given by equation 6-18 is fitted to the experimental data in addition to the model of Channell (1999) as presented in the results section.

6.3 Experimental

Analysis of the local cake properties through a set of constant pressure filtration experiments was used to investigate the effects of shear on cake structure. Specifically, the effect of shear on compressive yield stress and permeability was studied. The experimental focus was on execution of well controlled sheared filtration experiments under constant flux and constant pressure experiments.

Consulting Figure 6-4 it can be seen that floc size, floc structure, floc strength, cake lift/detachment and cake stiffness reduction are all affected by in-situ shear. The objective of the experimental design was to isolate the effect of shear on direct dewatering of the cake from the effect of the remaining variables.

Conversely, the effect of shear on floc size and structure and the resulting effect on filtration were not studied as the shear regime for such an analysis would almost certainly be too complicated to decouple each effect.

6.3.1 Apparatus to Conduct Sheared Filtration Studies

The experimental rig used for these studies is essentially the same setup as that described in section 4.4. The major design criterion was the creation of a low shear range environment where shear rate could be precisely controlled. To achieve this, the 4-blade axial flow impellor was replaced with a coni-cylindrical Couette as described

in section 6.1 and illustrated in Figure 6-3. The filtration cell containing the coni-cylindrical Couette was pressurised allowing for simultaneous shear and filtration.

For this study, sets of steady state filtrations were performed to determine the material properties according to the method described in Chapter 3. The filtration was driven to steady state for pressures of 12.5, 25, 50, 100 and 150 kPa for shear rates up to 4.8 s^{-1} (8 RPM). The steady state filtration was conducted with gradual introduction of the material as described in section 4.4.

The constant flux filtration data was obtained for several shear rates both below and above the predicted critical shear. The apparatus was operated as described in section 4.4 for Couette speeds of 2.5, 5, 8, 13 and 25 RPM, corresponding to shear rates of 1.5, 3, 4.8, 7.2 and 15 s^{-1} assumed to be acting at the cake/suspension interface.

6.3.2 Experiment Design

Yeast was again used as the model particle in all studies described here. The particles were prepared as described in section 3.4.5.3 with yeast being flocculated at a fixed pH.

In order to implement the steady state filtration analysis, several design considerations needed to be addressed. The key design considerations for flocs in this study were:

- low sensitivity of floc size and structure to shear; and
- low sensitivity of cake lift to shear.

The shear history of flocs in the experiments described here is presented in Figure 6-11.

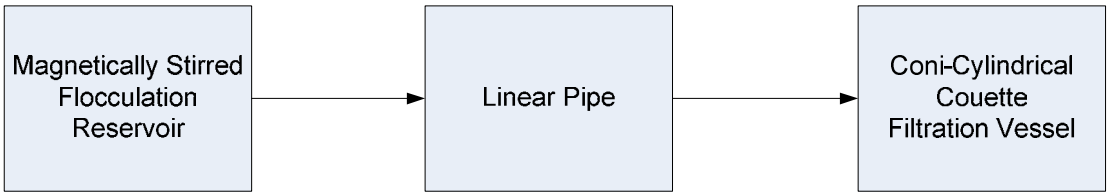

Figure 6-11 Shear history for yeast flocs from point of formation to filtration.

For low shear rates, the rate of floc growth for a mature population of flocs is governed by number, concentration and size distribution and is unlikely to be dominated by the breakage term (von Smoluchowski 1917). For a system of latex particles, Selomulya et al. (2005) showed how the size of flocs evolved from primary particles to a steady state size distribution for various shear rates. At higher shear rates the breakage of flocs results in a decline in floc size following an initial period of growth. For operation at or below $12s^{-1}$ it is reasonable to assume that breakage will not dominate the flocculation process even at long times, as verified by in-situ size measurement.

Presumably, flocs entering the filtration vessel would make a single pass of short duration through the filtration vessel as they settle into the conical shear zone adjacent to the cake. For short durations in a reduced shear environment it would be reasonable to assume that the floc size would be independent of shear rate. This assumption can be verified through in-situ measurement of floc-size. In this work the floc size was monitored by the FBRM probe (described in section 2.1.2.1).

Another important design consideration is the selection of shear rate for this study. An important assumption of the steady state filtration analysis is that 100% of the solids are retained in the cake. Measurement of particle counts of the suspension with the FBRM will determine if this condition is met.

6.4 Results and Discussion

6.4.1 Validation of Experimental Design

In order to implement the steady state filtration analysis, several assumptions need to be validated. In this section, results are presented showing that below a critical shear rate there appears to be 100% deposit of solids on the cake. In addition, at low shear rates, floc size is not sensitive to shear as measured by the FBRM given such short duration and relatively low particle counts in the filtration cell.

Table 6-2 shows the shear parameters for constant flux filtration experiments. The filtrations were run at 0, 2.5, 5, 8, 13 and 25 RPM. The mean floc size does not appear to be correlated to shear rate and size distributions appear to be similar. This confirms

that it is reasonable to assume that the flocs that land on the cake are consistent from run to run. The percentage of mass retained on the cake based on the measured size distribution is also shown in Table 6.2. The mono-disperse sphere size corresponding to the unity normalised velocity (cut off) shows that at the higher shear rates this value approached the average floc size. It is thus sensible to operate at shear rates below this.

Table 6-2 Summary of chord size (in μm unless otherwise stated) as measured by FBRM. The cut off size is calculated from the model presented in section 6.2.2 as being the size above which all spherical equivalent particles are rejected from the cake for the given shear rate.

Speed RPM	mean size @ t_{max}	d 10	d 50	d 90	Shear Rate s^{-1}	Cut Off	% retained
0	45.7	19.6	37.5	70.1	0		100%
2.5	40.4	17.6	34.7	58.7	1.5	467.7	100%
5	53.3	20.0	40.4	83.3	3	281.8	100%
8	45.8	16.6	31.7	85.5	4.8	199.5	99.90%
13	54.7	23.1	42.4	111.5	7.2	144.5	94.90%
25	57.2	18.8	44.4	91.8	15	84.1	88.40%

For shear rates corresponding to 0 to 8 RPM impellor speeds, it is reasonable to assume based on these models that 100% of the mass is retained. Particle counts as measured with the FBRM are shown in Figure 6-12. It is seen quite clearly that the particle counts at 25 RPM increase with time suggesting that the solid mass is accumulating in suspension. It is reasonable to suggest that this mass consists of matter resuspended from the cake by shear or not deposited in the first place. It is difficult to confirm if this matter is larger flocs based on the observed larger mean size at higher shear rate as the accumulation of mass would also promote growth. Due to the position of the probe it is unlikely a large floc would travel upwards to the probe and affect the measurement. The observed higher particle counts in this instance could possibly be due to floc breakage and dispersion of primary particles resulting in orthokinetic floc growth throughout the vessel.

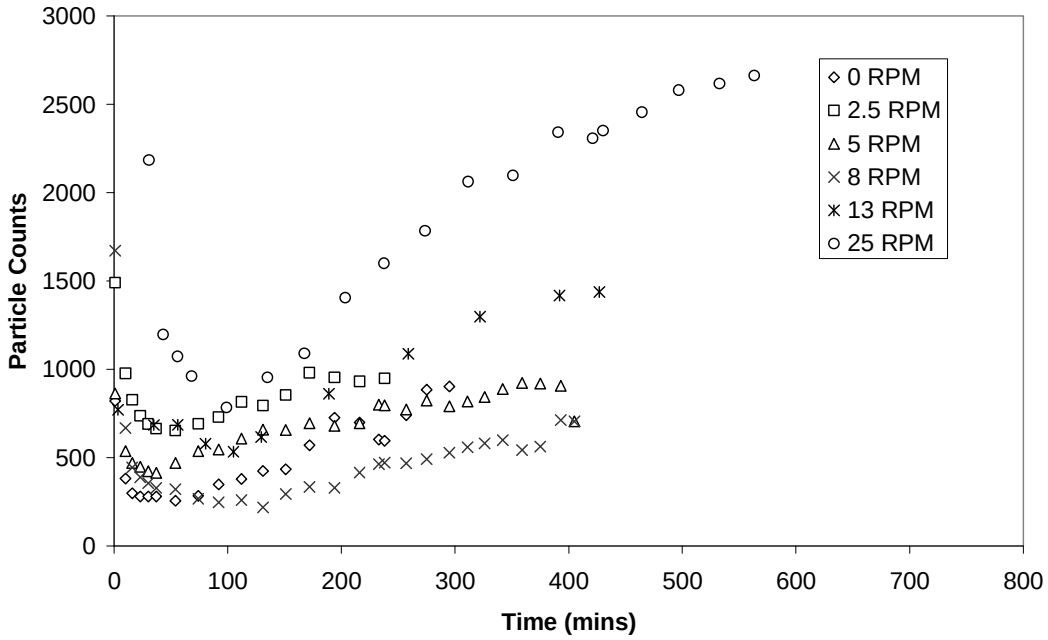

Figure 6-12 Particle counts versus time measurements at various shear rates showing that at 13 and 25 RPM Couette speed there is an increase in particle counts with time suggesting rejection of flocs from the membrane.

Figure 6-13 shows the mean floc chord length measured by the FBRM over the duration of the experiment. The size appears to follow an exponential decay to some average steady state size. This suggests that the cake early on in the filtration could be formed from larger flocs than towards the end of filtration. This is perhaps representative of the flocculation dynamics in the reservoir. It is also possible that such a transient is an artifact of the filtration vessel design.

Comparing the steady state floc size across all shear rates the trend is consistent between 40 and 60 μm from 100 minutes onwards. On this basis it is reasonable to assume that the cake is composed of matter of similar hydraulic conductivity in an uncompressed state. A further assumption of consistent fractal dimension must be made though no experimental evidence is available to confirm this.

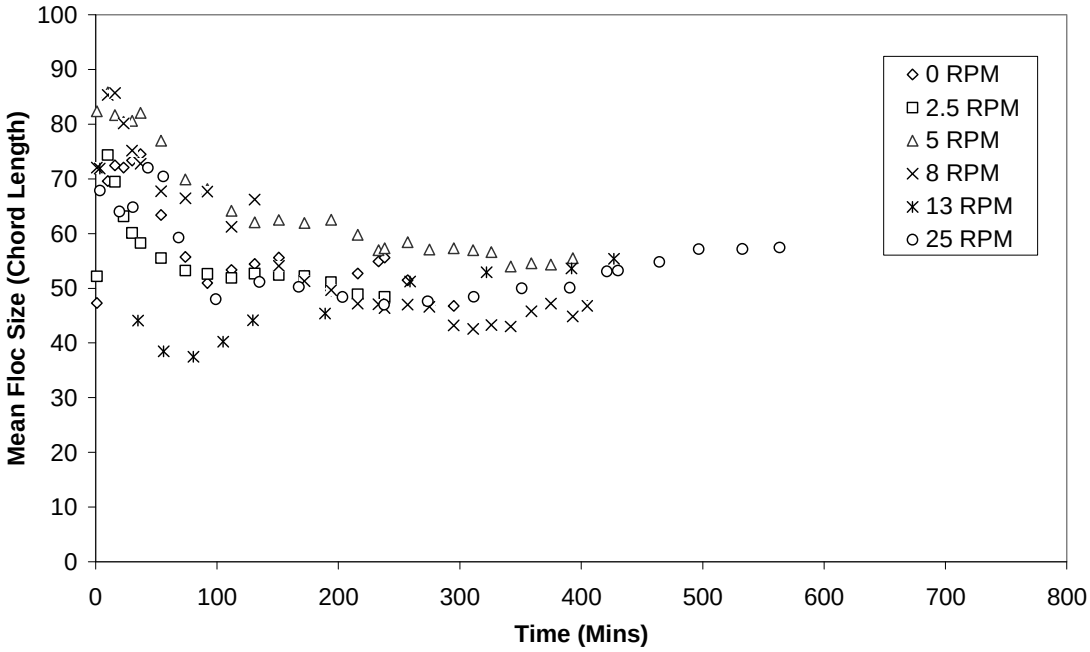

Figure 6-13 Mean floc chord length (μm) versus time plot shows evolution of floc size as flocs reside in the filtration cell. The floc size appears to be uncorrelated with Couette speed and similar.

6.4.2 Calculation of Material Properties

Calculation of the material properties in terms of compressive yield stress and permeability provides a means of probing the local properties of the filter cake. This is important information in ascertaining the macroscopic structural effects imposed by in-situ shear stress on the cake.

For this analysis a series of constant pressure filtration experiments were performed on a fixed mass of flocculated material under well defined shear. The cake was allowed to build up gradually. Data such as filtrate mass versus time were logged as was the final cake height at the end of the filtration run. The filtration was stopped either when steady state had been achieved (i.e. dJ/dt=0). Figure 6-14 shows the steady state flux at each of the nominal pressures for shear rates below the critical shear for cake lift. As expected, the flux is observed to increase in a monotonic non-linear manner with an increase in pressure. In all instances it appears that the flux plateaus at high pressures with no further gain in throughput obtained by increasing the driving force.

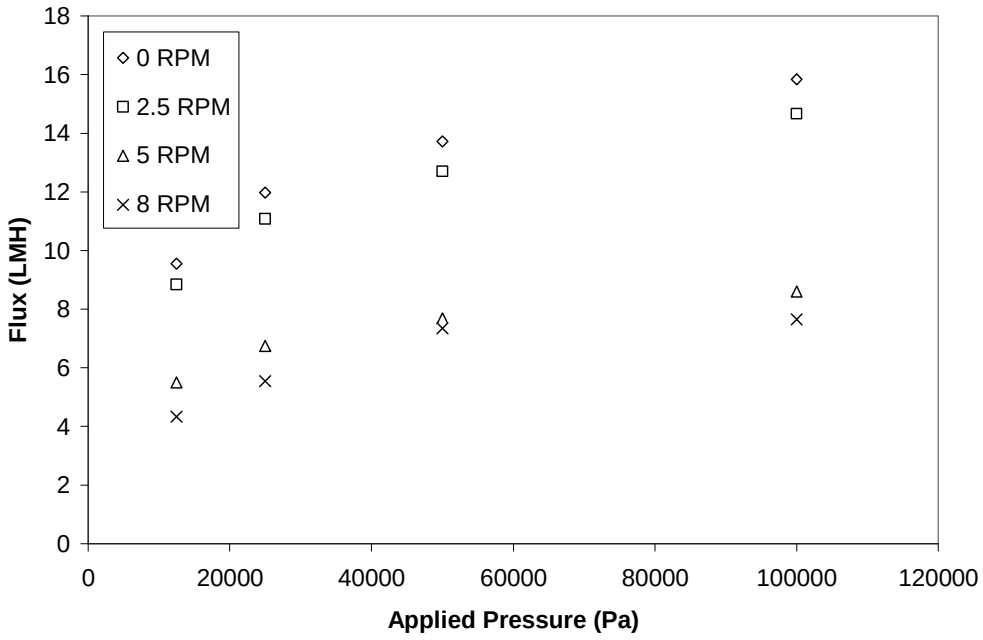

Figure 6-14 Steady state flux versus pressure for various shear rates used for inputs to the steady state filtration analysis.

The final cake height for each filtration run was measured by the method described in section 3.4. A summary of the measured heights for each run is given in Table 6-3. The final height in addition to the steady state flux at the nominal pressures is the inputs required to calculate the material properties according to the method outlined in Chapter 3. A summary of the calculated parameters for the compressive yield stress and permeability is given in Table 6-4.

As can be seen from Figure 6-14, a marginal difference between results obtained at 0 and 2.5 RPM is evident. Recall that the impellor configuration in the 0 RPM case is a 4 blade axial impellor placed at the top of the filtration cell at less than 5 RPM. This is done to provide gentle stirring to ensure even distribution of flocs as they form the cake. This type of configuration is the only viable way of operating near zero shear for the entire volume of the cell without compromising cake uniformity. It is reasonable to assume that such a configuration would result in transmission of 2.5 RPM equivalent shear throughout the cell.

As can be seen from Figure 6-14, a considerable jump in filtration behaviour is observed on increasing mixing speed from 2.5 RPM to 5 RPM.

Table 6-3 Summary of measured cake heights (m) showing the collapse in cake height with higher applied filtration pressures. Comparing the Experimental and calculated values via the steady state filtration approach shows a maximum 14.4% difference suggesting that the parameter fit calculation is reasonable.

	100 kPa Exp	100kPa Calc	% difference	12.5 kPa Exp	12.5 kPa Calc	% difference
0 RPM	0.0178	0.0178	0	0.018	0.0206	14.4
2.5 RPM	0.0183	0.0183	0	0.019	0.0215	13.2
5 RPM	0.017	0.017	0	0.018	0.0197	9.4
8 RPM	0.0165	0.0165	0	0.0174	0.0192	10.3

Table 6-4 Summary of material properties calculated by the steady state approach for shear rates below the point that cake lift was observed(see definition of material properties in section 3.2.1).

	Material Properties						
	C1	C2	C3	C4	C5	C6	R^2
0 RPM	7.53E+06	-6.20E+00	-1.83E+00	9.38E-02	6.12E-04	-1.46	0.99
2.5 RPM	1.19E+07	-5.80E+00	-1.19E+00	-1.34E+00	6.38E-04	-1.40	0.99
5 RPM	1.15E+07	-5.40E+00	-9.56E-01	9.74E-02	8.85E-02	-1.30	0.98
8 RPM	1.03E+07	-5.27E+00	-3.64E-01	1.29E-01	1.21E-03	-1.35	0.96

The compressibility of yeast for each shear rate is presented in Figure 6-15. The compressibility of the cakes formed at 5 and 8 RPM appear to be higher then the cakes formed at 0 and 2.5 RPM.

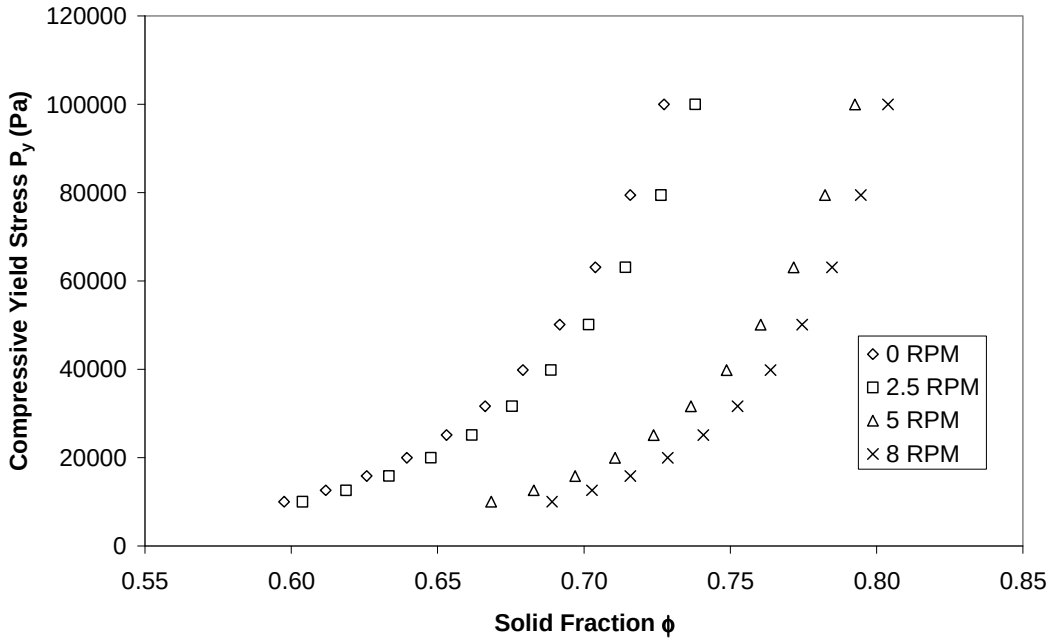

Figure 6-15 Compressive yield stress for sheared yeast flocs showing that it requires less compressive stress to collapse a cake subject to shear.

For the compressibility plots it can be concluded with reasonable certainty that cakes formed at higher shear are compressed to a greater extent, perhaps affected by the additional tangential stresses imposed by shearing. This is very similar to the results observed by Channell et al. (2000). The compressive yield stress curve in this instance (yeast) is offset which was also observed for AKP alumina. This is a significant result because it confirms that the shear stress increases cake compressibility for soft gel like particles. This has further implications for processes such as membrane cleaning where a more compact cake would require more energy and expense to mechanically break the tight network with higher bond density.

In order to ascertain the effects of shear on hydraulic conductivity at a local level it is necessary to compare the change in permeability in the cake as it is subject to solids compressive stress. Figure 6-16 shows a plot of permeability versus solid fraction. There appears to be little difference between the four plots which is in agreement with what was observed by Green (1997) for zirconia who suggests that shear does not alter the microstructure sufficiently to alter permeability.

Figure 6-17 shows the local permeability versus pressure for each of the filtration runs. The trend shows equal permeability at or near the top layer of the cake where the lowest pressure is experienced. The trends of each data set differ towards higher compressive pressures where the layers adjacent to the membrane have a pronounced difference in permeability. It is possible that the difference in permeability is solely attributable to the difference in compressibility alone. This is because the more compressed cake structure at high shears has less pore space available for permeation of fluid. This is certainly within the experimental range of the data.

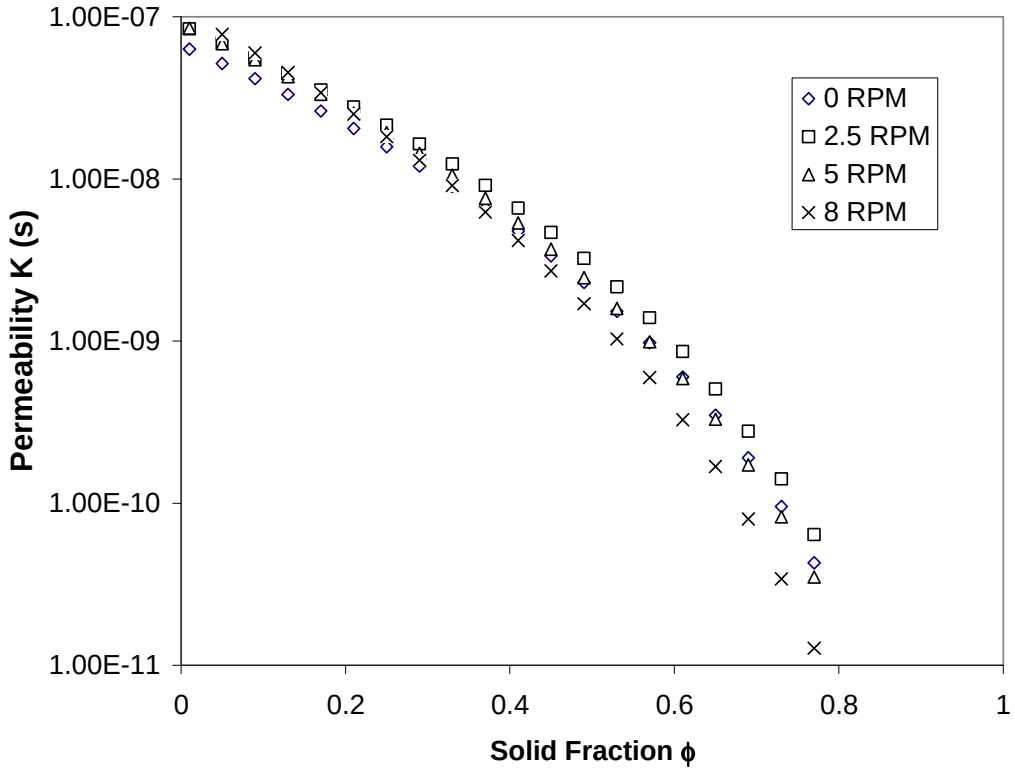

Figure 6-16 Permeability versus solid fraction plot showing a marginal difference between each.

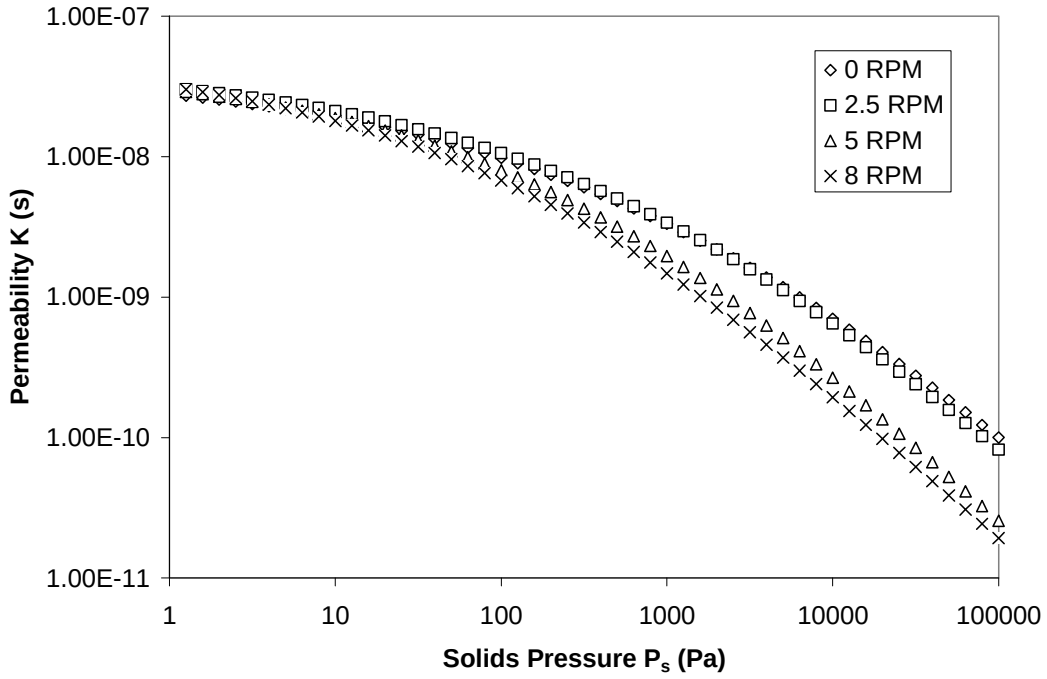

Figure 6-17 Sensitivity of permeability to solids compressive pressure showing that at higher shear the permeability is less across the cake.

The effect of shear on compressive yield stress was characterised by equation 6-7. According to Channell 1999, G^* is expected to be independent of solid fraction. G^* was determined by a fit to the data of $P_y(\phi,G)$ and $P_y(\phi,0)$ values calculated from the steady state approach. Figure 6-18 is a plot of G^* versus ϕ showing that the value of G^* at 5 and 8 RPM is approximately the same (i.e. G^*=6.75). At 2.5 RPM the model fit is likely to be incorrect based on the experimental data. Recall that the values for $P_y(\phi,0)$ are not obtained from a true zero shear and rather reflects some low shear that was used to distribute the material. It appears that results derived for 0 and 2.5 RPM shown in other plots appear similar. Thus, this zero shear is possibly approximate in magnitude to that experienced at 2.5RPM. Hence, it is not surprising to see that the model does not fit well here.

Thus, an equation describing how shear affects the compressive yield stress is given by

$$P_y(\phi,G) = P_y(\phi,0)\left[1-\left(\frac{G}{6.75}\right)^{\frac{1}{2}}\right] \qquad (6\text{-}19)$$

where the model appears to be a reasonable approximation between $5<G<8$ s^{-1}. Despite the known limitation with the penetration of the fluid velocity gradient into the cake phase, the model comprised of experimentally determined constants can be used to give the empirical equation 6-19.

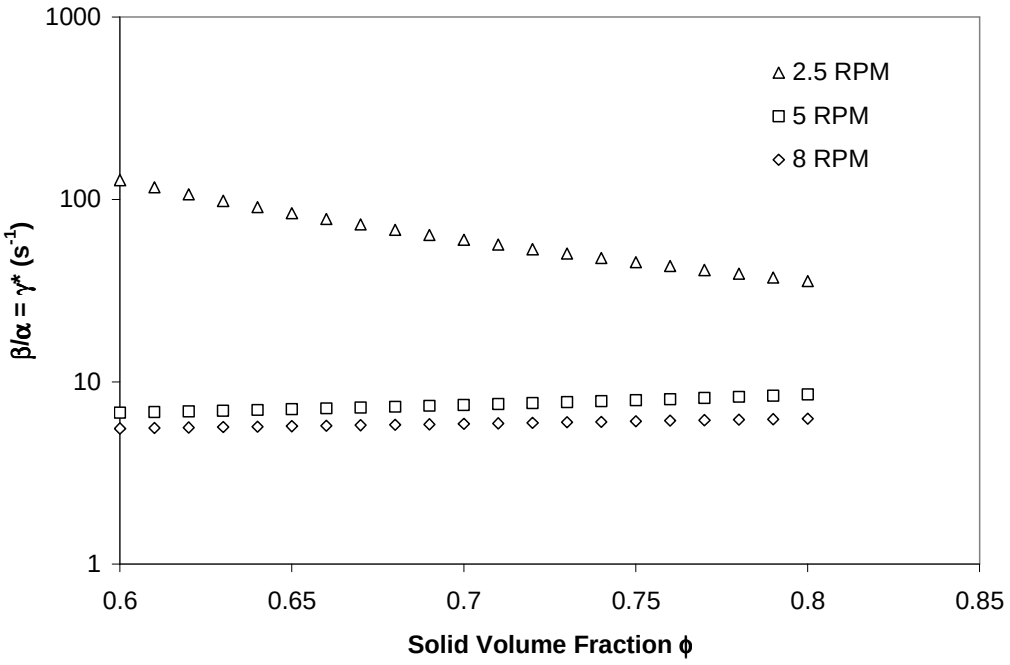

Figure 6-18 Plot of G^* versus solid fraction showing that equation 6-19 is not valid as G approaches zero shear.

6.4.3 Implications for Constant Flux Filtration

In Chapter 4, a model was established to describe the effect of compressibility and permeability on the TMP rise in constant flux filtration. An important aspect about the operation of real world membrane treatment processes is managing the TMP rise to some threshold value before removal of the fouling layer in order to restore permeability. This model has important implications for the application of shear in membrane filtration whether it is for preventing or minimising deposit of cake mass or enhancing particle collisions to increase floc size.

In the constant flux filtration experiments performed under shear, flux was maintained at 30 LMH for all runs. The feed was initiated and pressure adjusted via a feedback control loop to maintain the set point flux. Figure 6-19 shows the TMP rise for

various shear rates up to a maximum possible of 25 RPM. The flocculated yeast was prepared in the same fashion as for the constant pressure filtration experiments of Chapter 3. Here, it can be seen that the more rapidly increasing TMP occurs for higher shear rates. It is highly probable that the underlying reduction in compressive yield stress results in a lower permeability in the rate determining regions of the cake (i.e. the lower layers). The difference is most pronounced when cake mass, corresponding to 300mL of processed volume or greater, has been accumulated. At this point a higher pressure is needed to sustain a constant flux through a less permeable structure. For higher sheared cakes this reduced permeability caused by effects that have propagated from the surface through to the lower layers are evident by the rapid TMP rise. This effect even outweighs the cake lift effect at 13 and 25 RPM where considerable mass is removed from the cake. It is expected at much higher shears that the back transport effects would dominate as reported by workers on such systems as Vibratory Separation or VSEP (Al Akoum et al. 2002). However, the effect of high shear on floc breakage would become significant at this point.

The processed volume corresponding to 150 kPa (an indication of shear sensitivity) does not appear to vary by much more than 25% across the range of shear examined here. For a real system such as hollow fibre where there is intermittent gas slugs from air sparging it is probable that regions of non-uniform shear would result in wide variability in hydraulic conductivity, perhaps equal to or greater than experienced here.

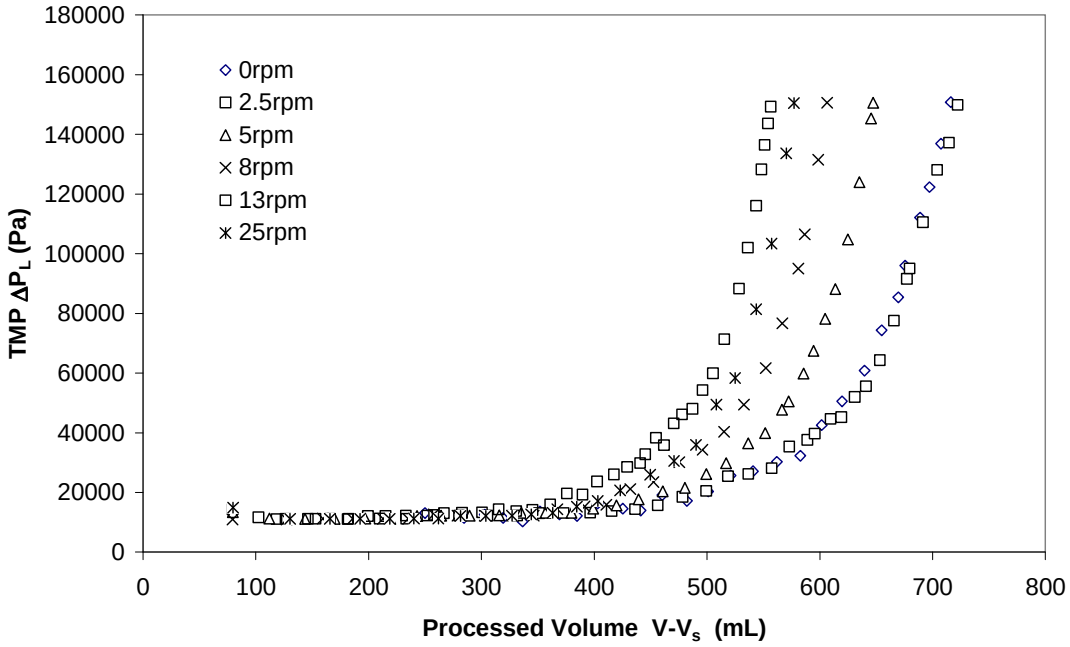

Figure 6-19 TMP rise at constant flux for various shear rates.

Equation 6-18 was fitted to the experimental data in Figure 6-19 via the SSE minimisation technique to determine the compressibility (n) for respective shear rates at a constant 30 LMH across all experiments. The results are presented in Figure 6-20 showing excellent fits for all TMP rise. A common time constant value of τ=77600s was extracted from the numerical technique on the assumption that this parameter is independent of shear. It is worth pointing out that the fit deviates at low pressure. This is due to the nature of the assumed model form (equation 6-17). The experimental data appears to not rise until 350mL of processed volume, which at this point there is a monotonic increase. The assumed model form cannot fit this trend perfectly at this point. This is a limitation of the assumed model form. It would be worth exploring other forms to accommodate this type of data.

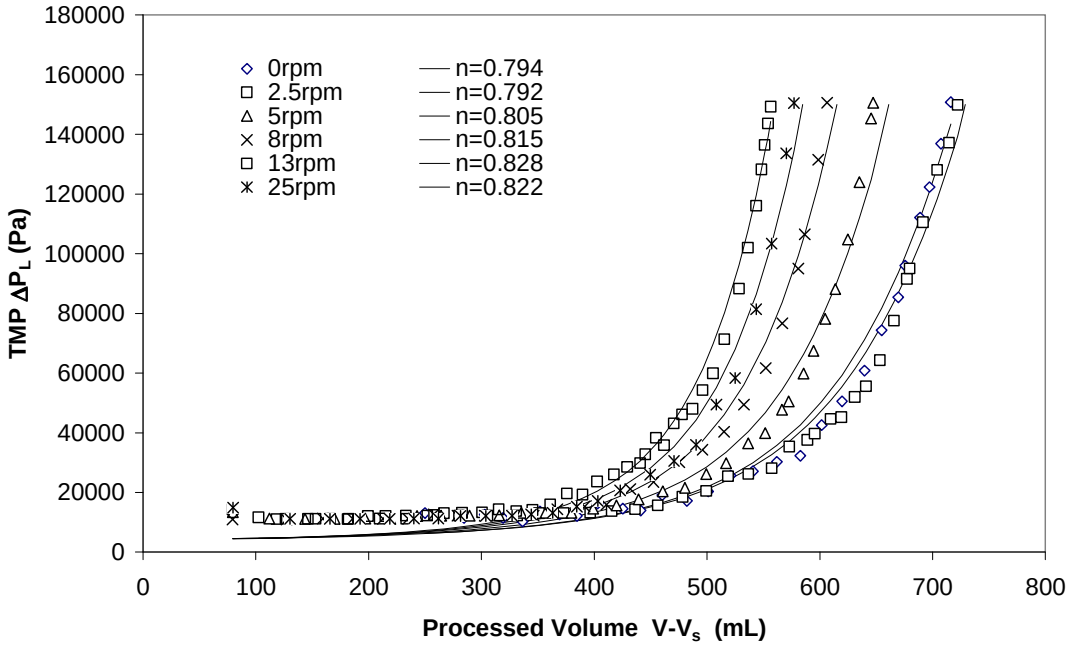

Figure 6-20 Equation 6-18 fitted to the experimental data extracting compressibility values (n) for each shear rate with a common time constant of τ=77600s.

The compressibility as a function of shear is plotted in Figure 6-21 showing a linear correlation of compressibility with shear up to a point where cake break off becomes significant. Values for k_3 and k_4 are calculated to be 0.0047 and 0.7926 respectively. The slope given by k_3 can be regarded as a measure of shear sensitivity. A material that exhibits a high G^* would be reflected in a low k_3 value. From a membrane filtration point of view, this characteristic is ideal as this implies that the one-dimensional response of the cake resists low shear. The only assumption can be made that this trend would extrapolate above the point of critical shear (break off) into regions where SMF operates even though these parameters cannot be measured in this regime. The modified general TMP rise model is a reasonable way to access these parameters in-situ.

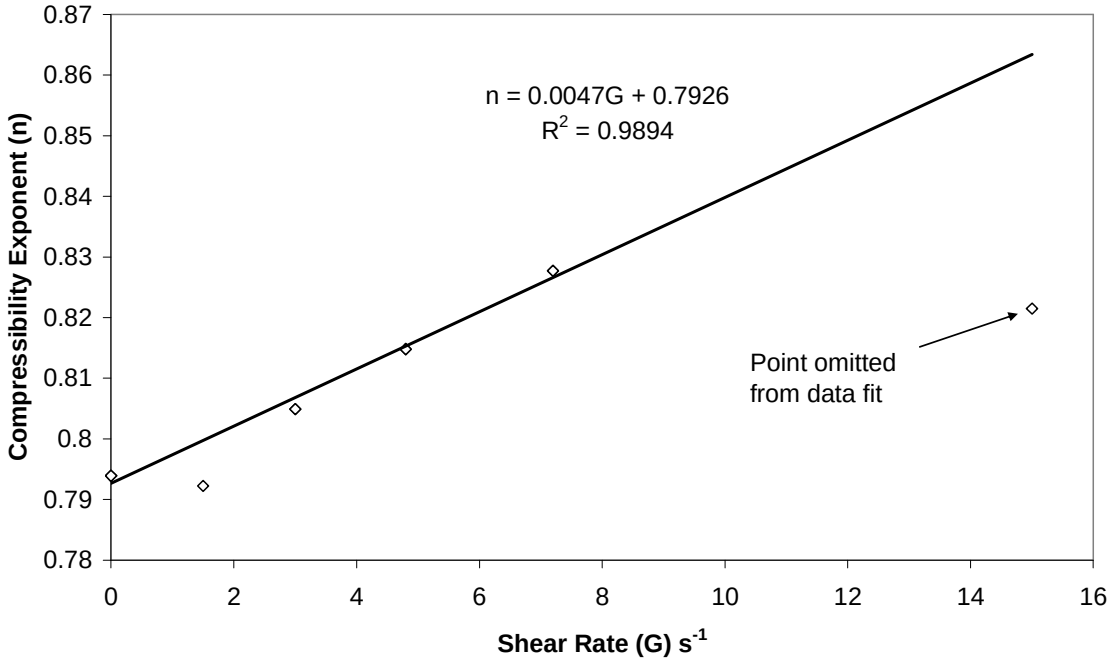

Figure 6-21 Compressibility as a function of shear showing a linear correlation up to G=7s^{-1} before the fit deviates at 15s^{-1}. This is more than likely due to cake break off compromising the assumption of a known rate of cake formation.

6.4.4 Recommendations

An empirical study over a much wider range of shear rates, perhaps exceeding the turbulent regime limit needs to be conducted in order to develop operational strategies and optimisation on sheared filtration processes. The optimum operating condition in terms of normalised flux including the expense to backwash and remove cake may lie in the high shear regime where the benefits of near 100% rejection of solids in dead-end configuration is achieved. At any point below this the operator faces the burden of detrimental effects on cake permeability resulting from application of shear.

Important future work will almost certainly involve varying the material properties of the suspension through choice of coagulants and original mixing conditions separate from filtration. The tools are certainly in place to measure the material properties in a suitable sheared cell for such a study. Addition of coagulants such as alum and aluminium chlorohydrate (ACH) and their effect on resisting shear stress are important for water treatment. Such a parameter as presented in equation 6-18 to

account for shear effects could potentially be used as a rheological measurement for assessing flocculants in membrane filtration subject to simultaneous shear and compression.

The choice of yeast in this system was made to represent a typical system in water treatment. The most important characteristic is its softness and ability to compress beyond the close packed limit for hard spheres. This is much like gelling systems such as clay that swell and immobilise water in their structure. Although there is moderate sensitivity to shear for yeast, there is scope to investigate the effects on mineral particles as surface waters can be a mix of soft and rigid particles. Future work should look at additives such as ACH and whether sufficient strength is provided to resist the effect of reduced stiffness.

6.5 Conclusion

The direct effect of shear stress imposed by a coni-cylindrical Couette on thin filter cakes formed from flocculated yeast was investigated. The shear rate was successfully varied in a regime where consistent floc size was observed in addition to consistent cake growth without significant particle rejection.

The steady state filtration analysis developed in earlier chapters was applied to sheared filtration data here. The local cake properties were calculated allowing deconvolution of the shear effects on compressibility and permeability. The results show that for higher shear rates the cakes formed yield at lower compressive pressures. Results also confirm a reduction in permeability under such circumstances.

Such a result can be explained by a reduction in cake stiffness early on in the life of any given incremental cake slice. Mechanically this can be described as offset in the load bearing chains thus weakening the vertical strength of the cake. Alternatively, a reduction in strength can be conceptually described in terms of the sheared dewatering model of Channell (1999) where shear stress effects penetrate the cake. According to this model, repeated reordering of load bearing chains subject to simultaneous forces in the normal and tangential (to the cake plane) directions occur. Based on the analysis presented here it is difficult to suggest whether the shear assisted dewatering

occurs only at the cake surface or deeper in the cake. However, it is not critical to the analysis presented here.

An empirical model describing the effect of shear on TMP was also fitted to the experimental data to present a practical way of determining the shear sensitivity of a material as an empirical parameter rather than the expression derived by Channell (1999). The relationship between compressibility and shear was shown to be linear over the low shear range up to the point where break-off becomes significant. Effects of cake break off were shown to be difficult to account for in modelling limiting the range of shears covered by the model. Future work should look to address this issue as SMF's operate in ranges where cake break off may be a significant factor.

Chapter 7: Conclusion and Recommendations

The demand imposed by industry to address the issue of fouling and cake collapse in dead-end membrane filtration has been largely the motivation for this study. This thesis investigated changing floc properties as a way of controlling fouling in membrane filtration, both through effects on the cake layer and effects on floc formation.

The approach taken has involved new methods to characterise the material properties during filtration. A steady state filtration approach was developed to address the complication of floc settling during filtration. Furthermore, analysing highly compressible cakes by the standard filtration approach, which assumes average cake properties, results in error due to a large gradient in porosity through the cake. A method based on local material properties was developed to address this.

Steady State Filtration Approach

A steady state filtration technique was developed in Chapter 3 to characterise the material properties of a flocculated suspension. By driving gas filtration to steady state, stable flux data at fixed pressures was obtained as input values for a numerical cake integration procedure. This technique was validated against data obtained using a piston filtration apparatus (Rowe Cell) for flocculated zirconia, yeast and soil. Good agreement was observed for both the compressive yield stress and permeability across these materials.

This technique was successfully implemented throughout this thesis to characterise the material properties of the filtered material.

Constant Flux Filtration Studies

In industry, constant flux filtration is the preferred mode of operation. In Chapter 4 a model was developed to predict constant flux filtration based on the derived cake material properties from the steady state work of Chapter 3. Good agreement between experimental and simulated TMP rise was observed, based on independently measured material properties. The remaining difference is likely attributed to additional consolidation effects that cannot be accounted for by material property based models. Another possible explanation is that the presence of loose unconsolidated material, that experiences high resistance from the lower layers, takes considerably longer than calculated to pass fluid through this layer.

Modification of the general equation for constant flux showed that significant improvements in predicting the TMP rise were gained through inclusion of a time constant to describe consolidation dynamics. Future work should look at the dependence of the time constant on cake material properties and new ways to describe the creep consolidation behaviour of cellular material.

Simulation Studies into Flocs and Filtration

A simulation of cake consolidation was developed in Chapter 5 based on the DEM. Flocs of known size and structure were placed in a "virtual suspension" and the consolidation physics simulated to investigate the hydraulic behaviour of packed flocs under compression.

Pore size distribution plots obtained from simulation studies showed that the cakes formed from larger flocs had larger pores in the relatively unconsolidated state. Larger pores were also favoured in the more compact flocs (D_f=2.3). Larger overall pore size was also more frequent after cake collapse in the larger/compact flocs. Calculation of permeability by CFD showed that the largest (D_f=2.3) floc had the highest permeability. It is reasonable to conclude that a higher frequency of large pores will lead to an increase in the hydraulic conductivity of the cake. This observation has significant implications for choice of shear during floc formation and should be investigated further with particular attention to confirming the results experimentally.

Shear and Filtration

The direct effect of shear stress imposed by a coni-cylindrical Couette on thin filter cakes formed from flocculated yeast was investigated. The shear rate was successfully varied between 1.5 and 4.8s^{-1} in a regime where consistent floc size was observed in addition to consistent cake growth without significant particle rejection. A potentially complex convolution of hydrodynamic effects was thus simplified.

The steady state filtration analysis was applied to constant pressure sheared filtration data between 1.5 and 4.8s^{-1}. The local cake properties were calculated which resolved the shear effects on compressibility and permeability. For increasing shear, it was demonstrated that the cake was more compressible and consequently less permeable. This was also evident in constant flux sheared filtration experiments where the TMP rise was fastest at higher shears. An empirical model for constant flux filtration derived in this study describes the relationship between shear and TMP rise below the point at which shear causes cake up lift. Such a model may suffice for most applications as the material properties approach in conjunction with the reaction rate model (Channell 1999) is not well suited to describing the hydrodynamic effect on membrane filtration.

For membrane filtration of compressible matter, the results show that simultaneous shear and filtration results in detrimental effects on filtration performance. Future work should look at the effect of shear induced cake collapse in moderate to high shear systems where these detrimental effects may or may not be significant compared to cake lift. The tools have been developed here to contribute to such a study. This would pave the way for a more complete understanding of the effect of shear on membrane filtration performance.

References

Al Akoum, O., Jaffrin, M. Y., Ding, L. H., Paullier, P. and Vanhoutte, C. (2002) *Journal of Membrane Science,* **197,** 37-52.

Altmann, J. and Ripperger, S. (1997) *Journal of Membrane Science,* **124,** 119-128.

Antelmi, D., Cabane, B., Meireles, M. and Aimar, P. (2001) *Langmuir,* **17,** 7137-7144.

Barr, J. D. and White, L. R. (2006) *AIChE Journal,* **52,** 545-556.

Bhatt, B. S. and Sacheti, N. C. (1994) *Journal of Physics D-Applied Physics,* **27,** 37-41.

Bian, R., Yamamoto, K. and Watanabe, Y. (2000) *Desalination,* **131,** 225-236.

Bird, R. B., Stewart, W. E. and Lightfoot, E. N. (2002) *Transport Phenomena,* John Wiley & Sons, New York

Botet, R. and Cabane, B. (2004) *Physical Review E,* **70**.

Bottero, J. Y., Tchoubar, D., Axelos, M. A. V., Quienne, P. and Fiessinger, F. (1990) *Langmuir,* **6,** 596-602.

Brenner, H. and Happel, J. (1958) *Journal of Fluid Mechanics,* **4,** 195-213.

Brinkman, H. C. (1947) *Applied Scientific Research Section a-Mechanics Heat Chemical Engineering Mathematical Methods,* **1,** 27-34.

Burger, R., Concha, F. and Karlsen, K. H. (2001) *Chemical Engineering Science,* **56,** 4537-4553.

Buscall, R., McGowan, I. J., Mills, P. D. A., Stewart, R. F., Sutton, D., White, L. R. and Yates, G. E. (1987) *Journal of Non-Newtonian Fluid Mechanics,* **24,** 183-202.

Buscall, R. and White, L. R. (1987) *Journal of the Chemical Society-Faraday Transactions I,* **83,** 873-891.

Bushell, G. C., Yan, Y. D., Woodfield, D., Raper, J. and Amal, R. (2002) *Advances in Colloid and Interface Science,* **95,** 1-50.

Cabane, B., Meireles, M. and Aimar, P. (2002) *Desalination,* **146,** 155-161.

Cabassud, C., Laborie, S., Durand-Bourlier, L. and Laine, J. M. (2001) *Journal of Membrane Science,* **181,** 57-69.

Carman, P. C. (1939) *Journal of Agricultural Science,* **29,** 262-273.

Channell, G. M. (1999) In *Chemical Engineering*, Vol. PhD University of Illinois, Urbana.

Channell, G. M., Miller, K. T. and Zukoski, C. F. (2000) *AIChE Journal,* **46,** 72-78.

Channell, G. M. and Zukoski, C. F. (1997) *AIChE Journal,* **43,** 1700-1708.

Cheremisinoff, N. P. (1986) *Encyclopedia of fluid mechanics* Gulf Pub. Co., Book Division, Houston.

Cho, B. D. and Fane, A. G. (2002) *Journal of Membrane Science,* **209,** 391-403.

Cho, M. H., Lee, C. H. and Lee, S. (2006) *Desalination,* **191,** 386-396.

Christensen, M. L. and Keiding, K. (2007) *AIChE Journal,* **53,** 598-609.

Chu, C. P., Chang, M. J. and Lee, D. J. (2003) *Separation Science and Technology,* **38,** 967-976.

Chu, C.P., Lee, D.J. and Tay, J.H. (2005), *Chemical Engineering Science,* **60**, 565-575.

Chu, C.P. and Lee, D.J. (2004) *Chemical Engineering Science,* **59**, 1875-1883.
Chu, C.P. and Lee, D.J. (2004), *Journal and Colloid Interface Science* **277,** 387-395.
Chu, C.P., Lee, D.J. and Peng, X.F. (2004). *Water Research,* **38**, 2125-2134.
Crittenden, J. (2004) *Water treatment principles and design / MWH,* John Wiley, Hoboken, N.J. .
Cundall, P. A. and Strack, O. D. L. (1979) *Geotechnique,* **29,** 47-65.
Darcy, H. (1856) (Ed, DALMONT, V.) Paris, pp. 647.
de Kretser, R. G., Usher, S. P., Scales, P. J., Boger, D. V. and Landman, K. A. (2001) *AIChE Journal,* **47,** 1758-1769.
Doi, M. and Chen, D. (1989) *Journal of Chemical Physics,* **90,** 5271-5279.
Font, R. and Perez, M. (2007) *Powder Technology,* **172,** 129-143.
Forrest, S. R. and Witten, T. A. (1979) *Journal of Physics a-Mathematical and General,* **12,** L109-L117.
Fuchs, W., Theiss, M. and Braun, R. (2006) *Separation and Purification Technology,* **52,** 46-52.
Gladman, B., de Kretser, R. G., Rudman, M. and Scales, P. J. (2005) *Chemical Engineering Research & Design,* **83,** 933-936.
Green, M. D. (1997) In *Department of Chemical Engineering,* Vol. PhD University of Melbourne, Melbourne.
Green, M. D. and Boger, D. V. (1997) *Industrial & Engineering Chemistry Research,* **36,** 4984-4992.
Gregory, J. and Dupont, V. (2001) *Water Science and Technology,* **44,** 231-236.
Guan, J., Amal, R. and Waite, T. D. (2001) *Water Science and Technology,* **44,** 215-220.
Happel, J. (1958) *AIChE Journal,* **4,** 197-201.
Happel, J. and Brenner, H. (1965) *Low Reynolds Number Hydrodynamics,* Prentice-Hall, Englewood Cliffs, NJ.
Head, K. H. (1980) *Manual of Soil Laboratory Testing,* Pentech Press, London.
Hermanowicz, S. W. (2007) In *IWA International Conference on Particle Separation*IWA, Toulouse.
Hiemenz, P. C. and Rajagopalan, R. (1997) *Principles of colloid and surface chemistry,* Marcel Dekker, New York.
Ho, C. C. and Zydney, A. L. (2002) *Journal of Membrane Science,* **209,** 363-377.
Howe, K. J. (2001) In *Civil Engineering,* Vol. PhD University of Illinois, Urbana.
Hsu, J. W. C., Speers, R. A. and Paulson, A. T. (2001) *Biophysical Chemistry,* **94,** 47-58.
Hughes, D. and Field, R. W. (2006) *Journal of Membrane Science,* **280,** 89-98.
Jiang, Q. and Logan, B. E. (1991) *Environmental Science & Technology,* **25,** 2031-2038.
Jin, Y. L. and Speers, R. A. (1998) *Food Research International,* **31,** 421-440.
Johansson, C. and Theliander, H. (2007) *Chemical Engineering Research & Design,* **85,** 220-228.
Kapur, P. C., Laha, S., Usher, S., deKretser, R. G. and Scales, P. (2002) *Journal of Colloid and Interface Science,* **256,** 216-222.
Khan, K. M. (2007) In *Chemical Sciences and Engineering,* Vol. PhD University of New South Wales, Sydney.
Kim, A. S. and Yuan, R. (2005) *Journal of Colloid and Interface Science,* **285,** 627-633.
Kim, A. S. and Yuan, R. (2005) *Journal of Membrane Science,* **249,** 89-101.
Kim, A. S. and Yuan, R. (2006) *Journal of Membrane Science,* **286,** 260-268.

Kocurek, J. and Palica, M. (2005) *Powder Technology,* **159,** 17-26.
Koenders, M. A., Liebhart, E. and Wakeman, R. J. (2001) *Chemical Engineering Research & Design,* **79,** 249-259.
Kovalsky, P. and Bushell, G. (2005) *Chemical Engineering Journal,* **111,** 181-188.
Kovalsky, P., Gedrat, M., Bushell, G. and Waite, T. D. (2007) *AIChE Journal,* **53,** 1483-1495.
Kovalsky, P., Santiwong, S., Bushell, B. and Waite, T. D. (2007) In *Chemical Water and Wastewater Treatment* Vol. IX (Eds, Hahn, H. H., Hoffmann, E. and Ødegaard, H.) IWA Publishing, London, pp. 279-288.
Kovalsky, P., Wang, X. M., Bushell, G. and Waite, T. D. (2008) *Journal of Membrane Science,* **in press**.
Kranenburg, C. (1994) *Estuarine Coastal and Shelf Science,* **39,** 451-460.
Kusters, K. A. (1991), Vol. PhD Eindhoven University of Technology, Netherlands.
Laborie, S., Cabassud, C., Durand-Bourlier, L. and Laine, J. M. (1998) *Desalination,* **118,** 189-196.
Landman, K. A., Stankovich, J. M. and White, L. R. (1999) *AIChE Journal,* **45,** 1875-1882.
Landman, K. A. and White, L. R. (1992) *AIChE Journal,* **38,** 184-192.
Landman, K. A. and White, L. R. (1994) *Advances in Colloid and Interface Science,* **51,** 175-246.
Landman, K. A. and White, L. R. (1997) *AIChE Journal,* **43,** 3147-3160.
Landman, K. A., White, L. R. and Buscall, R. (1988) *AIChE Journal,* **34,** 239-252.
Landman, K. A., White, L. R. and Eberl, M. (1995) *AIChE Journal,* **41,** 1687-1700.
Lanoiselle, J. L., Vorobyov, E. I., Bouvier, J. M. and Piar, G. (1996) *AIChE Journal,* **42,** 2057-2068.
Lattuada, M., Wu, H. and Morbidelli, M. (2003) *Journal of Colloid and Interface Science,* **268,** 96-105.
Le-Clech, P., Jefferson, B. and Judd, S. J. (2003) *Journal of Membrane Science,* **218,** 117-129.
Lee, D. J. and Wang, C. H. (2000) *Water Research,* **34,** 1-20.
Lee, S. A., Fane, A. G., Amal, R. and Waite, T. D. (2003) *Separation Science and Technology,* **38,** 869-887.
Li, X. Y. and Wang, X. M. (2006) *Journal of Membrane Science,* **278,** 151-161.
Liao, J. Y. H., Selomulya, C., Bushell, G., Bickert, G. and Amal, R. (2006) *Particle & Particle Systems Characterization,* **22,** 299-309.
Lin, C. L. and Miller, J. D. (2004) *International Journal of Mineral Processing,* **73,** 281-294.
Lin, Y. L., Lu, W. M., Wang, D. M. and Tung, K. L. (2003) *Fluid/Particle Separation Journal,* **15,** 13-26.
Lin, Y. L., Wang, D. M., Lu, W. M., Lin, Y. S. and Tung, K. L. (2008) *Chemical Engineering Science,* **63,** 195-203.
Lu, W. M., Huang, Y. P. and Hwang, K. J. (1998) *Journal of Chemical Engineering of Japan,* **31,** 969-976.
Lu, W. M., Huang, Y. P. and Hwang, K. J. (1998) *Separation and Purification Technology,* **13,** 9-23.
Lu, W. M. and Hwang, K. J. (1993) *Separations Technology,* **3,** 122-132.
Machenbach, I., Leiknes, T. and Odegaard, H. (2003) *Water Science and Technology: Water Supply,* **3,** 401-407.
Mandelbrot, B. (1967) *Science,* **156,** 636-&.
McCurdy, K., Carlson, K. and Gregory, D. (2004) *Water Research,* **38,** 486-494.

Meireles, A., Molle, C., Clifton, M. J. and Aimar, P. (2004) *Chemical Engineering Science,* **59,** 5819-5829.
Scott, P. (2004) *Case Study : Kranji Newater Reclamation Plant* USFilter, Towson, MD 21204.
Miller, K. T., Melant, R. M. and Zukoski, C. F. (1996) *Journal of the American Ceramic Society,* **79,** 2545-2556.
Mo, L. and Huang, X. (2003) *Desalination,* **159,** 1-9.
Mooney, M. and Ewart, R. H. (1934) *Physics-a Journal of General and Applied Physics,* **5,** 350-354.
Mulder, M. (1996) *Basic principles of membrane technology* Kluwer Academic, Dordrecht ; Boston
Ni, L. (2001) In *Material Science and engineering,* Vol. PhD University of New South Wales, Sydney.
Perry, R. H. and Green, D. W. (1997) *Perry's chemical engineers' handbook,* McGraw-Hill, New York
Philip, J. R. (1955) *Transactions of the Faraday Society,* **51,** 885-892.
Pikkarainen, A. T., Judd, S. J., Jokela, J. and Gillberg, L. (2004) *Water Research,* **38,** 455-465.
Pollice, A., Brookes, A., Jefferson, B. and Judd, S. (2005) *Desalination,* **174,** 221-230.
Potanin, A. A., Derooij, R., Vandenende, D. and Mellema, J. (1995) *Journal of Chemical Physics,* **102,** 5845-5853.
Potanin, A. A. and Russel, W. B. (1996) *Physical Review E,* **53,** 3702-3709.
Ravina, L. (1993) *Everything you want to know about*
Coagulation & Flocculation.... Zeta-Meter,Inc, Virginia.
Rhodes, M. J. (1998) *Introduction to particle technology* John Wiley, Chichester ; New York.
Riseman, J. and Kirkwood, J. G. (1950) *Journal of Chemical Physics,* **18,** 512-516.
Ruf, A., Worlitschek, J. and Mazzotti, M. (2000) *Particle & Particle Systems Characterization,* **17,** 167-179.
Rushton, A. (2000) *Solid-liquid filtration and separation technology* Wiley-VCH, Weinheim ; New York : .
Ruth, B. F., Montillon, G. H. and Montonna, R. E. (1933) *Industrial and Engineering Chemistry,* **25,** 76-82.
Santiwong, S. R., (2008) In *School of Civil and Environmental Engineering*, Vol. PhD University of New South Wales, Sydney. (Thesis Submitted)
Schafer, A. I., Fane, A. G. and Waite, T. D. (2001) *Water Research,* **35,** 1509-1517.
Selomulya, C. (2001) In *School of Chemical Engineering and Industrial Chemistry,* Vol. PhD University of New South Wales, Sydney.
Selomulya, C., Jia, X. and Williams, R. A. (2005) *Chemical Engineering Research & Design,* **83,** 844-852.
Selomulya, C., Liao, J. Y. H., Bickert, G. and Amal, R. (2006) *International Journal of Mineral Processing,* **80,** 189-197.
Shaw, D. J. (1992) *Introduction to colloid and surface chemistry. ,* Butterworth-Heinemann., Boston.
Shirato, M., Murase, T., Iwata, M. and Nakatsuka, S. (1986) *Chemical Engineering Science,* **41,** 3213-3218.
Smiles, D. E. (1970) *Chemical Engineering Science,* **25,** 985-&.

Smith, A. E., Zhang, Z. B., Thomas, C. R., Moxham, K. E. and Middelberg, A. P. J. (2000) *Proceedings of the National Academy of Sciences of the United States of America,* **97,** 9871-9874.
Sorensen, C. M. (1997) *Scattering and Absorption of Light by Particles and Aggregates,* CRC Press.
Sorensen, P. B., Moldrup, P. and Hansen, J. A. A. (1996) *Chemical Engineering Science,* **51,** 967-979.
Spicer, P. T. and Pratsinis, S. E. (1996) *Water Research,* **30,** 1049-1056.
Spicer, P. T., Pratsinis, S. E., Raper, J., Amal, R., Bushell, G. and Meesters, G. (1998) *Powder Technology,* **97,** 26-34.
Stickland, A. D., De Kretser, R. G. and Scales, P. J. (2005) *AIChE Journal,* **51,** 2481-2488.
Stickland, A. D., de Kretser, R. G., Scales, P. J., Usher, S. P., Hillis, P. and Tillotson, M. R. (2006) *Chemical Engineering Science,* **61,** 3818-3829.
Streeter, V. L. and Wylie, B. (1985) *Fluid mechanics* McGraw-Hill, New York
Svarovsky, L. (2000) *Solid-liquid separation* Butterworth-Heinemann, Boston
Thouy, R. and Jullien, R. (1996) *Journal De Physique I,* **6,** 1365-1376.
Tien, C. (2002) *Powder Technology,* **127,** 1-8.
Tien, C. and Bai, R. B. (2003) *Chemical Engineering Science,* **58,** 1323-1336.
Tiller, F. M. (1953) *Chemical Engineering Progress,* **49,** 467-479.
Tiller, F. M. and Huang, C. J. (1961) *Industrial and Engineering Chemistry,* **53,** 529-537.
Tiller, F. M., Lu, R., Kwon, J. H. and Lee, D. J. (1999) *Water Research,* **33,** 15-22.
Touhami, A., Hoffmann, B., Vasella, A., Denis, F. A. and Dufrene, Y. F. (2003) *Microbiology-Sgm,* **149,** 2873-2878.
Usher, S. P., De Kretser, R. G. and Scales, P. J. (2001) *AIChE Journal,* **47,** 1561-1570.
Usher, S. P. and Scales, P. J. (2005) *Chemical Engineering Journal,* **111,** 253-261.
Vandijk, H. J. M. and Walstra, P. (1986) *Netherlands Milk and Dairy Journal,* **40,** 3-30.
Vasan, S. S., Ghosh, R. and Cui, Z. F. (2002) *Desalination,* **146,** 219-224.
Veerapaneni, S. and Wiesner, M. R. (1996) *Journal of Colloid and Interface Science,* **177,** 45-57.
von Smoluchowski, M. (1917) *Phys. Chem,* **92,** 129-168.
Waite, T. D., Schafer, A. I., Fane, A. G. and Heuer, A. (1999) *Journal of Colloid and Interface Science,* **212,** 264-274.
Wakeman, R. J. (1978) *Transactions of the Institution of Chemical Engineers,* **56,** 258-265.
White, I., Smiles, D. E., Santomartino, S., van Oploo, P., Macdonald, B. C. T. and Waite, T. D. (2003) *Water Resources Research,* **39**.
Worlitschek, J. and Mazzotti, M. (2003) *Particle & Particle Systems Characterization,* **20,** 12-17.
Yang, R. Y., Zou, R. P. and Yu, A. B. (2000) *Physical Review E,* **62,** 3900-3908.
Yen, P. S. and Lee, D. J. (2001) *Water Research,* **35,** 4004-4009.
Zhang, Z. P., Liu, L. F., Yuan, Y. D. and Yu, A. B. (2001) *Powder Technology,* **116,** 23-32.